

ZR

动物学研究

Volume 35 Issue 5
18 September 2014

ZOOLOGICAL RESEARCH



CN 53-1229/Q ISSN 2095-8137
CODEN: ZOYADI
Bimonthly, Since 1980
www.zoores.ac.cn

ZOOLOGICAL RESEARCH

Volume 35, Issue 5 18 September 2014

CONTENTS

Articles

- Schistura megalodon* species nova, a new river loach from the Irrawaddy basin in Dehong, Yunnan, China
(Teleostei: Cypriniformes: Nemacheilidae) Marco Endruweit (353)
- Influence of a large dam on the longitudinal patterns of fish assemblages in Qingyi Stream
..... Xiao-Yun SUI, Zhi LU, Yun-Zhi YAN, Yi-Feng CHEN, Yin-Tao JIA (362)
- Population sizes and group characteristics of Siberian Crane (*Leucogeranus leucogeranus*) and Hooded Crane
(*Grus monacha*) in Poyang Lake Wetland Ming-Qin SHAO, Hong GUO, Jian-Hong JIANG (373)
- Gene cloning and induced expression pattern of IRF4 and IRF10 in the Asian swamp eel (*Monopterus albus*)
..... Qiao-Qing XU, Dai-Qin YANG, Rui TUO, Jing WAN, Ming-Xian CHANG, Pin NIE (380)
- Molecular cloning, sequence analysis, and cadmium stress-rated expression changes of BTG1 in freshwater
pearl mussel (*Hyriopsis schlegelii*) Kou PENG,
Cheng-Yuan WANG, Jun-Hua WANG, Jun-Qing SHENG, Jian-Wu SHI, Jian LI, Yi-Jiang HONG (389)
- Cloning the *sterol carrier protein 2* genes of Japanese toad (*Bufo japonicus formosus*) and Chinese toad
(*Bufo gargarizans*) and its tissue expression analysis
..... Yu-Cheng JI, Hui ZHUGE, Shan-Shan ZHANG, Shu-Fang ZHANG, Xian-Yu Yang (398)
- MicroRNA signature in response to nutrient restriction and re-feeding in fast skeletal muscle of grass carp
(*Ctenopharyngodon idella*) · Xin ZHU, Wu-Ying CHU, Ping WU, Tan YI, Tao CHEN, Jian-She ZHANG (404)
- Effects of surround suppression on response adaptation of V1 neurons to visual stimuli Peng LI,
Cai-Hong JIN, San JIANG, Miao-Miao LI, Zi-Lu WANG, Hui ZHU, Cui-Yun CHEN, Tian-Miao HUA (411)
- Protease-activated receptor (PAR)1, PAR2 and PAR4 expressions in esophageal squamous cell carcinoma
..... Si-Man LI, Ping JIANG,
Yang XIANG, Wei-Wei WANG, Yue-Chun ZHU, Wei-Yang FENG, Shu-De LI, Guo-Yu YU (420)
- Differences in cocaine-induced place preference persistence, locomotion and social behaviors between
C57BL/6J and BALB/cJ mice Jian-Li WANG, Bei WANG, Wen CHEN (426)
- Review**
- Progress on low susceptibility mechanisms of transmissible spongiform encephalopathies
..... Li-Li QING, Hui ZHAO, Lin-Lin LIU (436)
- 广告: 科铭牌生化检测试剂盒: 产品实用、服务实在和价格实惠 (446)
- Cover image:** *Spizixos canifrons*. Photo by Ben HAN

***Schistura megalodon* species nova, a new river loach from the Irrawaddy basin in Dehong, Yunnan, China (Teleostei: Cypriniformes: Nemacheilidae)**

Marco Endruweit*

601, Qingshan Road, Licang, Qingdao, Shandong, Qingdao 266001, China

Abstract: A new species of river loach, *Schistura megalodon* sp. nov., is described from the Irrawaddy basin in Yingjiang County, Dehong Autonomous Prefecture, Yunnan Province, China. The following combination of diagnostic characters serve to distinguish it from all other congeners in the given zoogeographical region: a large processus dentiformes in the upper jaw, a short pre-anus length of 65.4%–66.3% of SL, long paired fins (pectoral: 20.8%–24.2% of SL; pelvic: 17.9%–20.6% of SL), a wide body of 9.7%–11.3% of SL at anal fin origin, an incomplete lateral line, the absence of an orbital lobe, and a broad and distinct basicaudal bar with forward extensions.

Keywords: *Schistura megalodon*; Irrawaddy; Dehong; Yunnan

The Dehong Dai and Jingpo Autonomous Prefecture is situated at the westernmost corner of China's Yunnan Province and shares a border with Myanmar's Kachin State. This area is quasi-solely drained by the Irrawaddy River, also known as Ayeyarwady River, except for its southeastern corner which lies in the watershed of the Salween River. Yingjiang County as the largest of five counties stretches over the northern half of the prefecture. It has various climatic zones from temperate to tropical with altitudes ranging from 210 to 3 404 m (Wikipedia, 2014). The region along its border with Myanmar is inhabited by people of the ethnic minorities Jingpo and Lisu.

Examination of a jar of fishes in the collection room of the Kunming Institute of Zoology (KIZ), Chinese Academy of Science, from rivers around Tongbiguan town in Yingjiang County prompted an ichthyofaunistic survey to western Dehong. The survey yielded inter alia a lot of four specimens of a *Schistura* species that was compared with all congeners reported from the Irrawaddy. Nemacheilid loaches reported from the northeastern Irrawaddy are *Schistura sikmaiensis* (Hora, 1921), *S. vinciguerrae* (Hora, 1935), *S. polytaenia* (Zhu, 1982), *S. yingjiangensis* (Zhu, 1982), and *S. malaisei*

Kottelat, 1990. The taxon *Nemacheilus putaoensis* Rendahl, (1948) is considered a junior synonym of *S. sikmaiensis* (see Kottelat, 1990:208; 2012:118). In addition, the concerned lot was compared with affine species from neighboring watersheds. The concerned specimens turned out to be a distinct species which is, scientifically described herein.

MATERIALS AND METHODS

Meristics, morphometrics and related terminology follow explanations given in Kottelat (1990). Terminology of cephalic sensory system differs in otic canal for 'infraorbital canal A1'. Lateral head length excludes opercular membrane. Eye diameter is measured horizontally. Ultimate and penultimate rays of the dorsal and anal fin that share the same pterygiophore are counted as one. Principal caudal rays are counted upper lobe plus lower lobe including unbranched rays. The widely used term 'suborbital flap' for the protuberance of the lateral ethmoid in some species of nemacheilid loach is

Received: 03 March 2014; Accepted: 10 July 2014

*Corresponding author, E-mail: marco.endruweit@yahoo.de

misleading. This feature is neither located exactly suborbital - anteroinferior would be a better fit - nor it is proved movable as the term 'flap' anticipates. It is therefore herein replaced by the term 'orbital lobe'.

Measurements are taken point to point with a caliper and recorded to nearest 0.1 mm. Regional squamation densities and scale types were examined using a monocular Fenglin XSP-06 (50–200 times magnification).

Lateral and abdominal radiographs (x-rays) of the specimen were taken by a Kubtec Xpert 80 and used to count vertebrae and fin rays. Vertebral counts and associated terminology follow Clothier (1950) and Arratia et al (2010); the terminal compound centrum supporting the hypural series is counted as one vertebra. In addition, radiographs were used to noninvasively measure the width of the Weberian apparatus. It is measured radially at the center of the gas bladders over the entire complex.

Location coordinates including altitudes were determined using a Global Positioning System (GPS) Garmin handheld device.

Type series material was preserved in the field using a 10% formalin solution and after eight days transferred into 90% industrial ethanol. It is placed in the Kunming Institute of Zoology (KIZ), Chinese Academy of Sciences, Kunming, China.

Morphometrics and meristics of comparative species are from Kottelat (1990) and Zhu (1989).

Schistura megalodon species nova (Figures 1–6)



Figure 1 *Schistura megalodon* sp. nov.
Holotype, KIZ 2014001456, 40.7 mm SL, lateral, dorsal, ventral view.



Figure 2 *Schistura megalodon* sp. nov.
Holotype, KIZ 2014001456, life coloration.

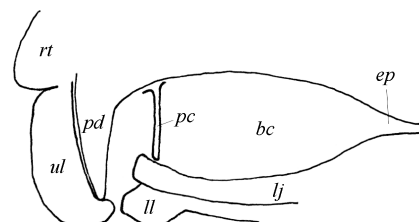


Figure 3 *Schistura megalodon* sp. nov.
Buccal enclosure, mouth closed, schematic depiction: bc, buccal cavity; ep, esophagus; lj, lower jaw; ll, lower lip; pc, palatal curtain; pd, processus dentiformes; rt, rostrum; ul, upper lip.



Figure 4 *Schistura megalodon* sp. nov.
Holotype, KIZ 2014001456, head, ventral view, scale bar: 1 mm.

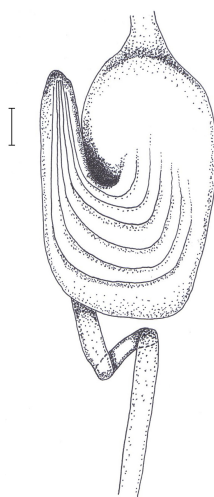
Type series material

Holotype: KIZ 2014001456, 40.7 mm SL; Erganyahe River, Jieyanghe River subbasin, Irrawaddy basin, close to Erganya village, East of Tongbiguan Nature National Reserve, West of Tongbiguan town, Yingjiang County, Dehong Autonomous Prefecture, Yunnan, China; N24°36', E97°36', 1323 m above sea level; collected by M. Endruweit & ZY. Sha, 2014-01-28.

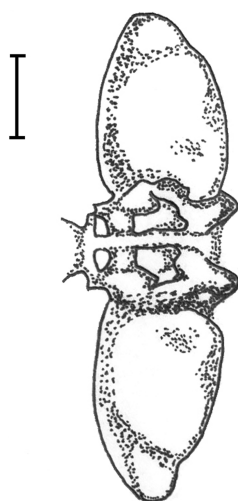
Paratypes: KIZ 2014001457, 3 ex., 33–41.7 mm SL; KIZ 2014001458 with an opened visceral cavity; paratypes collected with the holotype.

Diagnosis

Key diagnostic characters of *Schistura megalodon* are a large processus dentiformes in the upper jaw, a

Figure 5 *Schistura megalodon* sp. nov.

Paratype, KIZ 2014001458, gastrointestinal tract, ventral view, scale bar: 1 mm.

Figure 6 *Schistura megalodon* sp. nov.

Holotype, KIZ 2014001456, gas bladder complex, ventral view, scale bar: 1 mm.

short pre-anus length of 65.4%–66.3% of SL, long paired fins (pectoral: 20.8%–24.2% of SL; pelvic: 17.9%–20.6% of SL), a wide body of 9.7%–11.3% of SL at anal fin origin, an incomplete lateral line, the absence of an orbital lobe, and a broad and distinct basicaudal bar with forward extensions.

Description

Body compact, cylindriciform, posteriorly compressed with a short pre-pelvic length (51.3%–52.1% of SL), a short pre-anus length (65.4%–66.3% of SL), and a short pre-anal length (75.5%–78.2% of SL); body height nearly constant from nape to caudal fin base, slightly

deeper in front of dorsal fin (14.7%–16.7% of SL); body wide (at dorsal fin origin 13.2%–15.3% of SL; at A origin 9.7%–11.3%). Caudal peduncle deep (13%–14% of SL) and long (16.4%–17.5% of SL), its length-depth ratio being 1.23–1.33; crests absent.

Head moderately wide (max. 16.1%–17.5% of SL, at nares 10.3%–11.5%: 68.8%–71.6% of lateral HL) and slightly depressed (height at eye 11.1%–11.8% of SL; at nape 12.6%–14.4% of SL, 91.7%–107% of lateral HL). Eye located dorso-laterally, in large specimens (KIZ 2014001456, 40.7 mm SL; KIZ 2014001457, 41.7 mm SL) conspicuously more dorsally; eye small (18.1%–18.8% of dorsal HL); interorbital width moderate (31%–40% of dorsal HL); ratio interorbital width in eye diameter large (1.69–2.12); eyes not visible when viewed ventrally. Orbital lobe absent. Nares situated antero-dorsally to eye, immediately next to each other; anterior nostril is located at the outlet of a valve-like tube. Snout blunt; its dorsal profile convex. Two pairs of rostral and one pair of maxillary barbels, singly rooted. When stretched inner rostral barbel does not reach anterior rim of eye, outer rostral barbel reaches midline through eye, maxillary barbel exceeds posterior rim of eye. Mouth inferior and moderately arched (ratio width to length: 1.71–2); upper jaw with large, pointed processus dentiformes at symphysis; lower jaw gutter shaped and notched at symphysis when viewed ventrally. Processus dentiformes reaches over lower jaw when mouth is closed. A thin, vertical palatal curtain (Figure 3) shortly posterior to the tip of the lower jaw arranges a buccal enclosure, its distal edge is gutter shaped following the shape of lower jaw at the given position. Lips moderately thick, furrowed; upper lip axially vertically enlarged to muffle processus dentiformes, axially slightly notched; lower lip notched centrally, not forming lateral triangular pads, each side medially with about four lobes separated by furrows (Figure 4). Rostral, labial groove continuous and very deep; labial groove centrally discontinuous around lower lip.

Body densely scaled, between pectoral fin bases sparsely scaled with naked patches. Scales minute, cycloid, imbricate. Head not scaled. Lateral line incomplete, to below D base; approximately 35–40 pored scales. Cephalic sensory system well developed; supra-temporal and otic canals with three pores each, preo-perculo-mandibular canal with 10 pores, supraorbital canal with 8–9 pores, and infraorbital canal with 10–11 pores. An additional, well visible, short canal

of seven pores commences from the upper lip and runs nearly parallel to the infraorbital canal before they merge at the anterior rim of the eye. Infraorbital canal from rostrum to posterior rim of eye and anteriormost three pores of preoperculo-mandibular canal situated on (fixation-induced) elevated ridges.

A short esophagus leads into a comparatively large stomach; stomach simple, sac-like, u-shaped, multiply ridged, nearly horizontally arranged, its posterior wall does not reach tip of pectoral fin, ventrally fully muffled by a thin layer of spleen, outlet located anteriorly on the right side. Intestine straight with two loops in the central section; upper loop does not reach wall of stomach (Figure 5). Peritoneum hyaline with plenty of silver speckles accumulated at visceral arch.

Vertebral column with 4+(13–14) abdominal and 19 caudal vertebrae. Weberian apparatus spreads over from the atlas to the fourth vertebra; gas bladder complex (Figure 6) manubrium shaped with a slight median commissure, massive, transversely arranged, located superior to the second and third vertebra, wide (ratio to interorbital width is 1.2–1.46); gas bladders paired, isodiametric, ovoid, ossified; secondary gas bladder absent. Urostyletic centrum with three lower hypural plates directly detached and three upper hypural plates detached via a long pleurostylus. All principal caudal fin rays are supported via this structure. Dorsally there are 6–7 rudimentary rays along the posterior part of the caudal peduncle associated to neural spines of preural centra 2 to 4 and one epural; ventrally 4–5 rudimentary rays are associated to hemal spines of preural centra 2 and 3.

Fin formula: D iii, 7; P i, 9; V i, 6–7; A iii, 5; C i, 9+8, i. Paired fins comparatively long (P: 20.8%–24.2% of SL; V: 17.9%–20.6% of SL). Pectoral fin horizontally inserted, falcate; tip reaches anteriormost tip of ligaments of pelvic girdle, but does not reach origin of pelvic fin; in KIZ 2014001457 first ray of pectoral fin thickened and ventrally flattened. Pelvic fin rays surpass anus by far, but do not reach origin of anal fin; origin of pelvic fin at vertebra 4+11; suprapelvic lobe well developed, posteriorly free. Origin of anal fin at vertebra 4+21. Distal margin of dorsal fin slightly convex; insertion of dorsal fin at vertebra 4+11; insertion in larger specimens (KIZ 2014001456–7, 40.7–41.7 mm SL) slightly behind pelvic fin origin, in smaller specimens (KIZ 2014001458–9, 33–34.1 mm SL) slightly in front of pelvic fin origin. Caudal fin slightly emarginated, almost truncate, lobes equally long, tips widely rounded.

An overview of selected comparative morphometrics is given in Table 1.

Coloration of preserved specimens

Body with 10–12 dark brown bars on light brown ground coloration; usually four predorsal, 2–3 subdorsal, and 4–5 postdorsal bars; predorsal bars 2–3 times wider, more irregular and inconspicuous than subdorsal and postdorsal bars. Humeral spot inconspicuous, superimposed to first and second bar. Predorsal bars more conspicuous in smaller specimens (KIZ 2014001458–9). All bars interconnected over dorsum, not connected at ventral extremity, except last bar between anal fin and basicaudal bar. Basicaudal bar conspicuously black, wide, straight, with forward directed extensions at both extremities; in some specimens (KIZ 2014001457) additionally with backward directed extensions. Interspace between last body bar and basicaudal bar conspicuously light gray. Abdomen in front of anus light beige; posterior to anus light gray. Top of head with dark gray markings on light gray ground coloration; head ventrally light beige. Tip of anterior nostril tube black. Lower lip with a peculiar, dark gray mark on each side in larger specimens (see Figure 3).

Dorsal fin with large black anterobasal spot reaching onto membrane between first and second branched fin ray followed by a dark brown basal band over the entire length of the fin base; a median band along rays; membranes hyaline. Caudal fin basally with black bar as described ranging far onto the fin; a transverse gray band at around halfway and another slightly lighter band submarginally. Pectoral, pelvic and anal fins hyaline with a whitish-yellowish hue.

Life coloration

Basically identical to the coloration of preserved specimens with differences as follows: ground coloration light brown to purple; the first four pectoral fin rays yellow; unbranched and first two unbranched dorsal fin rays red distally; unbranched and uppermost two unbranched caudal fin rays of the upper lobe distally red.

Etymology

The specific epithet *megalodon* is a compound word borrowed from ancient Greek: μέγας for 'big' and ὄδους for 'tooth'; an allusion to the large processus dentiformes of the upper jaw; a noun in nominative, indeclinable.

Table 1 Comparative morphometrics of *Schistura megalodon* sp. nov. and of related species (values from Kottelat, 1990)

	<i>Schistura megalodon</i> sp. nov.					<i>S. malaisei</i>	<i>S. vinciguerrae</i>				<i>S. sikmaiensis</i>
	types series; n=4					Holotype	n=10				Neotype
	Holotype	Mean	Min	Max	SD		Mean	Min	Max	SD	
SL [mm]	40.7		33.0	41.7		45.9		40.3	65.2		58.7
In % of SL											
Dorsal HL	22.1	21.6	21.1	22.1	0.41	20	19.5	18.0	20.3	0.76	21.1
Lateral HL	24.8	23.9	22.4	24.8	1.13	24.6	20.3	18.3	21.3	0.87	24.5
Pre-dorsal length	53.6	53.2	52.1	54.2	0.90	52.3	51.4	48.9	52.6	1.09	53.5
Pre-pelvic length	51.4	51.7	51.3	52.1	0.43	57.1	51.5	49.7	52.6	0.95	58.8
Pre-anal length	75.7	76.6	75.5	78.2	1.23	79.5	76.1	74.1	77.7	1.00	80.8
Pre-anus length	66.3	65.9	65.4	66.3	0.39	74.7	68.8	66.8	71.3	1.30	77.8
Head depth (at eye)	11.3	11.4	11.1	11.8	0.26	11.1	9.9	8.9	10.7	0.50	12.8
Head depth (at nape)	14.3	13.5	12.6	14.4	0.96	12.6	11.9	10.7	13.0	0.61	14.7
Body depth	16.7	15.6	14.7	16.7	0.92	16.1	18.4	16.1	21.3	1.69	17.6
Depth caudal peduncle	14.0	13.4	13.0	14.0	0.43	13.5	12.2	11.6	12.6	0.39	12.3
Length caudal peduncle	17.2	17.0	16.4	17.5	0.48	13.3	15.6	14.6	16.2	0.51	12.6
Snout length	9.3	8.9	8.2	9.4	0.57	8.7	8.9	8.2	9.7	0.45	9.9
Head width (at nares)	11.5	10.8	10.3	11.5	0.66	10.7	9.4	8.2	10.1	0.50	11.1
Maximum head width	17.4	16.8	16.1	17.5	0.80	15.0	14.1	13.1	14.9	0.48	15.0
Body width (dorsal origin)	14.7	14.2	13.2	15.3	0.99	12.9	13.7	12.3	15.3	0.99	14.0
Body width (anal origin)	10.8	10.4	9.7	11.3	0.73	8.9	8.7	7.6	9.7	0.64	9.0
Eye diameter	4.2	4.0	3.8	4.2	0.16	4.6	4.0	3.2	4.5	0.38	3.9
Interorbital width	8.8	7.8	6.7	8.8	1.10	6.5	7.0	6.3	7.9	0.39	6.1
Length pelvic fin	17.9	19.2	17.9	20.6	1.20	16.6	18.7	16.9	20.7	1.02	17.2
Length pectoral fin	21.4	21.9	20.8	24.2	1.59	18.1	22.3	19.6	24.2	1.32	19.3

Ecology

The type series was obtained from the Erganyahe River (Figure 7). A montane, subtropical biome predominates this region. At the time of visit (late January, 2014, dry season) the stream was approximately 8–10 m wide and 0.3–0.5 m deep over riffles. Water parameter: 12 °C, 20 µs/cm, pH 5.9. The water was clear and running moderately to fast over boulders, rocks, pebbles, sand, and twigs. Aquatic macrophytes were absent. Aside *Schistura megalodon*, there were *Schizothorax malacanthus*, *Devario kakhienensis*, *Exostoma labiatum*, *Misgurnus anguillicaudatus*, and *Channa gachua*.

A full day of fishing just yielded the four specimens that compose the type series. *Schistura megalodon* is regarded as rare. This is in compliance with the statements of locals and Shuwei Liu (KIZ), who spend a



Figure 7 Erganyahe River, type locality of *Schistura megalodon* sp. nov., view northwards, downstream.

full spend a full day fishing at the Erganyahe River close to Erganya village in June 2013. He collected just one specimen that was identified conspecific basing on

photographs. The specimen concerned was not preserved (SW. Liu, pers. comm.).

The large processus dentiformes may be a trophic adaptation. It is hypothesized that it may be used as a tool to detach eggs and other food items from the substratum or it may be used for efficient digging. It is equally well developed in the type specimens and therefore most likely not a sexual dimorphic character.

The dorsal fin migrates backwards during ontogeny in *Schistura megalodon*. Its position relatively to the pelvic fin, thus, proves unsuitable as a diagnostic character. Smaller specimens of *S. megalodon* have the dorsal fin inserted slightly in front of the pelvic fin, while larger specimens have it inserted slightly behind the pelvic fin origin. This is manifested by the predorsal length: the two smaller paratypes (KIZ 2014001458–9, 33–34.1 mm SL) have a predorsal length of 52.1%–52.8 mm SL, the holotype (KIZ 2014001456, 40.7 mm SL) and the largest paratype (KIZ 2014001457, 41.7 mm SL) have a predorsal length of 53.6%–54.2% of SL.

Distribution

Schistura megalodon is only known from the type locality (Figure 8). A few kilometers downstream of the type locality the Erganyahe River marks the borderline between China and Myanmar flowing northwards prior to its influx in the Jieyanghe River. The new species is, thus, expected to occur on Burmese territory as well.

DISCUSSION

Certainly *Schistura megalodon* has been hitherto overlooked by taxonomists working on this group of fishes due to its diminutive size, its rather limited distributional range, its occurrence close in the politically sensitive border region of China and Myanmar and the therefore restricted accessibility, and its absolute scarcity in the habitat.

The palatal curtain in *Schistura megalodon* separates the pharynx into an anteriorly located prebuccal cavity and a posteriorly located buccal chamber. The buccal chamber is quasi sealed by the palatal curtain when the mouth is closed. This morphology reminds of the condition found in member of the genus *Neonoemacheilus* Zhu & Guo, 1985. However, in *Neonoemacheilus* the prebuccal cavity is formed by hypertrophied lips which is not the case in *S. megalodon*. Furthermore, *S. megalodon* does not possess characters diagnostic of *Neonoemacheilus* such as an orbital lobe in males and a

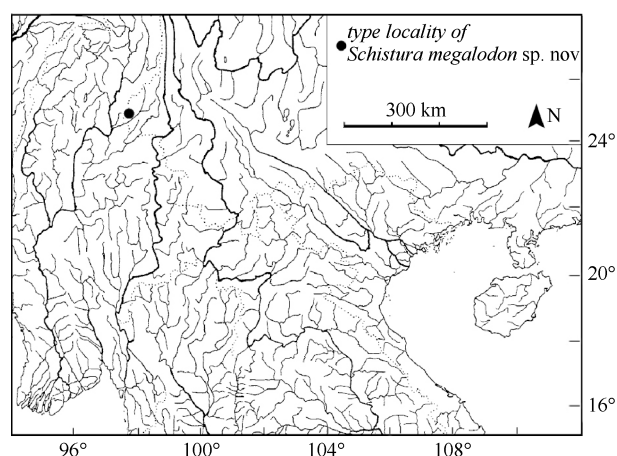


Figure 8 *Schistura megalodon* sp. nov., type locality

complete lateral line. It perfectly fits into the generic description of *Schistura* as provided by Kottelat (1990: 24) and is therefore herein treated as a member thereof.

Phenotypically close to *Schistura megalodon* is *S. cincticauda* (Blyth, 1860) from the Salween basin in Thailand. *Schistura megalodon* differs from *S. cincticauda* in having a smaller size (41.7 mm SL vs. 50 mm SL); a shorter pre-dorsal length (52.1%–54.2% of SL vs. 54.7%–58.8%); a longer caudal peduncle (16.4%–17.5% of SL vs. 12.2%–16.4%); a wider body at anal fin origin (9.7%–11.3% of SL vs. 7.7%–9.4%; 45.1%–52.2% of dorsal HL vs. 34%–45%); a smaller eye diameter (3.8%–4.2% of SL vs. 4.6%–5.7%; 18.1%–18.9% of dorsal HL vs. 21%–27%); suprapelvic lobe present vs. absent; and further differences in the color pattern.

Schistura megalodon is distinguished from *S. malaisei* by a shorter pre-pelvic length (51.3%–52.1% of SL vs. 57.1% of SL in *S. malaisei*); a shorter pre-anus length (65.4%–66.3% of SL vs. 71.1%–74.7%); a longer caudal peduncle (16.4%–17.5% of SL vs. 11.8%–13.3%); a wider head (16.1%–17.5% of SL vs. 15%–15.1%); a wider body (at dorsal fin origin: 13.2%–15.3% of SL vs. 12.9%; at anal fin origin: 9.7%–11.3% of SL vs. 8.9%–9.6%); a longer pelvic fin (17.9%–20.6% of SL vs. 14.7%–16.6%); a longer pectoral fin (20.8%–24.2% of SL vs. 17.6%–18.1%); and a different color pattern. *Schistura malaisei* was described from Putao in northern Myanmar.

Another similar nemacheilid loach described from the Irrawaddy basin in the Manipur State in India is *S. sikmaiensis*. *Schistura megalodon* is readily distinguishable from *S. sikmaiensis* by having iii, 7 dorsal fin rays vs. iv, 8; i, 9 pectoral fin rays vs. 11; lateral incomplete

with 35–40 pored scales vs. complete with 100–110 pored scales; a shorter pre-pelvic length (51.3%–52.1% vs. 58.8%); a shorter pre-anus length (65.4%–66.3% of SL vs. 77.8%); a shorter pre-anal fin (75.5%–78.2% vs. 80.8%); a less deep head (at eye: 11.1%–11.8% vs. 12.8%; at nape: 12.6%–14.4% vs. 14.7%); a less deep body (14.7%–16.7% vs. 17.6%); a deeper and longer caudal peduncle (depth: 13%–14% vs. 12.3%; length: 16.4%–17.5% vs. 12.6%); a shorter snout (8.2%–9.2% vs. 9.9%); a wider head (16.1%–17.5% vs. 15%); a wider body at anal fin origin (9.7%–11.3% vs. 9%); a wider interorbital distance (6.7%–8.8% vs. 6.1%); longer paired fins (pelvic fin: 17.9%–20.6% vs. 17.2%; pectoral fin: 20.8%–24.2% vs. 19.3%); processus dentiformes present vs. absent; and significant differences in color pattern. Kottelat (1990:210) designates the holotype of *Nemacheilus putaoensis* as neotype of *S. sikmaiensis* which makes *N. putaoensis* an objective junior synonym to *S. sikmaiensis*. Zhu (1989:62, Figure 42) lists one specimen of *N. putaoensis* from the Dayingjiang River in Yingjiang County and gives the species' distributional range as Jieyanghe River, the same subbasin from which *S. megalodon* is described. This river is an independent tier one tributary to the Irrawaddy itself and does not belong to the Dayingjiang subbasin. Zhu places *putaoensis* in *Nemacheilus* which actually implies the presence of an orbital lobe in males according to his generic diagnosis (1989:60). Both, the description and the accompanying figure, however, are lacking an orbital lobe. Zhu does not mention a processus dentiformes which fits well to the species' diagnosis.

Schistura vinciguerrae (Figure 9a) was described from Meekalan within the Tenasserim mountain range in southern Myanmar and is reported from the Irrawaddy basin Yingjiang County in Dehong by Kottelat (1990:219) and Zhu (1989:52). *Schistura megalodon* is distinguished from *S. vinciguerrae* by having iii, 7 dorsal fin rays vs. iv, 8–9; i, 9 pectoral fin rays vs. 11–12 in total; lateral incomplete with 35–40 pored scales vs. complete with 84–90 pored scales; a longer head length (dorsally: 21.1%–22.1% of SL vs. 18%–20.3%; laterally: 22.4%–24.8% vs. 18.3%–21.3%); a deeper and wider head (depth at eye: 11.1%–11.8% vs. 8.9%–10.7%; max. width: 16.1%–17.5% vs. 13.1%–14.9%); a shorter pre-anus length (65.4%–66.3% of SL vs. 66.8%–71.3%); a deeper and longer caudal peduncle (depth: 13%–14% vs. 11.6%–12.6%; length: 16.4%–17.5% vs. 14.6%–16.2%); a wider body at anal fin (9.7%–11.3% vs. 7.6%–9.7%), a

smaller maximum size of 41.7 mm SL vs. 71 mm SL; and a far different color pattern.



Figure 9 a. *Schistura vinciguerrae*, KIZ2012004064, 42.6 mm SL, Tanjiazhai, Tengchong County, Longchuanjiang River subbasin; b. *Schistura polytaenia*, KIZ2012004077, 49 mm SL, male, Mahei village, Tengchong County, Dayingjiang River subbasin.

Zhu (1982:107) describes *Schistura yingjiangensis* (as *Nemacheilus yingjiangensis*) from the Dayingjiang River in Yingjiang County and gives its distributional range as Dayingjiang and Longchuanjiang rivers (1989:65). *Schistura megalodon* is distinguished from *S. yingjiangensis* by i, 9 pectoral fin rays vs. i, 10; lateral line incomplete vs. complete; orbital lobe absent vs. present; pelvic clearly surpasses anus vs. does not surpass; smaller maximum size (41.7 mm SL vs. 61 mm SL); and a longer pre-dorsal length (52.1%–54.2% of SL vs. 44%–50%). In *S. megalodon* the lateral HL is 4.03–4.46 times in SL vs. 4.5–5 times; the eye diameter 1.69–2.12 times in interorbital width vs. 1.4–1.5 times; the eye diameter 5.69–6.15 times in lateral HL vs. 4.2–5 times; and interorbital width 2.81–3.36 times in lateral HL vs. 3.7–4 times. Besides, there are significant differences in the color pattern.

Schistura megalodon is easily distinguished from *S. polytaenia* (Figure 9b) described from the Longchuanjiang River in having constant 17 (9+8) branched caudal fin rays vs. 15–16; vertebrae 4+(32–33) vs. 4+(29–31); lateral line incomplete vs. complete; orbital lobe in males absent vs. present; pelvic fin clearly surpasses anus vs. does not reach; a broad and deeply black, conspicuous basicaudal bar with forward extensions at its extremities vs. short, brown, inconspicuous, does not reach extremities; and a body pattern of 10–12 bars interconnected over the dorsum vs. 18–30 bars and 9–13 saddles along the dorsum. In fact,

the color pattern along the flanks of *S. polytaenia* is highly irregular. It may be more appropriate to define it as mottled rather than barred. This is particularly true in specimens from the Mengjiahe River in Sudian, Yingjiang County.

Another nemacheilid species originally described from upper reaches of the Chaungmagyi River, a left bank, first tier tributary to the Irrawaddy, is the enigmatic *Nemacheilus* (described as *Nemachilus*) *acuticephalus*. Apparently, this species has not been collected since its original description (Hora, 1929). All subsequent authors (inter alia: Kottelat, 1990:97; Talwar & Jhingran, 1992:468) refer to this description. *Schistura megalodon* is distinguished from *N. acuticephalus* in having a broad, straight and distinct basicaudal bar with forward extensions and its extremities vs. a crescent-shaped and pale basicaudal bar not reaching extremities; 10 pectoral fin rays vs. 9; 9+8 branched caudal fin rays vs. 8+8 (taken from Hora, plate 14; see Kottelat); pelvic fin surpasses anus vs. not reaching anus; crests on caudal peduncle absent vs. prominent crests supported by rudimentary rays on the dorsal and ventral extremity of the caudal peduncle; caudal fin slightly emarginate vs. forked. Besides, there are differences in the color pattern. Kottelat placed *N. acuticephalus* in *Schistura*. This generic allocation seems to be incorrect. The prominent caudal peduncle crests, which are in *N. acuticephalus* at least dorsally widely supported by procurent rudimentary rays, are diagnostic for members of *Homatula*. Its mottled color pattern is also typical of members of *Homatula*. However, its small size of just 40 mm TL and the hitherto absence of this genus in the Irrawaddy basin act contradictorily. In order to finally access the generic allocation of *N. acuticephalus* an in depth examination of either the type series or a large batch of topotypic fresh material is recommend. Until this question is satisfactorily resolved the taxon is tentatively treated as *S. acuticephala* following Kottelat (2012:104).

Key to the species of the genus *Schistura* reported

or expected to occur in the Irrawaddy basin in China:

1. Orbital lobe in males present; lateral line complete2
1. Orbital lobe in males absent3
2. Eight branched dorsal fin rays; barred color pattern with postdorsal bars wider*Schistura yingjiangensis*
2. Seven branched dorsal fin rays; mottled color pattern.....*S. polytaenia*
3. Prominent crests supported by rudimentary rays on the dorsal and ventral extremity of the caudal peduncle; forked caudal fin.....*S. acuticephala*
3. Caudal peduncle crests absent4
4. Processus dentiformis in upper jaw absent; median notch in lower jaw absent; pre-anus length 77.8% of SL; lateral line complete.....*S. sikmaiensis*
4. Processus dentiformis in upper jaw present5
5. Median notch in lower jaw absent; pre-anus length 66.8%–71.3% of SL; lateral line complete*S. vinciguerrae*
5. Median notch in lower jaw present; lateral line incomplete.....6
6. Pre-anus length 71.1%–74.7% of SL; color pattern of irregular bars, in particular over the dorsum*S. malaisei*
6. Pre-anus length 65.4%–66.3% of SL; color pattern of regular bars*S. megalodon* sp. nov.

Acknowledgements: The author is thankful to the team around Jun-Xing YANG at KIZ, in particular to Xiao-Yong CHEN for literature support, to Li-Na DU for access to specimens in the collection room of KIZ and for various translations, to Shu-Shu SHEN for help with drawings and sketches, to Shu-Wei LIU for information exchange about the habitat, and to Rui MIN for access to laboratory equipment. Pierre MERCAN and Richard GREEN helped with literature. The discovery of this species would not be possible without the enthusiastic help of Zi-Ying SHA from Erganya village and the support of various Jingpo people inhabiting this area.

References

- Arratia G, Schulze HP, Wilson MVH. 2010. Mesozoic Fishes 5-Global Diversity and Evolution. *Verlag Dr. Friedrich Pfeil*, Munich, 560.
- Blyth E. 1860. Report on some fishes received chiefly from the Sitang River and its tributary streams, Tenasserim Provinces. *Journal of the Asiatic Society of Bengal*, **29**(2): 138-174.
- Clothier CR. 1950. A key to some Southern California fishes, based on vertebral characters. California Department of Fish and Game, Fish Bulletin, No. 79. Bureau of Marine Fisheries, 88.
- Hora SL. 1921. Fish and fisheries of Manipur with some observations on those of the Naga Hills. *Records of the Indian Museum, Calcutta*, **22**: 165-214.
- Hora SL. 1929. Notes on fishes in the Indian Museum. XVII. Loaches

- of the genus *Nemachilus* from Burma. *Records of the Indian Museum, Calcutta*, **31**: 311-334.
- Hora SL. 1935. Notes on fishes in the Indian Museum. XXIV. Loaches of the genus *Nemachilus* from eastern Himalayas, with the description of a new species from Burma and Siam. *Records of the Indian Museum, Calcutta*, 37(Pt1): 49-67, Pl. 1.
- Kottelat M. 1990. Indochinese Nemacheilines. Munich: Verlag Dr. Friedrich Pfeil, 262.
- Kottelat M. 2012. Conspectus cobitidum: An inventory of the loaches of the world (Teleostei: Cypriniformes: Cobitoidei). *The Raffles Bulletin of Zoology*, (S, 26): 1-199.
- Rendahl H. 1948. Die Süßwasserfische Birmas. I. Die Familie Cobitidae. *Arkiv för Zoologi*, **40A**(7): 1-116. (in German)
- Talwar PK, Jhingran AG. 1992. Inland fishes of India and adjacent countries. Volume 1. New Delhi, Bombay, Calcutta: Oxford & IBH Publishing Co. 541.
- Wikipedia contr. 2014. Yingjiang County. Published by Wikipedia, The Free Encyclopedia. Available from: http://en.wikipedia.org/wiki/Yingjiang_County. (accessed: 2014-02-26)
- Zhu SQ. 1982. Five new species of fishes of the genus *Nemachilus* from Yunnan Province, China. *Acta Zootaxonomica Sinica*, **7**(1): 104-111. (in Chinese)
- Zhu SQ. 1989. The loaches of the subfamily Nemacheilinae in China. Nanjing: Jiangsu Science and Technology Publishing House, 150. (in Chinese)
- Zhu SQ, Guo QZ. 1985. Descriptions of a new genus and a new species of noemacheiline loaches from Yunnan Province, China (Cypriniformes: Cobitidae). *Acta Zootaxonomica Sinica*, **10**(3): 321-325.

Influence of a large dam on the longitudinal patterns of fish assemblages in Qingyi Stream

Xiao-Yun SUI^{1,2}, Zhi LU¹, Yun-Zhi YAN³, Yi-Feng CHEN^{2,*}, Yin-Tao JIA²

1. School of Life Sciences, Peking University, Beijing 100871, China

2. Institute of Hydrobiology, Chinese Academy of Sciences, Wuhan 430072, China

3. College of Life Sciences, Anhui Normal University, Wuhu 241000, China

Abstract: Using seasonally collected data (2009–2010) from 15 sampling sites that represent first- to fifth-order streams within the Qingyi watershed, we examined the spatio-temporal patterns of fish assemblages along two longitudinal gradients to explore the effects of a large dam on fish assemblages at the watershed scale. No significant variation was observed in either species richness or assemblage structure across seasons. Species richness significantly varied according to stream order and gradient. Dam construction appeared to decrease species richness upstream substantially, while a significant decrease between gradients only occurred within fourth-order streams. Along the gradient without the large dam, fish assemblage structures presented distinct separation between two neighboring stream orders, with the exception of fourth-order versus fifth-order streams. However, the gradient disrupted by a large dam displayed the opposite pattern in the spatial variation of fish assemblages related with stream orders. Significant between-gradient differences in fish assemblage structures were only observed within fourth-order streams. Species distributions were determined by local habitat environmental factors, including elevation, substrate, water depth, current discharge, wetted width, and conductivity. Our results suggested that dam construction might alter the longitudinal pattern in fish species richness and assemblage structure in Qingyi Stream, despite the localized nature of the ecological effect of dams.

Keywords: Fish assemblage; Species richness; Spatiotemporal pattern; Longitudinal gradient; Dam building

Stream fish assemblages are structured by abiotic factors, biotic interactions, and historical processes (Hoeinghaus et al, 2007). The physicochemical stream environment exhibits spatial heterogeneity and temporal variability, and may cause spatiotemporal variations in fish assemblages (Meador & Matthews, 1992). Typically, among the multiple spatial factors affecting fish assemblages, longitudinal-gradient variations in environmental conditions substantially influence the distribution and abundance of stream fishes (Araújo et al, 2009; Inoue & Nunokawa, 2002; Taniguchi et al, 1998; Vannote et al, 1980). From headwaters to downstream, fish species richness generally increases due to increases in stream size (Matthews, 1986), habitat diversity (Gorman & Karr, 1978), and shelter availability (da Silva Abes & Agostinho, 2001), and the different rates of fish immigration and extinction (Power et al, 1988). Concurrently,

fish species composition may vary longitudinally by species addition and/or species replacement (Boys & Thoms, 2006; Gorman & Karr, 1978; Roberts & Hitt, 2010). The River Continuum Concept (RCC) describes the changes in community structure and species richness of organisms from headwaters to mouth waters and relates these changes to flow regime, water temperature, food availability, and substrate conditions (Vannote et al, 1980). However, due to various human activities (e.g., damming, pollution, erosion), few riverine ecosystems remain free-flowing over their entire course. Overlaying

Received: 17 December 2013; Accepted: 12 May 2014

Foundation items: This study was financially supported by the National Basic Research Program of China (2009CB119200) and the Natural Science Foundation of China (31071900, 31172120)

*Corresponding author, E-mail: chenyf@ihb.ac.cn

this pattern displayed by the RCC, the Serial Discontinuity Concept (SDC) claims that regulation by dams disrupts the underlying continuum and produces a series of lentic and lotic reaches, thereafter causing longitudinal shifts in abiotic and biotic parameters and processes (Ward & Stanford, 1983).

Dams impact stream fishes and invertebrates in diverse ways, such as blocking migratory pathways (March et al, 2003), fragmentizing habitats (Travnichek et al, 1993), altering natural flow regimes (Bonner & Wilde, 2000) and food webs (Power et al, 1996), decreasing water temperature downstream (Clarkson & Childs, 2000) and current velocity upstream (Bennett et al, 2002), disrupting riparian plant communities (Nilsson et al, 1997), and shifting water chemistry (Humborg et al, 1997). The extent to which stream fishes and invertebrates are affected by dams may be associated with the characteristics of dams (e.g., location, purpose, and management) and fauna (Cumming, 2004; March et al, 2003). For example, large dams without spillways are impermeable barriers for migratory organisms and may extirpate all native migratory fish from upstream habitat (Holmquist et al, 1998). In contrast, large dams with spillways provide a possible passage for some native fishes. To date, investigations have primarily identified the effects of dams on lotic reaches directly below dams, mainstream reservoirs directly above dams, and lotic reaches upstream of impoundments (Clarkson & Child, 2000; Cumming, 2004; Santucci et al, 2005; Travnichek et al, 1993). However, little attention has been paid to the effects of dams at the watershed scale.

Stream ecosystems in China are experiencing massive ecological perturbation due to diverse human activities, such as extensive agricultural and industrial production, urbanization, development, and hydraulic engineering construction, all of which threaten freshwater fish (Chen, 2005). Based on data collected from first- to fifth-order streams, representing two longitudinal gradients (one disrupted by a large dam and the other not) within a tributary (Qingyi Stream) of the lower reaches of the Yangtze River, the spatial and temporal patterns of fish assemblages were examined. Totally, our three key goals were to: (1) to determine how fish assemblage patterns vary longitudinally from first- to fifth-order streams; (2) to identify the correlations between local habitat and fish assemblages; and (3) to assess how a large dam affects the longitudinal patterns of fish assemblages at the watershed scale.

MATERIALS AND METHODS

Study area

Qingyi Stream originates from the northern portion of Huangshan Mountain, and flows northeast toward its confluence with the lower reaches of the Yangtze River. This watershed is approximately 309 km long and covers an area of 7 195 km². Due to the subtropical monsoon climate, temperature and precipitation in this area are quite asymmetric across seasons. Annual air temperature ranges from -2.1 °C (January) to 27.5 °C (July), with a mean of 17.8 °C. Annual precipitation is high (approximating 2000 mm/year), with most rainfall (79%) occurring in spring and summer (April to September) and only minor rainfall (less than 5%) occurring in the cold, dry winter (December to February) (Yan et al, 2011).

Chencun Hydropower Station was constructed at the mid-reaches of the Qingyi mainstream in the 1950s. It is the largest station along the lower reaches of the Yangtze River, with 119 m deep impoundment and covering an area of 88.6 km². Derived from Anhui Province topographic maps (1:300 000 scale), the Qingyi Stream is categorized as fifth-order (Strahler, 1957) at its mainstream. A total of 75 first-order, 34 second-order, 12 third-order, 4 fourth-order, and 1 fifth-order stream are included in this watershed. Among the fourth-order streams, the Qingxi, Shuxi, and Machuan streams flow into an artificial reservoir (i.e., Taiping Lake) formed by the impoundment of Chencun Hydropower Station, while Huishui Stream directly flows into the mainstream with its confluence downstream of the station (Figure 1).

Fish sampling

A total of 15 segments representing first- to fifth-order streams were surveyed seasonally during April, August, and October 2009, and January 2010. The sampling segments were derived from two longitudinal gradients. One gradient (A) was set from the headwaters of Qingxi and Shuxi streams to the lower reaches of the mainstream, representing the gradient disrupted by Chencun Hydropower Station, and the other gradient (B) was set from the headwaters of Huishui Stream to the mainstream, representing the gradient not disrupted by a station. Each surveyed segment was set on the topographic map based on their stream orders. Four segments ranging from first- to fourth-order streams were selected within Qingxi, Shuxi, and Huishui streams, respectively. Three other segments representing fifth-order streams were set at the mainstream (Figure 1). Sampling

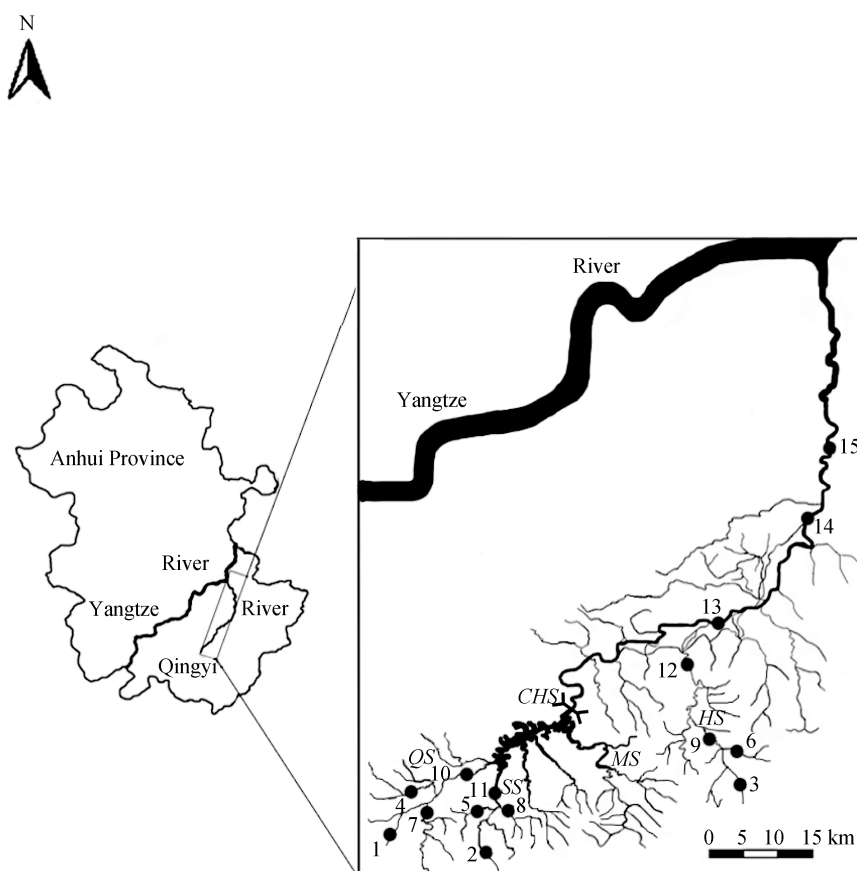
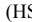


Figure 1 Map of the Qingyi Stream watershed in Anhui Province, China

Solid circles mark the 15 sampling sites. Sites 1–3, 4–6, 7–9, 10–12, and 13–15 represent first-, second-, third, fourth-, and fifth-order streams, respectively. Sites 1, 2, and 3 are located at Qingxi (QS), Shuxi (SS), and Huishui Streams (HS), respectively.  shows Chencun Hydropower Station.

sites were selected in the field based on habitat representativeness and accessibility. Each shallow-water (<1.0 m depth) site of first-, second-, and third-order streams was sampled using backpack electro-fishing by wading in two passes. Each site encompassed at least two mesohabitat units (pool and riffle). Each deep-water (>1.0 m depth) site of fourth- and fifth-order streams was sampled twice using boat electro-fishing along both riversides. Sampling sites were far (>1.0 km distance) from conspicuous human disturbance, such as dam, farmland, and urban land, and each sampling was conducted with comparable effort (i.e., 100 m long and approximately 40 min). Fish were identified to species level (except for *Ctenogobius* due to the deficiency in identifying tools), counted, and returned to sampling sites if alive. Voucher specimens were placed in 8% formaldehyde solution for further identification.

Environmental survey

Each sampling site was characterized using 10 variables to describe local habitat: elevation (m), wetted

width (m), water depth (m), water temperature (°C), pH, conductivity (mS/cm), dissolved oxygen (mg/L), current velocity (m/s), discharge (m³/s), and substrate. Elevation was determined by a portable GPS receiver. Wetted width was measured along five transects, regularly spaced across the stream channel. Water depth, temperature, dissolved oxygen, pH, and conductivity were surveyed at four equal-interval points along each transect. Water depths <1.0 m were measured using a graduated wading rod, and depths >1.0 m were measured using a supersonic echo sounder. Current velocity was taken at 60% of water depth at each point of each transect. Discharge of each channel was determined at the transect that yielded the most accurate measurement (smooth bottom and laminar flow). Along each transect, the proportion of substrate categories (particle size 1=0–1 mm; 2=1–5 mm; 3=5–25 mm; 4=25–50 mm; 5=50–100 mm; 6=100–500 mm; 7=500–1 000 mm; 8=>1 000 mm) was visually estimated, and an index of substrate coarseness ranging from 1 to 8 was derived for each site

following Bain et al (1985).

Data analysis

Each fish species collected in this study was examined for frequency of occurrence (F) and relative abundance (RA), estimated from $F_i=100(S_i/S)\%$ and $P_i=100(n_i/n)\%$, respectively, where S_i and S are the abundance of the samplings of which species i were collected and of total samplings, respectively, and n_i and n are the individual numbers of species i and total fish species, respectively. The above F and P values were determined independently for three groups of sampling segments, i.e., first- to fourth-order streams along gradient A and B and fifth-order streams, respectively. Species richness and fish abundance were analyzed using a separate three-way ANOVA model with stream order (first- to fifth-order), season (January, April, August, October), and dam (gradient A and B) as factors. One-way ANOVA was used to test differences in species richness across stream orders along gradients A and B, respectively. The Newman-Keuls test was used for post-hoc comparisons after ANOVA. Independent sample t -tests were used to compare species richness within the same ordered streams between the two gradients. All data were log-transformed to meet the assumptions of normality and homogeneity of variances.

Discrete spatial patterns in fish assemblages were identified using PRIMER 5 (Primer-E Ltd., 2001). Following a Bray-Curtis similarity matrix calculation, an analysis of similarity (ANOSIM) was used to test variations in fish assemblages across stream orders, seasons, and gradients. Firstly, variations associated with stream orders and seasons were analyzed separately for gradients A (two-way crossed ANOSIM) and B (one-way ANOSIM due to no replication), respectively. Secondly, variations associated with gradients and seasons were analyzed separately for each stream order using two-way crossed ANOSIM. The relationships among assemblages from each site and season were graphically presented using non-metric multi-dimensional scaling (NMS) analysis. The contribution of each species to differences among assemblage groups was identified using similarity percentages analysis (SIMPER) (Clarke & Warwick, 2001). The variability in fish assemblages in relation to local habitat environment was evaluated by canonical correspondence analysis (CCA) using CANOCA 4.5. All variables entered the CCA after a forward-selection procedure, showing their importance in explaining total

variability in species composition. The significance ($P<0.05$) of the CCA gradients was assessed by Monte Carlo permutation tests, and their importance measured by the eigenvalues of the first two axes (ter Braak & Verdonschot, 1995). All variables of fish assemblages (i.e., species richness and abundance) and habitat environment were $\log(X+1)$ transformed to meet assumptions of multivariate normality and to moderate the influence of extreme data. Species that occurred in less than two sites were excluded from the above analysis to avoid negligible weighting (Gauch, 1982).

RESULTS

Overview of species diversity

A total of 13 647 fish were captured throughout this study, representing 57 species, 15 families, and 5 orders. Species of family Cyprinidae comprised on average 59.6% of total species richness. Species richness per sampling site amounted to 11.9 ± 6.6 (mean \pm SD) species, and abundance per site was 227.6 ± 205.5 specimens. A total of 16, 24, 24, 47, and 44 species were collected in first- to fifth-order streams, respectively. *Cyprinus carpio*, *Mylopharyngodon piceus*, *Hemiculter leucisculus*, *Sarcocheilichthys sinensis*, *Abbottina obtusirostris*, *Macropodus chinensis*, *Mystus macropterus* and *Hyporhamphus intermedius* were only collected within fifth-order streams. Within the first- to fourth-order streams, 18 species were only collected from streams along gradient B, including *Distoechodon tumirostris*, *Elopichthys bambusa*, and *Spinibarbus hollandi*. *Saurogobio dabryi* was a unique species occurring in gradient A but not gradient B. *Zacco platypus*, *Acrossocheilus fasciatus*, *Pseudogobio vaillanti*, *Vanmanenia stenosoma* and *Ctenogobius* sp. were common ($>40\%$ of F) and relatively abundant ($>1\%$ of P) within both gradients. In addition, *Acheilognathus barbatulus*, *A. chankaensis*, *Rhodeus ocellatus*, *Squalidus argentatus* and *Misgurnus anguillicaudatus* were more frequent and abundant within gradient A, while *Opsariichthys bidens*, *Hemiculter bleekeri*, *Sarcocheilichthys parvus*, *Parabotia fasciata*, *Siniperca chuatsi*, *Odontobutis obscurus*, *Silurus asotus* and *Pseudobagrus albomarginatus* were more frequent and abundant in gradient B (Table 1).

Local species richness

Fish species richness significantly varied according to stream order and gradient, but not season (Table 2).

Table 1 Frequency of occurrence (%; left of dash) and relative abundance (%; right of dash) of fish collected within Qingyi Stream

Species	Code	First to fourth-order		Fifth-order
		Gradient A	Gradient B	
Cypriniformes				
<i>Abbottina rivularis</i>	ABR	50.0/1.7	31.3/2.3	83.3/2.9
<i>Abbottina tafangensis</i>	ABT*	3.1/<0.1	6.3/0.1	
<i>Abbottina obtusirostris</i>	ABO*			16.7/0.2
<i>Acheilognathus barbatulus</i>	ACB	53.1/3.9	12.5/0.3	58.3/0.8
<i>Acheilognathus chankaensis</i>	ACC	18.8/0.9	6.3/0.3	41.7/0.5
<i>Acrossocheilus fasciatus</i>	ACF	68.8/7.7	87.5/10.1	25.0/0.3
<i>Carassius auratus</i>	CAA	28.1/1.8	31.3/2.1	91.7/5.8
<i>Cobitis rarus</i>	COR	53.1/5.6	37.5/2.2	
<i>Cobitis sinensis</i>	COS	28.1/0.6	18.8/1.3	8.3/<0.1
<i>Cyprinus carpio</i>	CYC*			16.7/0.1
<i>Culter erythropterus</i>	CUE*		6.3/<0.1	
<i>Distoechodon tumirostris</i>	DIT*		6.3/0.1	
<i>Elopichthys bambusa</i>	ELB*		6.3/<0.1	
<i>Erythroculter ilishaeformis</i>	ERI		6.3/0.2	41.7/2.3
<i>Gnathopogon taeniellus</i>	GNT	18.8/0.6	25.0/0.4	
<i>Gobiobotia tungi</i>	GOT*		12.5/0.1	
<i>Hemiculter leucisculus</i>	HEL			75.0/7.9
<i>Hemiculter bleekeri</i>	HEB	6.3/0.2	31.3/4.3	58.3/1.2
<i>Hemibarbus labeo</i>	HEL		18.8/0.4	
<i>Hemibarbus maculatus</i>	HEM		31.3/0.7	16.7/0.1
<i>Misgurnus anguillicaudatus</i>	MIA	37.5/1.1	18.8/0.4	8.3/<0.1
<i>Mylopharyngodon piceus</i>	MYP			41.7/0.8
<i>Opsariichthys bidens</i>	OPB	21.9/1.0	56.3/1.6	66.7/2.1
<i>Phoxinus oxycephalus</i>	PHO	12.5/0.2	18.8/3.8	
<i>Pseudobrama simoni</i>	PSS		18.8/1.6	58.3/3.8
<i>Rhodeus ocellatus</i>	RHO	65.6/13.9	31.3/2.3	66.7/3.8
<i>Spinibarbus hollandi</i>	SPH*		12.5/0.1	
<i>Zacco platypus</i>	ZAP	100/34.7	93.8/26.0	58.3/5.5
<i>Parabramis pekinensis</i>	PAP		6.3/0.1	16.7/0.1
<i>Parabotia fasciata</i>	PAF	18.8/0.6	31.3/2.0	33.3/5.0
<i>Pseudorasbora parva</i>	PSP	15.6/0.6	25.0/2.7	50.0/2.2
<i>Pseudogobio vaillanti</i>	PSV	43.8/2.5	43.8/4.8	33.3/0.5
<i>Sarcocheilichthys sinensis</i>	SAS*			8.3/<0.1
<i>Sarcocheilichthys parvus</i>	SAP	3.1/0.1	25.0/2.9	66.7/2.8
<i>Sarcocheilichthys nigripinnis</i>	SAN		25.0/4.0	75.0/2.3
<i>Squalidus argentatus</i>	SQA	34.4/1.2	12.5/0.7	33.3/1.0
<i>Saurogobio dabryi</i>	SAD	6.3/0.1		8.3/<0.1
<i>Varicorhinus barbatulus</i>	VAB*		12.5/0.2	
<i>Vanmanenia stenosoma</i>	VAS	65.6/5.2	50.0/3.9	25.0/1.1
Perciformes				
<i>Channa argus</i>	CHA		18.8/1.4	91.7/6.1

(Continued)

Species	Code	First to fourth-order		Fifth-order
		Gradient A	Gradient B	
<i>Channa asiatica</i>	CHA*		6.3/0.1	8.3/0.1
<i>Siniperea roulei</i>	COR		12.5/0.3	33.3/0.3
<i>Ctenogobius</i> sp.	CTS	93.8/12.6	68.8/4.4	25.0/2.0
<i>Hypseleotris swinhonis</i>	HYS		12.5/0.2	9.3/0.1
<i>Mastacembelus aculeatus</i>	MAA	21.9/0.6	6.3/0.2	
<i>Macropodus chinensis</i>	MAC*			16.7/<0.1
<i>Odontobutis obscurus</i>	ODO	12.5/0.9	37.5/2.7	91.7/7.9
<i>Siniperca chuatsi</i>	SIC	3.1/<0.1	25.0/1.2	75.0/2.4
<i>Siniperca obscura</i>	SIO		6.3/0.2	50.0/0.6
Siluriformes				
<i>Glyptothorax fukiensis</i>	GLF*		6.3/0.9	
<i>Liobagrus styani</i>	LIS	31.3/1.0	31.3/0.6	
<i>Mystus macropterus</i>	MYM*			8.3/0.1
<i>Pelteobagrus fulvidraco</i>	PEF		25.0/3.9	100.0/21.1
<i>Pseudobagrus albomarginatus</i>	PSA	3.1/<0.1	37.5/0.9	66.7/4.1
<i>Silurus asotus</i>	SIA	3.1/0.1	25.0/0.5	41.7/0.7
Synbranchiformes				
<i>Monopterus albus</i>	MOA	31.3/0.5	18.8/0.4	33.3/0.9
Beloniformes				
<i>Hyporhamphus intermedius</i>	HEI*			8.3/0.9

*: Rare species occurring in less than two sites, not included in statistical analysis.

Table 2 Three-way ANOVA results of the spatial and temporal variations in fish species richness within Qingyi Stream

Factors	df	SS	MS	F	P	Student-Newman-Keuls
Stream orders	4	2.3	0.6	38.9	**	1st<2nd=3rd<4th<5th
Seasons	3	0.1	0.02	1.9	ns	
Gradients	1	0.1	0.1	4.0	*	
Orders×seasons	12	0.2	0.01	0.9	ns	
Seasons×gradients	3	0.02	0.01	0.5	ns	A<B
Orders×gradients	4	0.6	0.1	9.5	**	
Orders×seasons×gradients	12	0.1	0.01	0.8	ns	

Factors are stream orders (first–fifth), seasons (January, April, July, October) and gradient (A, B; with and without the effect of a large dam, respectively).

*: $P<0.05$, **: $P<0.01$, ns $P>0.05$. Student-Newman-Keuls test: $P<0.05$.

Species richness significantly increased with stream orders, with the exception of no significant difference between second- and third-order streams. Gradient B had more species than that of Gradient A. A significant interaction effect was observed for stream order by gradient (Table 2). Within Gradient A, the lowest and highest species richness occurred in first-order and fifth-order streams, respectively, and species richness did not vary significantly among second-, third- and fourth-order streams. Within Gradient B,

however, the highest species richness was observed in fourth-order streams, while first-, second- and third-order streams were not significantly different in species richness (Figure 2). When comparing species richness within the same-order streams between the two gradients, significant differences were only observed in fourth-order streams (t -test, $F=0.23$, $P<0.01$), but not in first- ($F=0.4$, $P=0.54$), second- ($F=1.5$, $P=0.21$), or third-order streams ($F=7.2$, $P=0.19$) streams.

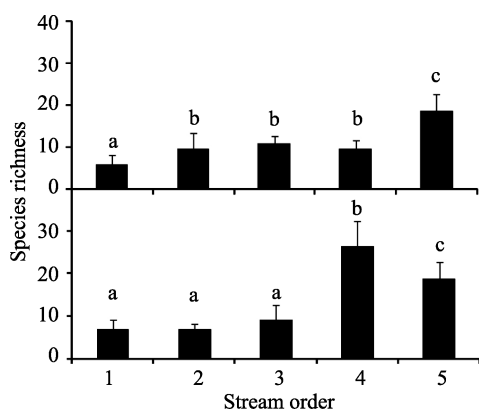


Figure 2 Fish species richness along two longitudinal gradients by stream orders within Qingyi Stream (upper: gradient A; lower: gradient B)

Different lowercases represent significant differences in species richness (One-way ANOVA, $P < 0.05$).

Fish assemblages

The two-way crossed ANOSIM results suggested that fish assemblages significantly differed across stream orders but not seasons, and were uniform for both longitudinal gradients of A and B (Table 3). Within gradient B, significant differences in inter-order fish assemblages were almost exclusively observed, with the exception of fourth- vs. fifth-order. Whereas, fish assemblages in fourth-order streams were similar with those in

Table 3 *R*-values and their significance levels (*P*) for comparisons of fish assemblages among stream orders and seasons using ANOSIM

	Gradient A		Gradient B	
	<i>R</i>	<i>P</i>	<i>R</i>	<i>P</i>
Order	0.50	0.001	0.66	0.001
1st vs. 2nd*	0.06	0.440	0.60	0.029
1st vs. 3rd	0.38	0.012	0.42	0.036
1st vs. 4th	0.29	0.049	1.00	0.029
1st vs. 5th	1.00	0.001	0.99	0.001
2nd vs. 3rd*	0.06	0.420	0.80	0.029
2nd vs. 4th*	0.06	0.370	1.00	0.029
2nd vs. 5th	0.98	0.001	0.96	0.002
3rd vs. 4th*	0.19	0.296	1.00	0.029
3rd vs. 5th	0.90	0.001	0.93	0.002
4th vs. 5th*	0.85	0.002	0.06	0.310
Season	-0.25	0.988	-0.10	0.971

One-way ANOSIM was conducted for gradient (B) without the effect of Chencun Hydropower Station, two-way crossed ANOSIM was conducted for gradient (A) disrupted by the station and both gradients (Both). Significance level was accepted at $P < 0.05$ (in bold). *: opposite significance level occurring between the two gradients.

second- and third-order but not fifth-order streams within gradient A (Table 3). For fish assemblages within the same-order streams, significant between-gradient differences were observed in fourth-order streams, but not in first-, second, and third-order streams (Table 4).

Table 4 *R*-values and their significance levels for comparisons of fish assemblages among seasons and between two gradients disrupted by a large dam or not using ANOSIM

	<i>R</i>		<i>P</i>	
	Season	Gradient	Season	Gradient
1st-order	-0.33	-0.25	0.876	0.815
2nd-order	-0.04	0.00	0.562	0.617
3rd-order	-0.31	-0.73	0.800	0.988
4th-order	-0.38	0.75	0.790	0.020
5th-order	-0.19		0.872	

Two-way crossed ANOSIM was conducted for first- to fourth-order streams, one-way ANOSIM was conducted for fifth-order streams. Significance level was accepted at $P < 0.05$ (in bold).

Based on NMS analysis, fish assemblages within gradient B varied substantially from headwaters to main-stream, despite the overlap between fourth- and fifth-order streams (Figure 3). In contrast, within gradient A, substantial overlaps were observed between neighboring orders from first- to fourth-order streams, while fish assemblages in fourth-order streams were distinct from those in fifth-order streams.

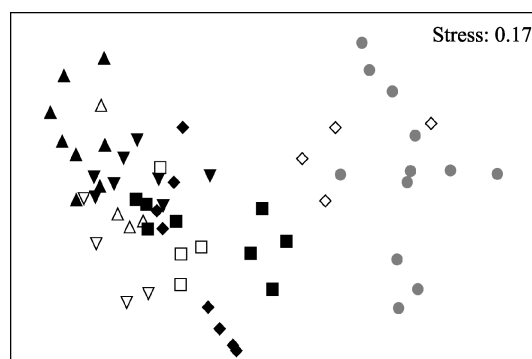


Figure 3 Non-metric multi-dimensional scaling (NMS) by stream orders and dams for fish assemblage data in Qingyi Stream. Black symbols, gradient disrupted by Chencun Hydropower Station; Open symbols, gradient without damming; Grey symbols, mutual part of both gradients. Normal triangle, reverse triangle, square, diamond, and rotundity, fish assemblages from first- to fifth-order streams, respectively.

SIMPER analysis revealed that *Z. platypus* was more abundant in first-, second- and third-order streams and less in fourth- and fifth-order streams within gradient B. The occurrence and abundance of *C. rarus*, *P. fasciata*,

R. ocellatus, and *S. nigripinnis* determined how fish assemblages varied substantially from first- to fourth-order streams. *Ctenogobius* sp. and *C. argus* contri-

buted most to the divergence in fish assemblages between fourth- and fifth-order streams within Gradient A (Table 5).

Table 5 Diagnostic species by SIMPER analysis for first- to fifth-order streams along gradients A and B within Qingyi Streams

	Gradient A			Gradient B		
	AvAbu.	AvSim.	Contri (%)	AvAbu.	AvSim.	Contri (%)
1st-order		AvSim., 46.3%			AvSim., 44.1%	
<i>Zacco platypus</i>	60.9	18.5	40.0	167.3	19.4	30.2
<i>Acrossocheilus fasciatus</i>	39.6	10.2	22.1	17.3	11.5	17.9
<i>Vanmanenia stenosoma</i>	16.3	5.1	11.0			
<i>Cobitis rarus</i>				23.5	12.4	19.3
2nd-order		AvSim., 51.6%			AvSim., 52.9%	
<i>Zacco platypus</i>	63.1	16.8	32.5	37.0	17.7	33.5
<i>Acrossocheilus fasciatus</i>	15.3	9.7	18.9	15.0	13.1	24.7
<i>Ctenogobius</i> sp.	14.4	7.4	14.4			
<i>Parabotia fasciata</i>				16.0	7.6	14.4
3rd-order		AvSim., 48.6%			AvSim., 57.8%	
<i>Zacco platypus</i>	44.8	11.9	24.6	95.8	15.9	27.6
<i>Rhodeus ocellatus</i>	22.1	9.9	20.5	69.7	11.4	19.7
<i>Ctenogobius</i> sp.	28.5	6.6	13.6	28.8	8.4	14.6
4th-order		AvSim., 51.0%			AvSim., 64.3%	
<i>Ctenogobius</i> sp.	24.6	11.9	23.4			
<i>Zacco platypus</i>	46.1	8.5	16.8			
<i>Acrossocheilus fasciatus</i>	12.6	6.1	11.9	51.8	5.2	8.1
<i>Sarcocheilichthys nigripinnis</i>				36.5	5.7	8.8
<i>Abbottina rivularis</i>				20.3	4.8	7.5
5th-order		AvSim., 52.9%			AvSim., 52.9%	
<i>Pseudobagrus albomarginatus</i>	58.0	7.0	15.1	58.0	7.0	15.1
<i>Channa argus</i>	16.8	4.5	9.2	16.8	4.5	9.2
<i>Carassius auratus</i>	15.8	3.4	7.3	15.8	3.4	7.3

The first three species contributing most to the average similarity within each order are shown. AvSim., average similarity (%); AvAbu., average abundance; Contri., contribution.

Relationships between species and environment

The first and second axes of the CCA ordination accounted for 49.7% and 12.4% of total variance in species richness and abundance among sampling sites, and for 54.7% and 13.6% of variance in species data and environmental relationship, respectively. From CCA, gradient A separated fish assemblages based on elevation, substrate, and flow velocity on the right, and wet width, water depth, discharge, and conductivity on the left. The species related to this gradient were *E. ilishaeformis*, *P. pekinensis*, *S. nigripinnis*, *H. labeo*, *C. rarus*, *C. argus*, *S. chuatsi*, *P. parva*, *C. auratus*, *A. chankaensis*, *R. ocellatus*, *C. sinensis*, *Ctenogobius* sp., *A. fasciatus*, and *Z. platypus* (left to right). Gradient B was caused by

water temperature and dissolved oxygen on the top and pH on the bottom, along which *P. oxycephalus*, *P. fasciata*, *A. chankaensis*, *P. vaillanti*, *M. albus*, *G. taeniellus*, and *S. argentatus* were distributed from top to bottom (Figure 4).

DISCUSSION

Our results showed that along a longitudinal gradient without the direct effect of a large dam, fish species richness was highest in fourth-order streams and showed no significant difference among first- to third-order streams. Following the increase in stream size and habitat diversity from headwaters to downstream, fish

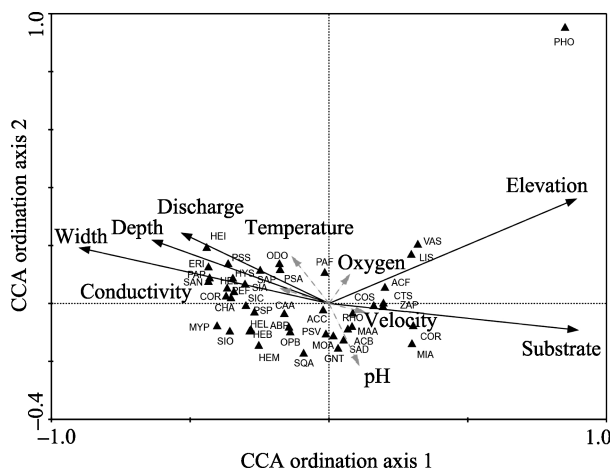


Figure 4 Canonical correspondence analysis (CCA) diagrams for environmental variables and fish assemblages in Qingyi Stream

Black arrows indicate the most important factors and grey arrows show the other factors. Species codes as in Table 1.

species richness generally increases downstream (Gorman & Karr, 1978; Matthews, 1986). Based on fish specimens collected from 89 shallow (first- to third-order) tributaries within the Qingyi watershed, Yan et al. (2011) discovered that local species richness was determined by local habitat variables (e.g., wetted width and water temperature) but not tributary spatial variables (e.g., stream order and link magnitude). Yan et al (2010) also revealed that stream order was not the optimal framework explaining spatial variation in fish assemblages within Puxi Stream, a tributary above Chencun Reservoir in the Qingyi watershed. The results in our study that fish species richness showed no substantial variation across first- to third-order streams appears to support fish species responding to local habitat features but not to stream classification schemes of humans (Matthews, 1998). In addition, our findings that the highest species richness occurred in fourth-order, not fifth-order, streams is consistent with the river continuum concept (RCC) claiming that maximum species diversity often occurs in mid-sized, not large, streams. Oberdorff et al (1993) also found a decline in fish species richness in the lower reaches of the Seine River, which was explained by anthropogenic disturbances decreasing habitat diversity.

In addition to species richness, fish also exhibit an alteration in zonation along the upstream-downstream gradient (Lasne et al, 2007; Miranda & Raborn, 2000). One of the most recognized theoretical classifications dividing running waters based on fish is longitudinal fish zonation proposed by Huet (1959); the brown trout,

grayling, barbel and bream zones exhibit alteration, in turn, from headwaters to lower reaches. However, associated with continuous, not abrupt, variation in the natural environments of many streams, fish assemblages vary by “addition” rather than by “replacement” (Matthews, 1998), which suggests a deficiency in the application of this zonation concept within these streams. In our results, despite some species only being collected in one ordered stream (e.g., *P. oxycephalus* and *C. molitorella* in first-order streams, *C. carpio*, *M. piceus*, and *H. leucisculus* in fifth-order streams), most fish species were distributed in at least two different ordered streams. Based on our SIMPER analysis, along the longitudinal gradient without the effects of a large dam, changes in the relative abundances of *Z. platypus*, *C. rarus*, *P. fasciata*, *R. ocellatus*, and *S. nigripinnis* contributed most to longitudinal species replacement. Our results suggest that “addition”, not “replacement”, was the main underlying mechanism explaining species distributions from upstream to downstream in Qingyi Stream. This spatial variation in species distributions could be explained by the relationship between species and the local habitat environment based on CCA. The spatial distributions of fish species in this study were affected by a series of local habitat environmental factors, such as elevation, substrate, water depth, current discharge, wetted width, and conductivity. At the watershed scale, Yan et al (2011) reported that fish assemblage structure in this study area was related to the combined effects of local habitat (i.e., elevation, substrate, and water depth) and spatial stream position (i.e., magnitude link and confluence link), suggesting that fish species distribution was associated with their ecological requirements, such as habitat preference and trophic ecology.

In Qingyi Stream, fish assemblages presented different patterns in their spatial variations between the two longitudinal gradients, which could be viewed as the effect of Chencun Hydropower Station. Fish showed significantly lower species richness and different species composition within the gradient disrupted by the dam compared with the gradient without the large dam. However, the substantial variations in fish assemblages between gradients were only observed in fourth-order streams. Numerous studies have revealed that dams may impact stream fish by blocking migratory pathways (March et al, 2003), decreasing current velocity upstream (Bennett et al, 2002), altering natural flow regime (Bonner & Wilde, 2000), and decreasing water temp-

erature downstream (Clarkson & Childs, 2000). In this study, when considering first- to fourth-order streams within the two gradients independently, a total of 18 fish species (e.g., *D. tumirostris*, *E. bambusa*, *S. hollandi*) were collected in gradient A only, and eight species (e.g., *O. bidens*, *H. bleekeri*, *S. parvus*) were more frequent and abundant in gradient A than in gradient B. This may be explained by two causes resulting from the effects of large dams on fish assemblages. Firstly, most of the 18 species only occurring in gradient A, including *H. bleekeri*, *E. ilishaeformis*, *H. maculatus*, and *S. roulei*, inhabited the lower reaches of the streams. The Chencun Hydropower Station may play a role in constraining their upstream movements, resulting in the local extinction of these fish in areas above the station. Secondly, dams may modify local habitat conditions upstream and

downstream (Bennett et al, 2002; Bonner & Wilde, 2000; Clarkson & Childs, 2000), which may decrease the fitness of endemic fish to naturally adapt to lotic conditions, eventually resulting in a decline in their abundance (Scott & Helfman, 2001). This may explain why some fish (e.g., *O. bidens*, *H. bleekeri*, *S. parvus*) showed lower abundance within the gradient disrupted by the dam. However, the influence of impoundment by dams on stream fish assemblage structure upstream was highly localized, which means that this influence was partially determined by proximity to impoundments (Falke & Gido, 2006a, b). Our results that significant between-gradient differences in fish assemblages only occurred in fourth-order, not lower-order, streams may support the findings of Falke & Gido (2006a, b), though some additional analyses may be necessary.

References

- Araújo FG, Pinto BCT, Teixeira TP. 2009. Longitudinal patterns of fish assemblages in a large tropical river in southeastern Brazil: evaluating environmental influences and some concepts in river ecology. *Hydrobiologia*, **618**(1): 89-107.
- Bain MB, Finn JT, Booke HE. 1985. Quantifying stream substrate for habitat analysis studies. *North American Journal of Fisheries Management*, **5**(3B): 499-500.
- Bennett SJ, Cooper CM, Ritchie JC, Dunbar JA, Allen PM, Caldwell LW, Mcgee TM. 2002. Assessing sedimentation issues within aging flood control reservoirs in Oklahoma. *Journal of the American Water Resources Association*, **38**(5): 1307-1322.
- Bonner TH, Wilde GR. 2000. Changes in the Canadian River fish assemblage associated with reservoir construction. *Journal of Freshwater Ecology*, **15**(2): 189-198.
- Boys CA, Thoms MC. 2006. A large-scale, hierarchical approach for assessing habitat associations of fish assemblages in large dryland rivers. *Hydrobiologia*, **572**(1): 11-31.
- Chen YY. 2005. Giving promotions to integrated management of river basins and protecting the life river of the Yangtze. *China Water Resources*, (8): 10-12. (in Chinese)
- Clarke KR, Warwick RM. 2001. Change in Marine Communities: an Approach to Statistical Analysis and Interpretation. 2nd ed. Plymouth: PRIMER-E.
- Clarkson RW, Childs MR. 2000. Temperature effects of hypolimnial-release dams on early life stages of Colorado River Basin big-river fishes. *Copeia*, **2000**(2): 402-412.
- Cumming GS. 2004. The impact of low-head dams on fish species richness in Wisconsin, USA. *Ecological Applications*, **14**(5): 1495-1506.
- Da Silva Abes S, Agostinho AA. 2001. Spatial patterns in fish distributions and structure of the ichthyocenosis in the Águs Nanci stream, upper Paraná River basin, Brazil. *Hydrobiologia*, **445**(1-3): 217-227.
- Falke JA, Gido KB. 2006a. Effects of reservoir connectivity on stream fish assemblages in the Great Plains. *Canadian Journal of Fisheries and Aquatic Sciences*, **63**(3): 480-493.
- Falke JA, Gido KB. 2006b. Spatial effects of reservoirs on fish assemblages in Great Plains streams in Kansas, USA. *River Research and Applications*, **22**(1): 55-68.
- Gauch HG. 1982. Multivariate Analysis in Community Ecology. New York: Cambridge University Press.
- Gorman OT, Karr JR. 1978. Habitat structure and stream fish communities. *Ecology*, **59**(3): 507-515.
- Hoetinghaus DJ, Winemiller KO, Birnbaum JS. 2007. Local and regional determinants of stream fish assemblage structure: inferences based on taxonomic vs. functional groups. *Journal of Biogeography*, **34**(2): 324-338.
- Holmquist JG, Schmidt-Gengenbach JM, Yoshioka BB. 1998. High dams and marine-freshwater linkages: effects on native and introduced fauna in the Caribbean. *Conservation Biology*, **12**(3): 621-630.
- Huet M. 1959. Profiles and biology of western European streams as related to fish management. *Transactions of the American Fisheries Society*, **88**(3): 155-163.
- Humborg C, Ittekkot V, Cociasu A, Bodungen BV. 1997. Effect of Danube River dam on Black Sea biogeochemistry and ecosystem structure. *Nature*, **386**(6623): 385-388.
- Inoue M, Nunokawa M. 2002. Effects of longitudinal variations in stream habitat structure on fish abundance: an analysis based on subunit-scale habitat classification. *Freshwater Biology*, **47**(9): 1594-1607.
- Lasne E, Bergerot B, Lek S, Laffaille P. 2007. Fish zonation and indicator species for the evaluation of the ecological status of rivers:

- example of the Loire basin (France). *River Research and Applications*, **23**(8): 877-890.
- March JG, Benstead JP, Pringle CM, Scatena FN. 2003. Damming tropical island streams: problems, solutions, and alternatives. *Bioscience*, **53**(11): 1069-1078.
- Matthews WJ. 1986. Fish faunal "breaks" and stream order in the eastern and central United States. *Environmental Biology of Fishes*, **17**(2): 81-92.
- Matthews WJ. 1998. Patterns in Freshwater Fish Ecology. New York: Chapman & Hall.
- Meador MR, Matthews WJ. 1992. Spatial and temporal patterns in fish assemblage structure of an intermittent Texas stream. *American Midland Naturalist*, **127**(1): 106-114.
- Miranda LE, Raborn SW. 2000. From zonation to connectivity: fluvial ecology paradigms of the 20th century. *Polskie Archiwum Hydrobiologii*, **47**(1): 5-19.
- Nilsson C, Jansson R, Zinko U. 1997. Long-term responses of river-margin vegetation to water-level regulation. *Science*, **276**(5313): 798-800.
- Oberdorff T, Guilbert E, Lucchetta JC. 1993. Patterns of fish species richness in the Seine River basin, France. *Hydrobiologia*, **259**(3): 157-167.
- Power ME, Dietrich WE, Finlay JC. 1996. Dams and downstream aquatic biodiversity: potential food web consequences of hydrologic and geomorphic change. *Environmental Management*, **20**(6): 887-895.
- Power ME, Stout RJ, Cushing CE, Harper PP, Hauer FR, Matthews WJ, Moyle PB, Statzner B, De Badgen IRW. 1988. Biotic and abiotic controls in river and stream communities. *Journal of the North American Benthological Society*, **7**(4): 456-479.
- Roberts JH, Hitt NP. 2010. Longitudinal structure in temperate stream fish communities: evaluating conceptual models with temporal data. *American Fisheries Society Symposium*, **73**: 281-302.
- Santucci VJ Jr, Gephard SR, Pescitelli SM. 2005. Effects of multiple low-head dams on fish, macroinvertebrates, habitat, and water quality in the Fox River, Illinois. *North American Journal of Fisheries Management*, **25**(3): 975-992.
- Scott MC, Helfman GS. 2001. Native invasions, homogenization, and the mismeasure of integrity of fish assemblages. *Fisheries*, **26**(11): 6-15.
- Strahler AN. 1957. Quantitative analysis of watershed geomorphology. *Transactions, American Geophysical Union*, **38**(6): 913-920.
- ter Braak CJF, Verdonschot PFM. 1995. Canonical correspondence analysis and related multivariate methods in aquatic ecology. *Aquatic Sciences*, **57**(3): 255-289.
- Taniguchi Y, Rahel FJ, Novinger DC, Gerow KG. 1998. Temperature mediation of competitive interactions among three fish species that replace each other along longitudinal stream gradients. *Canadian Journal of Fisheries and Aquatic Sciences*, **55**(8): 1894-1901.
- Travnichek VH, Zale AV, Fisher WL. 1993. Entrainment of ichthyoplankton by a warm water hydroelectric facility. *Transactions of the American Fisheries Society*, **122**(5): 709-716.
- Vannote RL, Minshall GW, Cummins KW, Sedell JR, Cushing CE. 1980. The river continuum concept. *Canadian Journal of Fisheries and Aquatic Sciences*, **37**(1): 130-137.
- Ward JV, Stanford JA. 1983. Serial discontinuity concept of lotic ecosystems. In: Fontaine TD, Bartell SM. Dynamics of Lotic Ecosystems. MI, Ann Arbor: Ann Arbor Science, 29-42.
- Yan YZ, Xiang XY, Chu L, Zhan YJ, Fu CZ. 2011. Influences of local habitat and stream spatial position on fish assemblages in a dammed watershed, the Qingyi Stream, China. *Ecology of Freshwater Fish*, **20**(2): 199-208.
- Yan YZ, He S, Chu L, Xiang XY, Jia YJ, Tao J, Chen YF. 2010. Spatial and temporal variation of fish assemblages in a subtropical small stream of the Huangshan Mountain. *Current Zoology*, **56**(6): 670-677.

Population sizes and group characteristics of Siberian Crane (*Leucogeranus leucogeranus*) and Hooded Crane (*Grus monacha*) in Poyang Lake Wetland

Ming-Qin SHAO^{*}, Hong GUO, Jian-Hong JIANG

College of Life Science, Jiangxi Normal University, Jiangxi Provincial Key Lab of Protection and Utilization of Subtropical Plant Resources, Nanchang Jiangxi 330022, China

Abstract: Both the Siberian Crane (*Leucogeranus leucogeranus*) and Hooded Crane (*Grus monacha*) have limited population sizes and are considered endangered by domestic Chinese and international agencies. To document the current size of their respective populations and characterize their groups, between October 2012 and April 2013 we undertook fieldwork at four nature reserve areas within the Poyang Lake wetlands. We divided Poyanghu National Nature Reserve (PYH) into the Wucheng (PWC) and Hengfeng areas (PHF), because each are each located in different counties. Our fieldwork showed that the Siberian Crane occurred mainly in PYH (364 in the PHF, 158 in the PWC) and the Nanjishan Wetland National Nature Reserve (NJS, with 200 individuals). The Hooded Crane was mainly distributed in PYH (302 in the PHF and 154 in the PWC). Family groups accounted for more than 50% of the total number of groups among both species, with Hooded Cranes forming more family groups than Siberian Cranes. Typically, these groups were formed of two adults with one offspring (Siberian Crane), and two adults with two offspring (Hooded Crane), with the mean family group size of the Siberian Crane and Hooded Crane being respectively 2.65 ± 0.53 ($n=43$) and 3.09 ± 0.86 ($n=47$) individuals per group. The mean collective group size of the Siberian Crane and Hooded Crane included 28.09 ± 24.94 ($n=23$) and 28.94 ± 27.97 ($n=16$) individuals per group, respectively, with the proportion of juveniles among Hooded Cranes being more than double that seen among the Siberian Cranes.

Keywords: Siberian Crane; Hooded Crane; Group characteristics; Poyang Lake wetland

The Siberian Crane (*Leucogeranus leucogeranus*) and Hooded Crane (*Grus monacha*) are frequent winter visitors of the Poyang Lake wetland area, but both species have suffered dramatic losses. Currently, the Siberian Crane is listed in the first category of the nationally protected wildlife species in China and regarded as a critically endangered species by IUCN, with a global population size ranging from 3,800 to 4,000 individuals (BirdLife International, 2008; Li et al, 2012). Though the Siberian Crane breeds in northwest Siberia, it frequently winters around Poyang Lake in Jiangxi Province and Dongting Lake in Hunan Province, with more than 90% of the known global population wintering around Poyang Lake (Zheng & Wang, 1998; Shan et al, 2012). The Hooded Crane has a somewhat larger global population—around 11 600 individuals—only ~1000 winter in China (BirdLife International 2008;

Zhou et al, 2010). The Hooded Crane is also listed in the first category of the nationally protected wildlife species in China, but is regarded as a vulnerable species by IUCN. Typically, the Hooded Crane breeds in eastern Siberia and Heilongjiang Province in China, but winters in an array of areas in eastern Asia, including Korea, Japan and China, predominately along lakes beside the middle and lower reaches of Yangtze River, including Poyang Lake in Jiangxi Province, Dongting Lake in Hunan Province, Shengjin Lake and Longgan Lake in Anhui Province, and Chongming Island in Shanghai (Jing et al, 2002b).

Received: 14 November 2013; Accepted: 15 July 2014

Foundation items: This study was supported by the National Natural Science Foundation of China (31260517; 31101651)

^{*} Corresponding author, E-mail: 1048362673@qq.com

To date, research on the wintering ecology of Siberian Crane and Hooded Crane has mainly focused on numbers and distribution (Liu, 2001; Li *et al.*, 2012; Shan *et al.*, 2012; Yan & Ding, 1988; Zhou & Ding, 1982;), genetic structure (Zhang *et al.*, 2012), behavior (Jing *et al.*, 2002b; Li *et al.*, 2007; Zhou *et al.*, 2010), diet (Zhao *et al.*, 2002) and habitat selection (Jing *et al.*, 2002a; Sun & Huang, 2010; Zhang *et al.*, 2010). However, despite the popularity and importance of the Poyang Lake are in the north of Jiangxi Province (and the largest freshwater lake in China), no comprehensive and quantitative assessment on population dynamic or age structure of these two species has been conducted. In the present study, we report the findings of several field observations of this area undertaken between October 2012 and April 2013, where we documented population size, group characteristics and age structure. To facilitate more targeted conservation and management of these two crane species, we focused on both documenting population size dynamics of the two crane species at different lakes in the area, and comparing the group characteristics and age structure of the two species.

STUDY AREAS AND METHODS

Poyang Lake (E115°47'–116°45', N28°22'–29°45') is a key wintering or stopover sites for migratory waterbirds in the East Asian-Australasian Flyway. Poyang Lake had a humid subtropical climate with the annual temperature averaging 16.7–17.7 °C, and average annual precipitation at 1400–1900 mm (Huang & Guo, 2007). Between October and April, the Poyang Lake undergoes a drought period, during which many habitats—e.g., grassland and mudflats—form and attract ~500000–600000 waterbirds annually. During the entire year, the wetland vegetation at the Poyang Lake is dominated by *Carex* spp., *Phragmites australis* and *Triarrhena lutarioriparia* (Liu *et al.*, 2006). For the present study, we selected four nature reserves in Poyang Lake to survey the population sizes and group characteristics of the Siberian and Hooded Cranes. To facilitate more accurate measurement, the Poyanghu National Nature Reserve (PYH) was divided into two areas, the Wucheng (PWC) and Hengfeng areas (PHF), since they are located in two counties and were investigated at different times. In the PWC, four lakes (Dahuchi, Baziqiang, Changhuchi, Zhushihu) were selected as observation sites, with additional surveys at two

lakes (Shahu, Banghu) in the PHF. We also surveyed 11 lakes at the Nanjishan Wetland National Nature Reserve (NJS; Zhanbeihu, Sanhu, Changhu, Fengweihu, Sanniwan, Baishahu, Linghu, Shangbeijia, Xiabeijia, Beishenhu, Shentanghu). A further 10 lakes in the Duchang Migratory Bird Nature Reserve (DC; Jishanhu, Zhongba, Xinmiaohu, Mayinghu, Huangjinzui, Binhu, Shuhu, Huamiaohu, Henggang, Xihu) and eight lakes from the Poyang Baishazhou Nature Reserve (BSZ; Zhuhu, Chemen, Rongqi, Sishilijie, Siwanghu, Xiaominghu, Daminghu, Biaoen) were also surveyed (Figure 1).

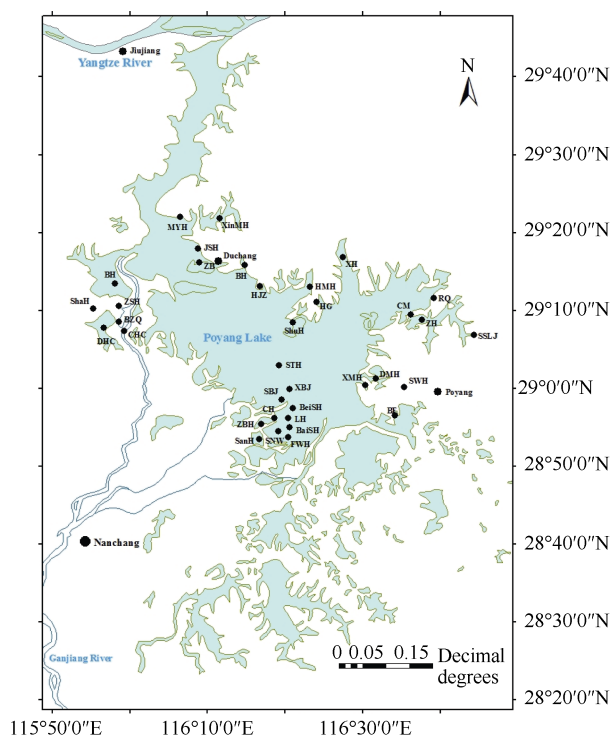


Figure 1 Surveyed areas around Poyang Lake

Abbreviations are as follows: Dahuchi: DHC, Baziqiang: BZQ, Changhuchi: CHC, Zhushihu: ZSH, Shahu: ShaH, Banghu: BH, Zhanbeihu: ZBH, Sanhu: SH, Changhu: CH, Fengweihu: FWH, Sanniwan: SNW, Baishahu: BaiSH, Linghu: LH, Shangbeijia: SBJ, Xiabeijia: XBJ, Beishenhu: BeiSH, Shentanghu: STH, Jishanhu: JSH, Zhongba: ZB, Xinmiaohu: XinMH, Mayinghu: MYH, Huangjinzui: HJZ, Binhu: BH, Shuhu: SH, Huamiaohu: HMH, Henggang: HG, Xihu: XH, Zhuhu: ZH, Chemen: CM, Rongqi: RQ, Sishilijie: SSLJ, Siwanghu: SWH, Xiaominghu: XMH, Daminghu: DMH, Biaoen: BE.

Between October 2012 and April 2013, six surveys, each lasting one or two days, were conducted from at each reserve at intervals of 20–30 days. For comparison, we divided the wintering season into three stages based on the population dynamics: early stage (October to December); middle stage (January to February); and late stage (March to April), in line with a previous study

(Zhou et al, 2010). Totally, between one and five fixed observation points were selected at each lake to count the number of adult or juvenile cranes, group size, group types of two crane species with binoculars (8×) and spotting scope (20–60×). The fixed points varied somewhat according to water level. We noted that the group types comprised of family, collective and special group (Liu et al, 2008), with the family group being subdivided into four types: 1) two adults; 2) two adults with one offspring; 3) two adults with two offspring; and 4) one adult with one offspring. The collective group referred to groups including five or more individuals, while the special group referred to a single adult or juvenile crane. Groups were defined as cranes that were usually within less than 50 m of each other and appeared to coordinate their activities, i.e., they stayed near one another and moved in the same direction (Lcheureux et al, 1995; Liu et al, 2009; Liu et al, 2010).

Our observation data were first checked with the Kolmogorov-Smirnov Test and were found to fit a normal distribution. Next, one-way ANOVA was used to test for differences in the average size of the family or collective groups at different stages, and the size of the family or collective groups between Siberian Crane and Hooded Crane. All data were analyzed with SPSS 19.0 (SPSS inc., Chicago, IL, USA).

RESULTS

Population size and distribution

The Siberian Crane was recorded at 18 of the 35 surveyed lakes located in the four nature reserve areas, but were mainly distributed at PYH and NJS. A large and steady population of Siberian Cranes was observed in Shahu, Banghu, Dahuchi, Baziqiang within the PYH, and

we also observed a large population in Sanhu, Baishahu, Shangbeijia, Beishenghu, Shentanghu at NJS. The Siberian Crane was not observed regularly at any of the other surveyed sites in the other reserves (Table 1).

The Hooded Crane was recorded at 10 lakes located within three of the nature reserve areas, but not in the DC (Table 1). The Hooded Crane was mainly distributed in Shahu, Banghu, Dahuchi, Changhuchi and Zhushihu of PYH, with a large and steady population of the Hooded Crane also observed in Banghu and Zhushihu. Though we also observed the Hooded Crane at the BSZ, the population was comparatively small.

The number of the Siberian Crane peaked in late December and early January when they were mainly distributed in Shahu (333 individuals), Baziqiang (151 individuals) and Beishenghu (182 individuals) but then decreased in mid-March (Table 1). Conversely, the number of Hooded Cranes was high in late January and peaked in later February and early March, when the cranes were mainly distributed in Banghu (226 individuals) and Zhushihu (135 individuals).

Group characteristics

During the course of our field observations, a total of 56 groups of Siberian Crane were observed, with family and collective groups being the most frequently encountered, accounting respectively for 55.54% and 41.07% of the total Siberian Crane groups observed during this investigation. The family groups of the Siberian Crane were the most frequently observed during all three stages. For the Hooded Cranes, 65 groups were observed during this study, with family and collective groups respectively accounting for 72.31% and 24.62% of the total groups. Similarly, the family groups of the Hooded Crane were also the most often observed groups during all three stages (Figure 2).

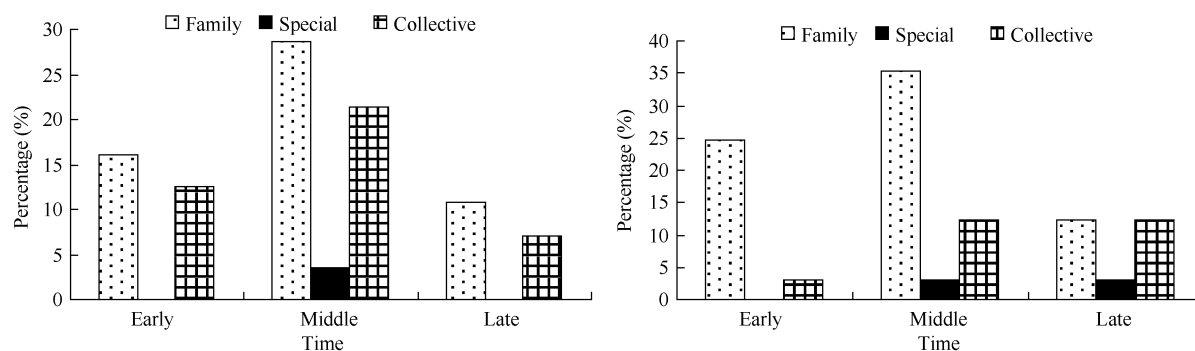


Figure 2 Temporal variation in group type among Siberian Cranes (left) and Hooded Cranes (right) around Poyang Lake

Table 1 Spatial and temporal distribution of Siberian Crane and Hooded Crane around Poyang Lake

Study area	Site	10/15*	11/19	1/2	1/27	3/7	4/13
PHF	Siberian Crane	Shahu	0	21	333	15	0
		Banghu	0	23	31	10	51
		total	0	44	364	25	51
	Hooded Crane	Shahu	0	0	2	0	76
		Banghu	0	25	0	113	226
		total	0	25	2	113	302
		10/14	11/12	12/24	1/16	2/25	3/18
PWC	Siberian Crane	Dahuchi	0	3	7	11	22
		Baziqiang	0	15	151	0	3
		total	0	18	158	11	25
	Hooded Crane	Dahuchi	0	2	9	33	15
		Baziqiang	0	0	4	0	4
		Chahuchi	0	57	0	0	0
		Zhushihu	0	15	15	27	135
		total	0	74	28	60	154
		10/19	11/11	12/23	1/20	2/22	3/9
NJS	Siberian Crane	Sanhu	0	0	3	30	0
		Fengweiuhu	0	0	0	0	3
		Baishahu	0	0	0	35	0
		Linghu	0	0	0	2	0
		Shangbeijia	0	0	15	48	39
		Beishenghu	0	0	182	14	0
		Shentanghu	—	—	—	39	0
		total	0	0	200	168	42
	Hooded Crane	Changhu	0	0	0	9	4
		Shangbeijia	0	0	0	4	0
		Xiabeijia	0	0	0	0	4
		total	0	0	0	13	4
		11/4	12/2	12/29	1/23	3/14	4/10
DC	Siberian Crane	Binhu	0	0	8	0	0
		Xiaoyang	0	0	5	0	0
		Chian	0	0	2	0	0
		total	0	0	15	0	0
		10/28	11/23	1/9	1/25	3/2	4/2
BSZ	Siberian Crane	Chemen	0	5	3	0	0
		Rongqi	0	0	3	3	6
		Xiaominghu	0	0	6	0	0
		Daminghu	0	0	3	7	8
		total	0	5	15	10	14
	Hooded Crane	Biaoen	—	0	0	0	4
Total	Siberian Crane		0	67	752	214	81
	Hooded Crane		0	99	30	186	464

* date, e.g., 10/15 = 15 October; — not surveyed; PHF: Poyang National Nature Reserve (Hengfeng); PWC: Poyang National Nature Reserve (Wucheng); NJS: Nanjishan Wetland National Nature Reserve; DC: Duchang Migratory bird Nature Reserve; BSZ: Poyang Baishazhou Nature Reserve

While family groups were the most common grouping for both the Siberian and Hooded Cranes, there composition differed between species. For the Siberian Crane, of four types of family groups, those with two adults and one offspring (51.61%) were most frequently observed, followed by family groups of two adults (38.71%). For the Hooded Cranes, family groups were typically two adults with two offspring (40.43%), though groups with two adults and one offspring (27.66%) and two adults (31.91%) were also regularly observed. No family group with one adult and one offspring was observed for the Hooded Crane at any of our survey sites (Figure 3).

The mean family group size of Siberian Crane and Hooded Crane were respectively 2.65 ± 0.53 ($n=43$) and 3.09 ± 0.86 ($n=47$) individuals per group (Figure 4). The mean collective group size of the Siberian Crane and Hooded Crane were respectively 28.09 ± 24.94 ($n=23$) and 28.94 ± 27.97 ($n=16$) individuals per group. The mean family group size of the Hooded Crane was significant larger than that of the Siberian Crane ($F=8.191$, $df=88$,

$P<0.05$). The collective group size between the two species of crane showed no significant difference ($F=0.01$, $df=37$, $P>0.05$).

During our survey, we observed no significant difference in the mean family group size for the Siberian Crane ($F=2.023$, $df=40$, $P>0.05$) throughout the three stages, but the mean family group size of the Hooded Crane was significantly lower in the early as compared to the late stage ($P<0.001$). Surveys of both species showed no significant differences in their mean collective group size between the three stages (Siberian Crane: $F=0.396$, $df=20$, $P>0.05$; Hooded Crane: $F=0.834$, $df=13$, $P>0.05$).

Age structure

Totally, 737 Siberian Cranes and 243 Hooded Cranes could be categorized as either being adults or juveniles. The percentage of juveniles among Siberian Cranes was 12.48%, while among Hooded Cranes was 29.22%. The numbers of juveniles displayed the same pattern among both species, being low in early or mid-winter, and high in late winter (Table 2).

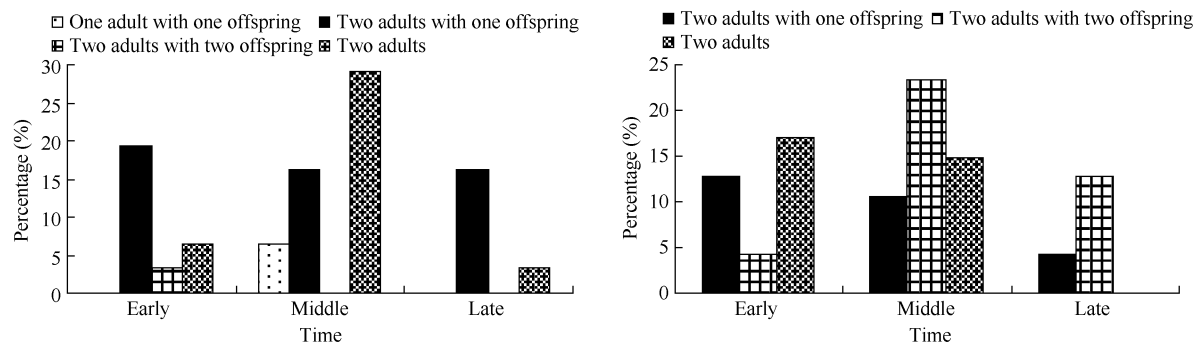


Figure 3 Statistics of four family group types of Siberian Cranes (left) and Hooded Cranes (right) at three different stages

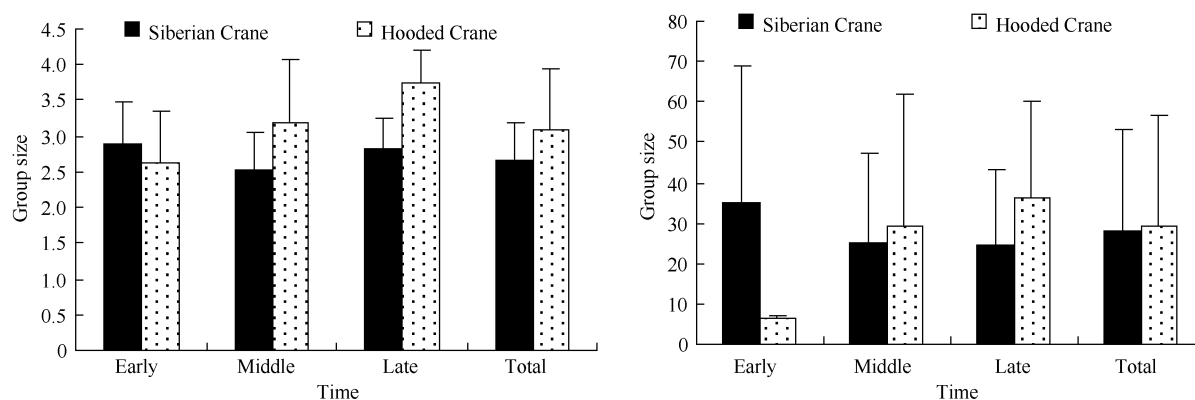


Figure 4 Temporal variation of family group size (left) and collective group size (right) of two Crane species in Poyang Lake

Table 2 Temporal variations in age structure of two species cranes in Poyang Lake

Species		Early stage	Middle stage	Late stage	Total
Siberian Crane	Proportion of juveniles	9.89%	6.92%	42.86%	12.48%
	No. of observed individuals	364	289	84	737
Hooded Crane	Proportion of juveniles	23.73%	27.61%	40.00%	29.22%
	No. of Observed individuals	59	134	50	243

DISCUSSION

Population sizes and distribution

In 1980, Zhou & Ding (1982) recorded the first sighting of more than 100 Siberian Cranes at Poyang Lake. Over the next six years, their numbers have increased gradually, peaking at 1 600+ individuals in 1987 (Yan & Ding, 1988). Between 1998 and 2010, the number of the Siberian Crane at Poyang Lake fluctuated from 1 627 to 3 954 individuals (Shan *et al.*, 2012). Recent research indicates that the global population size somewhere between 3 800–4 000 individuals (Li *et al.*, 2012). This increase suggests that Poyang Lake is an ideal wintering habitat for the Siberian Crane. During our study, we noted that these cranes are primarily distributed across two national nature reserves, with maximum numbers in PHF, PWC and NJS being 364, 158 and 200 individuals, accounting for 9.10%, 3.95% and 5.00% of the global population size, respectively. This shows that these two reserves are important habitats for the Siberian Crane. Compared with previous surveys of the Siberian Cranes, our results showed a smaller and more scattered distribution. For example, previous studies indicated that the Siberian Crane was mainly distributed in Banghu and seldom observed in the NJS (Shan *et al.*, 2012), but we observed a large number of these cranes in the NJS, and detected frequent local movements of the species among different lakes in NJS.

In recent years, continuous low water levels during spring and early summer in Poyang Lake have resulted in long-term drought and a decreased availability of food for many of the water birds that migrate there. The scattered distribution pattern of the Siberian Crane we observed during our surveys may accordingly be due to an insufficient food supply capable of support all the cranes in Banghu. Similarly, the departure time from Poyang Lake recorded for the Siberian Crane during this study was later than the time recorded in previous reports. One potential explanation for this difference may due to a delay in the wintering period due to climate change. Additionally, the juveniles we observed did not need to

breed, and may have delayed their migration after they had acquired enough energy at Poyang Lake, which may subsequently have decreased their mortality.

Our observations also showed that the Hooded Crane was mainly distributed in the PYH, with maximum numbers in PHF and PWC respectively at 302 and 154 individuals, indicating a larger number than previously observed in the entire Poyang Lake (Li *et al.*, 2012). While the Siberian Crane was mainly distributed in Shahu, Banghu, Dahuchi, Beishenghu, the Hooded Crane was only found in Banghu, Dahuchi and Zhushihu. Similarly, the Siberian Crane mainly selected shallow water areas or mudflats for forging habitats, while the Hooded Crane foraged mainly in the grasslands near the lakes. The migration of the Siberian Crane also took place somewhat earlier than that of the Hooded Crane. These ecological differences demonstrate the temporal and spatial separation indicate a positive coexistence of the two species.

Group characteristics

On the whole, both Siberian and Hooded Crane groupings were dominated by family and collective groups. The proportion of family groups for the Hooded Crane recorded in this study was higher than that observed in Chongming Island (Jing *et al.*, 2002b). Family groups for the Siberian Crane were dominated by two adults with one offspring and two adults with two offspring for the Hooded Crane. Compared with the Black-necked Crane, the Siberian Crane had a higher proportion of two adults with one offspring and a lower proportion of two adults with two offspring. The clutch size of the Hooded Crane was two ($n=4$) with a hatching rate of 100% (Guo *et al.*, 2005). A previous study in 1981 noted that family groups of the Hooded Crane were dominated by two adults with one offspring in Poyang Lake, but by two adults with two offspring in Japan in 1967 (Wang, 1988). The higher proportion of two adults with two offspring for the Hooded Crane that we noted during our observations indicates a high survival rate of juveniles. This assessment is also bolstered by the observed higher proportion of two adults with two offspring for the Hooded Crane at Poyang Lake than previously observed in Shengjinhu, or among

the Black-necked Crane (Liu, 2001; Liu et al, 2008).

Age structure

Our characterization of the age structure of both crane species showed some interesting differences between Hooded Cranes and Siberian Cranes. The proportion of juveniles of the Hooded Crane were more than double those seen among Siberian Cranes, suggesting that the proportion of juveniles of the Siberian Crane recorded in this study was similar to the numbers recorded in 1981, and also in line with observations of Black-necked Cranes (Zhou & Ding,

1982, Li, 1997). Typically, the numbers of juveniles of both the Hooded and Siberian Cranes follows an annual pattern, being low in December and January and high in November and February-April, which is again in line with observations of Black-necked Cranes (Liu et al, 2008). On 13 April 2013, we also noted 51 Siberian Cranes, including 30 juveniles, at Banghu, suggesting that the family group began to disintegrate during late wintering stage, with some juveniles leaving the family to cohabit with other juveniles or adults, which is quite similar to the behaviors of both Black-necked Cranes and the Common Crane *Grus grus* (Liu et al, 2008).

References

- Bird Life International. 2008. *Grus monacha*. In: IUCN 2009. IUCN Red List of Threatened Species. Version 2009.1.
- Guo YM, Qian FW, Liu XL, Xu CZ, Ma JZ. 2005. Preliminary report on breeding habit of Hooded Crane *Grus monacha* in Xiaoxing'an mountains. *Acta Zoologica Sinica*, **51**(5): 903-908. (in Chinese)
- Huang JG, Guo ZY. 2007. The wetland biodiversity and its conservation countermeasures in the Poyang Lake. *Research of Soil and Water Conservation*, **14**(1): 305-306, 309. (in Chinese)
- Jing K, Tang SM, Chen JK, Ma ZJ. 2002a. Primary Research on the Characteristics of Feeding Sites of *Grus monacha* in the East Tide Flat of Chongming. *Zoological Research*, **23**(1): 84-88. (in Chinese)
- Jing K, Tang SM, Chen JK, Ma ZJ. 2002b. Wintering ecology of the Hooded Crane in the eastern tideland of Changming Island. *Chinese Journal of Zoology*, **37**(6): 29-34. (in Chinese)
- Lcheureux N, Lucherini M, Festa-Bianchet M, Jorgenson JT. 1995. Density-dependent mother-yearling association in bighorn sheep. *Animal Behaviour*, **49**(4): 901-910.
- Li FS, Wu JD, Harris J, Burnham J. 2012. Number and distribution of cranes wintering at Poyang Lake, China during 2011–2012. *Chinese Birds*, **3**(3): 180-190.
- Li F, Wang QX, Lu S, Cai YJ. 2007. Time budget and activity rhythm of Siberian crane during day at Stopover site in spring in Zhalong Wetland. *Chinese Journal of Zoology*, **42**(3): 68-72. (in Chinese)
- Li LX. 1997. Population ecology and endangered categories evaluation of the Black-necked crane (*Grus nigricollis*). *Chinese Biodiversity*, **5**(2): 84-89. (in Chinese)
- Liu Q, Yang XJ, Zhu JG, Zhao JL, Yu HZ. 2008. Flock of Black-necked crane wintering at Napahai nature reserve, China. *Zoological Research*, **29**(5): 553-560. (in Chinese)
- Liu GK, Zhou CQ, Yang ZS, Long S, Pan L, Zeng GW, Li KJ, Tang L. 2010. Comparative study on group characteristics of dwarf blue sheep (*Pseudois schaeferi*) in spring and winter. *Acta Ecologica Sinica*, **30**(9): 2484-2490. (in Chinese)
- Liu XZ, Fan SB, Hu BH. 2006. Comprehensive and Scientific Survey of Jiangxi Nanjishan Wetland Nature Reserve. Beijing: Chinese Forestry Press.
- Liu ZS, Li XQ, Wang XM, Li ZG, Hu TH, Zhai H. 2009. Seasonal variations in group types and sizes of blue sheep (*Pseudois nayaur*) in the Helan Mountains, China. *Acta Ecologica Sinica*, **29**(6): 2782-2788. (in Chinese)
- Liu ZY. 2001. The vjunior observation of the *Grus monacha* shengjin Lake in Anhui province. *Journal of Anqing Teachers College (Natural Science)*, **7**(4): 79-81. (in Chinese)
- Shan JH, Ma JZ, Li YK, Qian FW, Tu XB. 2012. Population and distribution of the Siberian crane (*Grus leucogeranus*) wintering in the Poyang lakes over the past decade. *Zoological Research*, **33**(4): 355-361. (in Chinese)
- Sun ZY, Huang XF. 2010. Analysis on the characteristics of feeding habitat of the wintering Siberian crane in Poyang lake. *Chinese Journal of Zoology*, **45**(6): 46-52. (in Chinese)
- Wang QS. 1988. Hooded Cranes (*Grus monacha*). *Chinese Journal of Zoology*, **23**(4): 30-34. (in Chinese)
- Yan L, Ding TM. 1988. Investigation on Siberian Cranes (*Grus leucogeranus*) in Poyang Lake of Jiangxi province in winter. *Chinese Journal of Zoology*, **23**(4): 34-36. (in Chinese)
- Zhang BL, Liu QX, Song GX. 2010. Habitat suitability assessment for wintering hooded cranes in Dongtan, Chongming Island. *Journal of Northeast Forestry University*, **38**(7): 85-87. (in Chinese)
- Zhang LL, Zhou LZ, Dai YL. 2012. Genetic structure of wintering Hooded Cranes (*Grus monacha*) based on mitochondrial DNA D-loop sequences. *Chinese Birds*, **3**(2): 71-81.
- Zhao YY, Ma ZJ, Chen JK. 2002. Food habits of Hooded Crane (*Grus monacha*) in winter at the east Tidelands of Chongming island. *Journal of Fudan University (Natural Science)*, **41**(6): 609-613. (in Chinese)
- Zheng GM, Wang QS. 1998. China Red data Book of Endangered Animals (Aves). Beijing: Science Press.
- Zhou B, Zhou LZ, Chen JY, Cheng YQ, Xu WB. 2010. Diurnal time-activity budgets of wintering Hooded Cranes (*Grus monacha*) in Shengjin Lake, China. *Waterbirds*, **33**(1): 110-115.
- Zhou FZ, Ding WN. 1982. Wintering ecology of Siberian Cranes (*Grus leucogeranus*). *Chinese Journal of Zoology*, **17**(4): 19-21. (in Chinese)

Gene cloning and induced expression pattern of IRF4 and IRF10 in the Asian swamp eel (*Monopterus albus*)

Qiao-Qing XU^{1,2,3,*}, Dai-Qin YANG^{1,3}, Rui TUO¹, Jing WAN¹, Ming-Xian CHANG², Pin NIE²

1. School of Animal Science, Yangtze University, Jingzhou 434020, China

2. State Key Laboratory of Freshwater Ecology and Biotechnology, Institute of Hydrobiology, Chinese Academy of Sciences, Wuhan 430072, China

3. Hubei Collaborative Innovation Center for Freshwater Aquaculture, Wuhan 430070, China

Abstract: The Asian swamp eel (*Monopterus albus*) is one of the most economically important freshwater fish in East Asia, but data on the immune genes of *M. albus* are scarce compared to other commercially important fish. A better understanding of the eel's immune responses may help in developing strategies for disease management, potentially improving yields and mitigating losses. In mammals, interferon regulatory factors (IRFs) play a vital role in both the innate and adaptive immune system; though among teleosts *IRF4* and *IRF10* have seldom been studied. In this study, we characterized *IRF4* and *IRF10* from *M. albus* (*maIRF4* and *maIRF10*) and found that *maIRF4* cDNA consists of 1 716 nucleotides encoding a 451 amino acid (aa) protein, while *maIRF10* consists of 1 744 nucleotides including an open reading frame (ORF) of 1 236 nt encoding 411 aa. The *maIRF10* gene was constitutively expressed at high levels in a variety of tissues, while *maIRF4* showed a very limited expression pattern. Expression of *maIRF4* and *maIRF10* in head kidney, and spleen tissues was significantly up-regulated from 12 h to 48 h post-stimulation with polyinosinic: polycytidylic acid (poly I:C), lipopolysaccharide (LPS) and a common pathogenic bacteria *Aeromonas hydrophila*. These results suggest that IRF4 and IRF10 play roles in immune responses to both viral and bacterial infections in *M. albus*.

Keywords: *Monopterus albus*; IRF4; IRF10; Poly I:C; Up-regulation

Interferon regulatory factors (IRFs) are ancient molecules conserved throughout the evolution of metazoans and play a vital role in the innate and adaptive immune system (Tamura et al, 2008). To date, 11 IRF family members (IRF1–11) have been described in vertebrates and invertebrates (Huang et al, 2010), with IRF1–10 being present in most vertebrate species and IRF11 being found in non-vertebrate deuterostomes (Huang et al, 2010). Phylogenetic analysis of these 11 IRF proteins demonstrated that they can be subdivided into four groups that reflect their evolutionary history (Nehyba et al, 2009; Xu et al, 2010). Previous studies showed that in humans (*Homo sapiens*) and mice (*Mus musculus*), IRF4 was expressed in most types of immune cells, and has critical functions in B cell differentiation and immunoglobulin production (De et al, 2012). Likewise, IRF4 seems to also play important roles in the development and function of T helper cells, regulatory T (Treg) cells, dendritic cells (Xu et al, 2012) and CD4⁺ T

cell differentiation (Suzuki et al, 2004). Other studies on chickens (*Gallus gallus*) found that IRF4 was mainly expressed in the bursa, bursal lymphocytes (Nehyba et al, 2002), and thymus (Dougherty et al, 2009) and it is capable of repressing the expression of ovalbumin gene (Dougherty et al, 2009). ConA can induce the expression of IRF4 in splenic cells, while IFNs cannot induce the expression of IRF4 (Nehyba et al, 2002). Furthermore, among teleost, pathogen-associated molecular patterns (PAMPs) were found to stimulate the IRF4 expression in rainbow trout (*Oncorhynchus mykiss*) (Holland et al,

Received: 23 October 2013; Accepted: 25 April 2014

Foundation items: This study was financially supported by the Project from the National Natural Science Foundation of China (31101928), the State Key Laboratory of Freshwater Ecology and Biotechnology (2010FB02) and Public Welfare Scientific Research Project of Hubei Province (2012DBA29001)

*Corresponding author, E-mail: xuqiaoqing@yangtzeu.edu.cn

2010) and rock bream (*Oplegnathus fasciatus*) (Bathige et al, 2012).

Belonging to the same IRF4 subfamily, IRF10 was previously found to have been eliminated or rendered non-functional in both mice and humans (Nehyba et al, 2009). Curiously though, IRF10 can elevate the expression of major histocompatibility complex (MHC) class I molecules and guanylate-binding protein (GBP) and interfere with the induction of the type I IFN target genes in chickens (Nehyba et al, 2002). Both MHC class I and GBP play important roles in viral infections (Nehyba et al, 2002; Hu et al, 2011). Another feature of IRF10 is that similar to IRF4, it can also repress the expression of ovalbumin gene (Dougherty et al, 2009) and ConA can induce the expression of IRF10 in splenic cells (Nehyba et al, 2002). Furthermore, type I IFN and IFN- γ seem capable of inducing the expression of IRF10 in primary fibroblasts, though the expression of IRF10 is induced relatively late and needs other protein synthesis (Nehyba et al, 2002). In the Japanese flounder (*Paralichthys olivaceus*), bacteria or viral hemorrhagic septicemia virus (VHSV) can increase the expression of IRF10 in kidney tissue (Suzuki et al, 2011), though in zebrafish (*Danio rerio*) IRF10 was found to be a negative regulator of interferon transcription (Li et al, 2013). Clearly the diversity of roles and effects of IRF10 could use some clarification, especially regarding the role IRF10 plays in immune responses following viral or bacterial infections.

In recent years, the Asian swamp eel (*Monopterus albus*) has become one of the most economically important freshwater fish in East Asia. Unfortunately, data on immune genes of *M. albus* are scarce as compared to other commercially important fish. Given the eels economic importance, a clearer understanding of its immune responses may help to develop strategies for disease management, which may potentially aid in aquaculture, increase yields, or decrease losses of this species. In this study, we cloned full-length cDNAs of *M. albus* IRF4 (maIRF4) and maIRF10 and then investigated the tissue distribution of these two genes' expression. Paired with this analysis, we also opted to investigate a common pathogen afflicting the Asian swamp eel, *Aeromonas hydrophila*, the causative agent of Septicemia in this species (Yang et al, 2008; He et al, 2010). Pathogens of some disease such as stigmatosis in Asian swamp eel had not been investigated clearly. For this analysis, we measured the change in maIRF4 and maIRF10 gene

expression in the head kidney (HK), spleen (SP), and gills (GI) following stimulation with PAMPs, e.g. polyinosinic: polycytidylic acid (poly I:C) and lipopolysaccharide (LPS), and a common pathogenic bacteria, *A. hydrophila*.

MATERIAL AND METHODS

Fish

Eels of 150–200 g body weight were obtained from the aquaculture base of Yangtze University, China. Eels were maintained in fiberglass tanks supplied with a continuous flow of recirculating freshwater at 24 \pm 1 °C. Fish were fed once daily on water earthworms, and were acclimated for at least two weeks prior to experimentation.

Gene cloning and sequence analysis

cDNA samples were prepared from head kidney with the first strand cDNA synthesis kit (Fermentas, Canada). First, degenerate primers IRF4-F/IRF4-R and IRF10-F/IRF10-R were designed against conserved region and used for PCR amplification of the internal region of *maIRF4* and *maIRF10* that was obtained from cDNA samples. PCR products were respectively isolated using a Gel Extraction Kit (Tiangen, China), cloned into a pMD18-T vector (TaKaRa, Japan) and transformed into *Escherichia coli* strain DH5 α competent cells. Putative clones were then screened *via* PCR using the aforementioned primers, and the selected clones were sequenced. 5'-RACE and 3'-RACE were performed with gene-specific primers and adaptor primers to obtain the full-length cDNA sequence of *maIRF4* and *maIRF10*. Universal primers mix (UPM) was obtained from mixing UPM Long and UPM Short at a ratio of 1:100. For 3'-RACE, PCR was initially performed with primers UPM/3-F1 followed by a nested PCR with primers UPM/3-F2. For 5'-RACE, the adaptor primers AAP and AUAP were used. RNA from *M. albus* spleen was reverse-transcribed at 42 °C using the gene-specific primer 5-R1. Following synthesis of the first strand cDNA, the resulting purified cDNA was used in the TdT-tailing reaction, and the tailed cDNA was then amplified by primers 5-R2 and AAP. A dilution of the original PCR (0.1%) was re-amplified using AUAP and a nested 5-R3 primer (all primers listed in Table 1).

The nucleotide sequences generated were assembled and analyzed with AlignIR (LI-COR, Inc.). Sequence identities were calculated using the DNASTar

Table 1 Oligonucleotide primers used in the study

Name	Sequence (5'–3')	Usage
UPM Long	CTAATACGACTCACTATAGGGCAAGCAGTGGTATCAACGCAGAGT	3'-Race PCR universal primers
UPM Short	CTAATACGACTCACTATAGGGC	
AAP	GGCCACGCGTCGACTAGTACGGGIIIGGGIIIG	5'-Race PCR universal primers
AUAP	GGCCACGCGTCGACTAGTAC	
IRF4-F	GA(G)AGC(T)CAGCTGGACATCTC	Cloning for <i>maIRF4</i> internal fragment
IRF4-R	ACAGGAGCTGCCTGGCA(G)AAC	
IRF4-5-R1	CTCCCGCATCACAG	5' RACE 1 st round PCR
IRF4-5-R2	GAGAAAGGTGAAGGCTGGCTGT	5' RACE 2 nd round PCR
IRF4-5-R3	GGGATGATGCGGTAGACTTTGT	5' RACE 3 rd round PCR
IRF4-3-F1	ACGGAGACAAGCCCAACAAGC	3' RACE 1 st round PCR
IRF4-3-F2	GTCGGCTGCTGCCTCGTTTCC	3' RACE 2 nd round PCR
IRF10-F	GAGCGC(G)AA(G)CCAGCTGGACATC	Cloning for <i>maIRF10</i> internal fragment
IRF10-R	CTCC(G)CGCTCCAGC(T)TTGTTGGG	
IRF10-5-R1	CTGGGCTCTTGGTG	5' RACE 1 st round PCR
IRF10-5-R2	GCTCTTGGTGGTCACTTTCATT	5' RACE 2 nd round PCR
IRF10-5-R3	AAGCGGGCTGAAGAAGGTGATA	5' RACE 3 rd round PCR
IRF10-3-F1	AAGTGACCACCAAGAGCCCGAT	3' RACE 1 st round PCR
IRF10-3-F2	CAATGGCTCGCCTTCTTTGTCA	3' RACE 2 nd round PCR
β-actin F	CAGTCCTCCTAAGGCGATAA	Real-time quantitative PCR control
β-actin R	GCATCATCTCCAGCAAAGC	
IRF4-RT- F	ACGGAGACAAGCCCAACAAG	Real-time quantitative PCR
IRF4-RT -R	ACAAGTGGCTGCCCGTCTG	
IRF10-RT- F	ACAATGGCTCGCCTTCTTT	Real-time quantitative PCR
IRF10-RT- R	TGGGACCACTCCAATACAC	

5.0 (<http://www.mega-software.net/index.html/>). Multiple sequence alignments were generated using Clustal W 2.02. Phylogenetic trees were created by the neighbor-joining method using MEGA 5.01 and were bootstrapped 1,000 times.

Tissue distribution

Intestines (I), HK, trunk kidney (TK), GI, brain (BR), liver (L), SP, muscle (M), gonad (GO), whole blood (BL) and skin (SK) from four fish were collected and used for RNA isolation using TRIzol (Invitrogen, USA) in order to analyze the expression of *maIRF4* and *maIRF10* in healthy eels. Real-time PCR was conducted to detect the expression of *maIRF4* and *maIRF10* in these tissues. The expression of *maIRF4* and *maIRF10* in different tissues was calculated relative to the expression level of β-actin.

Real-time PCR analysis

The *maIRF4*, *maIRF10* and house-keeping gene β-actin cDNA fragments were generated via RT-PCR. A common reference with purified PCR products of the three genes was separately used for quantification. Primers used for detection of gene expression are detailed in Table 1. PCR reactions were performed using Chromo 4TM Continuous Fluorescence Detector (MJ Research). Amplifications were carried out at a final volume of 20 μL

containing 1 μL DNA sample, 10 μL 2×SYBR green Real time PCR Master Mix (Toyobo, Japan), 2 μL of each primer and 5 μL H₂O. PCR amplification consisted of 5 min at 95 °C, followed by 40 cycles consisting of 10 s at 94 °C, 20 s at 58 °C, 20 s at 72 °C and read plate at 82 °C. Melting curve analysis of amplification products was performed at the end of each PCR reaction in order to confirm that a single PCR product was detected. Each sample was run in duplicate to ensure accuracy.

Challenge trial using different stimulus

To study the effect of immunostimulants on the expression of *maIRF4* and *maIRF10*, four groups of fish (three fish each group) were respectively injected intra-peritoneally (i.p.) with either 500 μL 2 mg poly I:C/mL (Sigma), 500 μL 2 mg LPS/mL (*E. coli* O127:B8, Sigma), 1×10⁸ CFU *A. Hydrophila*/mL, or 500 μL PBS to serve as a control. Consecutively, at 0 h, 12 h, 24 h, 48 h after injection, three fish were killed, and tissues from the head kidney, gill and spleen were collected for total RNA extraction and gene expression detection via real-time PCR.

Statistical analysis

Fold change was calculated as (Ts/Tn)/(Cs/Cn) where Ts equals the treated sample assayed for the specific gene and Tn equals the treated sample assayed for the

normalizer gene (β -actin), and Cs and Cn respectively equals the calibrator group with the specific and normalizing gene (Purcell et al, 2004). One way-analysis of variance (ANOVA) and an LSD post hoc test was used to statistically analyze the expression data, with $P < 0.05$ being considered statistically significant.

RESULTS

Cloning and characterization of *maIRF4* and *maIRF10*

Analysis showed that *maIRF4* cDNA (GenBank accession no. JX463267) is approximately 1.7 kb in length, with an open reading frame (ORF) of 1 356 nucleotides, encoding a protein of 451 amino acid (aa) residues with a putative molecular weight of 51.7×10^3 and an isoelectric point (pI) of 9.61. Furthermore, the *maIRF4* cDNA contains 22 microsatellite dinucleotide (T-G) repeats in the 3' UTR. The full-length cDNA of *maIRF10* meanwhile comprises 1 744 nucleotides (GenBank accession no. JX463268). The ORF encodes a 411 aa protein, with a calculated molecular weight of 58.97×10^3 and a pI of 8.85. The 3'-UTR has two ATTTA motifs that mediate mRNA degradation (Iwai et al, 1991) and the polyadenylation signal (AATAAA) lies 27 bp upstream of the polyA tail.

Phylogenetic analysis showed that the IRF4 molecules diverged from the other IRF4 subfamily members (IRF8, 9, 10), with eel IRF4 clustering with the other teleost IRF4s (Figure 1). Furthermore, teleost IRF4 diverged into two clades, with *maIRF4* having the highest similarity with medaka IRF4-2 (Figure 1). The putative *maIRF4* protein was 45.6% to 84.0 % identical to IRF4 proteins from mammals, chickens, frogs and other fish (Figure 2), while *maIRF10* is 43.4% to 76.6% identical to its homologous proteins in mammals, birds, amphibians and other fish (Figure 3). Additionally, flounder IRF10 was the closest to *maIRF10*. *MaIRF4* and *maIRF10* had the DNA-binding domain and IRF association domain (Figure 2, Figure 3), both of which were important domains in the IRF family (Lohoff & Mak, 2005).

Tissue expression

Real-time PCR analyses showed that the expression of *maIRF4* in all tested tissues was quite low, with relative abundant in intestine (0.21×10^{-3} -fold), head kidney (0.16×10^{-3} -fold) and trunk kidney (0.14×10^{-3} -fold) (Figure 4). However, constitutive expression of *maIRF10* transcripts was detected in all tissues studied. Compared

with β -actin, expression was predominantly in head kidney (7.2×10^{-3} -fold) and whole blood (6.9×10^{-3} -fold). And a relatively low level of *maIRF10* expression was detected in brain (1.1×10^{-3} -fold) and spleen (0.4×10^{-3} -fold) (Figure 4).

Induced expression

In order to further investigate the differences pattern, *maIRF4* and *maIRF10* expression induced by poly I:C, LPS and *A. hydrophila* were examined. Stimulation by poly I:C up-regulated *maIRF4* expression at 12 h post-stimulation (hps) in head kidney (23.2-fold), spleen (15.3-fold) and gill (3.8-fold) tissue ($P < 0.05$). Subsequently, expression increased, reaching a peak in head kidney (45.8-fold), spleen (27.5-fold) and gill (5.4-fold) at 24 hps ($P < 0.05$) (Figure 5). Following LPS stimulation, *maIRF4* mRNA levels were initially increased in head kidney and spleen at 12 hps, and remained elevated at 24 hps before decreasing to basal levels in spleen. In gill only at 24 hps was a significant increase seen. After *A. hydrophila* stimulation, *maIRF4* transcript levels were enhanced in all three tissues studied at all time-points and peaked at 24 hps, with a fold change of 17.7 in head kidney, 13.6 in spleen and 6.51 in gill (Figure 5).

The level of *maIRF10* induction was always lower than that of *maIRF4*. *MaIRF10* expression was significantly up-regulated at all times-points by poly I:C in head kidney and in spleen but not in gills. The *maIRF10* expression level peaked at 24 h in head kidney (5.3-fold) and spleen (5.8-fold). Following LPS stimulation, *maIRF10* mRNA expression increased from 12 hps to 48 hps (up to 3.6-fold) in head kidney, but significant up-regulation occurred at 24 h (3.6-fold) in the spleen, with no significant change in gills. Following *A. hydrophila* stimulation, *maIRF10* transcript levels were also enhanced in head kidney and spleen at 12 and 24 hps, with a peak fold change of 6.3 and 4.9 at 24 hps, respectively. Notably, levels remained elevated to 48 hps in head kidney. No significant changes were detected in *maIRF10* expression in the gills at any time-point following stimulation by *A. hydrophila* (Figure 5).

DISCUSSION

Phylogenetic analysis showed that teleost IRF4 genes aggregated into two branches, suggesting that these two fish IRF groups arose through teleost-wide whole genome duplication (Figure 1). However, only one IRF4 gene was cloned in the Asian swamp eel. This may be

explainable by a twice genome duplication in the species while a third genome duplication occurred in other teleost (Zhou et al, 2002). The *malIRF4* gene is highly conserved compared with flounder IRF4 and medaka IRF4-2, respectively exhibiting 84.2% and 83.7% identity over the entire protein. The serine-rich domain is a target for virus induced phosphorylation that facilitates interaction with other IRF members and subsequent activation of virus clearance signaling pathways (Sun et al,

2007). This domain is present in zebrafish IRF4-1, fugu IRF4-1, medaka IRF4 (Figure 2) and rock bream (*O. fasciatus*) (Bathige et al, 2012) but absent from IRF4 in many other species including humans, chickens, xenopus (*Xenopus tropicalis*) (Figure 2), rainbow trout (Holland et al, 2010) and eel, indicating significant evolutionary divergence of IRF4. All IRF10 genes from birds, amphibians and fish are closely clustered and closely related to IRF4 (Figure 1). Compared with these

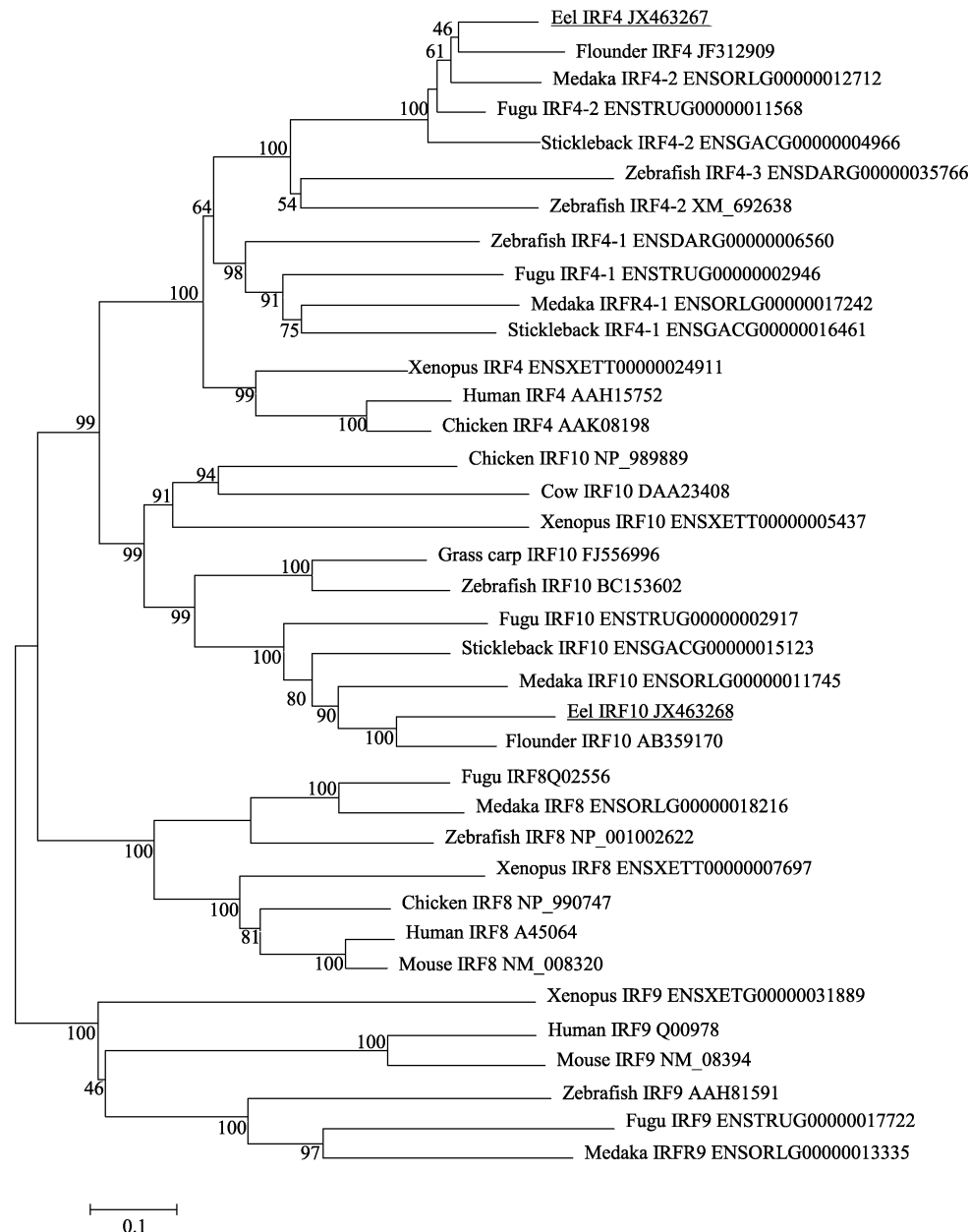
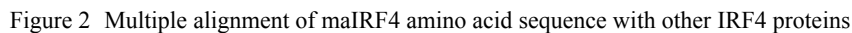


Figure 1 Phylogenetic tree analysis of IRF4, IRF8, IRF9 and IRF10 among vertebrates

A neighbor-joining phylogenetic tree of IRF proteins based on protein sequences analyzed with Clustal W and MEGA 5.0. Data were analyzed using Poisson correction, and gaps were removed by pairwise deletion. The degree of confidence for each branch point was determined by bootstrap analysis (1 000 times). The sequences of IRFs used for the analysis are derived from the GenBank and Ensembl Databases, with accession numbers added after the genes.



Generally, *IRF10* is expressed in all tissues while *IRF4* has a much more limited expression pattern. For example, among chickens *IRF10* is detected in all tissues, while only faint signals of *IRF4* mRNA were detected in all the previously tested tissues in chicken or mice (Dougherty et al, 2009; Takaoka et al, 2008). Consistent with these results, *maIRF10* mRNA was found to be abundant in all the tissues we analyzed, with predominant expression in whole blood, skin and head kidney, while *maIRF4* expression was significantly lower than that of *maIRF10* in all the same tissues (Figure 4). The highest expression of *maIRF4* was detected in the intest-

Previously, it was reported that IFN1, IFN- γ and ConA can up-regulate IRF10 expression (Nehyba et al, 2002). However, induction expression of IRF10 occurs relatively late, and is dependent on protein synthesis.

[illegible]

Figure 3 Multiple alignment of maIRF10 amino acid sequence with other IRF10 proteins

Symbol (*) represents identical residues, (:) conservative substitution and (.) similar residues. Missing amino acids are denoted by hyphens. The DNA-binding domain (DBD) and IRF association domain (IAD) are highlighted in grey. The conserved tryptophan (W) residues that comprise a “tryptophan cluster” are boxed.

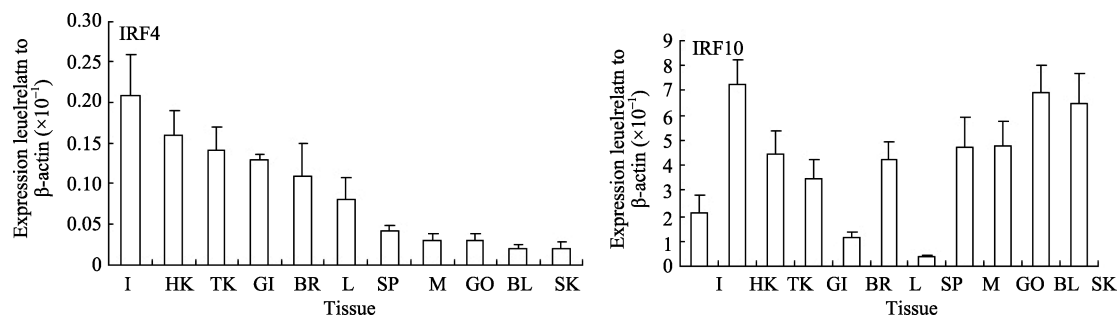


Figure 4 Expression analysis of maIRF4 and maIRF10 in different tissues

Real-time quantitative PCR was performed with cDNA samples prepared from whole blood (BL), brain (BR), gill (GI), skin (SK), muscle (M), intestines (I), spleen (SP), liver (L), gonad (GO), head kidney (HK) and trunk kidney (TK). Bars are averages plus standard deviations of tissue data from 4 fish.

Neither IFN1 or IFN- γ induce IRF4 expression, though IRF4 is known to be induced by ConA, plant lectins, CD3, phorbol-12-myristate-13-acetate (PMA) and IgM

cross-linking in chicken and mouse (Ma et al, 2006; Nehyba et al, 2002). In humans, dengue virus and T cell receptor cross-linking has likewise been known to

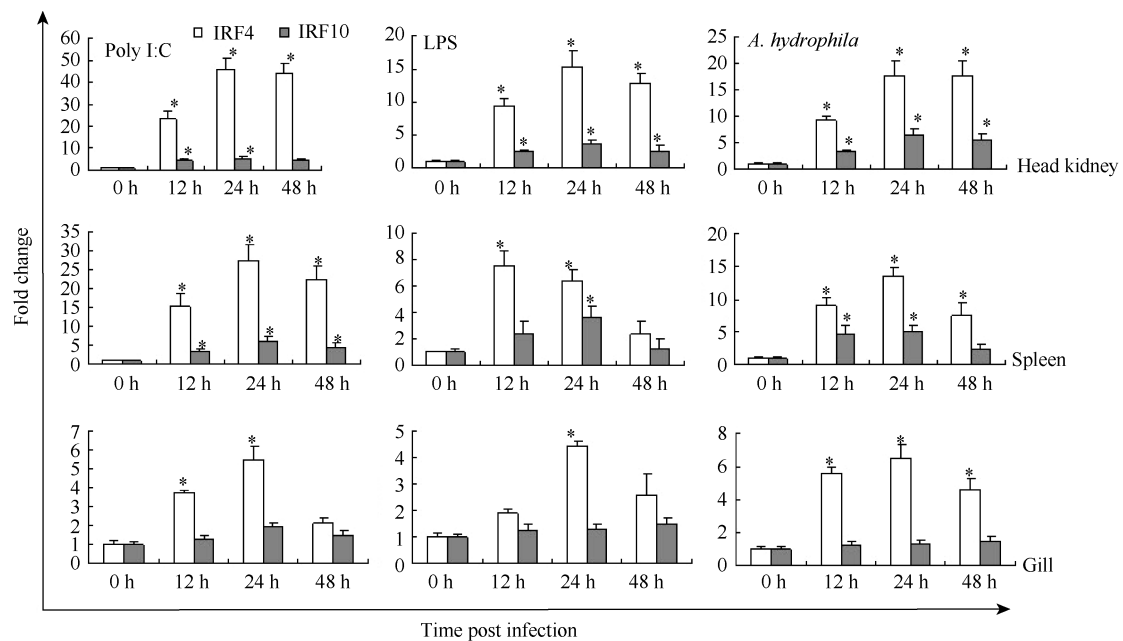


Figure 5 Expression levels of *maIRF4* and *maIRF10* induced by poly I:C, LPS and *Aeromonas hydrophila* in head kidney, spleen and gill. Fish were injected with each stimulant and 12 h, 24 h and 48 h, and tissues were then isolated for RNA extraction and cDNA synthesis. The transcript levels were obtained using real-time PCR and expressed relative to the 0 h healthy (control) fish and presented as the fold change after being normalized to the expression of β -actin. Bars denote averages plus standard deviations of tissues from 3 fish. * over the bar indicates a significant difference after a treatment by one-way ANOVA (*: $P < 0.05$).

increase *IRF4* mRNA levels (Chen et al, 2008; Matsuyama et al, 1995). Among the Asian swamp eel, we found that poly I:C, LPS and *A. hydrophila* induced *maIRF4* and *maIRF10* expression, wherein intraperitoneal injection of poly I:C significantly induced *maIRF4* and *maIRF10* expression from 12 hps to 48 hps (Figure 5). Although *maIRF4* and *maIRF10* expression induced by LPS or *A. hydrophila* was lower than that induced by poly I:C, there was a significant increase in expression in both the head kidney and spleen following both treatments (Figure 5). *maIRF4* expression peaked at a 45.8-fold increase in head kidney and *maIRF10* reached a maximal expression level (5.8-fold) at 24 hps following poly I:C stimulation. Similar results have been found in other fish: for example, in rainbow trout, *IRF4* was significantly up-regulated by PMA (4-fold above control levels) in splenocytes in vitro (Holland et al, 2010) while in the Japanese flounder, *IRF10* expression was up-regulated 7.8-fold at 6 hps by LPS and peaked at a 23.6-fold up-regulation at 6 hps following poly I:C stimulation of peripheral blood leukocytes (Suzuki et al, 2011).

Further comparison of *IRF10* and *IRF4* inducible expression highlighted a greater increase in *maIRF4*

expression as compared with that of *maIRF10*. These results are consistent with previous expression studies conducted on birds (Nehyba et al, 2002), which found that *IRF4* constitutively expressed at a low levels in most tissues and organs among chickens (Dougherty et al, 2009) and that inducible expression of *IRF10* requires protein synthesis, with *IRF10* playing a unique role in the later stages of antiviral defense (Nehyba et al, 2002). By contrast, in rainbow trout, LPS significantly down-regulated *IRF4* expression in splenocytes (Holland et al, 2010). Similarly, estrogen was also found to decrease the expression of *IRF4* and *IRF10* in chickens (Dougherty et al, 2009).

In summary, in this study the complete *maIRF4* and *maIRF10* genes of the Asian swamp eel were cloned for the first time. Analysis of the overall amino acid sequence, identity and phylogenetics, showed that the cDNA encoding *maIRF4* and *maIRF10* exhibited homology with other *IRF4* and *IRF10* proteins of tetrapod species and fish sequences currently deposited in public databases. Furthermore, *maIRF10* was constitutively expressed at high levels in all the tissues investigated, while the transcript level of *maIRF4* was found to be quite low in all organs. Stimulation by Poly I:C, LPS

and *A. hydrophila* were also shown to induce *maIRF4* and *maIRF10* expression, indicating that these two factors likely play a part in the immune reaction to both bacterial and viral infections.

References

- Bathige SD, Whang I, Umasuthan N, Lim BS, Park MA, Kim E, Park HC, Lee J. 2012. Interferon regulatory factors 4 and 8 in rock bream, *Oplegnathus fasciatus*: Structural and expressional evidence for their antimicrobial role in teleosts. *Fish Shellfish Immunology*, **33**(4): 857-871.
- Chen JC, Ng MML, Chu JH. 2008. Molecular profiling of T-helper immune genes during dengue virus infection. *Virology Journal*, **5**: 165.
- Dadoue JP, Pawlak A, Alfonsi MF, Siffroi JP. 2005. Identification of transcripts by macroarrays, RT-PCR and in situ hybridization in human ejaculate spermatozoa. *Molecular Human Reproduction*, **11**(2): 133-140.
- De Silva NS, Simonetti G, Heise N, Klein U. 2012. The diverse roles of IRF4 in late germinal center B-cell differentiation. *Immunological Reviews*, **247**(1): 73-92.
- Dougherty DC, Park HM, Sanders MM. 2009. Interferon regulatory factors (IRFs) repress transcription of the chicken ovalbumin gene. *Gene*, **439**(1-2): 63-70.
- Eguchi J, Yan QW, Schones DE, Kamal M, Hsu CH, Zhang MQ. 2008. Interferon regulatory factors are transcriptional regulators of adipogenesis. *Cell Metabolism*, **7**(1): 86-94.
- He Z, Ren HM, Yang DY, Yang GY, Biao Y, Wang S. 2010. The histopathological study of hemorrhagic septicemia by *Aeromonas hydrophila* isolated from rice field eel (*Monopterus albus*). *Freshwater Fisheries*, **40**(4): 56-61.
- Holland JW, Karim A, Wang T, Alnabulsi A, Scott J, Collet B. 2010. Molecular cloning and characterization of interferon regulatory factors 4 and 8 (IRF-4 and IRF-8) in rainbow trout, *Oncorhynchus mykiss*. *Fish and Shellfish Immunology*, **29**(1): 157-166.
- Hu Y, Wang J, Yang B, Zheng N, Qin M, Ji Y, Lin G, Tian L, Wu X, Wu L. 2011. Guanylate binding protein 4 negatively regulates virus-induced type I IFN and antiviral response by targeting IFN regulatory factor 7. *Journal of Immunology*, **187**(12): 6456-6462.
- Huang B, Qi ZT, Xu Z, Nie P. 2010. Global characterization of interferon regulatory factor (IRF) genes in vertebrates, Glimpse of the diversification in evolution. *BMC Immunology*, **11**: 22.
- Iwai Y, Bickel M, Pluznik DH, Cohen RB. 1991. Identification of sequences within the murine granulocyte-macrophage colony-stimulating factor mRNA 3'-untranslated region that mediate mRNA stabilization induced by mitogen treatment of EL-4 thymoma cells. *Journal of Biological Chemistry*, **266**(27): 17959-17965.
- Li S, Feng H, Wu N, Zhang YA. 2013. Irf10, a novel interferon regulatory factor in zebrafish. *Fish Shellfish Immunology*, **24-28** Oval Rd, London Nw1 7dx, England. Academic Press Ltd-Elsevier Science Ltd., 1718-1718.
- Lohoff M, Mak TW. 2005. Roles of interferon regulatory factors in T-helper-cell differentiation. *Nature Reviews Immunology*, **5**(2): 125-135.
- Ma S, Turetsky A, Trinh L, Lu R. 2006. IFN regulatory factor 4 and 8 promote Ig light chain kappa locus activation in pre-B cell development. *Journal of Immunology*, **177**(11): 7898-7904.
- Matsuyama T, Grossman A, Mittrücker HW, Siderovski DP, Kiefer F, Kawakami T, Richardson CD, Taniguchi T, Yoshinaga SK, Mak TW. 1995. Molecular cloning of LSIRI a lymphoid-specific member of the interferon regulatory factor family that binds the interferon-stimulated response element ISRE. *Nucleic Acids Research*, **23**(12): 2127-2136.
- Nehyba J, Hrdlicková R, Bose HR. 2009. Dynamic evolution of immune system regulators: the history of the interferon regulatory factor family. *Molecular Biology and Evolution*, **26**(11): 2539-2550.
- Nehyba J, Hrdlicková R, Burnside J, Bose HR. 2002. A novel interferon regulatory factor (IRF), IRF-10, has a unique role in immune defense and is induced by the v-Rel oncoprotein. *Molecular and Cellular Biology*, **22**(11): 3942-3957.
- Purcell MK, Kurath G, Garver KA, Herwig RP, Winton JR. 2004. Quantitative expression profiling of immune response genes in rainbow trout following infectious haematopoietic necrosis virus (IHNV) infection or DNA vaccination. *Fish and Shellfish Immunology*, **17**(5): 447-462.
- Sun BJ, Chang MX, Song Y, Yao WJ, Nie P. 2007. Gene structure and transcription of IRF-1 and IRF-7 in the mandarin fish *Siniperca chuatsi*. *Veterinary Immunology and Immunopathology*, **116**(1-2): 26-36.
- Suzuki S, Honma K, Matsuyama T, Suzuki K, Toriyama K, Akitoyo I, Yamamoto K, Suematsu T, Nakamura M, Yui K, Kumatori A. 2004. Critical roles of interferon regulatory factor 4 in CD11bhighCD8alpha-dendritic cell development. *Proceedings of the National Academy of Sciences of the United States of America*, **101**(24): 8981-8986.
- Suzuki Y, Yasuike M, Kondo H, Aoki T, Hirono I. 2011. Molecular cloning and expression analysis of interferon regulatory factor 10 (IRF10) in Japanese flounder, *Paralichthys olivaceus*. *Fish and Shellfish Immunology*, **30**(1): 67-76.
- Takaoka A, Tamura T, Taniguchi T. 2008. Interferon regulatory factor family of transcription factors and regulation of oncogenesis. *Cancer Science*, **99**(3): 467-478.
- Tamura T, Yanai H, Savitsky D, Taniguchi T. 2008. The IRF family transcription factors in immunity and oncogenesis. *Annual Review of Immunology*, **26**: 535-584.
- Xu QQ, Chang MX, Xiao FS, Huang B, Nie P. 2010. The gene and virus-induced expression of IRF-5 in grass carp *Ctenopharyngodon idella*. *Veterinary Immunology and Immunopathology*, **134**(3-4): 269-278.
- Xu WD, Pan HF, Ye DQ, Xu Y. 2012. Targeting IRF4 in autoimmune diseases. *Autoimmunity Reviews*, **11**(12): 918-924.
- Yang ZZ, Li DF, Wang YW. 2008. Rapid diagnosis of *Aeromonas hydrophila* Septicemia of *Monopterus albus* by PCR. *Journal of Aquaculture*, **29**(2): 11-13.
- Zhou RJ, Cheng HH, Tiersch TR. 2002. Differential genome duplication and fish diversity. *Reviews in Fish Biology and Fisheries*, **11**(4): 331-337.

Molecular cloning, sequence analysis, and cadmium stress-rated expression changes of BTG1 in freshwater pearl mussel (*Hyriopsis schlegelii*)

Kou PENG¹, Cheng-Yuan WANG¹, Jun-Hua WANG¹, Jun-Qing SHENG¹, Jian-Wu SHI¹, Jian LI¹, Yi-Jiang HONG^{1,2,*}

1. School of Life Sciences and Food Engineering, Nanchang University, Nanchang 330031, China

2. Institute of Life Science, Nanchang University, Nanchang 330031, China

Abstract: The B cells translocation gene 1 (*BTG1*) is a member of the BTG/TOB family of anti-proliferative genes, which have recently emerged as important regulators of cell growth and differentiation among vertebrates. Here, for the first time we cloned the full-length cDNA sequence of *Hyriopsis schlegelii* (*Hs-BTG1*), an economically important freshwater shellfish and potential indicator of environmental heavy metal pollution, for the first time. Using rapid amplification of cDNA ends (RACE) together with splicing the EST sequence from a haemocyte cDNA library, we found that *Hs-BTG1* contains a 525 bp open reading frame (ORF) encoding a 174 amino-acid polypeptide, a 306 bp 5' untranslated region (5' UTR), and a 571 bp 3' UTR with a Poly(A) tail as well as a transcription termination signal (AATAAA). Homologue searching against GenBank revealed that *Hs-BTG1* was closest to *Crassostrea gigas* *BTG1*, sharing 50.57% of protein identities. *Hs-BTG1* also shares some typical features of the BTG/TOB family, possessing two well-conserved A and B boxes. Clustering analysis of *Hs-BTG1* and other known BTGs showed that *Hs-BTG1* was also closely related to *BTG1* of *C. gigas* from the invertebrate BTG1 clade. Function prediction via homology modeling showed that both *Hs-BTG1* and *C. gigas* *BTG1* share a similar three-dimensional structure with *Homo sapiens* *BTG1*. Tissue-specific expression analysis of the *Hs-BTG1* via real-time PCR showed that the transcripts were constitutively expressed, with the highest levels in the hepatopancreas and gills, and the lowest in both haemocyte and muscle tissue. Expression levels of *Hs-BTG1* in hepatopancreas (2.03-fold), mantle (2.07-fold), kidney (2.2-fold) and haemocyte (2.5-fold) were enhanced by cadmium (Cd^{2+}) stress, suggesting that *Hs-BTG1* may have played a significant role in *H. schlegelii* adaptation to adverse environmental conditions.

Keywords: *Hyriopsis schlegelii*; *BTG1*; Gene cloning; mRNA expression; Cadmium stress

Exposure to heavy metals—cadmium in particular—is widely known to be toxic to humans and higher vertebrates, negatively affecting several key organs. Unfortunately, industrial pollution run-off often results in these metals making their way into water sources, where they are absorbed by the ecosystem's resident species. For example, oysters were previously found to accumulate environmental cadmium, suggesting that they may serve as potential indicator organisms for marine cadmium contamination (Lu et al, 1998). However, the toxicological activities and effects of such heavy metals among invertebrates such as freshwater shellfish are not well understood. This situation is especially acute in developing countries and regions such as China, where heavy levels of water pollution that has

accompanied industrial development.

One key reason that shellfish species like oysters can serve as viable indicators of environmental heavy metals is that they have remarkable adaptability to

Received: 12 December 2013; Accepted: 04 August 2014

Foundation items: This work was supported by the Key Scientific and Technological Programme of Jiangxi Province, China (20121BB-F60036); the Special Fund for Agro-scientific Research in the Public Interest, State Agriculture Ministry of China (200903028); the Science and Technology Landing Project of Jiangxi Province, China (KJLD12001); the Youth Fund of the Education Department of Jiangxi Province, China (GJJ14219) and the National Natural Science Foundation of China (31160534)

*Corresponding author, E-mail: yijianghong@126.com

different environments and are resistant to the toxic effects of metals like cadmium. Among freshwater shellfish, both the Japanese *Hyriopsis schlegelii* (*H. schlegelii*) and Chinese *H. cumingii* species of mussels exhibit similar characteristics. In 1997, *H. schlegelii* was introduced to China by the Reservoir Development Company in Fuzhou City, Jiangxi Province. Over the last decade, this species has become a key economic feature of freshwater shellfish production, largely due to decades of selective breeding that have results in strong disease resistance and environmental adaptability, as well as its enlarged shell width and other physical characteristics contributing to senior pearls cultivation (He et al, 2013; Peng et al, 2012a, b; Xie et al, 2011). In order to develop a better ecological farming, exploring molecular indicator capable of monitoring environmental pollution is particularly important for this mussel.

Testing for the presence and effects of cadmium among potential indicator species is not always straightforward, but gene expression analysis under various environmental factors stress is a commonly employed experimental method to explore candidate gene's corresponding function (Duan et al, 2013; Wang et al, 2011) and in doing so illustrating the effects of certain environmental pollutants on different organisms. In the present study, we sought to examine the *H. schlegelii* *B cell translocation gene 1* (*BTG1*), which has been cloned and studied in several species, including *Rattus norvegicus*, *Mus musculus*, *Gallus gallus*, *Xenopus laevis*, and *Danio rerio* (Fu et al, 2012), but not among many lower animals. *BTG1* is a member of the BTG/TOB family that was identified from B lymphoblastic leukemia with chromosomal translocation (Rouault et al, 1992). The BTG/TOB family is a class of anti-proliferative proteins involved in negative regulation of cell cycle (Winkler, 2010) and tumor cell growth (Mauxion et al, 2009). BTG/TOB proteins have a conservative BTG region of 100 – 120 amino acids at its amino-terminal (N terminal), containing two well-conserved A and B boxes (Mauxion et al, 2009; Winkler, 2010). Among mammals, the BTG/TOB family includes six members: BTG1, BTG2/PC3/Tis21, BTG3/ANA, BTG4/PC3B, TOB1/TOB, and TOB2 (Winkler, 2010), with both BTG1 and BTG2 belonging to the same subfamily with an approximate carboxyl terminal (C terminal) length (Mauxion et al, 2009). Previously, the BTG/TOB proteins were reported to be involved in several different physiological activities,

including regulation of embryonic development, cell differentiation and apoptosis, among others (Mauxion et al, 2009). Similarly, BTG/TOB proteins were also found to affect gene transcription and mRNA stability in cells via deadenylation (Yang et al, 2008; Mauxion et al, 2009). In this study, we obtained the full length cDNA of *Hs-BTG1* by library screening and RACE cloning to investigate whether BTG1 is involved in the response against heavy metal stress.

MATERIALS AND METHODS

Experimental materials and reagents

We obtained healthy *H. schlegelii* from the national seed market of *Hyriopsis* at Reservoir Development Company in Fuzhou City, Jiangxi Province. The *H. schlegelii*, with a shell length of 107 ± 6.5 mm, was cultured in a laboratory aquarium for one week (18–25 °C) prior to testing.

RNAase inhibitors, DNA Polymerases and Markers were purchased from TaKaRa. Gel extraction kit and plasmid extraction kit were purchased from Axygen, while DNase I (RNase Free) and a first strand cDNA synthesis kit were purchased from Promega. TRIzol was from Invitrogen. *E. coli* DH5 α cells were stored in our lab. Primers were synthesized by Shanghai Sangon Company. Cadmium chloride (CdCl₂·5H₂O, AR) was produced by the Shanghai Chemical Reagent and other conventional reagents of analytical grade were obtained from Sinopharm Group.

cDNA

Total RNA of different tissues was extracted using TRIzol prior to assessing its purity and concentration. Primary sample digestion by RNase-free DNase I was performed before cDNA synthesis. The organization-specific cDNA synthesis was conducted as described previously (He et al, 2013; Peng et al, 2012a, b).

cDNA library screening

We performed PCR amplification of monoclonal colony using random primers (M13) according to our established cDNA library from blood cells of *H. schlegelii* (Xie et al, 2011), under the following conditions: 94 °C 5 min; 94 °C 30 s, 45 °C 30 s, 72 °C 90 s, 33 cycles; 72 °C 7 min. Amplified fragments more than 500 bp in length were sequenced using M13 sequencing primers (Sangon), and then we obtained expressed sequence tags (ESTs) sequence of *Hs-BTG1*.

Full-Length cDNA cloning and molecular characterization

The 3' and 5' cDNA ends were amplified using SMART™ RACE Amplification Kit and Advantage 2 PCR Kit. Primers (*BTG1*-GSP1 and *BTG1*-GSP2; shown in Table 1) were designed using Primer Premier 5.0 according to the ESTs sequence of *Hs-BTG1*. Touchdown PCR amplification was performed using universal primers (UPM), 5' specific (*BTG1*-GSP1) and 3' specific (*BTG1*-GSP2) primers, with 5'-RACE-Ready and 3'-RACE-Ready cDNA as the template. PCR reaction system was as follows: 10× Advantage 2 PCR Buffer 5 µL, dNTP Mix 1 µL, 5'-RACE-Ready cDNA or 3'-RACE-Ready cDNA 2.5 µL, UPM 5 µL, *BTG1*-GSP1 or *BTG1*-GSP2 1 µL, Advantage 2 Polymerase Mix 1 µL, PCR-Grade water 34.5 µL, total volume 50 µL. Reaction

conditions were as follows: 94 °C 5 min; 94 °C 30 s, 72 °C 3 min, 5 cycles; 94 °C 30 s, 70 °C 30 s, 72 °C 3 min, 5 cycles; 94 °C 30 s, 68 °C 30 s, 72 °C 3 min, 28 cycles; 72 °C 10 min. Amplified products were recovered and purified using a gel extraction kit before being sequenced by Shanghai Sangon Company.

NCBI ORF Finder and BlastP were used for identifying the largest ORF and homologous amino acid sequences of *Hs-BTG*. SignalP 4.0 was used for predicting the signal peptide. ClustalW was used in multiple comparisons of the amino acid sequences from different species. Protein homology modeling was conducted by using SWISS-MODEL. Chimera 1.8 was used for the tertiary structure analysis. The phylogenetic tree was constructed using Neighbor-Joining (NJ) method with 1000 bootstraps in Mega 4.1.

Table 1 Primers used for cloning *Hyriopsis schlegelii* *BTG1* cDNA and expression quantification

Primer name	Sequence (5'–3')
M13 F	TGTAACGACGCGCCAGT
M13 R	CAGCAACAGCTATGAC
SMART II™ A Oligonucleotide (12 µmol/L)	AAGCAGTGGTATCAACGCAGAGTACGCGGG
3'-RACE CDS Primer A (3'-CDS; 12 µmol/L)	(T) ₂₅ V N (N=A, C, G, or T; V=A, G, or C)
5'-RACE CDS Primer A (5'-CDS; 12 µmol/L)	AAGCAGTGGTATCAACGCAGAGTAC(T) ₃₀ V N
10×Universal Primer A Mix (UPM)	(N=A, C, G, or T; V=A, G, or C)
Long Primer (0.4 µmol/L)	CTAATACGACTCACTATAGGGCAAGCAGTGGTA
Short Primer (2 µmol/L)	TCAACGCAGAGT
<i>Hs-BTG1</i> 5GSP1 (10 µmol/L)	CTAATACGACTCACTATAGGGC
<i>Hs-BTG1</i> 3GSP2 (10 µmol/L)	CGTGGTCCTCGTGCGAAATAGAATG
<i>Hs-BTG1</i> qPCR-F	TGCCACTTTGTTTCCAGTTGAGG
<i>Hs-BTG1</i> qPCR-R	GCTGGCTTATCGTGTTGGAAT
β -actin qPCR-F	CGGTACTGGCATCCTCTGAT
β -actin qPCR-R	AAGGTTACGCCCTTCCTCAT
	GCCATTTCTGCTCAAAGTC

Expression profile of *Hs-BTG1*

Totally, we tested 10 tissues from three mussels, including intestines, gills, gonads, mantle, ax foot, adductor muscle, blood cells, hepatopancreas, kidneys, and hearts. Total RNA was extracted and treated by RNase-free DNase I (Promega). 1.5 µg total RNAs were reverse transcribed using MMLV RT Kit (Promega) under following reaction conditions: 37 °C, 60 min, 75 °C 5 min, 4 °C, hold. Expression profiles of *BTG1* from different tissues were detected by quantitative PCR using SYBR Premix Ex Taq II kit (TaKaRa) with β -actin as an

internal reference. The amplification condition was as follows: 95 °C 5 min; 95 °C 30 s, 60 °C 30 s, 72 °C 30 s, 40 cycles; 72 °C 10 min. $2^{-\Delta\Delta CT}$ relative quantification method was used. Tissues that showed the lowest expression were set as controls. Each sample had three replicates, and all experiments were repeated in triplicate.

Cadmium (Cd²⁺) stress test

We determined the test concentrations following the method reported by literature (Kim et al, 2012). The standard Cd²⁺ concentration (≤ 0.005 mg/L) according to

"Water quality standard for fishery" GB7471 (0.005 mg/L) as well as 1 000 times the standard concentration (5mg/L) were respectively set as the control and experimental groups. The exposure method was static contact with $\text{CdCl}_2 \cdot 5\text{H}_2\text{O}$ infected water. Totally, 20 healthy mussels in each group were cultured in an aquarium with 20 L test solution. The water was changed by 50% every day and the concentration was maintained during the trial period. We randomly selected 3–4 mussels at exposure points of 0 h, 6 h, 12 h, 24 h, 48 h, 96 h, and from these total RNA from the hepatopancreas, kidneys, blood cells, and mantle was extracted. This experiment was repeated three times.

Target gene expression analysis under Cd^{2+} stress

We performed SYBR green-based real-time quantitative PCR assay (He et al, 2013; Peng et al, 2012a, b) to detect the expression changes of target gene in the 5 mg/L concentration of cadmium stress conditions. The final relative expression result is the product of two relative expression values: the $2^{-\Delta\Delta\text{CT}}$ value of the experimental group (5mg/L) at different time points relative to 0h, and the $2^{-\Delta\Delta\text{CT}}$ value of the experimental group relative to the control group at the same time point. The mRNA expression difference of *Hs-BTG1* was analyzed using SPSS 16.0 (SPSS, inc. Chicago, USA). $P < 0.05$ and $P < 0.01$ were set as significant and highly significant, respectively.

RESULTS

Sequence analysis of *Hs-BTG1*

The full length cDNA of *Hs-BTG1* was found to be 1 402 bp and involves a complete coding sequence of 525 bp, including an ORF encoding 174 amino acids, 306 bp 5'-UTR, 571 bp 3'-UTR, with a typical AATAAA and poly A tail (Figure 1; sequence submitted to NCBI, accession number KF015272). BlastP analysis (<http://blast.ncbi.nlm.nih.gov/Blast.cgi>) showed that the Hs-BTG1 has one typical conserved N terminal domain shared by BTG Superfamily (*i.e.*, BTG/TOB domain) which is characterized by two well-conserved boxes named A and B (Figure 1, Figure 2) (Fu et al, 2012; Sakaguchi et al, 2001; Winkler, 2010); SignalP-4.1 prediction identified no signal peptide sequence.

Homology and cluster analysis

Amino acid sequences of BTG1 from *H. schlegelii*, *C. gigas*, *D. rerio*, *X. laevis*, *G. gallus*, *M. musculus*, and

H. sapiens were compared using Clustal W (Figure 2), showing that Hs-BTG1 has the highest identity (50.57%) with BTG1 from *C. gigas*. Hs-BTG1 has lower identity with BTG1 in vertebrates, with an identity of 35.67% with human BTG1. We next performed a homology modeling of BTG1 from *H. schlegelii* and *C. gigas* according to reported 3D structure of human BTG1 protein (Yang et al, 2008; Winkler, 2010), and found each presents a similar 3D structure (Figure 2) with five α -helices and two antiparallel β -sheets.

Cluster analysis (Figure 3) using Mega4.1 (Neighbor-Joining, NJ) showed that BTGs of vertebrates and invertebrates clustered into two branches. In invertebrates, the Hs-BTG1 was clustered firstly together with the *C. gigas* BTG1, and then BTG1 of *L. gigantea*, *L. Singoriensis*, *A. florae*, and *C. formosanus* along with the aforementioned two BTG1 were clustered into one large branch. In vertebrates, another large branch was also formed mainly by some BTG1s from fish to humans, as well as BTG2 from *G. gallus*, *M. musculus*, and *H. sapiens*.

Expression profile of Hs-BTG1

Expression profile of *Hs-BTG1* in different tissues was analyzed via real-time quantitative PCR (RT-qPCR) (Figure 4). Expression of *Hs-BTG1* mRNA was detected in all 10 tissues—intestines, gills, gonads, mantle, ax foot, adductor muscle, blood cells, hepatopancreas, kidney, and heart—but was most highly expressed in the hepatopancreas and then the gills, with while blood cells exhibited the lowest expression of *Hs-BTG1*.

Expression change under Cadmium stress

Expression changes of *Hs-BTG1* in hepatopancreas, kidneys, blood cells, and mantle under Cadmium (Cd^{2+}) exposure for 0 h, 6 h, 12 h, 24 h, 48 h, 96 h were shown in Figure 5. In the hepatopancreas, *Hs-BTG1* expression significantly increased at 6 h, decreased at 12 h, then increased at 24 h, reaching a peak at 48 h (2.03-fold of the standard control group) and then falling back at 96h. The overall expression pattern in blood cells was quite similar, with the only difference being a continued decrease at 24 h, though the expression level also peaked at 48h (2.5-fold of the standard control group). In kidney tissue, the *Hs-BTG1* transcription dropped until an increase at 24 h (2.2-fold of the standard control group) before slowly returning to normal levels between 48 h-96 h. Similarly, *Hs-BTG1* expression level in mantle also reached the peak at 24 h (2.07-fold of the standard control

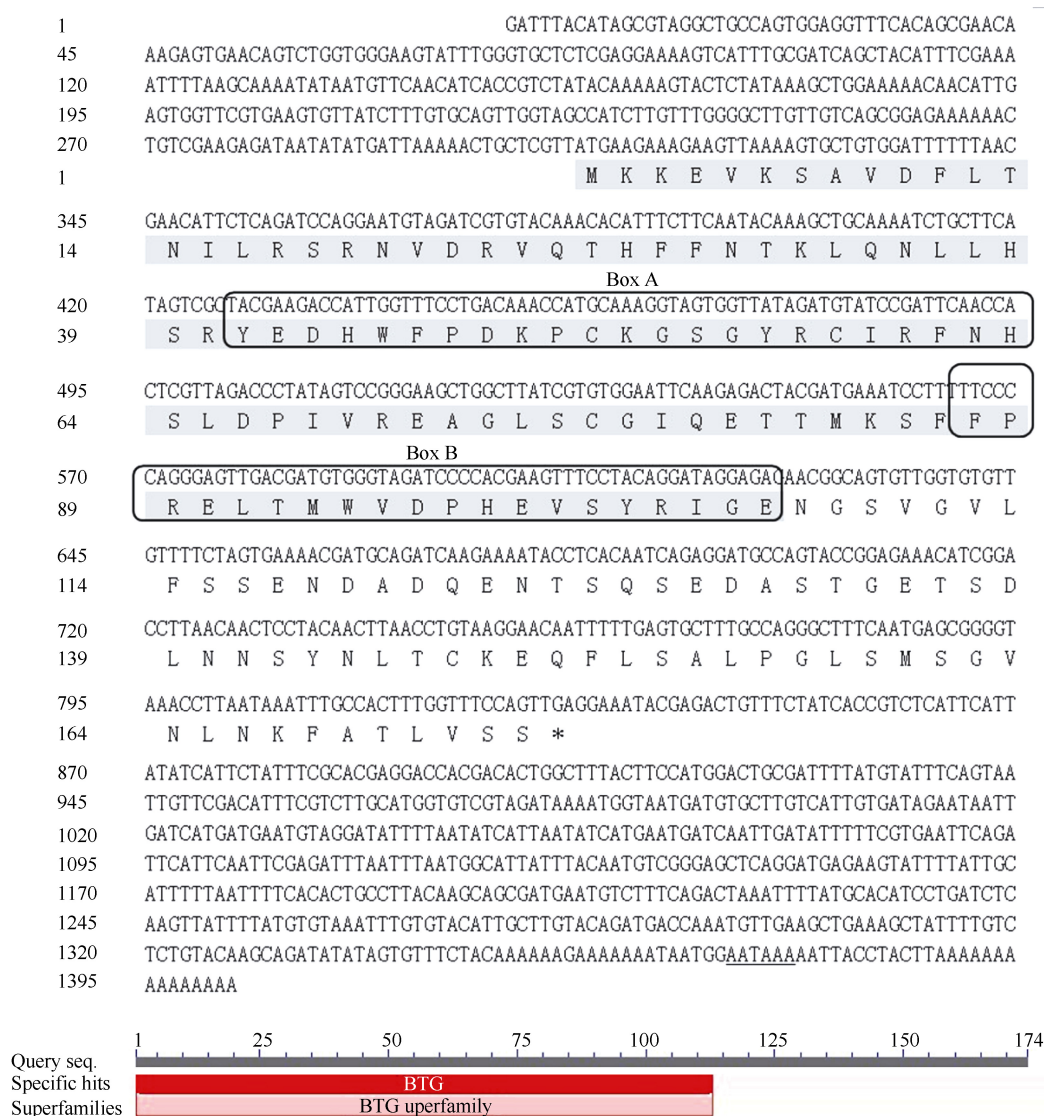


Figure 1 cDNA and deduced amino acid sequence of BTG1 in *Hyriopsis schlegelii*

Nucleotide and deduced amino acid sequence were numbered on the left. The BTG/TOB function domain was shaded and the two highly conserved domains (BTG Boxes A and B) were indicated with a rounded rectangle. The stop codon TGA and the polyadenylation signal AATAAA were tagged with an asterisk and underline, respectively. The lower image depicts the BlastP result for Hs-BTG1.

group), but decreased at 48 h, and then showed a slight increase at 96 h.

DISCUSSION

To date, there are 6 identified members of the BTG/TOB family in vertebrates, named for its BTG tag sequence in the N terminal. The BTG region contains two highly conserved homologous short motifs, namely A box (YKHHWFDRPNKSGYRCIRIN) and B box (LPSELTLWVDPFEVSYRIGE). These two boxes are separated by 20–25 nonconservative amino acids (Guehenneux et al, 1997; Sakaguchi et al, 2001; Fu et al,

2012). The A box seems to have an anti-proliferation function, while the B box appears act as the binding sites of its target molecule (Yang et al, 2008). Among mammals, the BTG/TOB family proteins can be classified into 3 subfamilies based on different sequence length of the C terminal: BTG1 and BTG2 as a subgroup, BTG3 and BTG4 as another subfamily, while TOB1 and TOB2 as the third subgroup (Matsuda et al, 2001; Mauxion et al, 2009; Winkler, 2010), with both BTG1 and BTG2 having a shorter C terminal and an extra 8–10 amino acids in the N terminal compared with other two subgroups (Winkler, 2010).

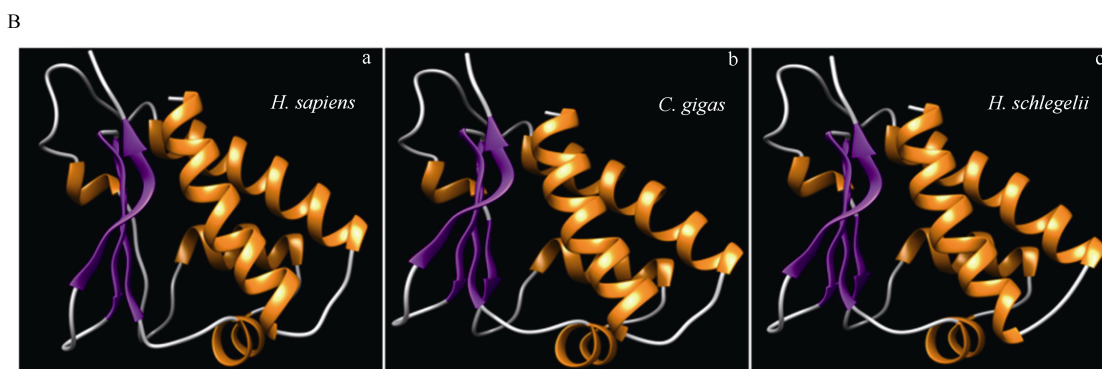
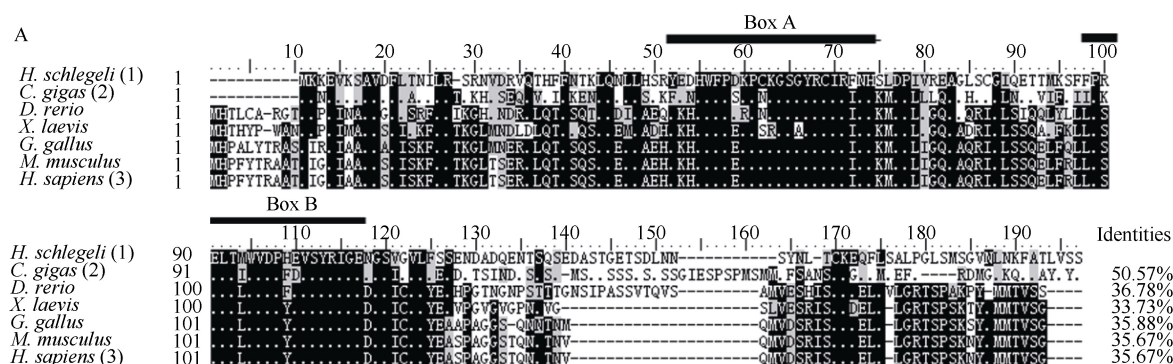


Figure 2 Multiple alignment of BTG1 between *Hyriopsis schlegelii* with other species

(A) Alignment of the deduced amino acid sequence of *H. schlegelii* BTG1 with the corresponding sequences from other species; (B) the tertiary (3D) structures of *Homo sapiens* BTG1 (a), *Crassostrea gigas* BTG1 (b), and *H. schlegelii* BTG1 (c) modeled in SWISS-MODEL. The highly conserved A Box and B Box regions are marked in (A) and a schematic representation of the α -helical (yellow) and β -sheet (purple) structural elements are present in (B). a. *H. sapiens*: NP_001722.1 BTG1, b. *C. gigas*: EKC27510.1 BTG1, c. *H. schlegelii* BTG1: AGT79958.1; *C. gigas*: EKC27510.1; *Danio rerio*: NP_956314.1; *Xenopus laevis*: NP_001080825; *Gallus gallus*: CAA45507.1; *Mus musculus*: NP_031595.1; *H. sapiens*: NP_001722.1. “...” indicates the same amino acid; “---” indicates the default at the corresponding sites.

Though *BTG1* is comparatively well characterized in mammals and other vertebrates, little has been done on freshwater shellfish. Here, for the first time, we identified a homologous gene (*Hs-BTG1*) of the BTG/TOB family in *H. schlegelii*. The motif structure of the deduced amino acid sequences also contains highly conserved A and B box. BlastP analysis showed that *Hs-BTG1* has the highest identity (50.57%) with *C. gigas* BTG1. Homology modeling further showed that both *H. schlegelii* and *C. gigas* BTG1 present similar 3D structure with the reported human BTG1 protein (Yang et al, 2008; Winkler, 2010). Interestingly, both *H. schlegelii* and *C. gigas* BTG1 have a truncated (for 8–10 amino acids) N terminal as compared with vertebrate BTG1, but the length of their C terminal is roughly consistent with the corresponding part of vertebrate BTG1. We also found that *Hs-BTG1* and *C. gigas* BTG1 were clustered together, both belonging to the invertebrate BTG1 large branch, while vertebrate BTG1 and BTG2 fell into another large branch. These

results concur with both BlastP and traditional classification, so consequently the sequence we obtained was classified into the first subgroup in the BTG/TOB family and termed as the homologue (*Hs-BTG1*) to other species BTG1.

It is worth noting that there are a very limited number of BTG/TOB members identified in invertebrates, making it difficult to accurately position the relationship between *Hs-BTG1* and other BTG/TOB members from the constructed cluster tree (Fu et al, 2012), which is supported by the low Bootstrap value in some branches. Additionally, while BTG1 from invertebrates (such as *C. gigas* and *H. schlegelii*) showed relatively low identity compared with vertebrate BTG1, they have conserved motif and similar 3D structure shared by the entire BTG family, implying that BTG1 of lower vertebrate animals may retain some conservative function and also possess different functions as compared to their vertebrate homologs (Matsuda et al, 2001).

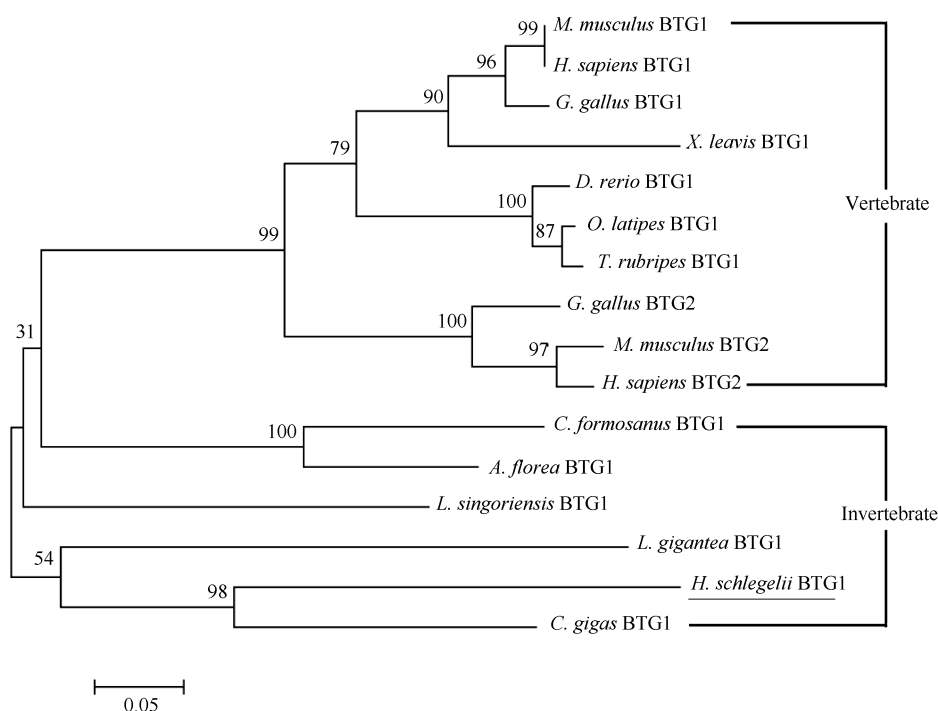


Figure 3 Phylogenetic tree of BTG1 from *Hyriopsis schlegelii* and other animals

Mus musculus BTG1: NP_031595.1; *Homo sapiens* BTG1: NP_001722.1; *Gallus gallus* BTG1: NP_990681.1; *Danio rerio* BTG1: NP_956314.1; *Oryzias latipes* BTG1: XP_004083105.1; *Takifugu rubripes* BTG1: XP_003972839; *Xenopus laevis* BTG1: NP_001080825; *G. gallus* BTG2: XP_418053; *M. musculus* BTG2: NP_031595.1; *H. sapiens* BTG2: NP_006754.1; *Coptotermes formosanus* BTG1: AGM32529; *Apis florea* BTG1: XP_003697190; *Lycosa singoriensis* BTG1: ABX75488; *Lottia gigantea* BTG1: ESO88805; *H. schlegelii* BTG1: AGT79958.1; *C. gigas* BTG1: EKC27510.1. The number in the branch is the bootstrap value.

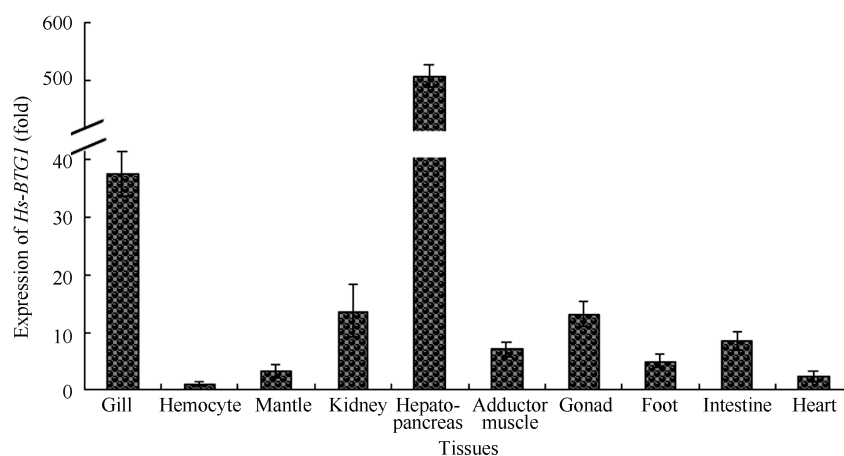


Figure 4 Expression level of *Hs-BTG1* mRNA in different tissues

The vertebrate BTG family was previously reported to be involved in a variety of biological processes, e.g., cell proliferation and differentiation. For example, *BTG1* expression is maximal in the G0/G1 phases of cell cycle and down-regulated throughout the G1 phase (Rouault et al, 1992; Matsuda et al, 2001), suggesting that the expression of BTG1 may inhibit cell proliferation by

keeping cell cycle arrest in the G0 phase. *In vitro* experiments further demonstrated that overexpression of BTG1 can inhibit cell proliferation and promote apoptosis (Rodier et al, 2001; Hata et al, 2007; Lee et al, 2003; Matsuda et al, 1992; Rouault et al, 1992). Several studies have shown that BTG1 is also involved in cell differentiation and early embryonic development, for

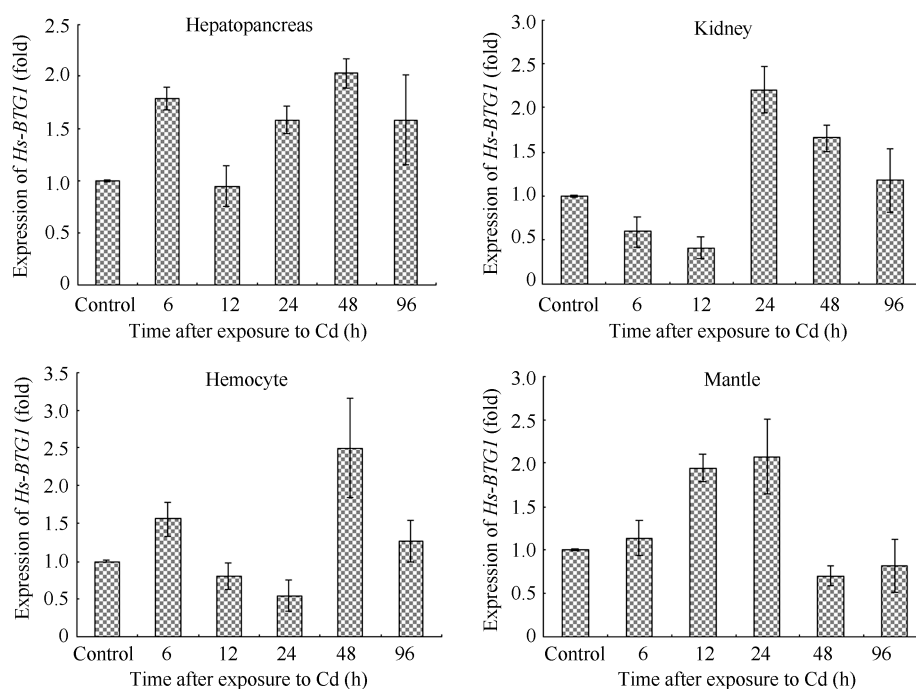


Figure 5 Fold inductions of *Hs-BTG1* mRNA levels in hepatopancreas (a), kidney (b), haemocytes (c) and mantle (d) after exposure to waterborne Cd exposure (5 mg/L)

Data represent group mean fold induction \pm SD ($n=3$ in each time). Asterisks indicate mean fold induction, which are significantly ($P < 0.05$) different from control values (0.005 mg/L).

example in regulating angiogenesis (Iwai *et al.*, 2004), promoting muscle cell differentiation (Busson *et al.*, 2005), and the gastrulation movement in early *Xenopus* embryo (Wessely *et al.*, 2005).

Several lines of evidence suggest that the biological function of BTG is correlated to its expression, such as in adult pigs and sheep where constitutive expression of BTG1 could be detected in several different tissues (Feng *et al.*, 2011; Zhang *et al.*, 2009). Another study found that the highest expression of human *BTG2* was in the renal proximal tubule, alveolar epithelial cells and prostate basal cell layer (Melamed *et al.*, 2002). During the early embryonic development of *Xenopus*, abnormal *XBTG1* expression may cause embryonic gastrulation failure (Saka *et al.*, 2000), while overexpression of a homologous gene *x-BTG-x* may induce a double axis of the embryo (Wessely *et al.*, 2005). Moreover, expression of *BTG-b* was detectable in embryonic induction region, as well as the forebrain, hindbrain and paraxial mesoderm in zebrafish (Sakaguchi *et al.*, 2001). Meanwhile, the highest level of *BTG1* expression in adult grass carp was found in the liver (Fu *et al.*, 2012), consistent with our present results, suggesting that a maintained high expression of *Hs-BTG1* may play an important role for

implementation of normal physiological function of the hepatopancreas.

As we noted earlier, gene expression analysis under various environmental stress factors is a common method of studying candidate gene's corresponding function(s) (Duan *et al.*, 2013; Wang *et al.*, 2011). In the present study, the highest *Hs-BTG1* transcription level was in the hepatopancreas, with the expression being significantly up-regulated when placed under conditions of heavy metal cadmium stress, and expression in other tissues (e.g., blood cells, mantle, and kidney) also increased under stress, though to a lesser extent. Since BTG1 was previously reported to have anti-proliferation and apoptosis effect in higher vertebrates (Corjay *et al.*, 1998; Lee *et al.*, 2003; Rouault *et al.*, 1992), we speculate that *Hs-BTG1* may also be involved in a similar function under cadmium stress. One intriguing observation garnered from this study was that *Hs-BTG1* in kidney tissues was notably up-regulated, but then fell back. A potential explanation may be that the kidney serves a temporary storage of accumulated environmental cadmium. If so, then inhibition of *Hs-BTG1* expression may contribute to proliferation of the renal cells, and then the increased cells would be able to accumulate

greater amounts of cadmium, while conversely a rapid increase of Hs-BTG1 caused by an exceeding threshold level for renal cells tolerance against cadmium may promote cell apoptosis. Though an intriguing possibility,

the exact mechanisms underlying cadmium stress regulation of *Hs-BTG1* in *H. schlegelii*, as well as other freshwater shellfish and invertebrates, remained to be further studied.

References

- Busson M, Carazo A, Seyer P, Grandemange S, Casas F, Pessemesse L, Rouault JP, Wrutniak-Cabello C, Cabello G. 2005. Coactivation of nuclear receptors and myogenic factors induces the major BTG1 influence on muscle differentiation. *Oncogene*, **24**(10): 1698-710.
- Corjay MH, Kearney MA, Munzer DA, Diamond SM, Stoltenberg JK. 1998. Antiproliferative gene BTG1 is highly expressed in apoptotic cells in macrophage-rich areas of advanced lesions in Watanabe heritable hyperlipidemic rabbit and human. *Laboratory Investigation*, **78**: 847-858.
- Duan YF, Liu P, Li JT, Li J, Gao BQ, Chen P. 2013. Cloning and expression analysis of Cathepsin L cDNA of *Exopalaemon carinicauda*. *Zoological Research*, **34**(1): 39-46. (in Chinese)
- Fu YJ, Huang FG, Yuan T, Gu JR, Luo GQ, Xu H. 2012. Molecular cloning, characterization and expression analysis of B cell translocation gene 1 in grass carp *Ctenopharyngodon idella*. *Journal of Fish Biology*, **80**(3): 669-678.
- Feng Z, Shen H, Du ZQ, Zhu MJ, Fan B, Rothschild MF, Zhao SH, Li CC. 2011. BTG1 as a new candidate gene for muscle growth in pigs: Cloning, expression and association analysis. *Journal of Animal Science and Biotechnology*, **2**(3): 121-130.
- Guehenneux F, Duret L, Callanan MB, Bouhas R, Hayette S, Berthet C, Samarut C, Rimokh R, Birot AM, Wang Q, Magaud JP, Rouault JP. 1997. Cloning of the mouse BTG3 gene and definition of a new gene family (the BTG family) involved in the negative control of the cell cycle. *Leukemia*, **11**(3): 370-375.
- He SH, Peng K, Hong YJ, Wang JH, Sheng JQ, Gu Q. 2013. Molecular properties and immune defense of two ferritin subunits from freshwater pearl mussel, *Hyriopsis schlegelii*. *Fish & Shellfish Immunology*, **34**(3): 865-874.
- Hata K, Nishijima K, Mizuguchi J. 2007. Role for Btg1 and Btg2 in growth arrest of WEHI-231 cells through arginine methylation following membrane immunoglobulin engagement. *Experimental Cell Research*, **313**(11): 2356-2366.
- Iwai K, Hirata K, Ishida T, Takeuchi S, Hirase T, Rikitake Y, Kojima Y, Inoue N, Kawashima S, Yokoyama M. 2004. An anti-proliferative gene BTG1 regulates angiogenesis *in vitro*. *Biochemical and Biophysical Research Communications*, **316**(3): 628-635.
- Kim JH, Rhee JS, Dahms HU, Lee YM, Han KN, Lee JS. 2012. The yellow catfish, *Pelteobagrus fulvidraco* (Siluriformes) metallothionein cDNA: molecular cloning and transcript expression level in response to exposure to the heavy metals Cd, Cu, and Zn. *Fish Physiology and Biochemistry*, **38**(5): 1331-1342.
- Lee H, Cha S, Lee MS, Cho GJ, Choi WS, Suk K. 2003. Role of antiproliferative B cell translocation gene-1 as an apoptotic sensitizer in activation-induced cell death of brain microglia. *Journal of Immunology*, **171**(11): 5802-5811.
- Lu CH, Xie WZ, Zhou GJ. 1998. Studies on *Crassostrea rivularis* as a biological indicator of cadmium pollution. *Journal of Fishery Science of China*, **5**(2): 79-83. (in Chinese)
- Mauxion F, Chen CY, Séraphin B, Shyu AB. 2009. BTG/TOB factors impact deadenylases. *Trends in Biochemical Sciences*, **34**(12): 640-647.
- Melamed J, Kernizan S, Walden PD. 2002. Expression of B-cell translocation gene 2 protein in normal human tissues. *Tissue Cell*, **34**(1): 28-32.
- Matsuda S, Rouault J, Magaud J, Berthet C. 2001. In search of a function for the TIS21/PC3/BTG1/TOB family. *FEBS Letters*, **497**(2-3): 67-72.
- Peng K, Wang JH, Sheng JQ, Zeng LG, Hong YJ. 2012a. Molecular characterization and immune analysis of a defensin from freshwater pearl mussel, *Hyriopsis schlegelii*. *Aquaculture*, **334-337**: 45-50.
- Peng K, Wang JH, Liu TT, Sheng JQ, Shi JW, Shao P, He SH, Hong YJ. 2012b. Expression analysis and immune response of the cathepsin L from freshwater pearl mussel, *Hyriopsis schlegelii*. *Acta Hydrobiologica Sinica*, **36**(6): 1128-1134. (in Chinese)
- Rouault JP, Rimokh R, Tessa C, Paranhos G, French M, Duret L, Garoccio M, Germain D, Samarut J, Magaud JP. 1992. BTG1, a member of a new family of antiproliferative genes. *EMBO Journal*, **11**(4): 1663-1670.
- Rodier A, Rochard P, Berthet C, Rouault JP, Casas F, Daury L, Busson M, Magaud JP, Wrutniak-Cabello C, Cabello G. 2001. Identification of functional domains involved in BTG1 cell localization. *Oncogene*, **20**(21): 2691-2703.
- Sakaguchi T, Kuroiwa A, Takeda H. 2001. Expression of zebrafish btg-b, an anti-proliferative cofactor, during early embryogenesis. *Mechanisms of Development*, **104**(1-2): 113-115.
- Saka Y, Tada M, Smith JC. 2000. A screen for targets of the Xenopus T-box gene Xbra. *Mechanisms of Development*, **93**(1-2): 27-39.
- Wang ZS, Qi ZT, Tian JY, Qiu M, Zhao WH, Wang AM, Huang JT, Guo XJ. 2011. Cloning of hemoglobin- $\alpha 1$ from half-smooth tongue sole (*Cynoglossus semilaevis*) and its expression under short-term hypoxia. *Zoological Research*, **32**(6): 641-646.
- Wessely O, Kim JI, Tran U, Fuentealba L, De Robertis EM. 2005. xBtg-x regulates Wnt/beta-Catenin signaling during early Xenopus development. *Developmental Biology*, **283**(1): 17-28.
- Winkler GS. 2010. The mammalian anti-proliferative BTG/Tob protein family. *Journal of Cellular Physiology*, **222**(1): 66-72.
- Xie K, Xu L, Sheng JQ, Zeng LG, Wang JH, Hong YJ. 2011. The full-length cDNA library of hemocyte induced by *Aeromonas hydrophila* and molecular characteristics of *Cyclophilin A* from *Hyriopsis schlegelii*. *Acta Hydrobiologica Sinica*, **35**(5): 783-789. (in Chinese)
- Yang X, Morita M, Wang H, Suzuki T, Yang W, Luo Y, Zhao C, Yu Y, Bartlam M, Yamamoto T, Rao Z. 2008. Crystal structures of human BTG2 and mouse TIS21 involved in suppression of CAF1 deadenylase activity. *Nucleic Acids Research*, **36**(21): 6872-6881.
- Zhang J, Du LX, Li HB, Wei CH. 2009. Semi-quantitative RT-PCR and bioinformatics analysis of sheep BTG1 gene. *Chinese Journal of Biochemistry and Molecular Biology*, **25**(10): 911-918. (in Chinese)

Cloning the *sterol carrier protein 2* genes of Japanese toad (*Bufo japonicus formosus*) and Chinese toad (*Bufo gargarizans*) and its tissue expression analysis

Yu-Cheng Ji^{3,#}, Hui ZHUGE^{2,#}, Shan-Shan ZHANG³, Shu-Fang ZHANG², Xian-Yu Yang^{1,*}

1. College of Animal Science and Technology, Zhejiang Agricultural and Forestry University, Lin'an 311300, China

2. The Nurturing Station for the State Key Laboratory of Subtropical Silviculture, Zhejiang Agricultural and Forestry University, Lin'an 311300, China

3. School of Forestry and Biotechnology, Zhejiang Agricultural and Forestry University, Lin'an 311300, China

Abstract: In this study, to clarify the bioactive polypeptides included in the skins and secretions of *Bufo*, we screened the Japanese toad (*Bufo japonicus formosus*) skin cDNA library by colony polymerase chain reaction (PCR), and obtained a transcript of 1 075 bp consisting of 137 bp 5' untranslated region (UTR), 515 bp 3' UTR and a 423 bp open reading frame (ORF) encoding a polypeptide of 140 amino acid residues (GenBank accession number: KF359945). Homolog analysis showed a 70%–96% homology with sterol carrier protein-2 (SCP-2) present in other animals, which is implicated in lipid metabolism of other organisms. The gene *SCP-2* of Chinese toad (*B. gargarizans*) was cloned from a first strand cDNA of *Bufo* skin (GenBank accession number: KF381341) via PCR, whose encoding polypeptide has only one amino acid difference from that of Japanese toad. Tissue distribution analysis showed that *SCP-2* expressed in all organs tested, though in the liver and spleen it manifested lower expression than in other organs. These findings might indicate *SCP-2* being one of the active ingredients in toad skin. These findings may in turn have implications for further drug development from traditional Chinese medicine sources.

Keywords: *Bufo gargarizans*; *Bufo japonicus formosus*; *SCP-2* cDNA cloning; Tissue expression

Amphibian skin and their secretions have been shown to contain large amount of biologically active compounds, suggesting a new potential source for drug discovery (Clark, 1997; Lai et al, 2002a, 2004; Novković et al, 2012; Rash et al, 2011; Zhao et al, 2014). The potential for novel therapeutics derived from these tissues is not unexpected; skin from the *Bufo* toad (Chan'pi), its cortex (Chan'yi) and secretions (Chan'su) have long been important components included in many prescriptions of traditional Chinese medicine (TCM) used in clinical treatments of several diseases, especially tumor control (Efferth et al, 2009; Liu et al, 2009; Tong, 2011; Xin et al, 2012). Previous reports showed that cinobufocini injection (water soluble extracts of toad skin) possessed excellent anti-tumor curative effects (Qi et al, 2010, 2011; Zhou et al, 2009), likely due to their unique polypeptides (Wu et al, 2012). Despite these

promising findings, little has been done to advance the use of the active compounds in toad skin, especially in China.

China itself is rich of amphibian species and has a long history of developing traditional medicine from unorthodox sources. Similarly, China is up and coming player in the pharmaceuticals and drug development. The key challenge in leveraging these two advantages is first gaining a clearer understanding of the underlying genetic and molecular mechanisms in many traditionally used

Received: 17 February 2014; Accepted: 25 March 2014

Foundation items: This study was supported by the National Natural Science Foundation of China (31071181, 31372149) and the Students' Innovative Training Program of ZAFU (20120207, 20120213)

[#]Authors contributed equally to this work

^{*}Corresponding author, E-mail: yangxy78@zafu.edu.cn

treatments, and second, finding better ways to utilize the available resources more efficiently (Lai et al, 2002b). We previously sought to elucidate the active polypeptide components included in toad-skin and its related materials by first screening the skin plasmid cDNA library of Japanese toad (*Bufo japonicus formosus*) via colony polymerase chain reaction (PCR) (Yuan et al, 2013; Zhang et al, 2013; Zhuge et al, 2013). As part of our other research efforts, we have also begun cDNA cloning from Chinese toad (*B. gargarizans*) skin first strand cDNA (Hu et al, 2013). During these processes, we were able to isolate the cDNAs encoding sterol carrier protein-2 (SCP-2) from both Japanese toad and Chinese toad.

SCP-2 was initially segregated and purified from mouse (*Mus musculus*) liver tissue (Osumi et al, 1980), which is distributed in peroxidase, mitochondria, endoplasmic reticulum and cytoplasm, and functions as intracellular transporters such as cholesterol, lecithin, fatty acid, ester acyl CoA etc (Kriska et al, 2010; Schroeder et al, 2000, 2007). Here we cloned *SCP-2* from two *Bufo* species and conducted RT-PCR analysis on the Chinese toad, and found that SCP-2 is likely one of the effective polypeptides included in toad-skin origin materials. These findings confirm our earlier observation that toad skin (and potentially other tissues) may be viable targets for future development of drug treatments and novel therapeutics.

MATERIALS AND METHODS

Experimental materials and reagents

The proprietary Japanese toad skin plasmid cDNA library held by the Japan Advanced Industrial Science and Technology (AIST, Tsukuba, Japan) was authorized for use by Zhejiang Agricultural and Forestry University (ZAFU) for research as part of a Material Transfer Agreement. Concerning this library, pSD64TR (3 250 bp) has been used as a vector, and *EcoR* I and *Xho* I as cloning sites. The upstream primer of the vector is SP6 (5'-ATTTAGGTGACACTATAGAA-3') and the downstream one is S.D.A. (5'-TTATGTAGCTTAGAGACTC-3'), respectively. The cDNA length ranged from 500–2000 base pairs (bp). For further testing, Chinese toad individuals were obtained from the East lake Campus of ZAFU, and then ice anaesthetized prior to dissection, wherein the organs were removed and cut into small pieces before being frozen in liquid nitrogen. The resulting samples were kept in a –70 °C refrigerator prior

to total RNA extraction.

The RNA extraction kit was purchased from Shanghai Bocai Biotechnology Company; Quantscript RT kit, pGM-T vector and *Escherichia coli* competent cells (DH5α) from Tiangen Biotechnology Limited Company; *Taq* PCR kit from TaKaRa Biotechnology Limited Company; and primer synthesis and DNA sequencing were commissioned by Shanghai Sang'ni Biotechnology Company.

B. japonicus formosus SCP-2 screening

Japanese toad cDNA screening was performed as described previously (Yuan et al, 2013). In brief, Japanese toad skin plasmid cDNA library was transformed into *E. coli* (DH5α), and colony PCR was performed using colony suspension as templates, and SP6 and XhoTT (5'-AGATCTCTCGAGTTTTTTTTTTTTT-3', a self-designed primer complementary with the area encompassing the connection point of cDNA polyA tail and the downstream cloning site of *Xho* I) as primers. Following this process, the recombinant plasmids were collected and double enzyme digested with *EcoR* I and *Xho* I to further confirm positivity, and then sent for sequencing with vector primers SP6 and S.D.A.

B. gargarizans SCP-2 cloning

For *SCP-2* cloning from Chinese toad, total RNA was extracted from its dorsal skin, and a first strand cDNA synthesized based on the manufacturer's protocols. Meanwhile, based on the Japanese toad *SCP-2* sequence, an upstream primer (SCP-2-S: 5'-CGTGGTCGTTACG TTATACAAG-3') and a downstream primer (SCP-2-R: 5'-GAAATTAGTGGCTTTTATTAAGTG-3') were designed for use in RT-PCR. The PCR product was ligated into a pGM-T vector and then sequenced with vector upstream primer T7 and downstream primer SP6.

Sequence Analysis

DNASTar/EditSeq was used to find the open reading frame (ORF) and deduce their encoding protein amino acid sequence. Potential phosphorylation sites were predicted via Net Phos 2.0. A further 17 *SCP-2* protein sequences from other animals were downloaded by NCBI blast program (<http://blast.ncbi.nlm.nih.gov/Blast.cgi>) and aligned with DNASTar/MegAlign. Phylogenetic tree based on *SCP-2* amino acid sequences was constructed using the neighbor-joining method by MEGA5.1 (bootstrap with 1 000 replications).

SCP-2 tissue expression analysis by RT-PCR

Total RNA samples were extracted from different Chinese toad organs including brain, heart, lung, liver, spleen, kidney, stomach, intestines, fallopian tube and skin, and their first strand cDNA were synthesized as mentioned above. Samples of the different tissue were analyzed via PCR for SCP-2 expression using a reference gene of β -actin (upstream primer: 5'-TTGAGAC CTTCAACACC-3'; downstream primer: 5'-CTTGATGT CACGCACAA-3').

RESULTS

SCP-2 screening and sequence analysis of *B. japonicus formosus*

Restriction enzyme digestion with *EcoR* I and *Xho* I showed one recombinant plasmid screened from Japanese toad skin plasmid cDNA library had a cDNA insert of about 1000 bp, which was later confirmed by sequencing analysis (Figure 1). The transcript is 1 075 bp consisting of 137 bp 5'UTR (untranslated region), 515 bp 3' UTR and a 423 bp ORF encoding a polypeptide of 140 amino acid residues, which showed high homology with sterol carrier protein-2 (SCP-2) found in other animals. The clone we screened in the present study (named *B. japonicus formosus* SCP-2), has been deposited into GenBank (accession number: KF359945).

SCP-2 cloning and sequence analysis of *B. gargarizans*

From Chinese toad skin first strand cDNA, a 920 bp

transcript was obtained consisting of 22 bp 5' UTR, 475 bp 3' UTR and 423 bp ORF encoding a polypeptide consisting of 140 amino acid residues (Figure 2). The only difference between two *Bufo* SCP-2 proteins is that Thr130 in Chinese toad was substituted by Ser in the Japanese toad. This clone was designated as *B. gargarizans* SCP-2 and deposited into GenBank (accession number: KF381341).

Phosphorylation site prediction of *Bufo* SCP-2

From the analysis of phosphorylation site prediction, 10 potential sites (Ser10, Ser11, Ser19, Ser77, Ser79, Ser82, Ser91, Ser93, Thr66 and Tyr44) were found in both *Bufo* species (Table 1), suggesting that SCP-2 expression might be regulated by the upstream factors.

Homology analysis of SCP-2 amino acids

Phylogenetic analysis showed that two *Bufo* species had a homology as high as 96% with *Xenopus (Silurana) tropicalis* and 92% with *Xenopus laevis*, with lower homology ranging from 70% to 91% among 15 other animals (Figure 3). The phylogenetic tree we constructed showed 9 different mammals (*Homo sapiens*, *Bos taurus*, *Rattus norvegicus*, *Mus musculus*, *Mesocricetus auratus*, *Capra hircus*, *Camelus ferus*, *Ictidomys tridecemlineatus* and *Sus scrofa*) gathered in a branch, 5 different birds (*Gallus gallus*, *Falco peregrinus*, *Falco cherrug*, *Pseudopodoces humilis* and *Melopsittacus undulatus*) in a branch, 1 reptile (*Anolis carolinensis*) in another branch, 2 frogs (*X. laevis* and *X. Silurana tropicalis*) in a branch, 2 toads (*B. gargarizans* and *B. japonicus formosus*) in a branch, and 2 fish in a branch (Figure 4),

```

CCACAGGCCCTGGCTCAGTGTGCAGAGCTCTGCTGGCAGCTCCGAGGTACGGCTGGGAAAAGACAGGTTCCGGGAGCCAAGCTCGCTCTGC 90
AGCACAACATCGGACTAGGGGGGGCCGTGCTGTTACGTTATACAAATGGCTTTCCGGACGCAGCAGCCAGATCTTCCCGTATCCAGC 180
      M G F P D A A A R S S R I Q
TGAATCCGACCAGCGCCGAAGACGGATTTAAAGCCCAGTTTGATTTCAAGGAAATTGAGAAGAAATTGAAACAGGAAGGGGAGCAGTATG 270
L N P T S A E D G F K A Q F V F K E I E K K L K E E G E Q Y
TTAAGAAGATTGGAGGAGTCTTTCCCTTTAAAGTGAAGGATGGACCTGGTGGAAAAGAGGCAAC TTGGTGGTTGATGTGAAGAACGGCA 360
V K K I G G V F A F K V K D G P G G K E A T W V V D V K N G
AAGGCTCTGTGTCCTTCGACTCCGATAAGAAAGCGGAC TGTACGATCTC AATGTCCGACTCTGACCTAT TGGCTCTGATGACCGGCCAGA 450
K G S V S F D S D K K A D C T I S M S D S D L L A L M T G Q
TCAATCCACAGACCGCTTTCTTCAGGGCAAGCTGAAAGTCACTGGAAATATGGGCTTGCCCATGAAGTGCAGAGCCTCCAGCTGCAGC 540
I N P Q T A F F Q G K L K V T G N M G L A M K L Q S L Q L Q
CTGTGAAGCCAAGCTCTGAGAGATCGTCCGTCCGATACATGAGAAATGCCAGCAGTACCCAGATGCCAACCCCTCTGATGCCAGAT 630
P V K A K L
GTCATCGATGCTGGGCTC TAGAGGACCAATCACAACTGCTGCTTTCCCTACCCAAGAAT AAAGAATCATGTCCCCTTTATTTCTAAGCAG 720
GTGGCAGTGCATC TGGCAGCTGTACATGTATATAGGTGTACGAATCCGGAATCTGGCTACGATGCCAGTCTGTTTGAAGATTAAGGC 810
GTTTGTAGGATGGGGCTTCTAACGGTGTGACTTAATCTGATGCTCTTCTGCTGCTCTTCAAC ACTAATGGATTTAAATAATTTCGGAG 900
GGCGATCTATAGCGCAGCAGTGATTTAATCCCTGTAATCTTGGGATAGGAGGCAGGTCTCTGCTCCGGCGCTGAACGCCACGGATGCAG 990
AATTCCTAACCTGTTAATAGTCAGAATAACACTTAATAAAAGCCACTAATTC GAAAAA AAAAAA AAAAAA AAAAAA AAAAAA 1075

```

Figure 1 SCP-2 cDNA and its deduced amino acid sequence of *Bufo japonicus formosus*

Start and stop codons were enclosed by line box. —: Polyadenylation signal; =: Poly(A) tail.

CGTGGTGGTTACGTTATACAAATGCGCTTTCCGGACGACGAGCCAGATCTTCCGTAATCCAGCTGAATCCAAACGAGCCCGAAGACGG 90
 1 M G F P D A A A R S S R I Q L N P T S A E D G
 ATTTAAAGCCAGTTTGTATTCAAGAAATCGAAGAAATTAAGAGGAGGAGGAGCAGTACGTTAAGAGATTGGAGGAGTCTTTGC 180
 F K A Q F V F K E I E K K L K E E G E Q Y V K K I G G V F A
 CTTTAAAGTGAAGGATGGACCTGGTGGAAAAGAGGCACTTGGTGGTTGATGTGAAGAACGGCAAGGCTCGGTGTCTTCGACTCCGA 270
 F K V K D G P G G K E A T W V V D V K N G K G S V S F D S D
 TAAGAAAGCCGATGTACGATCTCAATGTCCGACTCTGACCTATGGCTCTGATGACCGCCAGATCAATCCACAGACCGCTTTCTTCCA 360
 K K A D C T I S M S D S D L L A L M T G Q I N P Q T A I F F Q
 GGGCAAACTGAAAGTCAC TGGAAATATGGGTCTGGCCATGAAGTTCGAGACTCTCCAGCTGCAGCCTGTGAAAGCCAAGCTCTGAAGAGA 450
 G K L K V T G N M G L A M K L Q T L Q L Q P V K A K L
 TCGTGGCTGGATACATGAGAAAAGCCAGCAGTACAGCAGATGCCAACCTCTTCTGATGCCAGATGTATCGATGCTGGCATCTACAGGA 540
 CCAATCACAACTGCTGCTTCCCTACCCAAAGATAAAGAAATCATGTCCCTTTATTTCTAAGCAGGTGGCAGTGATCTGCCACGCTGT 630
 CATGTATATAGGTGTACGAATCCGGAGTCTACGATGCCAGTCTGTTAGAAATTAAGGCCTTTGTAGGATGGGGCTCTAACCGTGTGA 720
 CTTAATCTGGTGTCTTCTGTCTTCTCAACACTAATGGATTAAAATGATTT CAGAGCGGATCTATAGCGCAGCAGTGATTTAATCC 810
 CTGTAATCTTGGGATAGGAGGACGAGTCTCTGCGCCGGCCCTGAACGCCAGGATGCAGAAATCTCTAACTGTATAGTCAGAATAAC 900
 ACTTAATAAAGCCACTAAT 920
 2

Figure 2 SCP-2 cDNA and its deduced amino acid sequence of *Bufo gargarizans*

Start and stop codons were enclosed by line box. 1: Upstream primer, SCP-2-S; 2: Downstream primer, SCP-2-R; —: polyadenylation signal.

Bufo gargarizans MGFFDAAA--RSSRQLNPTS--AEDGFKAQVFKEIEKKLKEEGEQVKKIGGVFAFKVKDGGGGKEATW 67
Bufo japonicus formosus MGFFDAAA--RSSRQLNPTS--AEDGFKAQVFKEIEKKLKEEGEQVKKIGGVFAFKVKDGGGGKEATW 67
Xenopus laevis (NP_001088024.1) // MGFFDAAA--KSSGHRMATS--ASDGFKAQVFKEIEKKLKEEGEQVKKIGGVFAFKVKDGGGGKEATW 463
Xenopus (Silurana) tropicalis (NP_001015795.1) // MGFFDAAA--KSSGHRMATS--AEDGFKAQVFKEIEKKLKEEGEQVKKIGGVFAFKVKDGGGGKEATW 463
Danio rerio (NP_001006093.1) // MRVPEVS--SSARVQAVITSAAGLEGFKAHAFVQEEINKKLQEDGGEQVKKIGGVFAFKVKDGGGGKEATW 69
Oreochromis niloticus (XP_003444345.1) // MGFFDAAA--RNROICAVPTKA--BVDGFKADLVFKEIEKKLKEEGEQVKKIGGVFAFKVKDGGGGKEATW 467
Anolis carolinensis (XP_003220339.1) // MGFFDAAA--SDGRVTAVELSA--AVDGFKSHLVFKEIEKKLKEEGEQVKKIGGVFAFKVKDGGGGKEATW 419
Gallus gallus (XP_004936856.1) // V-----CT---VTGRFAAVFLSA--BVDGFKSHLVFKEIEKKLKEEGEQVKKIGGVFAFKVKDGGGGKEATW 64
Melopsittacus undulatus (XP_005151341.1) MGFFDAAA--RTHQIEAAPTSA--ASDGFKANLVFKEIEKKLKEEGEQVKKIGGVFAFKVKDGGGGKEATW 67
Ictidomys tridecemlineatus (XP_005316699.1) MGFFDAAA--STGRILAAVFLSA--AVDGFKSHLVFKEIEKKLKEEGEQVKKIGGVFAFKVKDGGGGKEATW 67
Falco cherrug (XP_005440424.1) MGFFDAAA--STGRILAAVFLSA--AVDGFKSHLVFKEIEKKLKEEGEQVKKIGGVFAFKVKDGGGGKEATW 67
Falco peregrinus (XP_005231734.1) MGFFDAAA--SNSRTAAVFLSA--AVDGFKANLVFKEIEKKLKEEGEQVKKIGGVFAFKVKDGGGGKEATW 67
Pseudopodoces humilis (XP_005521224.1) // MGFFDAAA--RTHQIEAAPTSS--AVDGFKANLVFKEIEKKLKEEGEQVKKIGGVFAFKVKDGGGGKEATW 429
Capra hircus (XP_005678455.1) // MGFFDAAA--RTHQIEAAPTSS--AVDGFKANLVFKEIEKKLKEEGEQVKKIGGVFAFKVKDGGGGKEATW 67
Camelus ferus (XP_006180210.1) // MGFFDAAA--RTHQIEAAPTSS--SVDFGKANLVFKEIEKKLKEEGEQVKKIGGVFAFKVKDGGGGKEATW 470
Bos taurus (DAA3T177.1) // MGFFDAAA--RSPQVEAAPTSS--TLDGFKANLVFKEIEKKLKEEGEQVKKIGGVFAFKVKDGGGGKEATW 67
Sus scrofa (XP_003482126.1) MGFFDAAA--RTHQIEAAPTSS--AGDGFKANLVFKEIEKKLKEEGEQVKKIGGVFAFKVKDGGGGKEATW 70
Mus musculus (AAA40099.1) MGFFDAAA--RTHQIEAAPTSS--AGDGFKANLVFKEIEKKLKEEGEQVKKIGGVFAFKVKDGGGGKEATW 70
Rattus norvegicus (CAA43060.1) MGFFDAAA--RTHQIEAAPTSS--AGDGFKANLVFKEIEKKLKEEGEQVKKIGGVFAFKVKDGGGGKEATW 68
Homo sapiens (NP_001007101.1) MGFFDAAA--RTHQIEAAPTSS--AGDGFKANLVFKEIEKKLKEEGEQVKKIGGVFAFKVKDGGGGKEATW 68
Mesocricetus auratus (XP_005072201.1) MGFFDAAA--RTHQIEAAPTSS--AGDGFKANLVFKEIEKKLKEEGEQVKKIGGVFAFKVKDGGGGKEATW 68

Bufo gargarizans VVDVKNKGKSVSFDSDKKADCTISMSDSDLLALMTGQINPQTAFQGGKLVGTGNMGLAMKLNQLQLQPVKAKL 140
Bufo japonicus formosus VVDVKNKGKSVSFDSDKKADCTISMSDSDLLALMTGQINPQTAFQGGKLVGTGNMGLAMKLNQLQLQPVKAKL 140
Xenopus laevis (NP_001088024.1) VVDVKNKGKSVVDVNSDKKADCTITMADADLLALMTGKMNPTAFQGGKLVGTGNMGLAMKLNQLQLQPVKAKL 536
Xenopus (Silurana) tropicalis (NP_001015795.1) VVDVKNKGKSVVDVNSDKKADCTITMADADLLALMTGKMNPTAFQGGKLVGTGNMGLAMKLNQLQLQPVKAKL 536
Danio rerio (NP_001006093.1) VVDVKNKGKSVHNSDKKADCTITMADADLLALMTGKMNPTAFQGGKLVGTGNMGLAMKLNQLQLQPVKAKL 142
Oreochromis niloticus (XP_003444345.1) VVDVKNKGKSVHNSDKKADCTITMADADLLALMTGKMNPTAFQGGKLVGTGNMGLAMKLNQLQLQPVKAKL 139
Anolis carolinensis (XP_003220339.1) VVDVKNKGKSVVDVNSDKKADCTITMADADLLALMTGKMNPTAFQGGKLVGTGNMGLAMKLNQLQLQPVKAKL 540
Gallus gallus (XP_004936856.1) VVDVKNKGKSVVDVNSDKKADCTITMADADLLALMTGKMNPTAFQGGKLVGTGNMGLAMKLNQLQLQPVKAKL 492
Melopsittacus undulatus (XP_005151341.1) VVDVKNKGKSVVDVNSDKKADCTITMADADLLALMTGKMNPTAFQGGKLVGTGNMGLAMKLNQLQLQPVKAKL 137
Ictidomys tridecemlineatus (XP_005316699.1) VVDVKNKGKSVVDVNSDKKADCTITMADADLLALMTGKMNPTAFQGGKLVGTGNMGLAMKLNQLQLQPVKAKL 140
Falco cherrug (XP_005440424.1) VVDVKNKGKSVVDVNSDKKADCTITMADADLLALMTGKMNPTAFQGGKLVGTGNMGLAMKLNQLQLQPVKAKL 140
Falco peregrinus (XP_005231734.1) VVDVKNKGKSVVDVNSDKKADCTITMADADLLALMTGKMNPTAFQGGKLVGTGNMGLAMKLNQLQLQPVKAKL 140
Pseudopodoces humilis (XP_005521224.1) VVDVKNKGKSVVDVNSDKKADCTITMADADLLALMTGKMNPTAFQGGKLVGTGNMGLAMKLNQLQLQPVKAKL 502
Capra hircus (XP_005678455.1) VVDVKNKGKSVLPNSDKKADCTITMADADLLALMTGKMNPTAFQGGKLVGTGNMGLAMKLNQLQLQPVKAKL 543
Camelus ferus (XP_006180210.1) VVDVKNKGKSVLPNSDKKADCTITMADADLLALMTGKMNPTAFQGGKLVGTGNMGLAMKLNQLQLQPVKAKL 543
Bos taurus (DAA3T177.1) VVDVKNKGKSVLPNSDKKADCTITMADADLLALMTGKMNPTAFQGGKLVGTGNMGLAMKLNQLQLQPVKAKL 140
Sus scrofa (XP_003482126.1) VVDVKNKGKSVLPNSDKKADCTITMADADLLALMTGKMNPTAFQGGKLVGTGNMGLAMKLNQLQLQPVKAKL 140
Mus musculus (AAA40099.1) VVDVKNKGKSVLPNSDKKADCTITMADADLLALMTGKMNPTAFQGGKLVGTGNMGLAMKLNQLQLQPVKAKL 143
Rattus norvegicus (CAA43060.1) VVDVKNKGKSVLPNSDKKADCTITMADADLLALMTGKMNPTAFQGGKLVGTGNMGLAMKLNQLQLQPVKAKL 143
Homo sapiens (NP_001007101.1) VVDVKNKGKSVLPNSDKKADCTITMADADLLALMTGKMNPTAFQGGKLVGTGNMGLAMKLNQLQLQPVKAKL 140
Mesocricetus auratus (XP_005072201.1) VVDVKNKGKSVLPNSDKKADCTITMADADLLALMTGKMNPTAFQGGKLVGTGNMGLAMKLNQLQLQPVKAKL 140

Figure 3 *Bufo* SCP-2 amino acid sequence alignment with other animal species

which is consistent with the traditional animal taxonomy.

SCP-2 expression in different organs of *B. gargarizans*

RT-PCR detection of *B. gargarizans* SCP-2 in the brain, heart, lung, liver, spleen, kidney, stomach, intestines, fallopian tube and dorsal skin (Figure 5) showed that SCP-2 was expressed in all tested organs, though the expression was lower in both liver and spleen as compared with other organs.

DISCUSSION

Previous studies found that SCP-2 is involved in adjusting concentrations of cholesterol inside and outside cell membranes via activation of cholesterol hydase, and participating in regulating cholesterol transport in the cell culture system (Kriska et al, 2010; Schroeder et al, 2000, 2007). Many human diseases—diabetes, arteriosclerosis, Zellweger, NPC disease and gallstones—have similarly

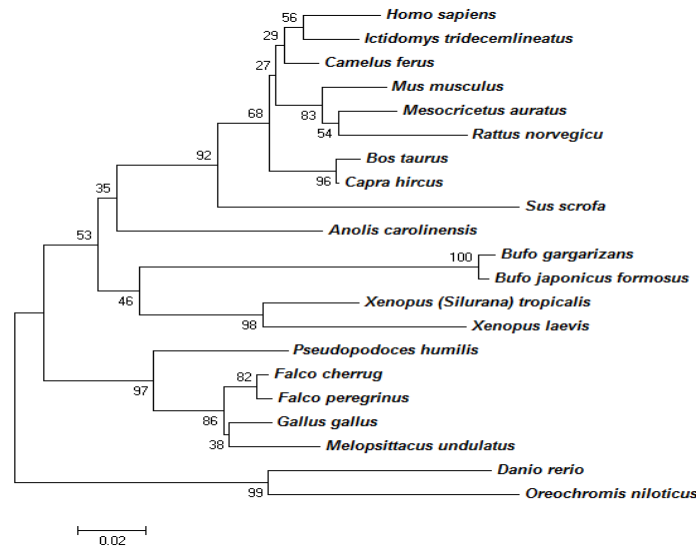


Figure 4 Phylogenetic tree of amino acid of SCP-2 between two *Bufo* species and 17 other species

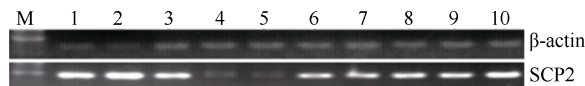


Figure 5 RT-PCR detection of *SCP-2* expression in different organs of *Bufo gargarizans*

M: DNA ladder; 1: brain; 2: lung; 3: heart; 4: liver; 5: spleen; 6: kidney; 7: stomach; 8: intestines; 9: fallopian tube; 10: dorsal skin.

Table 1 *Bufo* SCP-2 phosphorylation site prediction

Position	Context	Score	Prediction
10	AAARSSRIQ	0.552	*S*
11	AARSSRIQL	0.598	*S*
19	LNPTSAEDG	0.995	*S*
77	NGKGSVSFD	0.943	*S*
79	KGSVSFDSD	0.902	*S*
82	VSFDSKKA	0.994	*S*
91	DCTISMSDS	0.992	*S*
93	TISMSDDL	0.955	*S*
66	GKEATWVVD	0.577	*T*
44	EGEQYVKKI	0.926	*Y*

been found to have associations with abnormal expression of SCP-2 (Castelli, 1984; McLean et al, 1996). For example, NPC (Niemann-Picktype C) disease seems to be caused by NPC-peak C protein mutations, and a corresponding drop in liver SCP-2 expression was indicated (Schroeder et al, 2007). In diabetic mice models induced by streptozotocin, the level of SCP-2 in the liver was reduced 60%–90%, alongside a 60% reduction in ovarian SCP-2 (McLean et al, 1996). SCP-2

expression is also related to the formation of cholesterol calculus (Cui et al, 2011).

In the present study, our successful cloning of sterol carrier protein-2 (*SCP-2*) genes from both *B. gargarizans* and *B. japonicus formosus* (Figures 1, 2) indicated that SCP-2 expressed in toad skin as well as in other organs (Figure 5) has a high homology with that in other animals (Figure 3, 4). Due to the function of SCP-2 in adjusting lipid metabolism in numerous animal species and many *SCP-2* expression-related disorders among humans, it may be reasonable to predict that SCP-2 is one of potentially several important ingredients within toad skin.

Our study extends the basic knowledge necessary to assess the potential for *Bufo* skin and other organs for potential drug development. Previously, numerous reports summarized several descriptions on the clinical efficacy of Chan'su, such as detoxification, analgesia, anti-inflammation, antidiarrheal, and antitumor, etc. (Liu et al, 2009; Xin et al, 2012). Curiously though, we found that SCP-2, as a potentially important element in toad skin, is largely involved in adjusting lipid metabolism. However, few reports have ever noted the use of *Bufo* skin in treating lipid metabolism related diseases, aside from an old description concerning Chan'su that pointed out that administration of the medicine could make the symptoms of stasis and stagnation disappear in “BenCaoHuiYan”. This reference itself is rather intriguing, given that it appears in a Ming Dynasty era

book written by Zhu-mo NI published in 1624. Presuming our finding survive replication and further targeted studies are conducted to answer some of the remaining

questions this research poses, our present results offer a potentially novel way of looking at cholesterol-related disease therapeutics using *Bufo* origin materials.

References

- Castelli WP. 1984. Epidemiology of coronary heart disease: the Framingham study. *The American Journal of Medicine*, **76**(2A): 4-12.
- Clark BT. 1997. The natural history of amphibian skin secretions, their normal functioning and potential medical applications. *Biological Reviews of the Cambridge Philosophical Society*, **72**(3): 365-379.
- Cui YF, Li ZL, Zhao EP, Jia YF, Li DH, Zhang J, Cui NQ. 2011. Overexpression of sterol carrier protein 2 in patients with hereditary cholesterol gallstone. *BMC Gastroenterology*, **11**: 10.
- Efferth T, Davey M, Olbrich A, Rücker G, Gebhart E, Davey R. 2009. Activity of drugs from traditional Chinese medicine toward sensitive and MDR1- or MRP1-overexpressing multidrug-resistant human CCRF-CEM leukemia cells. *Blood Cells, Molecules, and Disease*, **28**(2): 160-168.
- Hu QL, Zhang SF, Yang XY, Yu MH, Zhuge H. 2013. *Bufo gargarizans mcl-1* cloning and its prokaryotic recombinant protein expression. *Acta Pharmaceutica Sinica*, **48**(10): 1624-1628. (in Chinese)
- Kriska T, Pilat A, Schmitt JC, Girotti AW. 2010. Sterol carrier protein-2 (SCP-2) involvement in cholesterol hydroperoxide cytotoxicity as revealed by SCP-2 inhibitor effects. *The Journal of Lipid Research*, **51**(11): 3174-3184.
- Lai R, Liang JG, Zhang Y. 2004. Antimicrobial peptides in amphibian skins and their application. *Zoological Research*, **25**(5): 465-468. (in Chinese)
- Lai R, Zhao Y, Yang DM, Zha HG, Lee WH, Zhang Y. 2002a. Comparative study of the biological activities of the skin secretions from six common Chinese amphibians. *Zoological Research*, **23**(2): 113-119. (in Chinese)
- Lai R, Zhao Y, Liu H, Zhang YJ, Lee WH, Zhang Y. 2002b. Bioactive substance of amphibian skin and a study on exploitation and utilization of Chinese amphibian resources. *Zoological Research*, **23**(1): 65-70. (in Chinese)
- Liu JS, Zhang DM, Kurihara H, Ye WC. 2009. Antitumor effects of venenum bufonis and its active components. *Journal of International Pharmaceutical Research*, **36**(2): 115-120. (in Chinese)
- McLean MP, Warden KJ, Sandhoff TW, Irby RB, Hales DB. 1996. Altered ovarian sterol carrier protein expression in the pregnant streptozotocin-treated diabetic rat. *Biology of Reproduction*, **55**(1): 38-46.
- Novković M, Simunić J, Bojović V, Tossi A, Juretić D. 2012. DADP: the database of anuran defense peptides. *Bioinformatics*, **28**(10): 1406-1407.
- Osumi T, Hashimoto T, Ui N. 1980. Purification and properties of acyl-CoA oxidase from rat liver. *The Journal of Biochemistry*, **87**(6): 1735-1746.
- Qi FH, Li AY, Zhao L, Zhang L, Du GH, Tang W. 2010. Apoptosis-inducing effect of cinobufacini on human hepatoma cell line HepG2 and its mechanism of action. *Acta Pharmaceutica Sinica*, **45**(3): 318-323. (in Chinese)
- Qi FH, Li AY, Inagaki Y, Kokudo N, Tamura S, Nakata M, Tang W. 2011. Antitumor activity of extracts and compounds from the skin of the toad *Bufo bufo gargarizans* Cantor. *International Immunopharmacology*, **11**(3): 342-349.
- Rash LD, Morales RA, Vink S, Alewood PF. 2011. De novo sequencing of peptides from the parotid secretion of the cane toad, *Bufo marinus* (*Rhinella marina*). *Toxicon*, **57**(2): 208-216.
- Schroeder F, Atshaves BP, McIntosh AL, Gallegos AM, Storey SM, Parr RD, Jefferson JR, Ball JM, Kier AB. 2007. Sterol carrier protein-2: New roles in regulating lipid rafts and signaling. *Biochimica et Biophysica Acta (BBA) - Molecular and Cell Biology of Lipids*, **1771**(6): 700-718.
- Schroeder F, Frolov O, Starodub BB, Atshaves W, Russell A, Petrescu H, Huang H, Gallegos AM, McIntosh A, Tahotna D, Russell DH, Billheimer JT, Baum CL, Kier AB. 2000. Pro-sterol carrier protein-2: role of the N-terminal presequence in structure, function, and peroxisomal targeting. *The Journal of Biological Chemistry*, **275**(33): 25547-25555.
- Tong ZY. 2011. The research progress of antitumor effects of venenum bufonis. *Journal of Military Surgeon in Southwest China*, **13**(2): 310-312. (in Chinese)
- Wu X, Gao B, Yang J, Bian BL, Wang HJ. 2012. In vitro anti-proliferation effect of peptides from cinobufacini injection. *Acta Pharmaceutica Sinica*, **47**(6): 822-826. (in Chinese)
- Xin XL, Zhang BJ, Su DH, Deng S, Huang SS, Ma XC. 2012. Pharmacology advances in studies on *Bufo bufo gargarizans*. *Progress in Modern Biomedicine*, **12**(3): 588-590, 600. (in Chinese)
- Yuan JQ, Xu Y, Yang XY, Zhuge H, Zhang SF. 2013. Cloning and sequence analysis of clusterin cDNA of *Bufo japonicus formosus*. *Biotechnology Bulletin*, (1): 156-161. (in Chinese)
- Zhang SF, Yuan JQ, Huang H, Zhuge H, Xu Y, Yang XY. 2013. Cloning and bioinformatics analysis of *MCL-1* cDNA of *Bufo japonicus formosus*. *Biotechnology Bulletin*, (4): 179-184. (in Chinese)
- Zhao F, Yan C, Wang X, Yang Y, Wang GY, Lee WH, Xiang Y, Zhang Y. 2014. Comprehensive transcriptome profiling and functional analysis of the frog (*Bombina maxima*) immune system. *DNA Research*, **21**(1): 1-13.
- Zhou X, Yang JK, Zhu LQ, Gao F, Xie RF, Gu XJ. 2009. Meta analysis on cinobufacini injection in hepatocellular carcinoma after transcatheter arterial chemoembolization. *Chinese Journal of New Drugs and Clinical Remedies*, **28**(9): 671-674. (in Chinese)
- Zhughe H, Yuan JQ, Zhang SF, Yang XY. 2013. Cloning and bioinformatic analysis of *TAGLN2* cDNA of *Bufo japonicus formosus*. *Acta Pharmaceutica Sinica*, **48**(2): 250-254. (in Chinese)

MicroRNA signature in response to nutrient restriction and re-feeding in fast skeletal muscle of grass carp (*Ctenopharyngodon idella*)

Xin ZHU^{1,2}, Wu-Ying CHU², Ping WU², Tan YI¹, Tao CHEN^{1,*}, Jian-She ZHANG^{2,*}

1. College of Veterinary Medicine, Hunan Agriculture University, Changsha Hunan 410128, China

2. Department of Bioengineering and Environmental Science, Changsha University, Changsha Hunan 410003, China

Abstract: The grass carp (*Ctenopharyngodon idella*) is one of the most important cultivated fish species in China. Mounting evidences suggests that microRNAs (miRNAs) may be key regulators of skeletal muscle among the grass carp, but the knowledge of the identity of myogenic miRNAs and role of miRNAs during skeletal muscle anabolic state remains limited. In the present study, we choose 8 miRNAs previously reported to act as muscle growth-related miRNAs for fasting-refeeding research. We investigated postprandial changes in the expression of 8 miRNAs following a single satiating meal in grass carp juveniles who had been fasting for one week and found that 7 miRNAs were sharply up-regulated within 1 or 3 h after refeeding, suggesting that they may be promising candidate miRNAs involved in a fast-response signaling system that regulates fish skeletal muscle growth.

Keywords: MicroRNA; Grass carp; Fasting; Refeeding; Skeletal muscle

The grass carp (*Ctenopharyngodon idella*) is one of the most important cultivated species in Chinese freshwater aquaculture. Generally, fast skeletal muscle comprises the largest tissue of the fish body (Zhang et al, 2009), and forms the main edible part of this species. Given the complicated development process as well as the importance of these tissues, gaining a clearer understanding of the mechanism underlying muscle development may provide key data for both developmental biologists and researchers attempting to improve grass carp musculature for aquaculture.

Several lines of research have implicated growth factors, regulatory proteins, and transcription factors as key actors involved in the regulation and maintenance of skeletal muscle mass among fish (Nihei et al, 2006; Steinbacher et al, 2006; Chu et al, 2010). Recent studies found that alongside transcriptional factors involved in muscle proliferation and differentiation, a set of microRNAs (miRNAs) may also play important roles in skeletal muscle development among vertebrate animals (Ge & Chen, 2011; Güller & Russell, 2010; Chu et al, 2013). MicroRNAs (miRNAs) are approximately 22-nt noncoding RNAs that act as negative regulators of gene expression, either via inhibiting mRNA translation or prom-

oting mRNA degradation through base pairing to the 3' untranslated region (UTR) of target mRNAs (Xie et al, 2005; Liu, 2008; Zhang & Wen, 2010). Furthermore, miRNAs regulate the expression of transcription factors and signaling mediators critical to both cardiac and skeletal muscle development and function (Callis & Wang, 2008; van Rooij et al, 2008). Studies using the mouse myogenic C2C12 cell line demonstrated miR-1 and miR-133 are involved in myoblast proliferation and differentiation via regulation of the expression of HDAC4 and SRF, respectively (Chen et al, 2006). Meanwhile, miR-1, miR-133a and miR-206 (muscle-specific miRNAs), were also noted to be differentially expressed in Japanese flounder (*Paralichthys olivaceus*) during metamorphosis, as well as in Nile tilapia (*Oreochromis niloticus*) among several developmental stages.

Received: 25 March 2014; Accepted: 17 July 2014

Foundation items: This study was supported by the National Natural Science Foundation of China (31230076; 31340054), the Natural Science Foundation of Hunan province (14JJ2135) and the State Key Laboratory of Freshwater Ecology and Biotechnology (2012FB01)

*Corresponding authors, E-mails: jzhang@ccsu.cn; chentao_114@163.com

Taken together, these findings imply that miRNAs likely play an important role in regulating muscle development (Fu et al, 2011; Yan et al, 2012a). Further evidences suggest that miRNAs act as key regulators of myogenesis, but unfortunately characterizing the identity of myogenic miRNAs and delineating the role of miRNAs during skeletal muscle anabolic state remains unclear.

The maintenance of skeletal muscle mass is a complex and controlled process, largely influenced by both nutritional and physiological states of different animals (Fuentes et al, 2012). Fasting-refeeding protocols have been commonly used as models to investigate the regulation of muscle growth in fish species that experience the transition from catabolic to anabolic states. In the present study, we analyzed the expression of 8 select miRNAs during skeletal muscle anabolic state using a fasting-refeeding experiment. The goal of our study was to better parse out the potential role of these miRNAs in skeletal muscle proliferation and differentiation. The 8 miRNAs (miR-1a, miR-133a-3p, miR-133b-3p, miR-146, miR-181a-5p, miR-206, miR-214 and miR-26a) were previously reported to act as muscle growth-related miRNAs (McCarthy & Esser, 2007; Flynt et al, 2007; Kuang et al, 2009; Yan et al, 2012b). In theory, these miRNAs and their target genes may comprise a coordinated regulating net to favor resumption of myogenesis as an early response to refeeding.

MATERIALS AND METHODS

Fasting-refeeding experiments and sampling

All grass carp individuals were reared under standard conditions at the Che Tian Jiang Reservoir in Loudi, Hunan, China. Two homogeneous groups of grass carp juveniles (average body weight 150 g, 90 days post-hatching (dph)) were reared respectively in two net cages (5 m×5 m×2 m) with fifty fish per tank. All juveniles were fed under standard conditions for 3 weeks, after which the juveniles underwent fasting for 1 week, and were then fed a single meal, which was distributed to all individuals until they appeared to be visually satiated. At each time point from 0 h (before the recovery meal), and at 1, 3, 6, 12, 24, 48 and 96 h (hours after the single meal), six fish were sampled, wherein fast muscles were dissected from the dorsal myotome of individuals. The resulting samples were then snap-frozen in liquid nitrogen and stored at -80 °C until further processing.

Quantitative real-time PCR for the miRNAs

Tissue samples were ground in liquid nitrogen, and total RNAs were extracted using TRIzol (Invitrogen, USA), and then treated with RNase-free DNase I (Promega, USA) in the presence of RNase inhibitor (Sigma, China Branch) followed by ethanol precipitation. The obtained RNAs were polyadenylated by poly (A) polymerase, and then reverse transcribed with one step PrimeScript miRNA cDNA synthesis Kit (TaKaRa, Dalian, China) and a Universal Adaptor Primer (a poly (T) primer ligated with an adapter) for miRNA quantitative assays.

The miRNA expression levels were quantified using real-time PCR with grass carp β -actin gene (GenBank No. DQ211096.1) as an internal control. The cDNA samples were used as templates for quantitative RT-PCR assays with SYBR Premix Ex Taq II (TaKaRa, Japan) and its amplification reaction was carried out on a Bio-Rad CFX96 system (USA). Each 2 μ L cDNA template was added to a total volume of 25 μ L reaction mix containing 12.5 μ L SYBR Green mix, 1 μ L of each miRNA or gene specific forward primer (as shown in Table 1, 10 μ mol/L) and 1 μ L of universal downstream primer (Uni-miR qPCR Primer, 10 μ mol/L, TaKaRa) or gene specific reverse primer, 8.5 μ L nuclease-free water. The protocols used are as follows: (i) pre-denaturation at 95 °C for 60 s; (ii) amplification and quantification, repeated 40 cycles of at 95 °C for 5 s and at 60 °C for 25 s; (iii) melting curve program (65-95 °C with heating rate of 0.1 °C/S and fluorescence measurement) (Zhou et al, 2010). The relative expression ratio (R) of target miRNA was calculated by $R=2^{-\Delta\Delta Ct}$ (Livak & Schmittgen, 2001; Bustin et al, 2009), where Ct is the cycle threshold. The basic equation employed was:

$$\Delta\Delta Ct = (Ct_{\text{target gene}} - Ct_{\text{housekeeping gene}})_{\text{experiment}} - (Ct_{\text{target gene}} - Ct_{\text{housekeeping gene}})_{\text{control}}$$

The miRNA expression levels were then analyzed by one-way ANOVA procedures and regression analysis of SPSS 17.0 (SPSS inc., Chicago, USA). Duncan's multiple range tests were used to compare the control (0 h before the recovery meal) and experimental (# hours after refeeding) groups. The differences were considered statistically significant when $P<0.05$. Data are shown as means \pm SE ($n=6$). Correlation of gene expression was analyzed by the Spearman rank order correlation test. Hierarchical clustering was performed using Cluster3.

Table 1 Primers used for miRNA detection

Name	Primer Sequence (5'–3')	Name	Primer Sequence (5'–3')
miR-1a-F	TGGAATGTAAAGAAGTATGTAT	miR-146-F	CGTGAGAACTGAATCCATAGATGG
miR-133a-3p-F	CGCGTTTGGTCCCTTCA	miR-133b-3p-F	TTGGTCCCTTCAACCAGCTA
miR-206-F	CGTGGAATGTAAGGAAGTGTGTGG	miR-214-F	ACAGCAGGCACAGACAGGCAG
miR-181a-5p-F	CGAACATTCAACGCTGTCTGGT	miR-26a-F	CGTTCAAGTAATCCAGGATAGGCT
β-actin-F	GCCGTGACCTGACTGACTACCT	β-actin-R	CGCAAGACTCCATACCCAAGAAG

Forward primers used for detection were detailed in the Methods; the reverse primer used for detection was universal downstream primer (Uni-miR qPCR Primer, 10 μmol/L, Takara).

RESULTS

Effect of fasting and refeeding on the expression of the miRNAs

A significant up-regulation of each of the 8 miRNAs was observed between 1–6 hours after the single meal ($P < 0.05$) (Figure 1). MiR-1a was sharply up-regulated within 1 h after refeeding and peaked at 6 h (Figure 1A). The expression of miR-133a-3p, miR-133b-3p, miR-146, miR-181a-5p, miR-206 and miR-214 were significantly increased at 3h ($P < 0.05$), reached the maximal levels at 3, 6 or 48 h postprandial (Figure 1B–G). While miR-26a responded slowly to refeeding, it significantly increased at 6 h ($P < 0.05$) and peaked at 48 h (Figure 1F). However, miR-1a, miR-133b-3p and miR-181a-5p significantly decreased at 12 h. All 8 miRNAs returned to the initial baseline values at 96 h.

Heat map summary of hierarchical clustering of miRNAs in skeletal muscle during fasting-refeeding periods

Hierarchical clustering analysis of miRNAs in muscle was done according to the similarity in their expression across different postprandial times (0–96 h). Hierarchical clustering of the miRNAs throughout the trial showed three clades (Figure 2). The first clade including 2 pairs of closely linked miRNAs (miR-133b-3p and miR-133a-3p, miR-206 and miR-181a-5p) that clustered together. The second clade clustered miR-26a with miR-146 expression.

DISCUSSION

MicroRNAs (miRNAs) are noncoding RNA molecules that regulate the stability and/or the translational efficiency of target mRNAs, and several miRNAs have been found to be specifically expressed or highly enriched in skeletal muscle. The expression of muscle-

specific miR-1, miR-133, miR-206, while miR-208 is regulated by muscle transcriptional networks involving SRF, MyoD and MEF2. (Flynt & Lai, 2008; Latronico *et al.*, 2007; Thum *et al.*, 2008; Van Rooij *et al.*, 2008; Callis *et al.*, 2008). Interestingly, non-muscle-specific miRNAs, e.g., miR-26a and miR-181, also regulate skeletal muscle differentiation (Wong & Tellam, 2008; Naguibneva *et al.*, 2006). While a great deal of attention has been paid to miRNAs involved in control of muscle development, a recent study suggests that several other miRNAs, including miR-499, miR-208b and miR-23a, also play an important role in human muscle growth (Drummond *et al.*, 2009). Among fish species, Huang *et al.* (2012) previously detected differentially expressed miRNA between 2 strains of Nile tilapia and identified miR-140, miR-192, miR-204, miR-218a, miR-218b, miR-301c, miR-460, miR-133, miR-152, miR-15a, miR-193a, miR-30b and miR-34 as being associated with body growth in tilapia.

Our present study focused on exploring the potential role(s) of miRNAs as a new layer of control in the postprandial regulation of the muscle development among grass carp. Typically, nutrient availability is among the most important environmental variable altering muscle growth (Valente *et al.*, 2012). As such, starvation and refeeding experiments have served as an effective model for studying the regulation of muscle growth in fish, including the Atlantic salmon (*Salmo salar*) (Bower *et al.*, 2009), rainbow trout (*Oncorhynchus mykiss*) (Montserrat *et al.*, 2007), and Atlantic halibut (*Hippoglossus hippoglossus*) (Hagen *et al.*, 2009). Similarly, in humans MiRNAs turned over quite rapidly (i.e. hours) in skeletal muscle following amino acid ingestion. However, little information is available regarding the early transcriptional changes of miRNA during the postprandial period, especially among fish. We therefore focused on exploring the postprandial regulation of growth-related miRNAs shortly after

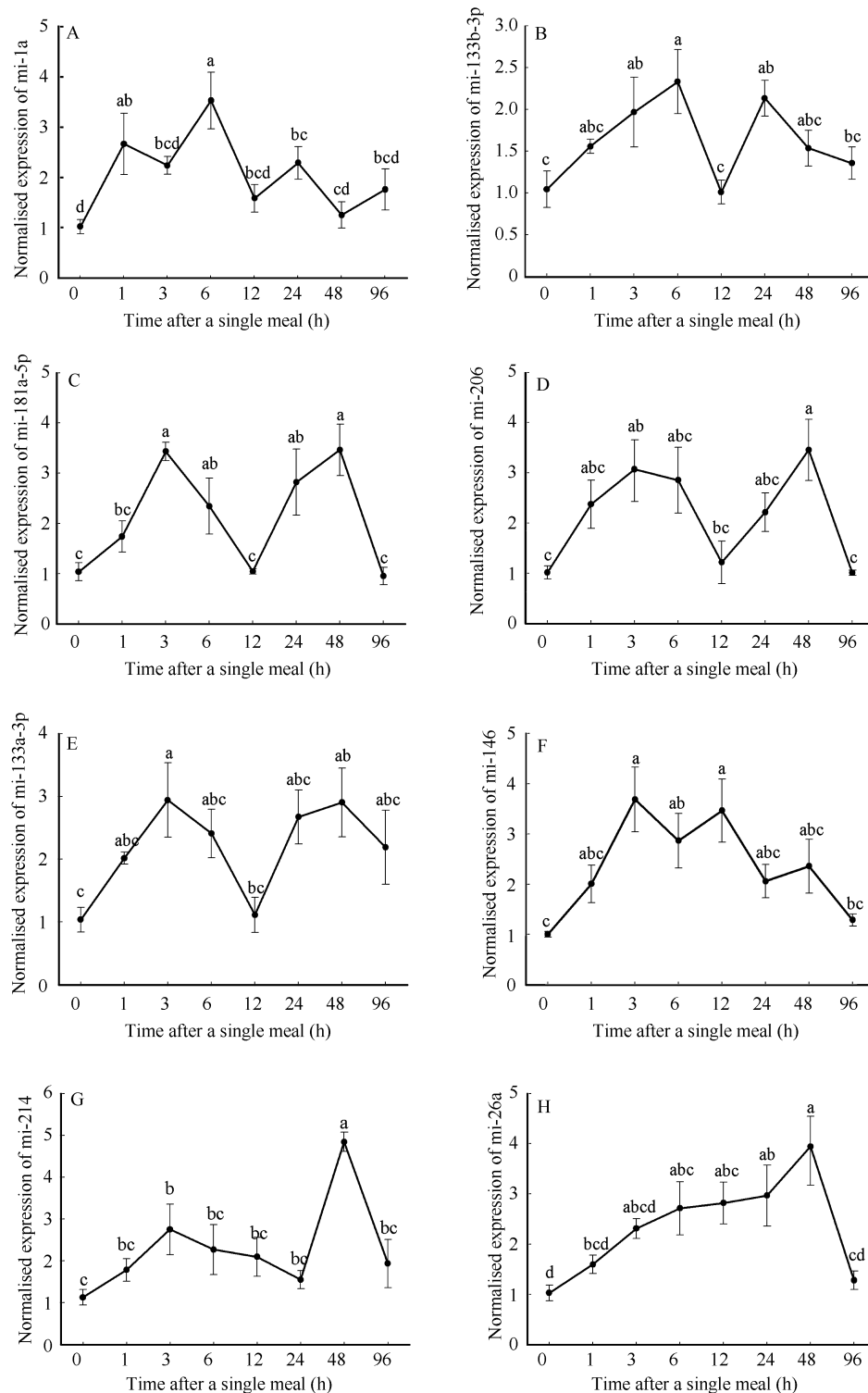


Figure 1 Relative expression of miRNAs with significant up-regulation following refeeding after 1 week fasting β -actin expression was detected as the internal control. All values are presented as mean \pm SE, $n=6$. Different letters indicate significant differences between columns ($P < 0.05$).

feeding a single meal in grass carp. Our results showed that miR-1a, miR-133a-3p, miR-133b-3p, miR-146, miR-181a-5p, miR-206 and miR-214 were significantly

elevated at 1 or 3 h after refeeding in the fast muscle of grass carp. Drummond et al (2009) previously found a rapid up-regulation of the miR-1, miR-208b, miR-23a

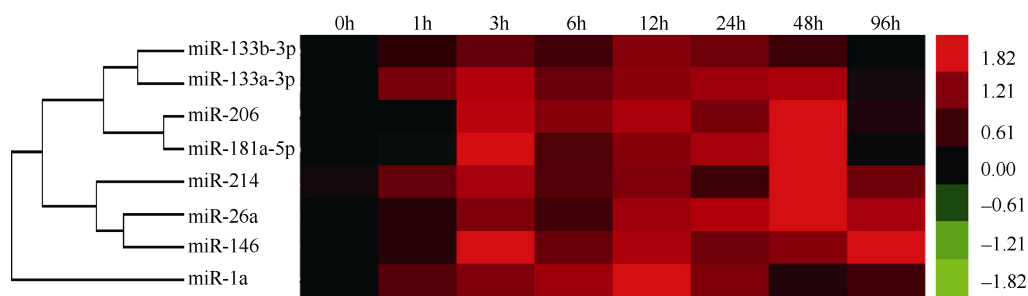


Figure 2 Heat map summary of hierarchical clustering of miRNAs in skeletal muscle during fasting-refeeding periods

Blue and yellow respectively denote a decrease or increase. The absolute signal intensity ranged from -1.82 to +1.82, with corresponding color changes from green to red.

and miR-499 following the amino acid ingestion in humans. These findings suggest that the identified miRNAs may be promising candidate miRNAs involved in a fast-response signaling system that regulates fish skeletal muscle growth. The other finding of significant decreased of miR-1a, miR-133b-3p and miR-181a-5p at 12 h after single meal suggests there may be other signaling pathways regulated by the miRNAs that limit excessive regulation of muscle growth.

A further finding of our study was that miR-206 and miR-181a-5p showed a dramatic and simultaneous up-regulation following feeding by a single meal. MiR-206 is known to be a muscle-specific miRNA, with its role in muscle development having been verified in some animal models, including mice, rats and zebrafish (Anderson et al, 2006; Kim et al, 2006; Mishima et al, 2009; Shan et al, 2009). MyoD acts as a transcriptional activator of the miR-206 pre-miRNA transcript, and subsequently the induced high levels of the mature miR-206 result in the down-regulation of specific target muscle growth-related genes (Rosenberg et al, 2006). MiR-181 is also thought to function partly through inhibition of Hox-A11 expression, a known repressor of MyoD, which is required for new muscle growth (Naguibneva et al, 2006). Taken together, these different

lines of evidence suggest that miR-181 may indirectly promote miR-206 expression, though some further study is needed. Moreover, our finding that two miRNAs (miR-181a-5p and miR-206) clustered together suggest a close relation and coordination regulation of these miRNAs towards resumption of myogenesis following refeeding.

In conclusion, the present results show that several miRNAs likely involved in fast skeletal muscle in grass carp respond quickly to refeeding of a single meal following fasting. Results of our analysis indicate that refeeding induced a coordinated regulation of several miRNAs involved in a strong resumption of myogenesis, wherein the 8 tested miRNAs transcripts were sharply up-regulated in muscle tissues in response to refeeding. This finding suggests that these miRNAs may be promising candidate miRNAs involved in regulating fish fast muscle growth. Further study is needed to experimentally assess the targets of these miRNAs and elucidate how they contribute to the regulation of skeletal muscle growth during anabolic state.

Acknowledgements: We would like to thank Yu-Long LI, Dun-Xue CHEN, Kai-Zhuo WANG and Jun-Zhi ZHANG for their help and support in sample collection.

References

- Anderson C, Catoe H, Werner R. 2006. MIR-206 regulates connexin43 expression during skeletal muscle development. *Nucleic Acids Research*, **34**(20): 5863-5871.
- Bower NI, Taylor RG, Johnston IA. 2009. Phasing of muscle gene expression with fasting-induced recovery growth in Atlantic salmon. *Frontiers in Zoology*, **6**: 18-30.
- Bustin SA, Benes V, Garson JA, Hellemans J, Huggett J, Kubista M, Mueller R, Nolan T, Pfaffl MW, Shipley GL, Vandesompele J, Wittwer CT. 2009. The MIQE guidelines: minimum information for publication

of quantitative real-time PCR experiments. *Clinical Chemistry*, **55**(4): 611-622.

Callis TE, Deng Z, Chen JF, Wang DZ. 2008. Muscling through the microRNA world. *Experimental Biology and Medicine*, **233**(2): 131-138.

Callis TE, Wang DZ. 2008. Taking microRNAs to heart. *Trends in Molecular Medicine*, **14**(6): 254-260.

Chen JF, Mandel EM, Thomson JM, Wu Q, Callis TE, Hammond SM,

- Conlon FL, Wang DZ. 2006. The role of microRNA-1 and microRNA-133 in skeletal muscle proliferation and differentiation. *Nature Genetics*, **38**(2): 228-233.
- Chu WY, Liu LS, Li YL, Chen L, Wang K Z, Li HH, Du SJ, Zhang JS. 2013. Systematic identification and differential expression profiling of microRNAs from white and red muscles of *Siniperca chuatsi*. *Current Molecular Medicine*, **13**(8): 1397-1407.
- Chu WY, Xia XJ, Chen DG, Fu GH, Liu C, Chen J, Liu F, Lu SQ, Zhang JS. 2010. Gene expression profiles of the muscle tissues of the commercial important teleost, *Siniperca chuatsi* L. *Aquaculture International*, **18**: 667-678.
- Drummond MJ, Glynn EL, Fry CS, Dhanani S, Volpi E, Rasmussen BB. 2009. Essential amino acids increase microRNA-499, -208b, and -23a and downregulate myostatin and myocyte enhancer factor 2c mRNA expression in human skeletal muscle. *The Journal of Nutrition*, **139**(12): 2279-2284.
- Flynt AS, Lai EC. 2008. Biological principles of microRNA-mediated regulation: shared themes amid diversity. *Nature Reviews Genetics*, **9**(11): 831-842.
- Flynt AS, Li N, Thatcher EJ, Solnica-Krezel L, Patton JG. 2007. Zebrafish miR-214 modulates Hedgehog signaling to specify muscle cell fate. *Nature Genetics*, **39**(2): 259-263.
- Fu Y, Shi Z, Wu M, Zhang J, Jia L, Chen X. 2011. Identification and differential expression of microRNAs during metamorphosis of the Japanese flounder (*Paralichthys olivaceus*). *PLoS ONE*, **6**(7): e22957.
- Fuentes EN, Ruiz P, Valdes JA, Molina A. 2012. Catabolic signaling pathways, atrogenes, and ubiquitinated proteins are regulated by the nutritional status in the muscle of the fine flounder. *PLoS ONE*, **7**(9): e44256.
- Ge Y, Chen J. 2011. MicroRNAs in skeletal myogenesis. *Cell Cycle*, **10**(3): 441-448.
- Güller I, Russell AP. 2010. MicroRNAs in skeletal muscle: their role and regulation in development, disease and function. *The Journal of Physiology*, **588**(pt21): 4075-4087.
- Hagen O, Fernandes JMO, Solberg C, Johnston IA. 2009. Expression of growth-related genes in muscle during fasting and refeeding of juvenile Atlantic halibut, *Hippoglossus hippoglossus* L. *Comparative Biochemistry and Physiology. Part B, Biochemistry & Molecular Biology*, **152**(1): 47-53.
- Huang CW, Li YH, Hu SY, Chi JR, Lin GH, Lin CC, Gong HY, Chen JY, Chen RH, Chang SJ, Liu FG, Wu JL. 2012. Differential expression patterns of growth-related microRNAs in the skeletal muscle of Nile tilapia (*Oreochromis niloticus*). *Journal of Animal Science*, **90**(12): 4266-4279.
- Kim, HK, Lee, YS, Sivaprasad U, Malhotra A, Dutta A. 2006. Muscle specific microRNA miR-206 promotes muscle differentiation. *The Journal of Cell Biology*, **174**(5): 677-687.
- Kuang W, Tan J, Duan Y, Duan J, Wang W, Jin F, Jin Z, Yuan X, Liu Y. 2009. Cyclic stretch induced miR-146a upregulation delays C₂C₁₂ myogenic differentiation through inhibition of Numb. *Biochemical and Biophysical Research Communications*, **378**(2): 259-63.
- Latronico MV, Catalucci D, Condorelli G. 2007. Emerging role of microRNAs in cardiovascular biology. *Circulation Research*, **101**(12): 1225-1236.
- Liu J. 2008. Control of protein synthesis and mRNA degradation by microRNAs. *Current Opinion in Cell Biology*, **20**(2): 214-221.
- Livak KJ, Schmittgen TD. 2001. Analysis of relative gene expression data using real-time quantitative PCR and the 2^{-ΔΔC_T} method. *Methods*, **25**(4): 402-408.
- McCarthy JJ, Esser KA. 2007. MicroRNA-1 and microRNA-133a expression are decreased during skeletal muscle hypertrophy. *Journal of Applied Physiology*, **102**(1): 306-313.
- Mishima Y, Abreu-Goodger C, Staton AA, Stahlhut C, Shou C, Cheng C, Gerstein M, Enright AJ, Giraldez AJ. 2009. Zebrafish miR-1 and miR-133 shape muscle gene expression and regulate sarcomeric actin organization. *Genes & Development*, **23**(5): 619-632.
- Montserrat N, Gabillard JC, Capilla E, Navarro MI, Gutiérrez J. 2007. Role of insulin, insulin-like growth factors, and muscle regulatory factors in the compensatory growth of the trout (*Oncorhynchus mykiss*). *General and Comparative Endocrinology*, **150**(3): 462-472.
- Naguibneva I, Ameyar-Zazoua M, Polesskaya A, Ait-Si-Ali S, Groisman R, Souidi M, Cuvelier S, Harel-Bellan A. 2006. The microRNA miR-181 targets the homeobox protein Hox-A11 during mammalian myoblast differentiation. *Nature Cell Biology*, **8**(3): 278-284.
- Nihei Y, Kobiyama A, Ikeda D, Ono Y, Ohara S, Cole NJ, Johnston IA, Watabe S. 2006. Molecular cloning and mRNA expression analysis of carp embryonic, slow and cardiac myosin heavy chain isoforms. *The Journal of Experimental Biology*, **209**(1): 188-198.
- Rosenberg MI, Georges SA, Asawachaicharn A, Analau E, Tapscott SJ. 2006. MyoD inhibits Fstl1 and Utrn expression by inducing transcription of miR-206. *The Journal of Cell Biology*, **175**(1): 77-85.
- Shan ZX, Lin QX, Fu YH, Deng CY, Zhou ZL, Zhu JN, Liu XY, Zhang YY, Li Y, Lin SG, Yu XY. 2009. Upregulated expression of miR-1/miR-206 in a rat model of myocardial infarction. *Biochemical and Biophysical Research Communications*, **381**(4): 597-601.
- Steinbacher P, Haslett JR, Six M, Gollmann HP, Sängler AM, Stoiber W. 2006. Phases of myogenic cell activation and possible role of dermomyotome cells in teleost muscle formation. *Developmental Dynamics: An Official Publication of the American Association of Anatomists*, **235**(11): 3132-3143.
- Thum T, Catalucci D, Bauersachs J. 2008. MicroRNAs: novel regulators in cardiac development and disease. *Cardiovascular Research*, **79**(4): 562-570.
- Valente LM, Bower NI, Johnston IA. 2012. Postprandial expression of growth related genes in Atlantic salmon (*Salmo salar* L.) juveniles fasted for 1 week and fed a single meal to satiation. *The British Journal of Nutrition*, **108**(12): 2148-2157.
- Van Rooij E, Liu N, Olson EN. 2008. MicroRNAs flex their muscles. *Trends in Genetics: TIG*, **24**(4): 159-166.
- Wong CF, Tellam RL. 2008. MicroRNA-26a targets the histone methyltransferase Enhancer of Zeste homolog 2 during myogenesis. *Journal of Chemical Biology*, **283**(15): 9836-9843.
- Xie X, Lu J, Kulbokas EJ, Golub TR, Mootha V, Lindblad-Toh K, Lander ES, Kellis M. 2005. Systematic discovery of regulatory motifs

- in human promoters and 3'UTRs by comparison of several mammals. *Nature*, **434**(7031): 338-345.
- Yan B, Guo JT, Zhao LH, Zhao JL. 2012a. microRNA expression signature in skeletal muscle of Nile tilapia. *Aquaculture*, **364-365**: 240-246.
- Yan X, Ding L, Li Y, Zhang X, Liang Y, Sun X, Teng CB. 2012b. Identification and profiling of microRNAs from skeletal muscle of the common carp. *PLoS ONE*, **7**(1): e30925.
- Zhang JS, Fu GH, Chu WY, Chen J, Liu Z, Liu F, Lu SQ, Liang P. 2009. cDNA cloning and expression analysis of myosin heavy chain gene(*MHC*)of the Mandarin fish, *Siniperca kneri*. *Aquaculture Research*, **40**(4): 412-418.
- Zhang YQ, Wen JF. 2010. Mirna system in unicellular eukaryotes and its evolutionary implications. *Zoological Research*, **31**(1): 39-42 [in Chinese]
- Zhou RX, Meng T, Meng HB, Cheng DX, Bin SY, Cheng J, Fu GH, Chu WY, Zhang JS. 2010. Selection of reference genes in transcription analysis of gene expression of the Mandarin fish, *Siniperca chuatsi*. *Zoological Research*, **31**(2): 141-146.

Effects of surround suppression on response adaptation of V1 neurons to visual stimuli

Peng LI, Cai-Hong JIN, San JIANG, Miao-Miao LI, Zi-Lu WANG, Hui ZHU, Cui-Yun CHEN, Tian-Miao HUA*

College of Life Sciences, Anhui Normal University, Wuhu 241000, China

Abstract: The influence of intracortical inhibition on the response adaptation of visual cortical neurons remains in debate. To clarify this issue, in the present study the influence of surround suppression evoked through the local inhibitory interneurons on the adaptation effects of neurons in the primary visual cortex (V1) were observed. Moreover, the adaptations of V1 neurons to both the high-contrast visual stimuli presented in the classical receptive field (CRF) and to the costimulation presented in the CRF and the surrounding nonclassical receptive field (nCRF) were compared. The intensities of surround suppression were modulated with different sized grating stimuli. The results showed that the response adaptation of V1 neurons decreased significantly with the increase of surround suppression and this adaptation decrease was due to the reduction of the initial response of V1 neurons to visual stimuli. However, the plateau response during adaptation showed no significant changes. These findings indicate that the adaptation effects of V1 neurons may not be directly affected by surround suppression, but may be dynamically regulated by a negative feedback network and be finely adjusted by its initial spiking response to stimulus. This adaptive regulation is not only energy efficient for the central nervous system, but also beneficially acts to maintain the homeostasis of neuronal response to long-presenting visual signals.

Keywords: Surround suppression; V1 neurons; Response adaptation; Cat

Viewing a long-presenting visual stimulus with specific patterns (e.g., orientation, motion direction and spatial frequency) often inhibits or perturbs perception of a subsequent test stimulus with similar attributes. This phenomenon is termed visual adaptation, and has attracted considerable attention since the 1960s (Clifford et al, 2007; Dao et al, 2006; Greenlee & Heitger, 1988; Hua et al, 2009; Kohn, 2007; Maffei et al, 1973; Marlin et al, 1988; Movshon & Lennie, 1979; Smith & Hammond, 1985). Since visual adaptation shows both evident interocular transfer and specificity to adapted stimulus attributes, it is generally regarded as a physiological process occurred in the cortical level, especially in the primary visual cortex (V1) (Duong & Freeman, 2007; Howarth et al, 2009), although subcortical neurons also exhibit a weak adaptation to visual stimulus (Brown & Masland, 2001; DeBruyn & Bonds, 1986; Smirnakis et al, 1997).

The neuronal mechanisms of adaptation to visual stimuli are still in debate (Hua et al, 2009; Kohn, 2007; Liu et al, 2013). The contrast gain control mechanism, which suggests a somatic afterhyperpolarization due to an increasing potassium ion current triggered by sodium ion influx during prolonged stimulation (Carandini & Ferster, 1997; Sanchez-Vives et al, 2000a; Sanchez-Vives et al, 2000b), cannot interpret the specificity of adaptation to stimulus attributes. Synaptic mechanisms can fully account for stimulus-specificity of adaptation

Received:20 February 2014; Accepted: 28 April 2014

Foundation Items: This research was supported by the National Natural Science Foundation of China (31171082), the Natural Science Foundation of Anhui Province (070413138), the Key Research Foundation of the Anhui Provincial Education Department (KJ200-9A167), the Foundation of Key Laboratories of Anhui Province and the Anhui Provincial Education Department

*Corresponding author, E-mail: tmhua@mail.ahnu.edu.cn

but lack of consistent experimental evidences. Some studies highlight the roles of excitatory synaptic depression in the adaptation process (Chung et al, 2002; McLean and Palmer, 1996; Reig et al, 2006; Vidyasagar, 1990). Some suggest that the changes of inhibitory synaptic activities may contribute to the adaptation effects (Hua et al, 2009; Yang et al, 2003). Others propose that adaptation may be caused by a network mechanism concerning a relative weight of recurrent excitation and inhibition in local neural circuitry (Teich & Qian, 2003). An important factor underlying these discrepancies is that previous studies fail to directly assess the correlations of the changes of neuronal response adaptation and the changes of local excitation / inhibition. Studies on microiontophoresis found that administrations of glutamate, gamma-aminobutyric acid (GABA) and GABA receptor's antagonists fail to change the adaptation strength of visual cortical neurons (DeBruyn & Bonds, 1986; Vidyasagar, 1990). However, it is premature to conclude that inhibition is not involved in the adaptation process because: i) the actual effects of iontophoretic drug delivery may be challenged if drug diffusion time, diffusion range and synaptic spatial alignment were concerned; ii) regulatory mechanisms from inhibitory synapses other than GABAergic ones may exist in adaptation (Ego-Stengel et al, 2002; McLean & Palmer, 1996; Waterhouse et al, 1990). Moreover, we recently found that relative to young adults, the adaptation of V1 neurons in the aged brain with compromised intracortical inhibition is actually enhanced (Hua et al, 2009).

The spiking response of a V1 neuron to a high-contrast stimulus placed within its classical receptive field (CRF) can be suppressed by a simultaneously presented stimulus within the surrounding nonclassical receptive field (nCRF), especially by the one with the similar orientation, motion direction and spatial frequency (Cavanaugh et al, 2002b; Haider et al, 2010; Series et al, 2003; Webb et al, 2005). This phenomenon, termed surround suppression, is induced by the increased activation of local inhibitory interneurons that are driven chiefly by the lateral horizontal connections and / or the feedback from higher visual cortical areas (Bair et al, 2003; Durand et al, 2007; Haider et al, 2010; Li & Freeman, 2011; Series et al, 2003; Smith et al, 2006). Therefore, the local inhibition (Akasaki et al, 2002; Fu et al, 2010; Walker et al, 2000) on the surround-suppressed neurons can be regulated by the varying stimulus size

outside the CRF.

In this study, grating stimuli of different sizes were presented outside the CRF to evaluate the effects of intracortical inhibition on the response adaptation of V1 neurons.

MATERIALS AND METHODS

Animals

Four healthy young adult cats (2–3 years old) were examined ophthalmoscopically prior to experimentation to confirm that no optical or retinal problems impaired their visual function. All experiment procedures were performed strictly in accordance with the guidelines published in the NIH Guide for the Care and Use of Laboratory Animals.

Electrophysiological recording preparation

All cats were prepared for acute *in vivo* single-unit recording using a previously described method (Hua et al, 2010; Hua et al, 2009; Hua et al, 2006; Meng et al, 2013). Briefly, anesthesia was induced by injection of ketamine HCl (40 mg/kg, im) and xylazine (2 mg/kg, im). After intubation of intravenous and tracheal cannulae, the cat was immobilized in a stereotaxic apparatus with ear, eye and bite bars. Glucose (5%)-saline (0.9%) solution containing a mixture of urethane (20 mg/h/kg) and gallamine triethiodide (10 mg/h per kg of body weight) was infused intravenously by a syringe pump to keep the animal anesthetized and paralyzed. Pupils were maximally dilated with atropine (1%) eye drops, and contact lenses (zero power) were used to protect the corneas from dryness. Neosynephrine (5%) was applied to retract the nictitating membranes. Artificial respiration was performed, and expired pCO₂ was maintained at approximately 3.8%. Anesthesia level was closely evaluated during the experiment by continuously monitoring the animal's heart rate (180–220 pulses/min) and electrocardiogram (ECG) throughout the experiment.

V1 was partly exposed (8 mm posterior to the earbar, 4 mm lateral to the midline) by removing the skull and dura over V1 (area 17) with the aid of a light microscope (77019, Reward, China). The small hole over V1 was filled with 4% agar saline solution prior to electrophysiological recording. The optic discs of the two eyes were reflected onto a movable transparent tangent screen positioned 57 cm from the animal's eyes and overlapped with a CRT monitor (resolution 1024×768, refresh rate 85 Hz) for visual stimuli presentation. The

area centralis of each eye was precisely located according to the position of the optic discs reflected onto the tangent screen (Bishop et al, 1962). After all the preparations were completed, single-unit recordings were performed using a glass-coated tungsten microelectrode (with an impedance of 3–5 MΩ) which was advanced by a hydraulic micromanipulator (Narishige, Japan). When the experiment was finished, the distance of each recorded cell's receptive field from the retinal central area was measured and calculated as visual acuity (1°/cm).

Visual stimuli and recording procedures

Visual stimuli were drifting sinusoidal gratings, which were generated in MATLAB with the aid of extensions provided by the high-level Psychophysics Toolbox (Brainard, 1997) and low-level Video Toolbox (Pelli, 1997). Once a cell's visually-evoked response was detected, the cell's receptive field center was preliminarily determined using bars of light emitted from a hand pantoscope and then precisely located by consecutively presenting a series of computer-generated flashing bars of light on the CRT. The cell's preferred stimulus attributes, including orientation, motion direction, spatial and temporal frequency were determined by comparing the cell's response to a series of grating stimulus packages. Then, the cell's responses to grating stimuli with optimal attributes but different sizes were recorded to build the response-stimulus size tuning curve (Figure 1A). We fitted the size tuning curve with a function described in previous papers (Cavanaugh et al, 2002a; Tailby et al, 2007):

$$R(x) = \frac{k_c \operatorname{erf}(x/w_c)^2}{1 + k_s \operatorname{erf}(x/w_s)^2} \quad (1)$$

Where, x is stimulus size, $R(x)$ is the neuronal response to a stimulus with size x , k_c and w_c are the gain and spatial extent of the center mechanism, k_s and w_s are the gain and spatial extent of the surround mechanism, erf is the error function.

From the fitting curve, we acquired three test stimulus sizes (a, b, c; Figure 1A), at which the cell's response reached maximum, half of the maximum and minimum value on the right side of the fitting curve, respectively. Size a is the optimal stimulus size that only stimulates the cell's CRF, but not induces surround suppression. Stimulus with size b and c can co-stimulate both CRF and nCRF, but may also evoke medium and

maximum surround suppression, respectively.

The contrast of each stimulus was set at 100%. The mean luminance of the display was 19 cd/m², and the environmental ambient luminance on the cornea was 0.1 lux.

Data acquisition and analysis

Action potentials of the recorded cells were amplified with a microelectrode amplifier (Nihon Kohden, Japan) and a differential amplifier (Dagan 2400A, USA), and then fed into a window discriminator with an audio monitor. The original voltage traces (Figure 1C, E, G) were digitized by an acquisition board (National Instruments, USA) controlled by IGOR software (WaveMetrics, USA), and saved for on- or off-line analysis. A cell's response to a grating stimulus was defined as the mean firing rate (spontaneous response subtracted) corresponding to the time of stimulus presentation, which was used to acquire the curves of tuning response to stimulus orientations, temporal and spatial frequencies. The optimal orientation of each cell was obtained as previously described. The optimal temporal and spatial frequency were determined respectively by comparing the cell's response to high contrast (100%) grating stimuli with different temporal and spatial frequencies, and selecting the temporal and spatial frequency with the maximum response.

The adaptation index (AI) was defined as the ratio of the cell's mean response during plateau period of adaptation to visual stimulation, a period when the cell's response reached a stable minimum value, to the mean initial response of the cell (Figure 1D, F, H). The change of AI with different stimulus sizes was plotted for each studied cell (Figure 1B). The smaller the AI is, the stronger the adaptation of the cell becomes. In order to assess the impact of surround suppression on the response adaptation, several neurons that did not exhibit surround suppression to visual stimuli presented in its nCRF were excluded from our data analysis. All studied neurons had a receptive field within 8° from the central area of the dominant eye.

All values were expressed as mean±SE. Variations between different stimulus sizes and subjects were assessed using analysis of variance (ANOVA) or *t*-test.

RESULTS

A total of 61 V1 cells from four young male adult cats were analyzed in this study (Table 1). All cells

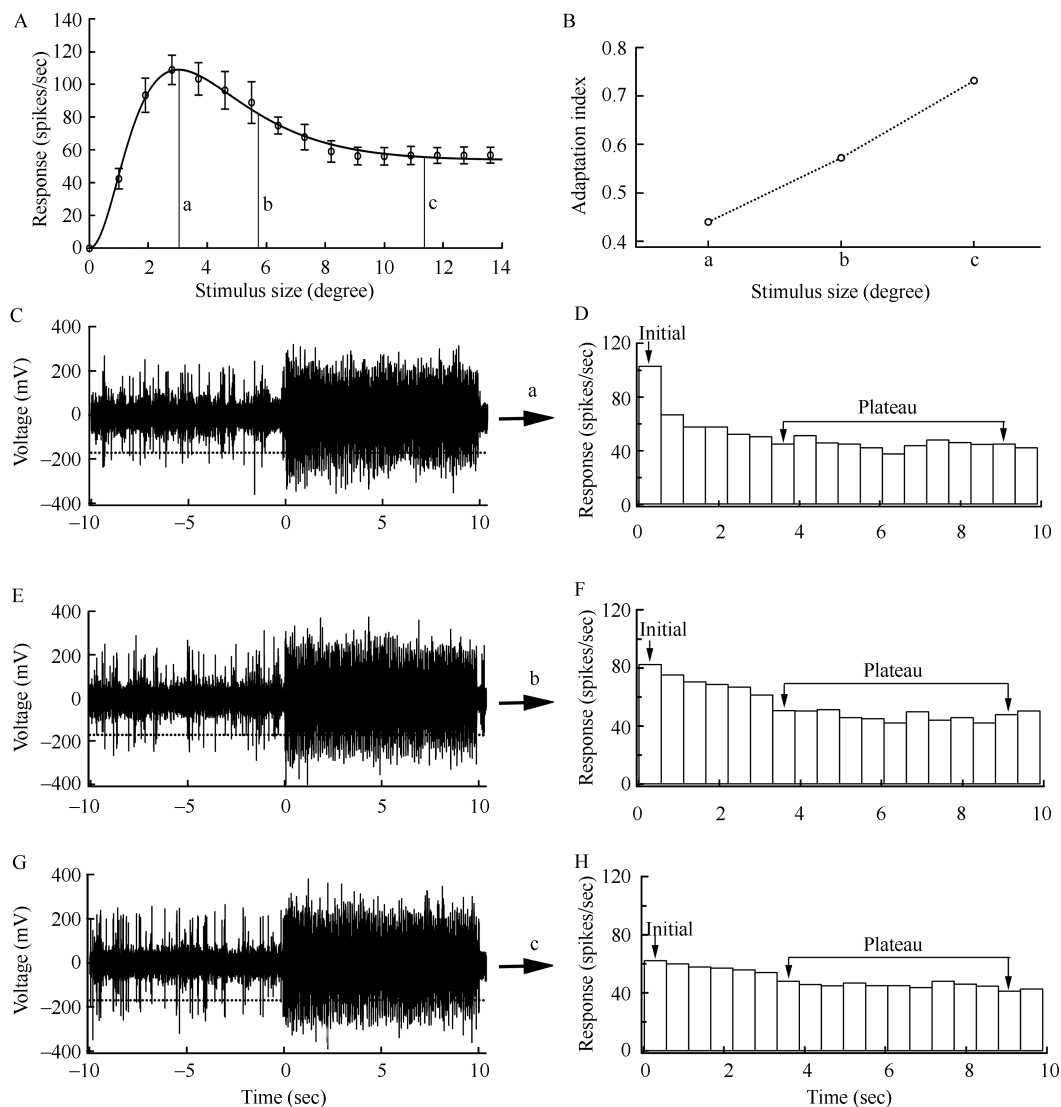


Figure 1 Response adaptation of a sample V1 cell to visual stimuli

A: The response-size tuning curve fitted with equation 1. B: AI changes with stimulus sizes. The AI at stimulus sizes a, b and c for this sample cell was 0.44, 0.57 and 0.73 respectively. Subsequently, the cell's response to prolonged stimulation (90 stimulus cycles) were recorded with three stimulus sizes, respectively, which were used to assess the cell's response adaptation changes with the magnitude of surround suppression. Each stimulus was presented monocularly to the dominant eye and repeated 4–6 times with a 3-minute interval between adjacent trials for the cell's functional recovery. Before each stimulus was presented, spontaneous activity was acquired during a 10 s period while a mean luminance was shown on the CRT. C, E and G: Voltage traces of the sample cell's response to 90 cycles of preferred visual stimuli with size a, b and c respectively, which were employed to evaluate the cell's response adaptation strength. Spontaneous activity was obtained during the first 10 s period while mean luminance was shown on the screen. The dashed horizontal line in each voltage trace indicated the threshold for action potential counting. D, F and H: PSTHs show the cell's average response (counted across each 5 stimulus cycles, with spontaneous activity subtracted) changes as a function of time. Spikes in the first bar were defined as the average initial response, and the mean spikes from the 7th to the 17th bar as an average response, a period when the cell's response decreased to a stable minimum level.

showed an evident adaptation to prolonged visual stimuli (90 stimulus cycles) as indicated by the AI value ranged from 0.104 to 0.760.

Changes of neuronal response adaptation with the stimulus size outside the CRF

The comparison of mean AI of studied neurons with

three stimulus sizes (a, b and c) showed that the surround suppression effects on the adaptation strength of neuronal response to visual stimuli from weak to strong were a, b and c, respectively. The ANOVA analysis showed significant differences in the averaged AI value of all the studied neurons with three different stimulus

Table 1 Mean adaptation index of V1 neurons at different stimulus sizes in each cat

Subject	Cell number (<i>n</i>)	Adaptation index at different stimulus size		
		a	b	c
Cat1	19	0.33±0.021	0.41±0.028	0.45±0.028
Cat2	17	0.33±0.021	0.40±0.020	0.48±0.025
Cat3	13	0.28±0.034	0.36±0.036	0.46±0.033
Cat4	12	0.18±0.018	0.22±0.025	0.29±0.032

a, b and c: the stimulus size at which the cell's response reached maximum, half of the maximum and minimum value on the right side of the response-stimulus size fitting curve, respectively.

sizes ($F_{(2, 183)}=25.7$, $P<0.0001$). These differences were independent of subjects ($F_{(6, 183)}=0.38$, $P>0.5$), although the mean AI exhibited a significant variance from cat to cat ($F_{(3, 183)}=22.4$, $P<0.0001$) (Figure 2A). The mean AI of each individual cat was found significantly different with different stimulus sizes (cat1: $F_{(2, 57)}=6.12$, $P<0.01$; cat2: $F_{(2, 51)}=9.472$, $P<0.001$; cat3: $F_{(2, 39)}=6.927$, $P<0.01$; cat4: $F_{(2, 360)}=4.935$, $P<0.05$). The mean AI at stimulus size b was significantly less than that at stimulus size c (t -test, $P<0.0001$), whereas, was significantly larger than that at stimulus size a (t -test, $P<0.0001$) (Figure 2B, C), indicating that the neuronal response adaptation decreased with the increase of surround suppression. These results suggest that the response adaptation of V1 neurons to visual stimuli is negatively correlated with the

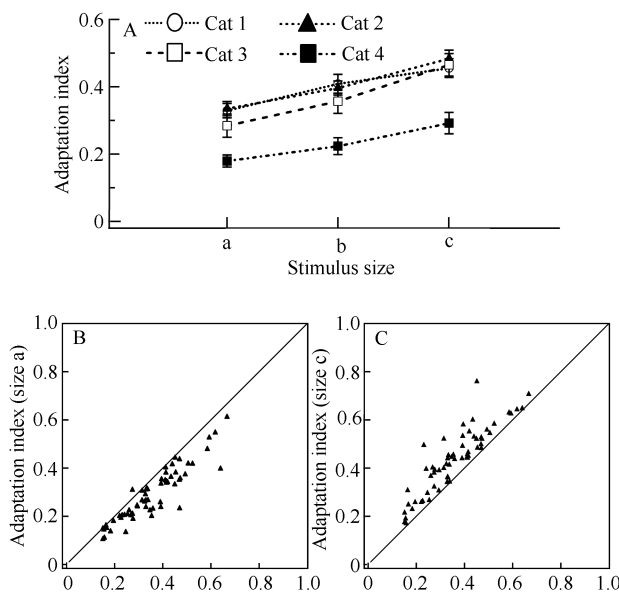


Figure 2 Average AI changes of studied neurons with different stimulus size

A: mean AI at different stimulus sizes of individual cat; B and C: AI at stimulus size a v.s. size b and size c v.s. size b of all the cells from all cats, respectively.

surround suppression that was modulated by the stimulus size.

Changes of neuronal response with the stimulus size

The increase or decrease of AI could result from a change of the initial response (IR) of neurons to visual stimuli, a change of the plateau response (PR), the response during the plateau period of adaptation, or any combination thereof. As such, we compared the IR (the mean response to the first five cycles of visual stimuli) and PR (the mean response of visual stimuli cycles from the 36th to the 85th, which represents a minimal and stable response after adaptation) of V1 neurons to prolonged visual stimuli with different stimulus sizes, respectively.

ANOVA analysis showed significant differences in the averaged IR of the studied neurons with different stimulus sizes ($F_{(2, 183)}=111.207$, $P<0.0001$). These differences were independent of subjects ($F_{(6, 183)}=0.536$, $P>0.5$), although the mean IR varied significantly from cat to cat ($F_{(3, 183)}=14.633$, $P<0.0001$) (Figure 3A). The mean IR of each individual cat also showed significant differences at different stimulus sizes (cat1: $F_{(2, 57)}=21.810$, $P<0.0001$; cat2: $F_{(2, 51)}=75.240$, $P<0.0001$; cat3: $F_{(2, 39)}=23.203$, $P<0.0001$; cat4: $F_{(2, 36)}=20.203$, $P<0.0001$). The mean IR at stimulus size b was significantly

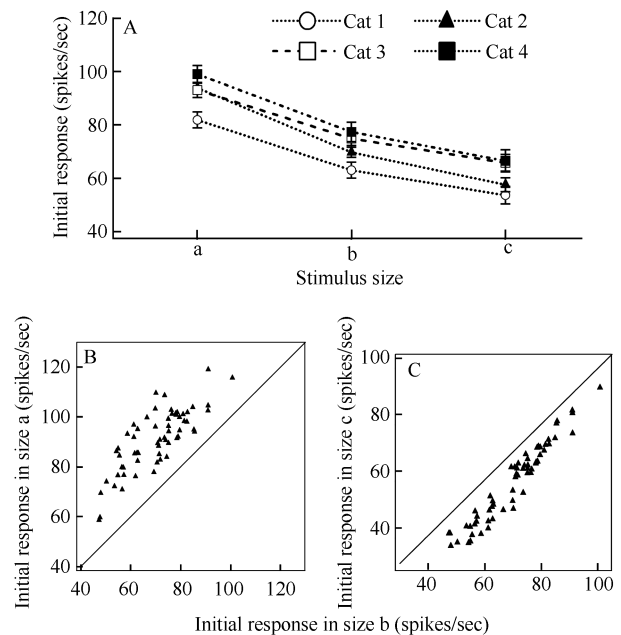


Figure 3 Average IR of neurons to prolonged visual stimuli with different sizes

A: The mean IR at different stimulus sizes of individual cat; B and C: The IR at stimulus size a v.s. size b and size c v.s. size b of all the cells from all cats.

larger than that at stimulus size c (*t*-test, $P < 0.0001$), whereas, was significantly less than that at stimulus size a (*t*-test, $P < 0.000001$) (Figure 3B, C), indicating that the IR of neurons to prolonged visual stimuli reduced greatly with the increase of surround suppression.

However, although the mean PR varied significantly from cat to cat ($F_{(2, 183)} = 0.667$, $P < 0.0001$), no significant differences were found in either all the studied neurons from all the cats ($F_{(2, 183)} = 0.403$, $P > 0.1$) or individual cat (cat1: $F_{(2, 57)} = 0.466$, $P > 0.5$; cat2: $F_{(2, 51)} = 1.173$, $P > 0.1$; cat3: $F_{(2, 39)} = 0.561$, $P > 0.5$; cat4: $F_{(2, 36)} = 0.237$, $P > 0.5$) with different stimulus sizes (Figure 4). These results indicate that the responses of neurons during the plateau period of adaptation to visual stimuli are stable and do not change significantly with the changes of surround suppression.

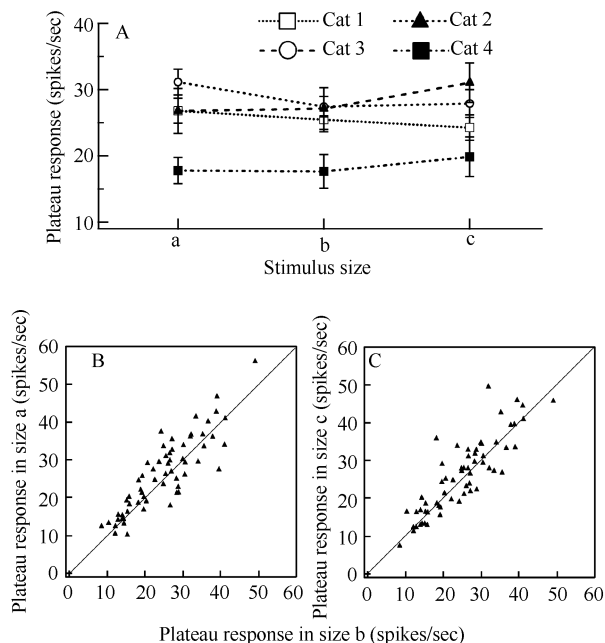


Figure 4 Average plateau response of neurons to prolonged visual stimuli with different sizes

A: The mean plateau response at different stimulus sizes for individual cat; B and C: the plateau response at stimulus size a vs. size b and size c vs. size b for all the cells from all cats.

Therefore, the response adaptation changes of the studied neurons with different surround suppression may attribute to the changes of their IR to prolonged visual stimuli, whereas, the PR maintains relatively stable.

DISCUSSION

Adaptation mechanisms

Visual cortical neurons exhibit a reduction in firing rate to prolonged visual stimulation. However, the

underlying mechanisms remain in debate, and previous studies proposed several hypotheses. For example, the response adaptation is caused by the activity fatigue of the neuron because the prolonged stimulation may evoke sustained firing and the fatigued neurons respond less than they normally do (Carandini, 2000; Sekuler & Pantle, 1967). The contrast gain control mechanism suggests that adaptation leads to a strong somatic afterhyperpolarization due primarily to the activation of voltage-gated potassium channels, triggered by the sodium influx during generation of action potentials (Carandini & Ferster, 1997; Sanchez-Vives et al, 2000a; Sanchez-Vives et al, 2000b). Although the above two mechanisms can interpret the neuronal response reduction during visual adaptation, they are unfortunately unable to account for the specificity of adaptation to the adapted stimulus attributes, such as orientation.

To date, more studies support the synaptic mechanism due to its advantage in explaining the stimulus-specificity of visual adaptation. However, debates concerning the contributions of excitation and inhibition in local circuitry to the adaptation still exist. Some studies emphasize the importance of excitatory synaptic depression in mediating the adaptation process (Chung et al, 2002; Nowak et al, 2005; Reig et al, 2006). Some suggest an involvement of inhibitory synaptic activation in the adaptation effect, and others propose a network mechanism based on recurrent excitation and inhibition models (Kohn, 2007). Current evidences on the role of local inhibition in the adaptation process are mutually inconsistent. An *in vivo* study reported that the iontophoretic delivery of GABA_A receptor antagonists could significantly improve the adaptation strength of relay cells in the dorsal geniculate nucleus (LGNd) and the administration of baclofen, a GABA_B receptor agonist, could decrease the adaptation strength (Yang et al, 2003). However, similar manipulation of GABA inhibition failed to alter the amplitude of visual cortical cells to visual stimuli (DeBruyn & Bonds, 1986; Vidyasagar, 1990). Interestingly, V1 neurons of aged cats showed stronger adaptation to visual stimuli than that of young adult cats (Hua et al, 2009). This enhanced adaptation of V1 neurons during aging may indirectly suggest that neuronal response adaptation is correlated with the changes of intracortical inhibition (Hua et al, 2008; Hua et al, 2006; Leventhal et al, 2003).

In the present study, we evaluated the effects of surround suppression on the adaptation strength of V1

neurons. By manipulating the levels of surround suppression using different stimulus sizes outside the CRF, we found that the amplitude of response adaptation of V1 neuron decreased significantly with the increase of surround suppression due to the decrease of the neuron's IR to the adapted stimulus. These results indicate that the surround suppression might only modify a neuron's IR but not the adaptation process and the adaptation strength depends closely on the neuron's IR to the adapted stimulus. IR decreases with the increase of surround suppression and the decrease of response adaptation, vice versa. Therefore, the response adaptation of V1 neurons may under the dynamic regulation of a negative feedback mechanism. Our results, together with several recent findings (Benucci et al, 2013; Compte & Wang, 2006; Levy et al, 2013; Liu et al, 2013) suggest that visual adaptation may depend on a network mechanism that involves an interplay between inhibitory and excitatory neurons in the local neural circuitry.

Benefits of visual adaptation

The functional benefits of adaptation remain unclear due to the inconsistent evidences suggest that adaptation sometimes decreases sensitivity for the adapting stimuli, and sometimes it changes sensitivity for stimuli very different from the adapting ones (Gepshtein et al, 2013). Some studies claimed that adaptation could improve the detectability of the adapting stimuli (Abbonizio et al, 2002; Greenlee & Heitger, 1988; Määtänen & Koenderink, 1991). Others reported that adaptation increased

perception of novel stimuli in the environment while suppressing the perception of adapted stimuli (Dragoi et al, 2002; Hosoya et al, 2005; Sharpee et al, 2006). Benucci et al (2013) measured adaptation in the response of populations of V1 neurons to stimulus ensembles with markedly different statistics of stimulus orientation, and found that adaptation might act as a mechanism of homeostasis by maintaining time-averaged response quality and orientation selectivity independence across the population of neurons.

In this study, we determined the response adaptation changes of V1 neurons with different degree of surround suppression. We found that the response adaptation of V1 neurons decreased significantly with the increase of surround suppression due to the reduction of its IR to the adapted stimulus, whereas, the response of neurons during the plateau period of adaptation remained stable. These results are consistent with previous studies (Cavanaugh et al, 2002a) and suggest that V1 neurons may dynamically adjust its adaptation strength according to its initial spiking activities evoked by the adapted stimulus: adaptation enhances if initial activities are high or otherwise weakens if initial activities are low. The response of the neuron can eventually be reduced to the similar level, which is independent of the amplitude of initial response. This adaptation strategy may be critical in maintaining the homeostasis of neuronal response to long-lasting visual signals and aiding the energy efficiency/frugality of brain activities (Hua et al, 2009).

References

- Abbonizio G, Langley K, Clifford CW. 2002. Contrast adaptation may enhance contrast discrimination. *Spatial Vision*, **16**(1): 45-58.
- Akasaki T, Sato H, Yoshimura Y, Ozeki H, Shimegi S. 2002. Suppressive effects of receptive field surround on neuronal activity in the cat primary visual cortex. *Neuroscience Research*, **43**(3): 207-220.
- Bair W, Cavanaugh JR, Movshon JA. 2003. Time course and time-distance relationships for surround suppression in macaque V1 neurons. *Journal of Neuroscience*, **23**(20): 7690-7701.
- Benucci A, Saleem AB, Carandini M. 2013. Adaptation maintains population homeostasis in primary visual cortex. *Nature Neuroscience*, **16**(6): 724-729.
- Bishop PO, Kozak W, Vakkur GJ. 1962. Some quantitative aspects of the cat's eye: axis and plane of reference, visual field co-ordinates and optics. *Journal of Physiology*, **163**(3): 466-502.
- Brainard DH. 1997. The psychophysics toolbox. *Spatial Vision*, **10**(4): 433-436.
- Brown SP, Masland RH. 2001. Spatial scale and cellular substrate of contrast adaptation by retinal ganglion cells. *Nature Neuroscience*, **4**(1): 44-51.
- Carandini M. 2000. Visual cortex: Fatigue and adaptation. *Current Biology*, **10**(16): R605-607.
- Carandini M, Ferster D. 1997. A tonic hyperpolarization underlying contrast adaptation in cat visual cortex. *Science*, **276**(5314): 949-952.
- Cavanaugh JR, Bair W, Movshon JA. 2002a. Nature and interaction of signals from the receptive field center and surround in macaque V1 neurons. *Journal of Neurophysiology*, **88**(5): 2530-2546.
- Cavanaugh JR, Bair W, Movshon JA. 2002b. Selectivity and spatial distribution of signals from the receptive field surround in macaque V1 neurons. *Journal of Neurophysiology*, **88**(5): 2547-2556.
- Chung S, Li X, Nelson SB. 2002. Short-Term depression at thalamocortical synapses contributes to rapid adaptation of cortical sensory responses *in Vivo*. *Neuron*, **34**(3): 437-446.

- Clifford CW, Webster MA, Stanley GB, Stocker AA, Kohn A, Sharpee TO, Schwartz O. 2007. Visual adaptation: neural, psychological and computational aspects. *Vision Research*, **47**(25): 3125-3131.
- Compte A, Wang XJ. 2006. Tuning curve shift by attention modulation in cortical neurons: a computational study of its mechanisms. *Cerebral Cortex*, **16**(6): 761-778.
- Dao DY, Lu ZL, Doshier BA. 2006. Adaptation to sine-wave gratings selectively reduces the contrast gain of the adapted stimuli. *Journal of Vision*, **6**(7): 739-759.
- DeBruyn EJ, Bonds AB. 1986. Contrast adaptation in cat visual cortex is not mediated by GABA. *Brain Research*, **383**(1-2): 339-342.
- Dragoi V, Sharma J, Miller EK, Sur M. 2002. Dynamics of neuronal sensitivity in visual cortex and local feature discrimination. *Nature Neuroscience*, **5**(9): 883-891.
- Duong T, Freeman RD. 2007. Spatial frequency-specific contrast adaptation originates in the primary visual cortex. *Journal of Neurophysiology*, **98**(1): 187-195.
- Durand S, Freeman TC, Carandini M. 2007. Temporal properties of surround suppression in cat primary visual cortex. *Vision Neuroscience*, **24**(5): 679-690.
- Ego-Stengel V, Bringuier V, Shulz DE. 2002. Noradrenergic modulation of functional selectivity in the cat visual cortex: an in vivo extracellular and intracellular study. *Neuroscience*, **111**(2): 275-289.
- Fu Y, Wang XS, Wang YC, Zhang J, Liang Z, Zhou YF, Ma YY. 2010. The effects of aging on the strength of surround suppression of receptive field of V1 cells in monkeys. *Neuroscience*, **169**(2): 874-881.
- Gepshtein S, Lesmes LA, Albright TD. 2013. Sensory adaptation as optimal resource allocation. *Proceedings of the National Academy of Sciences of the United States of America*, **110**(11): 4368-4373.
- Greenlee MW, Heitger F. 1988. The functional role of contrast adaptation. *Vision Research*, **28**(7): 791-797.
- Haider B, Krause MR, Duque A, Yu Y, Touryan J, Mazer JA, McCormick DA. 2010. Synaptic and network mechanisms of sparse and reliable visual cortical activity during nonclassical receptive field stimulation. *Neuron*, **65**(1): 107-121.
- Hosoya T, Baccus SA, Meister M. 2005. Dynamic predictive coding by the retina. *Nature*, **436**(7047): 71-77.
- Howarth CM, Vorobyov V, Sengpiel F. 2009. Interocular transfer of adaptation in the primary visual cortex. *Cerebral Cortex*, **19**(8): 1835-1843.
- Hua T, Bao P, Huang CB, Wang Z, Xu J, Zhou Y, Lu ZL. 2010. Perceptual learning improves contrast sensitivity of V1 neurons in cats. *Current Biology*, **20**(10): 887-894.
- Hua TM, Kao CC, Sun QY, Li XR, Zhou YF. 2008. Decreased proportion of GABA neurons accompanies age-related degradation of neuronal function in cat striate cortex. *Brain Research Bulletin*, **75**(1): 119-125.
- Hua TM, Li GZ, Tang CH, Wang ZH, Chang S. 2009. Enhanced adaptation of visual cortical cells to visual stimulation in aged cats. *Neuroscience Letters*, **451**(1): 25-28.
- Hua TM, Li XR, He LH, Zhou YF, Wang YC, Leventhal AG. 2006. Functional degradation of visual cortical cells in old cats. *Neurobiology of Aging*, **27**(1): 155-162.
- Kohn A. 2007. Visual adaptation: physiology, mechanisms, and functional benefits. *Journal of Neurophysiology*, **97**(5): 3155-3164.
- Leventhal AG, Wang Y, Pu M, Zhou Y, Ma Y. 2003. GABA and its agonists improved visual cortical function in senescent monkeys. *Science*, **300**(5620): 812-815.
- Levy M, Fournier J, Fregnac Y. 2013. The role of delayed suppression in slow and fast contrast adaptation in V1 simple cells. *Journal of Neuroscience*, **33**(15): 6388-6400.
- Li B, Freeman RD. 2011. Neurometabolic coupling differs for suppression within and beyond the classical receptive field in visual cortex. *Journal of Physiology*, **589**(Pt 13): 3175-3190.
- Liu RL, Wang K, Meng JJ, Hua TM, Liang Z, Xi MM. 2013. Adaptation to visual stimulation modifies the burst firing property of V1 neurons. *Zoological Research*, **34**(3): E101-E108.
- Mänttinen LM, Koenderink JJ. 1991. Contrast adaptation and contrast gain control. *Experimental Brain Research*, **87**(1): 205-212.
- Maffei L, Fiorentini A, Bisti S. 1973. Neural correlate of perceptual adaptation to gratings. *Science*, **182**(4116): 1036-1038.
- Marlin SG, Hasan SJ, Cynader MS. 1988. Direction-selective adaptation in simple and complex cells in cat striate cortex. *Journal of Neurophysiology*, **59**(4): 1314-1330.
- McLean J, Palmer LA. 1996. Contrast adaptation and excitatory amino acid receptors in cat striate cortex. *Visual Neuroscience*, **13**(6): 1069-1087.
- Meng JJ, Liu RL, Wang K, Hua TM, Lu ZL, Xi MM. 2013. Neural correlates of stimulus spatial frequency-dependent contrast detection. *Experimental Brain Research*, **225**(3): 377-385.
- Movshon JA, Lennie P. 1979. Pattern-selective adaptation in visual cortical neurones. *Nature*, **278**(5707): 850-852.
- Nowak LG, Sanchez-Vives MV, McCormick DA. 2005. Role of synaptic and intrinsic membrane properties in short-term receptive field dynamics in cat area 17. *Journal of Neuroscience*, **25**(7): 1866-1880.
- Pelli DG. 1997. The VideoToolbox software for visual psychophysics: transforming numbers into movies. *Spatial Vision*, **10**(4): 437-442.
- Reig R, Gallego R, Nowak LG, Sanchez-Vives MV. 2006. Impact of cortical network activity on short-term synaptic depression. *Cerebral Cortex*, **16**(5): 688-695.
- Sanchez-Vives MV, Nowak LG, McCormick DA. 2000a. Cellular mechanisms of long-lasting adaptation in visual cortical neurons in vitro. *Journal of Neuroscience*, **20**(11): 4286-4299.
- Sanchez-Vives MV, Nowak LG, McCormick DA. 2000b. Membrane mechanisms underlying contrast adaptation in cat area 17 in vivo. *Journal of Neuroscience*, **20**(11): 4267-4285.
- Sekuler R, Pantle A. 1967. A model for after-effects of seen movement. *Vision Research*, **7**(5): 427-439.

- Series P, Lorenceau J, Fregnac Y. 2003. The "silent" surround of V1 receptive fields: theory and experiments. *Journal of Physiology*, **97**(4-6): 453-474.
- Sharpee TO, Sugihara H, Kurgansky AV, Rebrik SP, Stryker MP, Miller KD. 2006. Adaptive filtering enhances information transmission in visual cortex. *Nature*, **439**(7079): 936-942.
- Smirnakis SM, Berry MJ, Warland DK, Bialek W, Meister M. 1997. Adaptation of retinal processing to image contrast and spatial scale. *Nature*, **386**(6620): 69-73.
- Smith AT, Hammond P. 1985. The pattern specificity of velocity aftereffects. *Experimental Brain Research*, **60**(1): 71-78.
- Smith MA, Bair W, Movshon JA. 2006. Dynamics of suppression in macaque primary visual cortex. *Journal of Neuroscience*, **26**(18): 4826-4834.
- Tailby C, Solomon SG, Peirce JW, Metha AB. 2007. Two expressions of "surround suppression" in V1 that arise independent of cortical mechanisms of suppression. *Visual Neuroscience*, **24**(1): 99-109.
- Teich AF, Qian N. 2003. Learning and adaptation in a recurrent model of V1 orientation selectivity. *Journal of Neurophysiology*, **89**(4): 2086-2100.
- Vidyasagar TR. 1990. Pattern adaptation in cat visual cortex is a co-operative phenomenon. *Neuroscience*, **36**(1): 175-179.
- Walker GA, Ohzawa I, Freeman RD. 2000. Suppression outside the classical cortical receptive field. *Visual Neuroscience*, **17**(3): 369-379.
- Waterhouse BD, Azizi SA, Burne RA, Woodward DJ. 1990. Modulation of rat cortical area 17 neuronal responses to moving visual stimuli during norepinephrine and serotonin microiontophoresis. *Brain Research*, **514**(2): 276-292.
- Webb BS, Dhruv NT, Solomon SG, Tailby C, Lennie P. 2005. Early and late mechanisms of surround suppression in striate cortex of macaque. *Journal of Neuroscience*, **25**(50): 11666-11675.
- Yang Y, Jin J, Zhou Y, Shou T. 2003. GABA(A) and GABA(B) receptors mediated inhibition affect the pattern adaptation of relay cells in the dorsal lateral geniculate nucleus (LGNd) of cats. *Brain Research*, **959**(2): 295-303.

Protease-activated receptor (PAR)1, PAR2 and PAR4 expressions in esophageal squamous cell carcinoma

Si-Man LI¹, Ping JIANG¹, Yang XIANG², Wei-Wei WANG³, Yue-Chun ZHU¹, Wei-Yang FENG¹, Shu-De LI¹, Guo-Yu YU^{1,*}

1. Kunming Medical University, Kunming 650500, China

2. Key Laboratory of Animal Models and Human Disease Mechanisms of the Chinese Academy of Sciences & Yunnan Province, Kunming Institute of Zoology, Kunming 650223, China

3. Third Affiliated Hospital of Kunming Medical University, Department of Thoracic Surgery, Kunming 650000, China

Abstract: Here, we used reverse transcription-PCR (RT-PCR) and western blot to detect protease-activated receptor (PAR) 1, PAR 2 and PAR 4 expression in cancer tissues and cell lines of esophageal squamous cell carcinoma, and investigated the co-relationship between PAR expression and clinic-pathological data for esophageal cancer. The methylation of *PAR4* gene promoter involved in esophageal carcinoma was also analyzed. By comparing the mRNA expressions of normal esophageal tissue and human esophageal epithelial cells (HEEpiC), we found that among the 28 cases of esophageal squamous cell carcinoma, *PAR1* (60%) and *PAR2* (71%) were elevated in 17 and 20 cases, respectively, and *PAR4* (68%) expression was lowered in 19 cases. Whereas, in human esophageal squamous cells (TE-1 and TE-10), *PAR1* and *PAR2* expression was increased but *PAR4* was decreased. Combined with clinical data, the expression of PAR1 in poorly differentiated ($P=0.016$) and middle and lower parts of the esophagus ($P=0.016$) was higher; expression of PAR4 in poorly differentiated carcinoma was lower ($P=0.049$). Regarding TE-1 and TE-10 protein expression, we found that in randomized esophageal carcinoma, PAR1 ($P=0.027$) and PAR2 ($P=0.039$) expressions were increased, but lowered for PAR4 ($P=0.0001$). In HEEpiC, TE-1, TE-10, esophageal and normal esophagus tissue samples (case No. 7), the frequency of methylation at the 19 CpG loci of *PAR4* was 35.4%, 95.2%, 83.8%, 62.6% and 48.2%, respectively. Our results indicate that the expression of PAR1 and PAR2 in esophageal squamous cell carcinoma is increased but PAR4 is decreased. Hypermethylation of the promoter of the *PAR4* gene may contribute to reduced expression of PAR4 in esophageal squamous cell carcinoma.

Keywords: PAR1; PAR2; PAR4; Esophageal squamous cell carcinoma; PCR; Western Blot; Methylation

The development of esophageal squamous cell carcinoma (ESCC) is a complicated process with multiple pathological stages. Among various regulatory factors, proteases play critical roles in activating signal transduction pathways and regulating gene expression (Ikeda et al, 1999). Protease-activated receptors (PARs) are a subfamily of the single seven-transmembrane G-protein-coupled receptors and include PAR1, PAR2, PAR3 and PAR4 (Macfarlane et al, 2001). PAR1, PAR3 and PAR4 are thrombin receptors, and PAR2 is trypsinase/tryptase receptor (Xu et al, 1998). Ribeiro et al (2009) found high expression of PAR1 but low expression of PAR2 in the tissues of ESCC; however, Wang et al (2010) found high expression of PAR2 in ESCC. PAR4 is a recently discovered novel subtype expressed in high amounts in

colon cancer and hepatocarcinoma and induces the proliferation and migration of cancer cells (Gratio et al, 2009; Kaufmann et al, 2007). PAR4 expression in stomach cancer tissues (Zhang et al, 2011) and adenocarcinoma of the lung are low (Jiang et al, 2013), but its expression in ESCC remains unclear.

Here, we determined the expression of PAR1, PAR2 and PAR4 in tissues of ESCC and analyzed correlations

Received: 28 March 2014; Accepted: 20 May 2014

Foundation items: This study was supported by the National Natural Foundation of China (81160302), the Major Research Project of Yunnan Province (2011FZ109), and Research project of Yunnan Education Bureau (2014Y153)

*Corresponding author, E-mail: yuguoyu2011@hotmail.com

between *PAR4* promoter hypermethylation and the development of ESCC. Our aim was to provide theoretical evidence for clinical diagnosis, treatment and prognosis of ESCC and provide a basis for drug research.

MATERIALS AND METHODS

Experimental materials

Human esophageal epithelial cells (HEEpiC) and human esophageal squamous cells (TE-1, TE-10) were obtained from the Cell Bank of Kunming Institute of Zoology, Chinese Academy of Sciences. Tissues of 28 cases (male=21, female=5; 51-81 years old) of diagnosed ESCC were from hospitals affiliated with the Kunming Medical University, Yunnan, China. All patients were clean of any chemotherapy or radiation treatment prior to surgery. The carcinoma tissues and corresponding normal control tissues (at least 5 cm away from carcinoma tissue) obtained during surgery were quick frozen in liquid nitrogen and stored at -80°C . All the experimental protocols were approved by the Ethics Committee of Kunming Medical University.

Experimental procedures Cell culture

TE-1 and TE-10 cells were cultured with RPM-11640 (Takara, Beijing, China) completed culture medium containing 10% FBS and incubated at 37°C with 5% CO_2 (relative humidity=95%). Culture medium was changed 1–2 days later. Cells were subcultured 3–5 days later and digested with 0.25% trypsinase: 0.03% EDTA (1:1). HEEpiC were cultured with HEEpiC-specific (Takara, Beijing, China) culture medium and the culture procedure was the same as that for TE-1 cells.

Reverse transcription-PCR (RT-PCR)

Total RNA of ESCC tissues, TE-1, TE-10 and HEEpiC were extracted using a RNA extraction kit (Tiangen Biotech, Beijing, China). The purity and integrity of total RNA were tested. cDNAs were reverse transcribed from

total RNAs of tissues and cells (2 ng–2 μg) using a reverse transcription kit (Takara, Beijing, China) and then stored at -20°C . Gene amplifications were performed by taking cDNAs as templates and *GAPDH* as internal reference. Primers for *GAPDH*, *PAR1*, *PAR2* and *PAR4* are shown in Table 1. PCR products were run by 2% agarose gel electrophoresis and observed under ultraviolet light and photographed.

Western blot

Carcinoma tissues and corresponding normal control tissues were randomly selected from three cases. Cultured cells in logarithmic growth were rinsed twice with pre-chilled PBS (4°C) and then lysed with $6\times$ SDS (0.6 mL) and water-bathed (95°C) for 15 min. After the polymerization of resolving gel (12%) and stacking gel (5%), samples were loaded. Tris-glycine electrophoresis buffer ($\times 1$) was poured into the running chamber and loaded samples were run for 1 h at a constant current of 160 V. Then the gel was transferred onto the PVDF membrane for 2 h at a constant current of 250 mA and 4°C . The blots were removed from the transfer unit and blocked by placing in 3% BSA-TBST blotting solution for 2 h with shaking at room temperature. After washing, the blot was incubated with the primary antibodies for PAR1, PAR2, PAR4 and β -actin over night at 4°C . After washing, the blot was incubated with secondary antibodies. After another three washes, the blot was revealed via HRP-ECL chemiluminescence detection and scanned using the SynGene scanning system. The illumination densities of the detected protein bands were transferred into optical density values (OD values). The developing strength of each target protein band and its internal reference (β -actin) were determined by OD values. The ratio of the OD values of each target protein band to its internal reference (β -actin) was taken as the result of RT-PCR.

Table 1 Primers and reaction conditions used in RT-PCR

Gene	Primer sequences	NCBI Accession Number	Annealing temperature ($^{\circ}\text{C}$)	Product (bp)
<i>GAPDH</i>	F: 5'-ATGGGGAAGGTGAAGGTCG-3'	NM_001101.3	60	308
	R: 5'-GGGGTCATTGATGGCAACAATA-3'			
<i>PAR1</i>	F: 5'-GCCGCTGCTTCAGTCTGTGC-3'	NM_001992.3	67	648
	R: 5'-GGCCAGACAAGTGAAGGAAGC-3'			
<i>PAR2</i>	F: 5'-CCATCCAAGGAACCAATAGATC-3'	NM_005242.3	60	643
	R: 5'-ATGTCCTCCACCAAGAGCTGCTCA-3'			
<i>PAR4</i>	F: 5'-GGCAACCTCTATGGTGCCTA-3'	NM_003950.2	58	244
	R: 5'-TTCGACCCAGTACAGCCTTC-3'			

Bisulfite genomic sequencing PCR

Genomic DNAs of TE-1, TE-10, HEEpiC and the No. 7 tissue sample were extracted using a genome DNA extraction kit (Takara, Beijing, China) and their concentrations were determined. The CpG sites in *PAR4* were amplified with the MethylCode Bisulfite Conversion Kit (Invitrogen, US). PCR products were eluted and purified with the AxyPrep DNA elution kit (Axygen). Primer sequences were: F-5'-TTTAAGGGTGATTTAGGAAA GGTTCAGAG-3' and R-5'-ACTATAACCTCAAACCTC CTACCTC-3'. The products of ligation were transformed with DH5 α component cells. Transformation products were spread on LB plates (with Ampicillin) and grown overnight. Clones were selected and sent for sequencing.

Statistical analyses

Data were analyzed using SPSS 17.0 (SPSS Inc., Chicago, USA). Correlations between PAR expression and clinical pathologies were tested using Fisher's exact tests. The illumination strength of protein expression is expressed as mean \pm SD and comparisons between expressions were conducted using *t*-tests. Statistical significance was set at $P < 0.05$.

RESULTS

mRNA expression of *PAR1*, *PAR2* and *PAR4* and correlation with clinical manifestation

When the expression of *GAPDH* of each sample was at a similar level, the brighter the mRNA band was, the higher the expression level of *PAR* was, and *vice versa*. Among the 28 cases of ESCC, 17 (60%) and 20 (71%) cases were found with increased expression of *PAR1* and *PAR2*, respectively. Totally, 19 (68%) cases were found with decreased *PAR4*. In TE-1 and TE-10, the expression of *PAR1* and *PAR2* was high. The expression of *PAR4* mRNA in TE-1 and TE-10 was lower than in HEEpiC. The expression level of *PAR1*, *PAR2* and *PAR4* mRNA in the tissues and cells from cases 7, 8 and 9 are shown in Figure 1. Combined with clinical pathological data, the expression of *PAR1* in central and low located ESCC was significantly higher than in upper ESCC ($P = 0.007$ and $P = 0.008$, respectively). The expression of *PAR2* in phase III+IV ESCC was significantly higher than in phase I+II ($P = 0.004$). Significantly lower expression of *PAR4* was found in lower ESCC, compared with central and upper ESCC ($P = 0.036$). No significant correlation for the expression of *PAR1*, *PAR2* and *PAR4*

and patients' gender, sex and distant or lymph node metastases were found (Table 2).

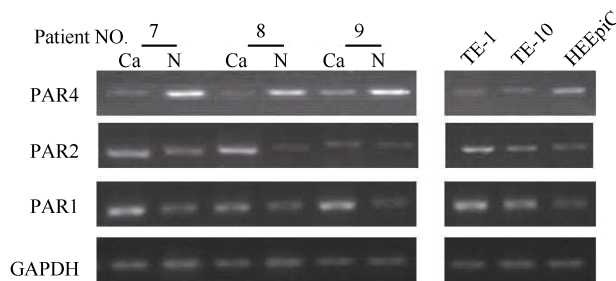


Figure 1 *PAR1*, *PAR2* and *PAR4* mRNA expression in esophageal squamous cell carcinoma and normal control tissues

Protein expression of *PAR1*, *PAR2* and *PAR4* in tissues and cells of ESCC

Protein expression was determined by taking β -actin as the internal reference (Figure 2). The expression of *PAR1* and *PAR2* proteins were increased ($P < 0.05$), whereas, those of *PAR4* were decreased ($P < 0.05$). The light degrees of protein expression of *PAR1*, *PAR2* and *PAR4* in sample tissues are shown in Table 3. The expression of *PAR1* and *PAR2* were high and that of *PAR4* was low in TE-1 and TE-10 cells.

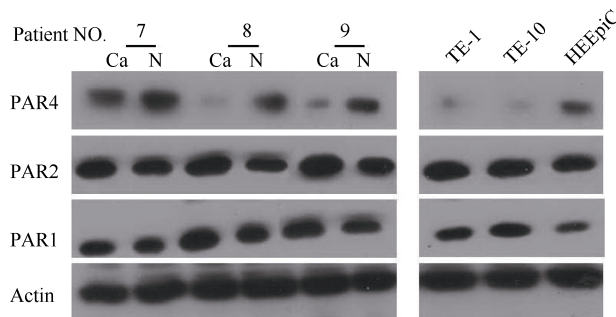


Figure 2 Protein expression of *PAR1*, *PAR2* and *PAR4* in tissues and cells of esophageal squamous cell carcinoma

PAR4 promoter hypermethylation in tissues and cells of ESCC

The BSP results of the PCR products of CpG sites in *PAR4* are shown in Table 4. In HEEpiC, TE-1 and TE-10, esophageal and normal esophagus tissue from case No. 7, the methylation frequency of the 19 CpG sites in *PAR4* was 35.4%, 95.2%, 83.8%, 62.6% and 48.2%, respectively.

DISCUSSION

PAR2 over-expression is commonly found in malignant tumors. In this study, among 28 cases of ESCC, 20 (71%) cases were found with high *PAR2*

Table 2 Correlation between *PAR1*, *PAR2* and *PAR4* mRNA levels and clinical manifestation of esophageal squamous cell carcinoma

Clinical data	Case numbers (<i>n</i>)	<i>PAR1</i>			<i>PAR2</i>			<i>PAR4</i>		
		Decreased	Increased	<i>P</i> -value	Decreased	Increased	<i>P</i> -value	Decreased	Increased	<i>P</i> -value
Age (year)										
≤65	13	5	8	1.000	3	10	0.686	8	5	0.689
>65	15	6	9		5	10		11	4	
Gender										
Male	21	9	12	0.668	4	17	0.142	15	6	0.646
Female	7	2	5		4	3		4	3	
Clinical stage										
I + II	16	8	8	0.253	7	9	0.088	11	5	1.000
III+IV	12	3	9		1	11		8	4	
Location of the tumor										
Upper	4	4	0	0.016*	0	4	0.549	2	2	0.574
Central and lower	24	7	17		5	16		17	7	
Differentiation										
Well and moderated	17	10	7	0.016*	7	10	0.099	9	8	0.049*
Poor	11	1	10		1	10		10	1	
Distant metastasis										
Positive	1	0	1	1.000	0	1	1.000	1	0	1.000
Negative	27	11	16		8	19		18	9	
Lymph node metastasis										
Positive	11	4	7	1.000	2	9	0.419	8	3	0.704
Negative	17	7	10		6	11		11	6	

*: $P < 0.05$.**Table 3** Gray values of PAR expression in sample tissues

Gene	Cancer tissue	Normal tissue	<i>t</i>	<i>P</i>
<i>PAR4</i>	0.18±0.05	0.42±0.12	9.77	0.0001**
<i>PAR2</i>	0.84±0.28	0.69±0.25	7.97	0.039*
<i>PAR1</i>	0.74±0.31	0.58±0.21	2.26	0.027*

*: $P < 0.05$; **: $P < 0.01$.

mRNA expression. The expression of *PAR2* mRNA was also increased in TE-1 and TE-10 cells. The gray value indicates that PAR2 protein expression is increased in ESCC ($P=0.039$). PAR2 can be activated by trypsinase, human mast cell tryptase (MCT), coagulation factor VIIa and tissue factor complex (Caruso et al, 2006; Uusitalo-Jarvinen et al, 2007). The *in vitro* synthesized SLIGKV by the degradation of PAR2 can also activate PAR2 (Déry et al, 1998). Activated PAR2 may release vascular endothelial growth factor (VEGF), Interleukin-6 (IL-6) and IL-8 of tumor cells and thereafter promote the generation and invasion of novel vessels by malignant

tumors (Knecht et al, 2007; Matej et al, 2007). Activated PAR2 may also increase the reverse activity of epidermal growth factor (EGF) and the release of transformation growth factor α (TGF α), and thus promote the proliferation of gastrointestinal cancer cells in stomach cancer, colon cancer, pancreatic cancer and ESCC (Darmoul et al, 2004; Fujimoto et al, 2006; Yada et al, 2005).

PAR1 and PAR4 are both thrombin receptors. Among the 28 cases of ESCC examined in the present study, 17 (60%) cases were found with high expression of *PAR1* mRNA; however, 19 (68%) cases were found with low expression of *PAR4* mRNA. The expression of *PAR1* mRNA was increased in TE-1 and TE-10 cells, whereas, that of *PAR4* was decreased. The gray value indicates that PAR1 protein expression was increased in ESCC ($P=0.027$) and that of PAR4 was significantly decreased ($P=0.0001$). High PAR1 expression was found in ESCC, particularly in central and lower ($P=0.016$) and poorly differentiated ESCC ($P=0.049$), whereas, the low expression of PAR4 was found in ESCC, particularly in

poorly differentiated ESCC.

Table 4 Methylation frequency of the 19 CpG sites in *PAR4* of cells and tissue of esophageal squamous cell carcinoma

CpG position	Gene	3	12	41	68	95	124	195	215	227	259	275	292	327	330	332	341	345	350	377	Total
Me-CpG (%)	HEEPIC	18	73	0	64	27	55	73	9	46	0	46	55	27	0	0	0	73	55	55	35.4
	TE-1	100	100	90.9	100	100	81.8	100	30	100	100	82	91	100	100	91	91	100	100	100	95.2
	TE-10	82	100	100	100	100	100	100	91	100	100	46	73	55	55	100	100	100	55	30	83.8
	Cancer tissue	64	46	30	46	64	9	64	100	91	100	100	100	91	91	9	46	46	30	64	62.6
	Normal tissue	91	64	9	55	64	30	55	9	55	100	100	9	0	55	55	30	64	30	46	48.2

To investigate the underlying mechanisms of PAR4 and ESCC, methylation of the *PAR4* promoter in tissues and cells of ESCC was evaluated. The results show that the methylation frequencies of *PAR4* promoters in sample tissues of ESCC (62.6%) and TE-1 and TE-10 (83.8% and 95.2%, respectively) were both high. Together with the fact that the expression of *PAR4* mRNA and protein is lower in tissues and cells of ESCC, these findings indicate that the methylation frequency of *PAR4* promoters may play a role in its expression in ESCC.

Kawabata et al (1999) found the relaxation induced by PAR4 aggravates duodenal-gastric-esophageal reflux, and trypsinase within the reflux liquid may activate PAR4, thus promoting the incidence of ESCC. Han et al (2011) found that the promoting effects of PAR4 on anti-angiogenesis factors, including endostatin, thrombo-standin 1, $\alpha 2$ macroglobulin, plasminogen activator, ang-iostatin and enzyme inhibitors may remarkably inhibit

the generation of novel vessels and tumors. Human blood platelets only express PAR1 and PAR4. Activated PAR4 inhibits the release of VEGF but promotes the exp-ression of endostatin, whereas, the effects of activated PAR1 are the opposite (Ma et al, 2005). Longitudinal gastrointestinal smooth muscles are intensified by PAR1 but relaxed by PAR4. PAR4 also prevents over intension in smooth muscles induced by PAR1 and thrombin (Lan et al, 2000). Cunningham et al (2012) found that similar interactions between PAR2 and PAR4 may play a role in locating receptors and cellular signal transduction.

In sum, here we investigated the expression charac-teristics of PAR1, PAR2 and PAR4 in ESCC tissues to broaden our understanding of PARs in ESCC. As G-protein-coupled receptors, the complicated biological distribution and function of PAR1, PAR2 and PAR4 remain unclear and their activity and interactions require further attention.

References

- Caruso R, Pallone F, Fina D, Gioia V, Peluso I, Caprioli F, Stolfi C, Perfetti A, Spagnoli LG, Palmieri G, Macdonald TT, Monteleone G. 2006. Protease-activated receptor-2 activation in gastric cancer cells promotes epidermal growth factor receptor *trans*-activation and proliferation. *The American Journal of Pathology*, **169**(1): 268-278.
- Cunningham MR, McIntosh KA, Pediani JD, Robben J, Cooke AE, Nilsson M, Gould GW, Mundell S, Milligan G, Plevin R. 2012. Novel role for proteinase-activated receptor 2 (PAR₂) in membrane trafficking of proteinase-activated receptor 4 (PAR₄). *Journal of Biological Chemistry*, **287**(20): 16656-16669.
- Darmoul D, Gratio V, Devaud H, Laburthe M. 2004. Protease-activated receptor 2 in colon cancer: trypsin-induced MAPK phosphorylation and cell proliferation are mediated by epidermal growth factor receptor transactivation. *Journal of Biological Chemistry*, **279**(20): 20927-20934.
- Déry O, Corvera CU, Steinhoff M, Bunnett NW. 1998. Proteinase-activated receptors: novel mechanisms of signaling by serine proteases. *The American Journal of Physiology*, **274**(6): C1429-C1452.
- Fujimoto D, Hirono Y, Goi T, Katayama K, Hirose K, Yamaguchi A. 2006. Expression of protease activated receptor-2 (PAR-2) in gastric cancer. *Journal of Surgical Oncology*, **93**(2): 139-144.
- Gratio V, Walker F, Lehy T, Laburthe M, Darmoul D. 2009. Aberrant expression of proteinase-activated receptor 4 promotes colon cancer cell proliferation through a persistent signaling that involves Src and ErbB-2 kinase. *International Journal of Cancer*, **124**(7): 1517-1525.
- Han N, Jin K, He KF, Cao J, Teng LS. 2011. Protease-activated receptors in cancer: A systematic review. *Oncology Letters*, **2**(4): 599-608.
- Ikeda G, Isaji S, Chandra B, Watanabe M, Kawarada Y. 1999. Prognostic significance of biologic factors in squamous cell carcinoma of the esophagus. *Cancer*, **86**(8): 1396-1405.
- Jiang P, Yu GY, Zhang Y, Xiang Y, Hua HR, Bian L, Wang CY, Lee WH, Zhang Y. 2013. Down-regulation of protease-activated receptor 4 in lung adenocarcinoma is associated with a more aggressive phenotype. *Asian Pacific Journal of Cancer Prevention*, **14**(6): 3793-3798.
- Kaufmann R, Rahn S, Pollrich K, Hertel J, Dittmar Y, Hommann M, Henklein P, Biskup C, Westermann M, Hollenberg MD, Settmacher U.

2007. Thrombin-mediated hepatocellular carcinoma cell migration: cooperative action via proteinase-activated receptors 1 and 4. *Journal of Cellular Physiology*, **211**(3): 699-707.
- Kawabata A, Kuroda R, Nishikawa H, Kawai K. 1999. Modulation by protease-activated receptors of the rat duodenal motility *in vitro*: possible mechanisms underlying the evoked contraction and relaxation. *British Journal of Pharmacology*, **128**(4): 865-872.
- Knecht W, Cottrell GS, Amadesi S, Mohlin J, Skåregårde A, Gedda K, Peterson A, Chapman K, Hollenberg MD, Vergnolle N, Bunnett NW. 2007. Trypsin IV or mesotrypsin and p23 cleave protease-activated receptors 1 and 2 to induce inflammation and hyperalgesia. *Journal of Biological Chemistry*, **282**(36): 26089-26100.
- Lan RS, Stewart GA, Henry PJ. 2000. Modulation of airway smooth muscle tone by protease activated receptor-1, -2, -3 and -4 in trachea isolated from influenza A virus-infected mice. *British Journal of Pharmacology*, **129**(1): 63-70.
- Ma L, Perini R, McKnight W, Dickey M, Klein A, Hollenberg MD, Wallace JL. 2005. Proteinase-activated receptors 1 and 4 counter-regulate endostatin and VEGF release from human platelets. *Proceedings of the National Academy of Sciences of the United States of America*, **102**(1): 216-220.
- Macfarlane SR, Seatter MJ, Kanke T, Hunter GD, Plevin R. 2001. Proteinase-activated receptors. *Pharmacological Reviews*, **53**(2): 245-282.
- Matej R, Mandáková P, Netíková I, Poucková P, Olejár T. 2007. Proteinase-activated receptor-2 expression in breast cancer and the role of trypsin on growth and metabolism of breast cancer cell line MDA MB-231. *Physiological Research*, **56**(4): 475-484.
- Ribeiro FS, Simão TA, Amôêdo ND, Andreollo NA, Lopes LR, Acatauassu R, Rumjanek FD, Albano RM, Pinto LF, Monteiro RQ. 2009. Evidence for increased expression of tissue factor and protease-activated receptor-1 in human esophageal cancer. *Oncology Reports*, **21**(6): 1599-1604.
- Uusitalo-Jarvinen H, Kurokawa T, Mueller BM, Andrade-Gordon P, Friedlander M, Ruf W. 2007. Role of protease activated receptor 1 and 2 signaling in hypoxia-induced angiogenesis. *Arteriosclerosis, Thrombosis, and Vascular Biology*, **27**(6): 1456-1462.
- Wang X, Liu HT, Li S, Li K, Lin N, Fan QX, Zheng YL. 2010. Prognostic value of protease-activated receptor 2 expression in oesophageal squamous cell carcinoma. *The Journal of International Medical Research*, **38**(4): 1381-1388.
- Xu WF, Andersen H, Whitmore TE, Presnell SR, Yee DP, Ching A, Gilbert T, Davie EW, Foster DC. 1998. Cloning and characterization of human protease-activated receptor 4. *Proceedings of the National Academy of Sciences of the United States of America*, **95**(12): 6642-6646.
- Yada K, Shibata K, Matsumoto T, Ohta M, Yokoyama S, Kitano S. 2005. Protease-activated receptor-2 regulates cell proliferation and enhances cyclooxygenase-2 mRNA expression in human pancreatic cancer cells. *Journal of Surgical Oncology*, **89**(2): 79-85.
- Zhang Y, Yu GY, Jiang P, Xiang Y, Li WL, Lee W, Zhang Y. 2011. Decreased expression of protease-activated receptor 4 in human gastric cancer. *The International Journal of Biochemistry & Cell Biology*, **43**(9): 1277-1283.

Differences in cocaine-induced place preference persistence, locomotion and social behaviors between C57BL/6J and BALB/cJ mice

Jian-Li WANG^{1,*}, Bei WANG^{1,2}, Wen CHEN²

1. College of Biology Sciences and Engineering, Beifang University of Nationalities, Yinchuan 750021, China

2. College of Life Sciences, Shaanxi Normal University, Xi'an 710062, China

Abstract: C57BL/6J and BALB/cJ mice display significant differences in sociability and response to drugs, but the phenotypic variability of their susceptibility to cocaine is still not well known. In this study, the differences between these two mice strains in the persistence of cocaine-induced conditioned place preference (CPP), as well as the locomotion and social behaviors after the 24-hour withdrawal from a four-day cocaine (20 mg/kg/day) administration were investigated. The results showed that the cocaine-induced CPP persisted over two weeks in C57BL/6J mice, while it diminished within one week among BALB/cJ mice. After 24-hours of cocaine withdrawal, high levels of locomotion as well as low levels of social interaction and aggressive behavior were found in C57BL/6J mice, but no significant changes were found in BALB/cJ mice, indicating that cocaine-induced CPP persistence, locomotion and social behavior are not consistent between these two strains, and that overall C57BL/6J mice are more susceptible to cocaine than BALB/cJ mice at the tested doses.

Keywords: Cocaine; Conditioned place preference; Locomotion; Social behavior; Withdrawal

C57BL/6J and BALB/cJ mice are two widely used strains in biomedical research, especially in behavioral neurosciences. Because these two strains have different neurochemical and endocrinological substrates (Ågmo et al, 1999; Scislowska-Czarnecka et al, 2004; Bach et al, 2011; Kundakovic et al, 2013), they display different responding patterns on many behavioral tasks. For example, BALB/cJ mice are with less sociability (the tendency to seek social interaction) (Sankoorikal et al, 2006; Brodtkin, 2007; Moy et al, 2007) but higher levels of anxiety-like behaviors (Bouwknicht & Paylor, 2002; Priebe et al, 2005; Verleye et al, 2011). C57BL/6J mice performs better in learning and memory tasks (Crawley et al, 1997; Van Dam et al, 2006; Shi et al, 2008). C57BL/6J mice exhibit approaching responses toward a novel environment, while BALB/cJ mice exhibit avoidance (Belzung & Berton, 1997; Belzung & Barreau, 2000). Bardo et al (1996) previously claimed that high levels of novelty seeking are associated with an increased risk of drug abusing. Studies also indicated that C57BL/6J and BALB/cJ mice differ in several aspects of drug abuse. For example, C57BL/6J mice are prone to cocaine self-administration (Deroche et al, 1997; Thom-

sen & Caine, 2011) and display a cocaine-induced conditioned place preference (CPP), however, BALB/cJ mice fail to demonstrate place preference to cocaine at the previously tested doses (Belzung & Barreau, 2000). Additionally, morphine preferences of C57BL/6J and BALB/cJ mice are differentially affected by social group and isolation during the CPP test (Kennedy et al, 2012).

Drug abuse is often associated with sociability, emotion and memory (Curtis & Wang, 2007; Perrine et al, 2008; Niigaki et al, 2010). Given the differences in these aspects between C57BL/6J and BALB/cJ mice, the comparisons of drug abuse between the two strains may provide more background information. CPP is a widely used paradigm in studying the rewarding effects of drugs and modeling some aspects of long term drug-seeking and relapse (Schechter & Calcagnetti, 1993; Sakoori &

Received: 01 February 2014; Accepted date: 20 April 2014

Foundation items: This research was supported by the National Natural Science Foundation of China (31260513), the National Natural Science Foundation of Ningxia (NZ14077) and the Science Foundation of Beifang University of Nationalities (2012Y052)

*Corresponding author, E-mail: wang_jianli@163.com

Murphy, 2005). The drug paired cues play a critical role in the reinstatement of drug-seeking behaviors after a period of abstinence (Crombag et al, 2008; Su et al, 2013). Although differences in the susceptibility to the reinforcing properties of cocaine, morphine, and ethanol have been described among inbred mice strains (Cunningham et al, 1992; Eisener-Dorman et al, 2011), the persistence of CPP during cocaine withdrawal in C57BL/6J and BALB/cJ mice remains unclear. Zhang et al previously (2002) proposed that the persistence of cocaine-induced CPP is strain dependent. Accordingly, the present study investigated: (1) the phenotypic variability between these two mice strains in cocaine-seeking behaviors reflected by the persistence of cocaine-induced CPP; (2) the differences in locomotion and social behaviors after the 24-hour cocaine withdrawal.

MATERIALS AND METHODS

Animals

Male C57BL/6J and BALB/cJ mice at 8-week of age were obtained from the Laboratory Animal Center of Xi'an Jiaotong University (Shaanxi, China). The animals were housed in groups of four in standard transparent Makrolon cages (42 cm×26 cm×20 cm, length×width×height). The colony room was illuminated on a 12:12 light-dark cycle (lights on 2000h) and the temperature was maintained at 23±2 °C. Food and water were available *ad libitum*. Mice were allowed to adapt to housing conditions for one week and were handled daily by the same technician for three days prior to testing. All protocols and procedures were approved by the Animal Care and Use Committee of Shaanxi Normal University.

Chemicals and injection

Cocaine-hydrochloride (Northwest Pharmaceutical Co., Ltd. Sinopharm, Xi'an, China) was diluted in saline (0.9% NaCl) and was administrated subcutaneously (s.c. 20 mg/kg) (Zhang et al, 2002; Eisener-Dorman et al, 2011).

Conditioned place preference test

The place preference apparatus consisted of two large compartments (34 cm×25 cm×32 cm, length×width×height) with different visual cues (one had gray walls and the other had white-black striped walls) separated by a small middle compartment (11 cm×25 cm×32 cm, length×width×height). The middle compartment was an acclimation chamber with a door (7 cm×9 cm, height×width) in the center of the base.

Pre-test: On the day prior to conditioning, all animals were tested to determine any individual innate preference to either of the large lateral chambers. The mice (C57BL/6J, $n=12$; BALB/cJ, $n=12$) were given free access to each cue-decorated chamber when received a subcutaneous injection of physiological saline. Following 10-minute acclimation, the time spent in two lateral chambers was recorded for 15 minutes by a camera (Sony, HDR-XR260E) mounted 70 cm above the arena. After each trial, the chamber was thoroughly cleaned with 70% ethanol solution.

Conditioning with cocaine: Each strain of mice (C57BL/6J, $n=8$; BALB/cJ, $n=9$) were conditioned with cocaine. Both cocaine and equivalent volume of physiological saline injections were given on the same day for four consecutive days. Specifically, in the morning, subjects were placed in one of the outer chambers with cocaine injections and were placed in the opposite chamber with saline injections at afternoon. Two injections per day in an alternating counter balanced sequence for four days, thus, providing four associative pairings for cocaine and saline. Mice were conditioned for 2 h after injections. The morning session and the afternoon session were at least 6 hr apart to allow time for cocaine clearance (Thiel et al, 2008).

Post-test: CPP testing was conducted 24 hour after the last conditioning trial. Mice in a drug-free and a saline-free state were allowed to free access to each compartment. The time spent in two lateral chambers was recorded for 15 minutes.

The persistence of CPP: Mice were housed in their home cages after the CPP testing. The day of post-test was taken as intermission day zero and then the place preference testing was conducted on intermission day 7, 15 in BALB/cJ and on day 7, 15, 25 in C57BL/6J mice, respectively.

Open-field test

Another group of C57BL/6J and BALB/cJ mice was used in open-field test and social interaction test. Mice were randomly assigned into cocaine-treated groups ($n=8$) and control groups ($n=8$). The cocaine-treated groups (CC: C57BL/6J mice treated with cocaine, BC: BALB/cJ mice treated with cocaine) were administrated with cocaine (20 mg/kg) at 0900h for four consecutive days. Control groups (CS: C57BL/6J mice treated with saline, BS: BALB/cJ mice treated with saline) were administrated with saline instead. Locomotion and anxiety-like behaviors were assessed in an open field chamber 24 hr after the last injection. The open field chamber (50 cm×50 cm×25 cm, length×

width×height) made of white glacial polyvinyl chloride was brightly and evenly illuminated by four 60 W lamps mounted 1.5 m above (400 lux in the center of arena). The square arena was divided into 16 quadrants (four central and 12 peripheral) (Fiore & Ratti, 2007). Mouse was placed in the center of the arena and allowed to explore for 5 minute. The time spent in the central and peripheral zones and numbers of crossings between quadrants were recorded. The anxiety-like behaviors were assessed by the time spent in the center of the arena and the locomotion was determined by the numbers of crossings.

Same-sex social interaction test

The social interaction test was conducted between 1500h and 1700h. To eliminate possible influences from sexually motivated behaviors, only male-male dyads were used. The stimulus mouse was an unfamiliar, sexually naive individual that was approximately of the same age and size as the tested mouse. Testing were conducted in a neutral plastic cage (44 cm×22 cm×16 cm, length×width×height) with wood shavings bedding (2 cm) and a removable opaque divider in the middle. The stimulus and tested mouse was confined in each side of the cage for 3 minute, then the divider was removed and the activities of the mice were recorded for 15 min by a video-recorder mounted 70 cm above.

Mice behaviors were classified as investigatory behavior (sniffing face, body or anogenital area), aggressive behavior (pouncing, i.e. jumps or lunges; fighting, i.e. tumbling or biting; chasing), body contact (staying together with another mouse or amicable grooming); self-grooming (cephalocaudal progression that begins with rhythmic movements of the paws around the mouth and face, ears, descending to the ventrum, flank, anogenital area and tail) and other behaviors (digging, jumping, climbing the cage and resting).

Statistical analysis

All behavioral variables were scored from video footage according to established definitions by a naïve observer using Observer 5.0 (Noldus, Netherlands). Statistical analyses were carried out via SPSS 10.0 (SPSS Inc., Chicago, Illinois, USA). Data were checked for normality using the one-sample Kolmogorov–Smirnov test. The expression of place conditioning was analyzed using repeated-measures, with the intermission day as a repeated measure. Paired-samples *t*-test was used to evaluate the differences in time spending during the pre-test and intermittent tests. Data from the open-field test and the social interaction test were compared

using two-way ANOVA with strains and cocaine treatment as factors. Group differences were compared using *post-hoc* test except aggressive behavior which was abnormally distributed and was compared using Mann–Whitney *U*-test. All data were expressed as mean±*SE*. Statistical significance was taken at $P < 0.05$.

RESULTS

Conditioned place preference

The pre-test indicated that neither C57BL/6J ($t_{(11)}=1.76$, $P=0.106$) nor BALB/cJ mice ($t_{(11)}=0.484$, $P=0.638$) showed preferences to either of the chambers (Figure 1A). Post-testing and intermittent testing

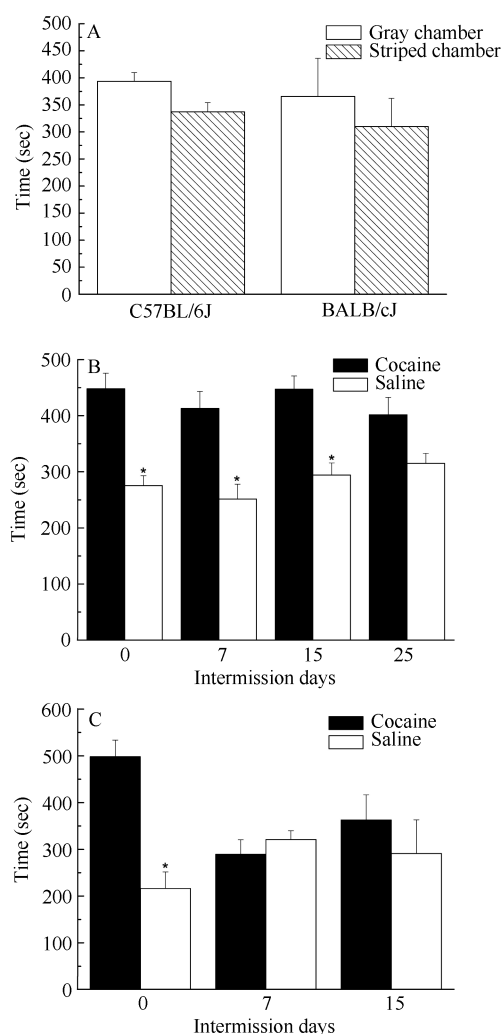


Figure 1 Time spent in saline- or cocaine-paired compartments by C57BL/6J and BALB/cJ mice

A: Pre-test; B and C: Post-test and intermittent test in C57BL/6J and BALB/cJ mice following cocaine conditioning, respectively; The day of post-test was taken as intermission day 0; *: $P \leq 0.05$; **: $P \leq 0.01$.

indicated that cocaine could induce place preference in both mice strains (C57BL/6J, $F_{(3,28)}=217.381$, $P<0.001$; BALB/cJ, $F_{(2,24)}=7.101$, $P<0.001$). However, a significant interaction between cocaine conditioning and intermission day was found only in BALB/cJ mice ($F_{(2,24)}=7.239$, $P=0.003$) but not in C57BL/6J mice ($F_{(3,28)}=1.043$, $P=0.384$).

A significant preference to the cocaine-paired compartment was shown in both mice strains on the day of post-testing (intermission day 0) (C57BL/6J: $t_{(7)}=3.849$, $P=0.006$; BALB/cJ: $t_{(8)}=4.092$, $P=0.03$) (Figure 1B, C) and persisted to intermission day 7 ($t_{(7)}=3.304$, $P=0.013$) and 15 ($t_{(7)}=3.862$, $P=0.006$), but not on day 25 ($t_{(7)}=1.985$, $P=0.094$) in C57BL/6J mice (Figure 1B). However, this preference persistence was not found in BALB/cJ mice on either day (day 7: $t_{(8)}=0.779$, $P=0.458$; day 15: $t_{(8)}=0.638$, $P=0.054$) (Figure 1C).

Open field behavior

The main effect of strain was significant in the time spent in the central area ($F_{(3,28)}=4.736$, $P=0.038$) and transitions ($F_{(3,28)}=28.776$, $P<0.001$). However, the interactions between strain and cocaine administration had no effects on either the total transitions ($F_{(3,28)}=2.028$, $P=0.165$) or the time spent in the central area ($F_{(3,28)}=3.461$, $P=0.073$).

Although no differences were found in the time spent in the central area between C57BL/6J and BALB/cJ control mice (*Mean difference*=1.158, $P=0.996$), C57BL/6J control mice showed a higher level of locomotor activity (total transitions) (*Mean difference*=46.000, $P=0.02$). Cocaine-administrated C57BL/6J

mice showed a greater number of total transitions than both the C57BL/6J control mice (*Mean difference*=35.375, $P=0.04$) and the cocaine-administrated BALB/cJ mice (*Mean difference*=79.250, $P<0.001$), as well as spent more time in the central area (*Mean difference*=14.799, $P=0.008$) than the cocaine-administrated BALB/cJ mice. However, cocaine-administration did not affect either the total transition ($F_{(3,28)}=2.580$, $P=0.119$) or the time spent in the central area ($F_{(3,28)}=0.178$, $P=0.677$) in BALB/cJ mice (Figure 2).

Same-sex social interaction

The male-male interactions indicated that strain and cocaine both significantly affected the social investigations (strain [duration: $F_{(3,28)}=18.216$, $P<0.001$, frequency: $F_{(3,28)}=107.113$, $P<0.001$]; cocaine [duration: $F_{(3,28)}=8.817$, $P=0.006$, frequency: $F_{(3,28)}=20.502$, $P<0.001$]), the contact behaviors (strain [duration: $F_{(3,28)}=30.856$, $P<0.001$, frequency: $F_{(3,28)}=F_{(3,28)}=356.608$, $P<0.001$]; cocaine [duration: $F_{(3,28)}=8.891$, $P=0.006$, frequency: $F_{(3,28)}=F_{(3,28)}=0.888$, $P=0.354$]) and the frequencies of self-grooming (strain: $F_{(3,28)}=66.336$, $P<0.001$; cocaine: $F_{(3,28)}=14.131$, $P<0.001$). The frequencies of aggressive behaviors between two mice strains were significantly different ($F_{(3,28)}=33.618$, $P<0.001$). Moreover, significant interactions between strain and cocaine were found in the social investigation (duration: $F_{(3,28)}=15.386$, $P=0.001$; frequency: $F_{(3,28)}=16.084$, $P<0.001$), the self-grooming (Duration: $F_{(3,28)}=14.598$, $P=0.001$; Frequency: $F_{(3,28)}=25.121$, $P<0.001$), duration of contact behavior ($F_{(3,28)}=9.675$, $P=0.004$) and aggressive behaviors ($F_{(3,28)}=4.423$, $P=0.045$).

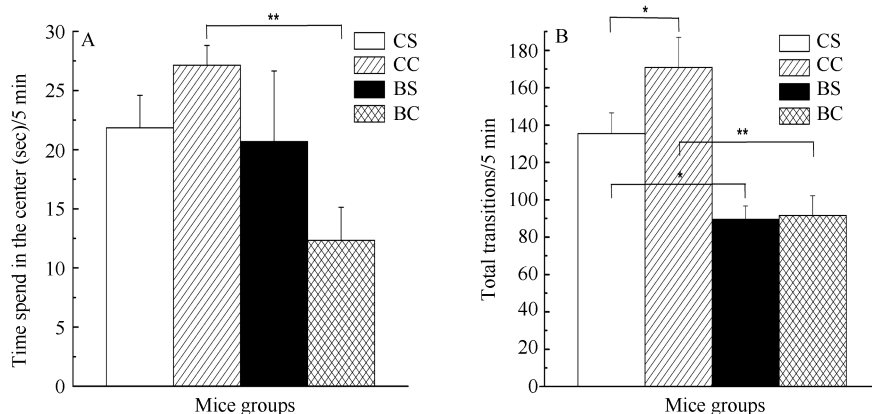


Figure 2 Open-field behavior of C57BL/6J and BALB/cJ mice after the 24 h cocaine withdrawal

A: The time spent in the central area; B: Total transitions; *: $P<0.05$; **: $P<0.01$; CS and CC: C57BL/6J mice administrated with saline and cocaine, respectively; BS and BC: BALB/cJ mice administrated with saline and cocaine, respectively.

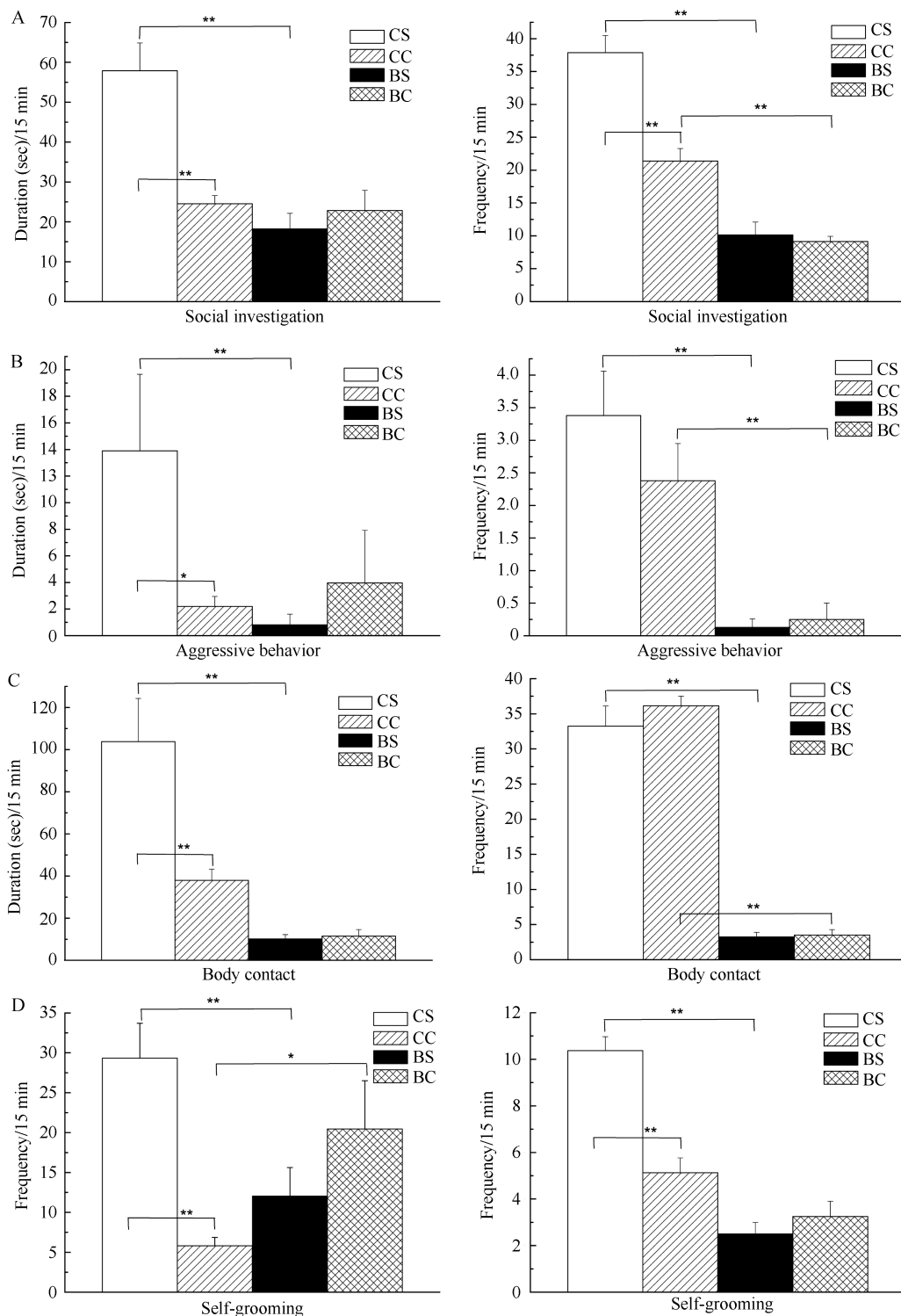


Figure 3 Duration and frequency of same-sex social interactions in C57BL/6J and BALB/cJ mice after the 24 h of cocaine withdrawal

A: Investigation; B: Aggression; C: Body contact; D: Self-grooming; *, $P \leq 0.05$, **, $P \leq 0.01$; CS and CC: C57BL/6J mice administrated with saline and cocaine, respectively; BS and BC: BALB/cJ mice administrated with saline and cocaine, respectively.

C57BL/6J control mice showed high levels of the social investigations (duration: *mean difference*=39.646,

$P < 0.001$; frequency: *mean difference*=27.750, $P < 0.001$), the aggressive behaviors (duration: $U=3$;

$P=0.001$; frequency: $U=1$, $P<0.001$) and the contact behavior (duration: *mean difference*=93.608, $P=0.000$; frequency: *mean difference*=30.005, $P<0.001$) compared with the BALB/cJ control mice. Moreover, the levels of the self-grooming behaviors between these two control mice groups were also significantly different (duration: *mean difference*=17.296, $P=0.007$; frequency: *mean difference*=7.875, $P<0.001$) (Figure 3).

Cocaine-administrated C57BL/6J mice exhibited attenuations in the social investigations (duration: *mean difference*=-33.360, $P<0.001$; frequency: *mean difference*=-16.500, $P<0.001$), the self-grooming behaviors (duration: *mean difference*=-23.524, $P<0.001$; frequency: *mean difference*=-5.250, $P<0.001$), the contact behaviors (duration: *mean difference*=-65.813, $P=0.001$; frequency: *mean difference*=-2.875, $P=0.230$) and the aggressive behaviors (duration: $U=9$, $P=0.015$; frequency: $U=22$, $P=0.328$) than those of their control mice (Figure 3).

Cocaine withdrawal had no apparent effect on social investigations (duration: *mean difference*=4.6140, $P=0.506$; frequency: *mean difference*=-1.000, $P=0.717$), aggressive behaviors (duration: $U=31.5$, $P=0.927$; frequency: $U=31.5$, $P=0.927$), contact behaviors (duration: *mean difference*=1.390, $P=0.928$; frequency: *mean difference*=0.250, $P=0.916$) or self-grooming behaviors (duration: *mean difference*=8.401, $P=0.166$; frequency: *mean difference*=0.750, $P=0.383$) in BALB/cJ mice (Figure 3).

Compared with cocaine-administrated BALB/cJ mice, cocaine-administrated C57BL/6J mice were more engaged in social investigations (duration: *mean difference*=1.6725, $P=0.809$; frequency: *mean difference*=12.250, $P<0.001$), aggressive behaviors (duration: $U=15$, $P=0.083$; frequency: $U=6.5$, $P=0.005$), contact behaviors (duration: *mean difference*=26.495, $P=0.095$; frequency: *mean difference*=32.625, $P<0.001$), but less in self-grooming behaviors (duration: *mean difference*=-14.630, $P=0.02$; frequency: *Mean difference*=0.875, $P=0.35$) (Figure 3).

DISCUSSION

Persistence of cocaine-induced place preference

Although Belzung & Barreau (2000) claimed that cocaine may be not able to induce place preference in BALB/cJ mice, in this study, after cocaine conditioning, both C57BL/6J and BALB/cJ mice showed a significant

preference to the cocaine-paired compartment, indicating that cocaine induces rewarding effects in both mice strains (Miner, 1997; Zhang et al, 2002; Eisener-Dorman et al, 2011). Since the rewarding effects of cocaine could be influenced by administration patterns (Zhang et al, 2002), this discrepancy may be due to the fact that Belzung & Barreau (2000) chose a dose of 10 mg/kg and a conditioning trial of half-hour, instead of 20 mg/kg and two-hour, respectively, as in this present study. These phenomena indicate that the CPP establishment could be affected by both the doses of cocaine and the duration of reinforcement.

In this study, the cocaine-associated preference diminished within one week after the withdrawal in BALB/cJ mice, but persisted at least two weeks after the withdrawal in C57BL/6J mice, which is consistent with previous studies indicating that the cocaine-induced CPP could be maintained by repeated testing two or four weeks after conditioning (Mueller & Stewart, 2000; Zhang et al, 2002). Tran-Nguyen et al (1998) found that the cocaine-seeking behaviors were getting more intense during the course of cocaine withdrawal in rats. Su et al (2013) reported that the cocaine-induced CPP could remain viable at three weeks of the withdrawal. Mueller & Stewart (2000) found that in animals tested only once, a spontaneous reduction in CPP was shown at six weeks after conditioning. These findings suggest that CPP may be variably maintained or extinguished dependent upon the timing and frequency of testing following conditioning (Sakoori & Murphy, 2005). Intermittent re-testing for CPP itself may act as a secondary reinforce that strengthens the association between drug experience and environment and may actually help maintain cocaine-induced CPP (Mueller & Stewart, 2000; Sakoori & Murphy, 2005). However, no such reinforcement was shown in BALB/cJ mice. The genetic variations in pharmacokinetic may not account for the differences in cocaine responsiveness observed because no difference in the incorporation of [3 H]-cocaine has been found between C57BL/6J and BALB/cJ mice (Seale, 1991). An alternative explanation of the differences in the persistence of CPP expression is the poor capacity of learning and memory of BALB/cJ mice (Crawley, 2000; Shi et al, 2008) because the CPP task involves learning processes (Fleming et al, 1994; Thiel et al, 2008). Similarly, Oler & Markus (1998) found that young rats showed a stronger retention for conditioning context after conditioning than aged rats. Thus, the persistence of

CPP expression indicates that the development of ordinary memory and addictive memory between C57BL/6J and BALB/cJ mice are quite different.

Studies suggested that place conditioning may be used to model some aspects of long term drug-seeking, drug relapse, and the hedonic properties of drugs (Sakoori & Murphy, 2005). Our results indicate that the persistence of cocaine-induced CPP during prolonged withdrawal may contribute to the sustained vulnerability to “relapse” of cocaine-seeking behavior. Moreover, compared with C57BL/6J mice, BALB/cJ mice are characterized by higher levels of anxiety-like behaviors, lower locomotor activities and are less sociability (Crawley *et al.*, 1997; Sankoorikal *et al.*, 2006; Brodtkin, 2007; Moy *et al.*, 2007). The different CPP persistence showed in this study between the two mice strains is in accordance with the previous study indicating that the highly social species have different susceptibility to the effects of drug compared with the less social species (Curtis & Wang, 2007).

Cocaine-induced locomotor activities

In this present study, the 24-hour cocaine withdrawal had no effect on the anxiety-like behaviors of the two mice strains, which is consistent with previous reports (Niigaki *et al.*, 2010; Stoker & Markou, 2011). However, in rats, cocaine withdrawal is associated with increased anxiety-like behaviors in the elevated plus maze (Perrine *et al.*, 2008; Hall *et al.*, 2010). Moreover, the anxiogenic effects of abstinence from cocaine are also correlated with different protocols (e.g. the elevated plus maze, the open field or the light-dark box) (Stoker & Markou, 2011; de Oliveira Citó Mdo *et al.*, 2012).

In this study, after a 24-hour cocaine withdrawal, the level of locomotor activities of C57BL/6J mice increased while that of BALB/cJ mice was maintained at the same level. These results are consistent with previous studies indicating that a marked increase or dose-dependent stimulant effects on locomotor activities in response to cocaine have been found in C57BL/6J mice (Zhang *et al.*, 2002; Eisener-Dorman *et al.*, 2011; Thomsen & Caine, 2011). BALB/cJ mice are less sensitive to the cocaine-associated stimulant effects on locomotor activities (Ito *et al.*, 2007; Eisener-Dorman *et al.*, 2011; Thomsen & Caine, 2011), though some reports claimed that BALB/cJ mice show hyperlocomotor activities in response to cocaine (Miner, 1997; Kuzmin *et al.*, 2000). In the open field test, the increased locomotion

activities were found in rats after 24-hour of abstinence from cocaine (de Oliveira Citó Mdo *et al.*, 2012). However, some studies showed that cocaine withdrawal suppresses locomotor activities in rats (Baldo *et al.*, 1999; Koeltzow & White, 2003). One potential explanation for these discrepancies is that the locomotor activity may be influenced by the measurement environment (e.g. the open field, the conditioning chamber or the light-dark box) or cocaine dosage, administration pattern and withdrawal time (Zhang *et al.*, 2002; Niigaki *et al.*, 2010; Eisener-Dorman *et al.*, 2011; Stoker & Markou, 2011; de Oliveira Citó Mdo *et al.*, 2012). For example, the context in which a drug is experienced can significantly influence both acute and sensitized responses to the drug (Badiani & Robinson, 2004; Eisener-Dorman *et al.*, 2011). A specific interaction between the cocaine and the environment may result in context-dependent sensitization in BALB/c mice (Eisener-Dorman *et al.*, 2011). The present results indicate that cocaine withdrawal induces locomotion changes in C57BL/6J mice.

Cocaine-induced social behaviors

In this present study, when interacting with same-sex individuals, C57BL/6J mice were more active in social investigation, body contact and aggression than those of BALB/cJ mice, which are consistent with previous reports (Sankoorikal *et al.*, 2006; Brodtkin, 2007; An *et al.*, 2011). Fairless *et al.* (2008) demonstrated that the size of the corpus callosum relative to brain weight is associated with sociability among these two mice strains. Moreover, compared with the saline control, cocaine withdrawal induced remarkable decreases in social investigation, contact behavior and aggressive behavior in C57BL/6J mice as described in previous reports (Rademacher *et al.*, 2002; Estelles *et al.*, 2007). Although cocaine induces complicated changes in social behaviors, no agreement has been reached on its specific effects on aggression (Moeller *et al.*, 1997; Dhossche, 1999). Some studies also indicated that other than strains or species, the aggressive behaviors may also be affected by the patterns of drug administration (single or binge administration), the dosing regimens and the specific temporal window assessed (Estelles *et al.*, 2004, 2007; Wang *et al.*, 2012).

Interestingly, no significant effects of cocaine withdrawal on either the social behaviors or the locomotor activities were found in BALB/cJ mice, indicating that there may be a dissociation between cocaine-induced

CPP and locomotion or social behavior in BALB/cJ mice. Compared with C57BL/6J mice, different mechanisms may underlie such effects in BALB/cJ mice. Combined the persistence of CPP test, these results indicate that C57BL/6J mice are more susceptible to cocaine withdrawal than BALB/cJ mice. However, because BALB/cJ mice are characterized with low levels of social investigation and contact behavior, it is possible that what we have observed in this study is only a 'floor effect' of cocaine on the two behaviors.

Mesolimbic dopamine (DA) is responsible for cocaine-induced behavior and locomotor activation (Sarnyai, 1993; Tran-Nguyen et al, 1998). Hyperlocomotion induced by psychostimulants is mediated by the mesolimbic dopaminergic system, whereas stereotyped behaviors are mediated by the nigrostriatal dopaminergic system (Ito et al, 2007). The balances of the activation of dopaminergic neurons between mesolimbic and nigrostriatal systems may play an important role to engender corresponding behavioral outcomes (Ito et al, 2007). The differences between C57BL/6J and BALB/cJ mice in dopaminergic function within the prefrontal cortex and the striatum have been reported (Hervé et al, 1979; Helmeste & Seeman, 1982). Thus, the differences

in dopaminergic neurotransmission between C57BL/6J and BALB/cJ mice may have induced their different behavioral response to cocaine. Moreover, these two mice strains have different hypothalamic–pituitary–adrenal (HPA) responses to stressors (Anisman et al, 1998). Therefore, the interactions between the HPA axis and the DA system may also affect their sensitized behavioral responses (Wang et al, 2010). Additionally, Deroche et al (1997) found that the genetically based differences in sociability between the two strains may play an important role in determining the sensitivity to cocaine. Taken together, the susceptibility to cocaine in the two mice strains may be mediated by the complex interaction between neurobehavioral and epigenetic outcomes and genetically based differences.

In conclusion, this study demonstrates that the cocaine-associated rewarding effects, drug seeking behaviors, locomotor activities and social behaviors are inconsistent in C57BL/6J and BALB/cJ mice strains; C57BL/6J mice are more susceptible to cocaine than BALB/cJ mice at the doses tested in the present study. Further studies are necessary to explore the specific neural mechanisms underlying these differences.

References

- Ågmo A, Belzung C, Deloire X, Grassin M, Lewis S. 1999. Blockade of anxiolytic-like actions of chlordiazepoxide by naloxone in the elevated plus-maze: Comparisons between SWISS, C57BL/6 and BALB/c mice. *Psychobiology*, **27**(1): 105-113.
- An XL, Zou JX, Wu RY, Yang Y, Tai FD, Zeng SY, Jia R, Zhang X, Liu EQ, Broders H. 2011. Strain and sex differences in anxiety-like and social behaviors in C57BL/6J and BALB/cJ mice. *Experimental Animals*, **60**(2): 111-123.
- Anisman H, Lacosta S, McIntyre D, Kent P, Merali Z. 1998. Stressor-induced corticotropin-releasing hormone, bombesin, ACTH and corticosterone variations in strains of mice differentially responsive to stressors. *Stress*, **2**(3): 209-220.
- Bach H, Arango V, Huang YY, Leong S, Mann JJ, Underwood MD. 2011. Neuronal tryptophan hydroxylase expression in BALB/cJ and C57BL/6J mice. *Journal of Neurochemistry*, **118**(6): 1067-1074.
- Badiani A, Robinson TE. 2004. Drug-induced neurobehavioral plasticity: the role of environmental context. *Behavioural Pharmacology*, **15**(5-6): 327-339.
- Baldo BA, Markou A, Koob GF. 1999. Increased sensitivity to the locomotor depressant effect of a dopamine receptor antagonist during cocaine withdrawal in the rat. *Psychopharmacology*, **141**(2): 135-144.
- Bardo MT, Donohew RL, Harrington NG. 1996. Psychobiology of novelty seeking and drug seeking behavior. *Behavioural Brain Research*, **77**(1-2): 23-43.
- Belzung C, Barreau S. 2000. Differences in drug-induced place conditioning between BALB/c and C57BL/6 mice. *Pharmacology Biochemistry & Behavior*, **65**(3): 419-423.
- Belzung C, Berton F. 1997. Further pharmacological validation of the BALB/c neophobia in the free exploratory paradigm as an animal model of trait anxiety. *Behavioural Pharmacology*, **8**(6-7): 541-548.
- Bouwknicht JA, Paylor R. 2002. Behavioral and physiological mouse assays for anxiety: a survey in nine mouse strains. *Behavioural Brain Research*, **136**(2): 489-501.
- Brodin ES. 2007. BALB/c mice: low sociability and other phenotypes that may be relevant to autism. *Behavioural Brain Research*, **176**(1): 53-56.
- Crawley JN, Belknap JK, Collins A, Crabbe JC, Frankel W, Henderson N, Hitzemann RJ, Maxson SC, Miner LL, Silva AJ, Wehner JM, Wynshaw-Boris A, Paylor R. 1997. Behavioral phenotypes of inbred mouse strains: implications and recommendations for molecular studies. *Psychopharmacology*, **132**(2): 107-124.
- Crawley JN. 2000. What's Wrong with My Mouse? New York: Wiley-Liss Press.
- Crombag HS, Bossert JM, Koya E, Shaham Y. 2008. Context-induced relapse to drug seeking: a review. *Philosophical Transactions of the Royal Society B*, **363**(1507): 3233-3243.

- Cunningham CL, Niehus DR, Malott DH, Prather LK. 1992. Genetic differences in the rewarding and activating effects of morphine and ethanol. *Psychopharmacology*, **107**(2-3): 385-393.
- Curtis JT, Wang Z. 2007. Amphetamine effects in microtine rodents: a comparative study using monogamous and promiscuous vole species. *Neuroscience*, **148**(4): 857-866.
- de Oliveira Citó Mdo C, da Silva FC, Silva MI, Moura BA, Macêdo DS, Woods DJ, Fonteles MM, de Vasconcelos SM, de Sousa FC. 2012. Reversal of cocaine withdrawal-induced anxiety by ondansetron, buspirone and propranolol. *Behavioural Brain Research*, **231**(1): 116-123.
- Deroche V, Caine SB, Heyser CJ, Polis I, Koob GF, Gold LH. 1997. Differences in the liability to self-administer intravenous cocaine between C57BL/6 x SJL and BALB/cByJ mice. *Pharmacology Biochemistry & Behavior*, **57**(3): 429-440.
- Dhossche DM. 1999. Aggression and recent substance abuse: absence of association in psychiatric emergency room patients. *Comprehensive Psychiatry*, **40**(5): 343-346.
- Eisener-Dorman AF, Grabowski-Boase L, Tarantino LM. 2011. Cocaine locomotor activation, sensitization and place preference in six inbred strains of mice. *Behavioral and Brain Functions*, **7**: 29.
- Estelles J, Lluch J, Rodri'guez-Arias M, Aguilar MA, Mi'narro J. 2007. Cocaine exposure during adolescence affects anxiety in adult mice. *Brain Research Bulletin*, **71**(4): 393-403.
- Estelles J, Rodri'guez-Arias M, Aguilar MA, Mi'narro J. 2004. Social behavioural profile of cocaine in isolated and grouped male mice. *Drug and Alcohol Dependence*, **76**(2): 115-123.
- Fairless AH, Dow HC, Toledo MM, Malkus KA, Edelmann M, LiH, Talbot K, Arnold SE, Abel T, Brodtkin ES. 2008. Low sociability is associated with reduced size of the corpus callosum in the BALB/cJ inbred mouse strain. *Brain Research*, **1230**: 211-217.
- Fiore L, Ratti G. 2007. Remote laboratory and animal behaviour: an interactive open field system. *Computers & Education*, **49**(4): 1299-1307.
- Fleming AS, Korsmit M, Deller M. 1994. Rat pups are potent reinforcers to the maternal animal: Effects of experience, parity, hormones, and dopamine function. *Psychobiology*, **22**(1): 44-53.
- Hall BJ, Pearson LS, Buccafusco JJ. 2010. Effect of the use-dependent, nicotinic receptor antagonist BTMPS in the forced swim test and elevated plus maze after cocaine discontinuation in rats. *Neuroscience Letters*, **474**(2): 84-87.
- Helmeste DM, Seeman P. 1982. Amphetamine-induced hypolocomotion in mice with more brain D2 dopamine receptors. *Psychiatry Research*, **7**(3): 351-359.
- Hervé D, Tassin JP, Barthelemy C, Blanc G, Lavielle S, Glowinski J. 1979. Difference in the reactivity of the mesocortical dopaminergic neurons to stress in the BALB/c and the C57BL/6 mice. *Life Science*, **25**(19): 1659-1664.
- Ito S, Mori T, Namiki M, Suzuki T, Sawaguchi T. 2007. Complicated interaction between psychostimulants and morphine in expression of phenotype of behavior in the dopaminergic system of BALB/c mice. *Journal of Pharmacological Sciences*, **105**(4): 326-333.
- Kennedy BC, Panksepp JB, Runckel PA, Lahvis GP. 2012. Social influences on morphine-conditioned place preference in adolescent BALB/cJ and C57BL/6J mice. *Psychopharmacology*, **219**(3): 923-932.
- Koeltzow TE, White FJ. 2003. Behavioral depression during cocaine withdrawal is associated with decreased spontaneous activity of ventral tegmental area dopamine neurons. *Behavioral Neuroscience*, **117**(4): 860-865.
- Kundakovic M, Lim S, Gudsnuk K, Champagne FA. 2013. Sex-specific and strain-dependent effects of early life adversity on behavioral and epigenetic outcomes. *Frontiers in Psychiatry*, **4**: 78.
- Kuzmin A, Johansson B, Fredholm BB, Ogren SO. 2000. Genetic evidence that cocaine and caffeine stimulate locomotion in mice via different mechanisms. *Life Science*, **66**(8): PL113-PL118.
- Miner LL. 1997. Cocaine reward and locomotor activity in C57BL/6J and 129/SvJ mice and their F1 cross. *Pharmacology Biochemistry & Behavior*, **58**(1): 25-30.
- Moeller FG, Dougherty DM, Rustin T, Swann AC, Allen TJ, Shah N, Cherek DR. 1997. Antisocial personality disorder and aggression in recently abstinent cocaine dependent subjects. *Drug and Alcohol Dependence*, **44**(2-3): 175-182.
- Moy SS, Nadler JJ, Young NB, Perez A, Holloway LP, Barbaro RP, Barbaro JR, Wilson LM. 2007. Mouse behavioral tasks relevant to autism: phenotypes of 10 inbred strains. *Behavioural Brain Research*, **176**(1): 4-20.
- Mueller D, Stewart J. 2000. Cocaine-induced conditioned place preference: reinstatement by priming injections of cocaine after extinction. *Behavioural Brain Research*, **115**(1): 39-47.
- Niigaki ST, Silva RH, Patti CL, Cunha JL, Kameda SR, Correia-Pinto JC, Takatsu-Coleman AL, Levin R, Abilio VC, Frussa-Filho R. 2010. Amnesic effect of cocaine after the termination of its stimulant action. *Progress in Neuro-Psychopharmacology & Biological Psychiatry*, **34**(1): 212-218.
- Oler JA, Markus EJ. 1998. Age-related deficits on the radial maze and in fear conditioning: hippocampal processing and consolidation. *Hippocampus*, **8**(4): 402-415.
- Perrine SA, Sheikh IS, Nwaneshiudu CA, Schroeder JA, Unterwald EM. 2008. Withdrawal from chronic administration of cocaine decreases delta opioid receptor signaling and increases anxiety- and depression-like behaviors in the rat. *Neuropharmacology*, **54**(2): 355-364.
- Priebe K, Brake WG, Romeo RD, Sisti HM, Mueller A, McEwen BS, Brake WG. 2005. Maternal influences on adult stress and anxiety-like behavior in C57BL/6J and BALB/cJ mice: a cross-fostering study. *Developmental Psychobiology*, **47**(4): 398-407.
- Rademacher DJ, Schuyler AL, Kruschel CK, Steinpreis RE. 2002. Effects of cocaine and putative a typical antipsychotics on rat social behavior. An ethopharmacological study. *Pharmacology Biochemistry & Behavior*, **73**(4): 769-778.
- Sakoori K, Murphy NP. 2005. Maintenance of conditioned place preferences and aversion in C57BL6 mice: effects of repeated and drug state testing. *Behavioural Brain Research*, **160**(1): 34-43.
- Sankoorikal GMV, Kaercher KA, Boon CJ, Lee JK, Brodtkin ES. 2006. A mouse model system for genetic analysis of sociability: C57BL/6J

- versus BALB/cJ inbred mouse strains. *Biological Psychiatry*, **59**(5): 415-23.
- Sarnyai Z. 1993. Measurement of cocaine-induced stereotyped behavior in response to neuropeptides. In: Conn PM. *Methods in Neurosciences Paradigms for the Study of Behavior*. San Diego CA: Academic Press, 153-165.
- Schechter MD, Calcagnetti DJ. 1993. Trends in place preference conditioning with a cross-indexed bibliography; 1957-1991. *Neuroscience & Biobehavioral Reviews*, **17**(1): 21-41.
- Scisłowska-Czarnecka A, Chadzińska M, Pierzchała-Kozieć K, Plytycz B. 2004. Long-lasting effects of social stress on peritoneal inflammation in some strains of mice. *Folia Biologica (Krakow)*, **52**(1-2): 97-104.
- Seale TW. 1991. Genetic differences in response to cocaine and stimulant drugs. In: Crabbe JC, Harris J, Harris RA. *The Genetic Basis of Alcohol and Drug Actions*. New York: Plenum Press.
- Shi JW, Zou H, Jin ML. 2008. Assessing exploratory behavior and memory in ICR, BALB/c and C57BL/6 mice using habituation. *Zoological Research*, **29**(1): 49-55.
- Stoker AK, Markou A. 2011. Withdrawal from chronic cocaine administration induces deficits in brain reward function in C57BL/6J mice. *Behavioural Brain Research*, **223**(1): 176-181.
- Su ZI, Santoostaroam A, Wenzel J, Ettenberg A. 2013. On the persistence of cocaine-induced place preferences and aversions in rats. *Psychopharmacology*, **229**(1): 115-123.
- Thiel KJ, Okun AC, Neisewander JL. 2008. Social reward-conditioned place preference: a model revealing an interaction between cocaine and social context rewards in rats. *Drug and Alcohol Dependence*, **96**(3): 202-212.
- Thomsen M, Caine SB. 2011. Psychomotor stimulant effects of cocaine in rats and 15 mouse strains. *Experimental and Clinical Psychopharmacology*, **19**(5): 321-341.
- Tran-Nguyen LT, Fuchs RA, Coffey GP, Baker DA, O'Dell LE, Neisewander JL. 1998. Time-dependent changes in cocaine-seeking behavior and extracellular dopamine levels in the amygdala during cocaine withdrawal. *Neuropsychopharmacology*, **19**(1): 48-59.
- Van Dam D, Lenders G, De Deyn PP. 2006. Effect of Morris water maze diameter on visual-spatial learning in different mouse strains. *Neurobiology of Learning and Memory*, **85**(2): 164-172.
- Verleye M, Dumas S, Heulard I, Krafft N, Gillardin JM. 2011. Differential effects of etifoxine on anxiety-like behaviour and convulsions in BALB/cByJ and C57BL/6J mice: any relation to over expression of central GABAA receptor beta2 subunits? *European Neuropsychopharmacology*, **21**(6): 457-470.
- Wang JL, Zhang LX, Zhang P, Tai FD. 2012. Cocaine-induced rewarding properties, behavioural sensitization and alteration in social behaviours in group-housed and post-puberty isolated female mandarin voles. *Behavioural Pharmacology*, **23**(7): 693-702.
- Wang YC, Wang CC, Lee CC, Huang AC. 2010. Effects of single and group housing conditions and alterations in social and physical contexts on amphetamine-induced behavioral sensitization in rats. *Neuroscience Letter*, **486**(1): 34-37.
- Zhang Y, Mantsch JR, Schlussman SD, Ho A, Kreek MJ. 2002. Conditioned place preference after single doses or "binge" cocaine in C57BL/6J and 129/J mice. *Pharmacology Biochemistry & Behavior*, **73**(3): 655-662.

Progress on low susceptibility mechanisms of transmissible spongiform encephalopathies

Li-Li QING¹, Hui ZHAO^{1,*}, Lin-Lin LIU¹

Laboratory of Conservation and Utilization of Bio-resources, Yunnan University, Kunming 650091, China

Abstract: Transmissible spongiform encephalopathies (TSEs), also known as prion diseases, are a group of fatal neurodegenerative diseases detected in a wide range of mammalian species. The “protein-only” hypothesis of TSE suggests that prions are transmissible particles devoid of nucleic acid and the primary pathogenic event is thought to be the conversion of cellular prion protein (PrP^C) into the disease-associated isoform (PrP^{Sc}). According to susceptibility to TSEs, animals can be classified into susceptible species and low susceptibility species. In this review we focus on several species with low susceptibility to TSEs: dogs, rabbits, horses and buffaloes. We summarize recent studies into the characteristics of low susceptibility regarding protein structure, and biochemical and genetic properties.

Keywords: Transmissible spongiform encephalopathy; Low susceptibility; Dog; Rabbit; Horse; Buffalo; *PRNP*; *SPRN*

Transmissible spongiform encephalopathy (TSE), or prion disease, is an invariably fatal neurodegenerative disease detected in a wide range of mammalian species, including Scrapie in goats (*Capra hircus*) and sheep (*Ovis aries*); bovine spongiform encephalopathy (BSE) in cattle (*Bos taurus*); chronic wasting disease (CWD) in elaphure (*Elaphurus davidianus*) and moose (*Alces americanus*); feline spongiform encephalopathy (FSE) in cats (*Felis catus*); transmissible mink encephalopathy (TME) in minks (*Mustela vison*); and Creutzfeldt-Jakob disease (CJD), variant Creutzfeldt-Jakob disease (vCJD), fatal familial insomnia (FFI), Gerstmann-Straussler-Scheinker syndrome (GSS) and Kuru in humans (*Homo sapiens*) (Collins et al, 2004; Prusiner, 1982). Humans and other animals infected with TSE are clinically and pathologically characterized with neuronal progressive vacuolation, stellate cell gliosis, spongiform lesions in gray matter, amyloid deposition and eventually disastrous degeneration and death (Prusiner, 1998). No effective treatments have been found and the World Health Organization has named TSE and AIDS as two major health problems of the 21st century.

The “protein-only” hypothesis of TSE suggests that the pathogenic factors of TSE are not bacteria or a virus, but a protein devoid of nucleic acid, which has been named prion protein (PrP). PrP is encoded by the prion protein gene (*PRNP*) (Prusiner, 1982). Normal cellular PrP (PrP^C) expresses in the cells of mammalian species and the number of amino acid residues varies from 253 to 264 across species (Wopfner et al, 1999) and are all highly conserved (Figure 1). PrP has two signal peptide sequences, a N-terminal and a C-terminal. Mature PrP has an intra-molecular disulfide bond and two glycosylation sites, and is anchored on the cell membrane surface via glycosylphosphatidylinositol (GPI) at the C-terminal (Aguzzi et al, 2008). According to the protein-only hypothesis TSE is a conformational disease and under certain circumstances cellular PrP^C mistakenly

Received: 04 May 2014; Accepted: 20 June 2014

Foundation items: This item was supported by the National Natural Science Foundation of China (31060302 and 31260032), the Trans-gene Special Project of the Ministry of Agriculture of China (2011ZX-08009-003-006) and the Natural Science Foundation of Yunnan Province (2010CD010).

*Corresponding author, E-mail: zhaohui@ynu.edu.cn

	1	10	20	30	40	50	60	70	
Human	--MANLGCWMLVLFVATWSDLGLCKKRPKPGG-WNTGG-SRYPGQGSPPGNNRYPPQGGGGWGQPHGGG-W								65
Chimpanzee									65
Rhesus									65
Deer	MVKSHI	S.I	M.V	G					68
Elk	MVKSHI	S.I	M.V	G					68
Mouse		Y.L.A	TM.T.V				-T		64
Rat		Y.L.A	T.CT.V				S.T		65
Pig	MVKSHI	G.I	A.I	G					68
Sheep	MVKSHI	S.I	M.V	G					68
Goat	MVKSHI	S.I	M.V	G					68
Rabbit		H.Y	L.V	G		S			66
Dog	MVKSHI	G.I	L.V		G				68
Cat	MVKGHI	G.I	V	G				A.G	69
House	MVKSHV	G.I	V						67
Cattle	MVKSHI	S.I	M.V	G					68
Buffalo	MVKRHI	S.I	VM.V	G			S		68
	80	90	100	110	120	130	140		
Human	GQPHGGG-WGQPHGG-----GWGQPHGGG-WGQGGGTHSQWNKPSKPKTNMKHMAGAAAAGAVVGGL							125	
Chimpanzee								125	
Rhesus								125	
Deer				G	-	N.H	S.V	128	
Elk				G	-		V	128	
Mouse	S		S		N		L.V	124	
Rat				S	N		L.V	125	
Pig				G	S.G		V	129	
Sheep				G	-S		V	128	
Goat				G	-S		V	128	
Rabbit					N	G	S.V	126	
Dog			G	-	G	S	N.V	129	
Cat	A.G	A.GG	-	A.G	G	G		132	
House				G	-S.G		V	127	
Cattle			GWGQPHGG	G	-G		V	136	
Buffalo			GWGQPHGG	G	-			126	
	150	160	170	180	190	200	210		
Human	GGYMLGSAMSRPIIHFGSDYEDRYRENMHRYFNQVYYRFMDSEYSNQNNFVHDCVNITIKQHTVTTTTKG							195	
Chimpanzee								195	
Rhesus		L.N		Y	V.Q	S		195	
Deer		L.N		Y	V.Q.N	T	V	198	
Elk		L.N		Y	V.Q.N	T	V	198	
Mouse		M.N.W		Y	V.Q			194	
Rat		ML.N.W		Y	V.Q			195	
Pig		L		Y	V.Q	S	V	199	
Sheep		L.N		Y	V.Q		V	198	
Goat		L.R.N		Y	V.Q		V	198	
Rabbit		L.N		Y	V.Q	S	V	196	
Dog		L.N		Y	V.Q	R	V	199	
Cat		L.N		Y	V.Q		VR	202	
House		L.N		Y	VS		V	197	
Cattle		L			V.Q		V.E	206	
Buffalo		L.N			V.Q		V.E	206	
	220	230	240	250	260	270			
Human	ENFTETDVKMMERVVEQMCITQYERESQAYY--QRGSSMVLFSPPFVILLISFLIFLIVG						253		
Chimpanzee							253		
Rhesus							253		
Deer			K				256		
Elk			Q	A.VI			256		
Mouse			Q.E	A.VI			256		
Mouse		V	QK	DGR.S.T			254		
Rat		V	QK	DGR.S.-A			254		
Pig		I	QK.YE.A	A.VI		L	257		
Sheep		I.I	Q	A.VI			256		
Goat		I.I	Q	A.VI			256		
Rabbit		I.I	Q	A	AAGVL		254		
Dog		M.I	V	QK.E	A.AI	P	L.L	257	
Cat		M.I	V	QK.E	A.AI	P	L.L.L.G	260	
House		I	QK.YE.FQ	A.V		V.F	255		
Cattle		I	Q	A.VI			264		
Buffalo		I	Q	A.VI		L	264		

Figure 1 Amino acid sequences of PrP in 16 mammals (data from GenBank)

Human (NM_000311.3), chimpanzee (NM_001009093.3), Rhesus (NM_001047152.1), deer (AY330343.1), elk (EU082291.1), mouse (NM_011170.3), rat (NM_012631.2), pig (NM_001008687.1), sheep (NM_001009481.1), goat(JF729302.1), rabbit (NM_001082021.1), dog (NM_001013423.1), cat (EU341499.1), horse(NM_001143798.1), cattle (NM_181015.2), buffalo (KC.1). 137634.

converts into the disease-associated isoform (PrP^{Sc}). Although the primary structures of PrP^C and PrP^{Sc} are the same, their secondary structures are quite different. PrP^C is enriched with α -helix (42% are α -helix, 3% are β -fold), whereas PrP^{Sc} is enriched with β -fold (43% are β -fold, 30% are α -helix) and is protease resistant (McKinley *et al.*, 1983; Pan *et al.*, 1993; Prusiner, 1982). The massive intracellular accumulation of PrP^{Sc} induces formations of oligomer and amyloid fibrils, and eventually neuronal degeneration (Barron *et al.*, 2007; Caughey *et al.*, 2009). PrP plays vital roles in the pathological process of TSE. Knockout and low expression of PrP effectively abolishes or reduces susceptibility to TSEs, respectively (Brandner *et al.*, 1996; Büeler *et al.*, 1993), whereas high expression is associated with susceptibility and a shortened incubation time for disease development (Manson *et al.*, 1994).

TSE susceptibility is species-specific. Previous studies show high susceptibility in hamsters (*Mesocricetus auratus*) to TSE, as they can be infected by various PrP^{Sc} virus strains isolated from human, cattle, goats, mice (*Mus musculus*) and minks (Bessen & Marsh, 1992; Gibbs & Gajdusek, 1973; Kimberlin & Walker, 1977; Thomzig *et al.*, 2006). Similar high susceptibility is also found in mice (Chandler, 1961; Gibbs & Gajdusek, 1973; Hill *et al.*, 2000; Lasmézas *et al.*, 1997; Thomzig *et al.*, 2006). However, rabbits could not be infected by PrP^{Sc} strains isolated from human, goats and mice (Barlow & Rennie, 1976; Gibbs & Gajdusek, 1973). During the outbreak of BSE in the UK, infections in humans and several species of feline were reported, but no infection was found in dogs (*Canis familiaris*) or horses (*Equus caballus*) (Aldhous, 1990; Kirkwood & Cunningham, 1994). Collectively, species with confirmed susceptibility to TSE include humans, rhesus monkeys (*Macaca mulatta*), hamsters, mice, minks, elaphures, moose, goats, sheep, cattle and raccoons (*Procyon lotor*) (Imran & Mahmood, 2011). Only a few species, such as dogs (*Canis familiaris*), rabbits (*Oryctolagus cuniculus*) and horses (*Equus caballus*) have been recognized as TSE resistant (Fernandez-Funez *et al.*, 2011; Yuan *et al.*, 2013; Zhang, 2011a). Interestingly, although more than 190,000 cattle were infected by BSE, and buffaloes (*Bubalus bubalis*) and cattle are closely related, no buffalo has been reported with BSE infection (<http://www.oie.int>) and are of low susceptibility to BSE (Zhao *et al.*, 2012). In this review, based on TSE susceptibility, animals have been classified into TSE susceptible animals and TSE low susceptible animals.

The pathological mechanisms of TSE are yet to be clarified. Although highly susceptible animals are important to understanding this disease, studies on animals with low susceptibility provide a new angle from which to examine TSE. Here, we review recent research developments on protein structures, biochemical characteristics and genetic features of four animals (dogs, rabbits, horses and buffaloes) with low susceptibility to TSE.

Dogs

During the outbreak of BSE in the UK, several species of feline were reportedly infected, including cheetahs (*Acinonyx jubatus*), pumas (*Puma concolor*) and cats (Kirkwood & Cunningham, 1994). Since 1990, about 100 cats and 29 captive felines, including 15 cheetahs, four lions (*Panthera leo*), three leopard cats (*Prionailurus bengalensis*), three pumas, three tigers (*Panthera tigris*) and one Asian golden cat (*Catopuma temminckii*), have been diagnosed with FSE (Imran & Mahmood, 2011). The presumed infection source was PrP^{Sc}-contaminated food; however, dogs and cats are provided similar food and no dogs were reported with TSE (Imran & Mahmood, 2011; Kirkwood & Cunningham, 1994; Wopfner *et al.*, 1999). With further laboratory cell experiments, dogs have been recognized as a species with low TSE susceptibility. For example, when Madin-Darby canine kidney cells (MDCK) were infected with brain tissue homogenates from CJD patients or RML prion strain isolated from scrapie animals, although the biosynthesis and processing of PrP^C in MDCK are similar with those in N2aPK1 cells of murine neuroblastoma, which are highly susceptible to TSE, no PrP^{Sc} was found in MDCK. When infected MDCK were used to infect N2aPK1 cells, no PrP^{Sc} was found in N2aPK1 cells either (Ploymenidou *et al.*, 2008; Zhang & Liu, 2011).

The gene polymorphism of *PRNP* is correlated with TSE susceptibility (Westaway *et al.*, 1994). In humans, at least 30 mutations of *PRNP* are intertwined with TSE susceptibility (Lloyd *et al.*, 2011). In dogs, the amino acid residue 187 and 229 of the PrP sequence are histidine and glycine, respectively, whereas, they both are arginine in cats (Wopfner *et al.*, 1999). No FSE-related polymorphic site was found by screening encoding sequences of *PRNP* in 609 animals (including 15 FSE infected cases) and 29 species from 22 genera of the Order Carnivora, but Stewart *et al.* (2012) did notice that amino acid residue 163 in all canines is either aspartate or glutamic acid, indicating this locus may have some

connection to TSE susceptibility.

The three-dimensional structure of PrP^C may be another tool in resolving the puzzle of TSE susceptibility (Lin & Wen, 2011). To understand the structural differences of PrP^C in animals with low and high susceptibility to TSE, Lysek et al (2005) carried out a study on nuclear magnetic resonance (NMR) structures of PrP^C in dogs (*canine* PrP, cPrP), cats (*feline* PrP, fPrP), pigs (*sus scrofa* PrP, scPrP) and goats (*ovine* PrP, ovPrP). Their overall three-dimensional structures are quite close, consisting of a N-terminal (constituted of about 100 amino acid residues in random coil) and a globular domain in the C-terminal (including three α -helices and a pair of short, reverse paralleled β -folds constituting about 100 amino acid residues). The globular domain in the C-terminal is species-specific, e.g., four amino acids (Asp159Asn, Arg177His, Lys185 Arg and Gly229Arg) are different between cPrP^C and fPrP^C; Asp-159 and Arg-177 in cPrP^C make it unique in potential distribution; in fPrP^C, scPrP^C and ovPrP^C same positive potential distribution patterns are observed in their C-terminals.

The conversion of PrP^C into PrP^{Sc} is critical in TSE pathogenesis. Besides PrP^C and PrP^{Sc}, the existence of

the third state- β intermediate state, consisting mainly of β -fold in circular dichroism (CD) (Hornemann & Glockshuber, 1998), has raised attention due to its capability in introducing TSE (Collinge & Clarke, 2007). Khan et al (2010) claimed that in different species, the propensities in forming the β intermediate state are one of the vital factors influencing TSE susceptibility. Using dual wavelength CD, Khan et al (2010) compared the structures of the globular domain in high-susceptible (hamsters and mice) and low-susceptible species to TSE (rabbits, horses and dogs) and found that under inducing conditions with different pH values and urea concentrations, the propensities of forming the β intermediate state vary in different species. At pH 7.0, urea concentrations have no effect on PrP^C and no β intermediate state is observed in all five species; at pH 5.0, the structure of hamster PrP^C (hPrP^C) is most unstable and easily forms the β intermediate state; at pH 4.0, the PrP^C in all five species is unstable and easily forms the β intermediate state, the lowest concentration of β intermediate state occurs in dogs (Figure 2). The propensities in forming the β intermediate state (hamsters > mice > rabbits > horses > dogs) can also be adopted in evaluating

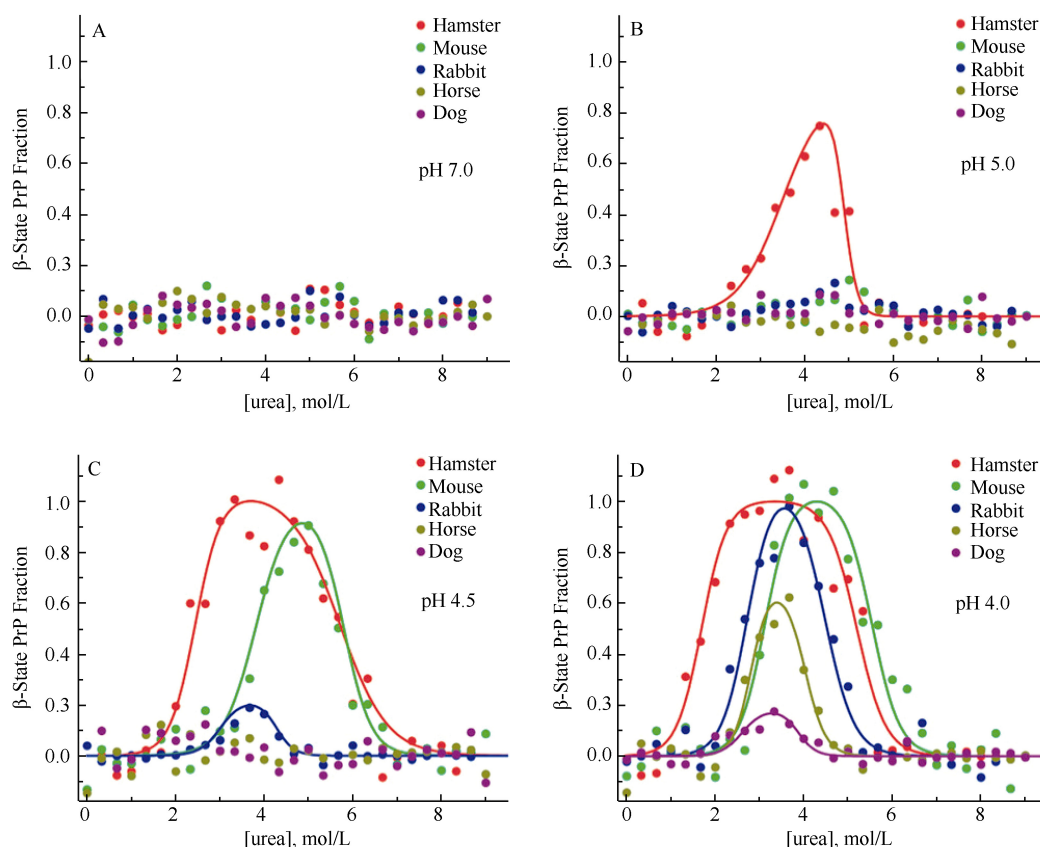


Figure 2 Propensities of conversions of PrP^C into the β intermediate state in different species at pH 7.0 (A), 5.0 (B), 4.5 (C) and 4.0 (D) and different concentrations of urea (modified from Khan et al, 2010)

species' susceptibilities to TSE (Fernandez-Funez *et al.*, 2011). Using molecular kinetic methods, Zhang & Liu (2011) found stable molecular structures of wild cPrP^C under both neutral and acidic pH conditions, and in the neutral condition the salt bridge between D177 and R163 improves structural stability. These studies help to explain the mechanism of low TSE susceptibility in dogs and general TSE pathogenesis.

Rabbits

No cases of spontaneous TSE infection in rabbits have been reported to date. In 1973, Gibbs & Gajdusek failed to infect rabbits with either brain tissues from human CJD or Kuru patients or brain tissues from scrapie animals and minks with TME. In 1976, Barlow & Rennie failed to infect rabbits with ME7 strains isolated from animals with scrapie. By constructing rabbit PrP^C (RaPrP^C) over-expressed murine neuroblastoma tumor cell lines, Vorberg *et al.* (2003) confirmed that RaPrP^C can neither be infected by RML strains nor convert into the PrP^{Sc}. The *in vivo* experiments conducted by Fernandez-Funez *et al.* (2010) support the view that rabbits are TSE resistant species. Fernandez-Funez *et al.* (2010) expressed full length PrP of hamsters, mice and rabbits in *drosophilae* voided of endogenous PrP, and found that cavernous transformation and isomers similar with PrP^{Sc} can only be found in the brains of transgenic *drosophilae* expressing shPrP^C and mouse PrP^C (moPrP^C), but not in *drosophilae* expressing RaPrP^C. Moreover, Bellotti & Chiti (2008) reported that TSE correlates with the deposition of amyloid fibrils. Zhou *et al.* (2011) found that Ficoll 70 and dextran 70 significantly accelerate the fibrillation of hPrP^C and bPrP^C, but prevent fibrillation of RaPrP^C; however, different from hPrP^C and bPrP^C, RaPrP^C does not have fragments resisting protease K digestion.

Initially it was presumed that one of the possible reasons rabbits are resistant to TSE infection is that certain transforming factors are lacking in their cellular environment or some inhibitory factors are expressed and the conversion of PrP^C to PrP^{Sc} is prevented. This presumption was later proved wrong. When PK13 cells, expressing shPrP^C, moPrP^C and vole (*Microtus spp.*) PrP^C, respectively, were infected with shPrP^{Sc}, moPrP^{Sc} and vole PrP^{Sc}, massive replications of PrP^{Sc} were observed, indicating that factors necessary for PrP conversion exist in rabbit cells (Courageot *et al.*, 2008;

Vilette *et al.*, 2001). Rabbits and mice share 87% similarity in amino acid sequences (33 amino acids are different, including 22 in mature peptides). When amino acid residues 99, 108, 173 and 214 in moPrP^C were mutated into the corresponding amino acid residues in RaPrP (Asn99Gly, Leu108Met, Asn173Ser and Val214Ile, respectively) and were overexpressed in mouse neuroblastoma (MNB), and then RML prion strains were used to infect MNB, the mutants of moPrP^C could not convert into PrP^{Sc}, indicating that several amino acid residues in RaPrP^C can prevent the replication of isomers of PrP^{Sc} (Vorberg *et al.*, 2003). About 33% of the different amino acids in moPrP^C and RaPrP^C locate around the attachment site of the GPI-anchor. Nisbet *et al.* (2010) stably transfected RK13 cells voided of endogenous PrP^C with a constructed double-mutant (Ser230Gly and Ser231Val) model of moPrP^C, MoPrP-RbGPI, and then infected RK13 cells expressing MoPrP-RbGPI using human prion strains M1000 or MU-02 isolated from mice brain homogenates. The results showed that MoPrP-RbGPI could change neither the attachment of the GPI-anchor nor the location of PrP^C on cells, but no PrP^{Sc} produce either, indicating that rabbit-specific amino acids may interfere with PrP^{Sc} and PrP^C contact and eventually prevent conversion of PrP^C to PrP^{Sc} (Nisbet *et al.*, 2010). These findings indicate that the resistance of rabbits to TSE may be attributable to their unique RaPrP^C structure (Lin & Wen, 2011). Wen *et al.* (2010a) adopted NMR techniques to study the solution structure of RaPrP^C and found that compared to hPrP^C, mPrP^C and bPrP^C, RaPrP^C features a unique charge distribution pattern. A large consecutive positive potential area exists on the protein surface of RaPrP^C which may interfere to interact with molecules such as chaperon protein X, prevents the proliferation of PrP^{Sc} (Wen *et al.*, 2010a). Khan *et al.* (2010) found a critical helix-capping motif interacting with the third α -helix and regulating the β -intermediate state by exploring the crystal structure of RaPrP^C. As we mentioned earlier, the complexities of PrP^C forming the β -intermediate state in different species are correlated with their susceptibility to TSE. Compared with ShPrP^C and moPrP^C, RaPrP^C is difficult to transform into the β -intermediate state (Figure 2) (Khan *et al.*, 2010). The irregular curling fragment, called an α 2- β 2 loop, locates between the second β -fold and the second α -helix (165-172). The epitope consisting of the α 2- β 2 loop and the C-terminal of the third α -helix is considered capable of recognizing protein X and

regulating progression of TSE (Kaneko et al, 1997). Protein dynamics analysis shows that RaPrP^C has a constructively highly ordered β 2- α 2 loop (Wen et al, 2010a) which may function as a species barrier for TSE dissemination (Lin & Wen, 2011). However, compared with wild RaPrP^C, S173N and I124V mutations affect the interactions of the β 2- α 2 loop with the third α -helix, and thereafter decrease the stability of the entire construct (Wen et al, 2010a, b). In addition, when the salt bridges between D202-R156 and D178-R164 were removed in hPrP^C and moPrP^C, although secondary protein structures remained intact, the helix structures of RaPrP^C were destroyed, indicating that salt bridges are important to the stability of RaPrP^C (Zhang, 2009, 2010, 2011a).

Recently, Joaquin Castilla's research group has raised questions about the view that rabbits are resistant to TSE. They amplified rabbit brain homogenates using serial automated protein misfolding cyclic amplification (saPMCA) and then inoculated this *in vitro* novel PrP into the brains of three other rabbits. One rabbit was found with TSE symptoms 766 days after inoculation even although no exogenous PrP^{Sc} was involved. Then the brain homogenates from this infected rabbit could 100% infect RaPrP^C over-expressed transgenic mice. Therefore, Chianini et al (2012) claims that rabbits are not TSE resistant. Furthermore, using saPMCA, when the amplified proteins from mixtures of rabbit brain homogenates and BSE prion strains were inoculated into the brains of RaPrP^C over-expressed transgenic mice, the resultant strains similar to BSE prion strains were discovered (Vidal et al, 2013). Fernández-Borges et al (2012) claims that *in vivo* infective experiments are imperfect when forming the conclusion that rabbits are resistant to TSE, especially when supported only by the observation that rabbits can not be infected with TSE naturally.

Horses

As there is no reports of horses being naturally infected with TSE, horses are recognized as low susceptibility species (Zhang, 2011a). Relative to dogs and rabbits, fewer studies have looked at low susceptibility in horses. Studies on the conversion of PrP^C into the β intermediate state show that under unstable conditions at pH 4, the PrP^C of hamsters, mice, rabbits, dogs and horses can convert into the β intermediate state, but the lowest level of β intermediate state is found in

horses (Figure 2), indicating that equus caballus PrP^C (ecPrP^C) is relatively stable (Khan et al, 2010). Structural NMR on ecPrP^C found two horse-specific amino acid alterations in its β 2- α 2 loop (Ser-167 and Lys-173, respectively), among which, S167 affects the highly ordered solution structure of the β 2- α 2 loop and may influence the low susceptibility of horses to TSE (Pérez et al, 2010). However, when amino acid residue 167 in moPrP^C was mutated from asparagine into ecPrP^C-specific serine (MoPrP^{D167S}), although MoPrP^{D167S} and ecPrP^C share similar NMR structures and their β 2- α 2 loops in solutions are both relatively highly ordered, spongiform lesions were found in mice expressing MoPrP^{D167S} and neural diseases can be induced with the accumulation of PrP^{Sc} in the brain (Sigurdson et al, 2011). Therefore, the ordered state of the β 2- α 2 loop in solution alone does not fully explain different susceptibilities to TSE (Lin & Wen, 2011). Moreover, as the salt bridge in RaPrP^C stabilizes protein structures, similar salt bridges consisting of GLU196-ARG156-HIS187, ARG156-ASP202 and GLU211-HIS177 are also found in ecPrP^C (Zhang, 2011b). The structures of ecPrP^C and cPrP^C are stable under both neutral and acidic conditions (Zhang, 2011a). A common phenomenon found among RaPrP^C, ecPrP^C and cPrP^C, is the salt bridge ASP177-ARG163 connects with the β 2- α 2 loop of PrP and is probably correlated with TSE susceptibility (Zhang, 2011a). Nevertheless, the low susceptibility of horses to TSE requires further work.

Buffalo

BSE was initially found in the UK in 1986, rapidly spread to over 25 countries, and caused major economic losses (Harman & Silva, 2009; Wells et al, 1987). BSE can also infect humans via the food chain and cause human vCJD (Collinge et al, 1996; Hill et al, 1997). The multiple pathogenic pathways of TSE, including spontaneous mutant, inheritance and infection (Nicholson et al, 2008), may explain why even after meat and bone meal was strictly forbidden, more than 15 000 BSE infected cattle were found in the UK (<http://www.oie.int>). Worldwide, there were over 190 000 *taurus* cattle, 1 *Bos indicus*, and 1 *Bos indicus* \times *Bos taurus* cross reported with BSE infections (data of OIE, Novakofski et al, 2005; Seuberlich et al, 2006). Although buffaloes and cattle are quite close phylogenetically, no case of BSE infected buffalo was ever reported, suggesting that genetic factors

are crucial to BSE susceptibility (Zhao *et al.*, 2012). The expression level of PrP is closely correlated with BSE susceptibility. Studies show that the *PRNP* gene of cattle has two indel (insertion and deletion) polymorphisms (a 23-bp indel in putative promoter, and a 12-bp indel in intron 1). These Indel polymorphisms affect gene expression (Msalya *et al.*, 2011; Sander *et al.*, 2005) and eventually BSE susceptibility (Haase *et al.*, 2007; Juling *et al.*, 2006; Sander *et al.*, 2004). Studies on polymorphisms in buffalo in Anatolia (Oztabak *et al.*, 2009), Pakistan (Imran *et al.*, 2012), Indonesia and Thailand (Uchida *et al.*, 2014) show significant differences in frequency distributions between buffaloes and cattle. Recently, genotyping analysis on Chinese buffalo showed that the distribution frequencies of BSE susceptibility related to genotypes and alleles, including the 23-bp deletion allele (D₂₃) and 12-bp deletion allele (D₁₂), were significantly lower than those of healthy cattle and BSE infected cattle, indicating that the low PrP expressed in buffalo may influence BSE susceptibility. Our later experiments proved that in tissue of the cerebellum, brain stem, mesenteric lymph nodes and bronchial lymph nodes, the expression of PrP is lower in buffalo than in cattle (submitted data).

Although *PRNP* play a vital role in the pathogenesis of TSE, the underlying pathological mechanisms of TSE remain unclear. Some propose that other than prions, there may be other factors or proteins regulating the pathogenesis and pathological process of TSE (Daude & Westaway, 2011; Watts *et al.*, 2007). The *SPRN* (shadow of prion protein) gene and its encoded protein Shadoo (Sho) have drawn lots of attention due to their roles in the pathogenesis of TSE. Comparative genomics analysis indicates that Sho is a newly discovered member of the prion protein family. Sho has been found in mammals such as mice and humans and is highly conserved from fish to mammals (Premzl *et al.*, 2003). Sho and PrP^C have a lot in common regarding structure and expression (Wang *et al.*, 2014). In PrP^{Sc} infected animal brains or nervous cell, with increasing PrP^{Sc} expression, the level of Sho decreases dramatically (Watts *et al.*, 2007, 2011; Westaway *et al.*, 2011). Beck *et al.* (2008) reported that the insertion of a base (heterozygous) within the encoding area of *SPRN* induces a frame-shift mutation which is correlated with vCJD. So, it is highly possible that Sho regulates the process of TSE by functioning as an inhibitory factor (Daude & Westaway, 2011). Our analysis of differences in the genetics and expression of *SPRN* between buffalo and cattle show that in the

hydrophobic domain (HD) within the encoding area, cattle have a 12-bp indel polymorphism which induces insertion/deletion of four amino acids. However, this phenomenon was not observed in buffalo (Zhao *et al.*, 2012). The HD of Sho not only protects against physiological stressors in nervous cell, but also helps Sho to interconnect with PrP^C (Wang *et al.*, 2010). This interconnection is a prerequisite of Sho regulating the pathogenesis of disease (Wang *et al.*, 2010). The exploration of the indel polymorphism within the Sho HD structural area is critical in fully understanding underlying mechanisms of TSE. Our luciferase reporter and immuno-blotting experiments confirm that compared to cattle, buffaloes have higher promoter activity and higher Sho expression, consistent with our prediction that buffalos have more transcription factor binding sites than cattle (Zhao *et al.*, 2012). These findings suggest that the low susceptibility of buffalos to BSE is probably attributable to significant genetic differences in *SPRN*.

Further Research

Joaquin Castilla's research group denies there are TSE resistant mammals, and believes that with improvements in detection any species can be found to be at risk of TSE infection (Fernandez-Borges *et al.*, 2012). However, from available data, TSE susceptibility does vary between species and we can classify animals as high susceptibility species and low susceptibility species. Scientists worldwide have applied various techniques to the study of TSE pathogenesis and have mainly focused on the genetic polymorphism of *PRNP*, expression levels of *PRNP*/PrP, three-dimensional structure and stability of PrP^C and dynamics of *PRNP*. However, the pathogenesis of TSE remains unclear. Lin & Wen (2011) claim that the three-dimensional structure of PrP^{Sc} and the physiological function of PrP^C are keys to resolving this puzzle but these two research directions have proved extremely difficult, even after two decades of attention. With breakthroughs in novel technologies and methods however, progress is likely. Studies on TSE low susceptibility molecules and newly discovered *SPRN* (Wang *et al.*, 2014) provide important clues about the formation of PrP^{Sc} and our understanding of TSE pathogenesis. Due to similarities in Sho and PrP^C regarding structure and function, especially their important roles in the pathogenesis and development of TSE, exploration of the biological functions of Sho and its regulatory effect on TSE will be vital.

References

- Aguzzi A, Sigurdson C, Heikenwaelder M. 2008. Molecular mechanisms of prion pathogenesis. *Annual Review of Pathology: Mechanisms Of Disease*, **3**(1): 11-40.
- Aldhous P. 1990. BSE: Spongiform encephalopathy found in cat. *Nature*, **345**(6272): 194.
- Barlow RM, Rennie JC. 1976. The fate of ME7 scrapie infection in rats, guinea-pigs and rabbits. *Research in Veterinary Science*, **21**(1): 110-111.
- Barron RM, Campbell SL, King D, Bellon A, Chapman KE, Williamson RA, Manson JC. 2007. High titers of transmissible spongiform encephalopathy infectivity associated with extremely low levels of PrP^{Sc} *in vivo*. *Journal of Biological Chemistry*, **282**(49): 35878-35886.
- Beck JA, Campbell TA, Adamson G, Poulter M, Uphill JB, Molou E, Mead S. 2008. Association of a null allele of SPRN with variant Creutzfeldt-Jakob disease. *Journal of Medical Genetics*, **45**(12): 813-817.
- Bellotti V, Chiti F. 2008. Amyloidogenesis in its biological environment: challenging a fundamental issue in protein misfolding diseases. *Current Opinion in Structural Biology*, **18**(6):771-779.
- Bessen RA, Marsh RF. 1992. Identification of two biologically distinct strains of transmissible mink encephalopathy in hamsters. *Journal of General Virology*, **73**(2): 329-334.
- Brandner S, Raeber A, Sailer A, Blättler T, Fischer M, Weissmann C, Aguzzi A. 1996. Normal host prion protein (PrP^C) is required for scrapie spread within the central nervous system. *Proceedings of the National Academy of Sciences of the United States of America*, **93**(23): 13148-13151.
- Büeler H, Aguzzi A, Sailer A, Greiner, RA, Autenried P, Aguet M, Weissmann C. 1993. Mice devoid of PrP are resistant to scrapie. *Cell*, **73**(7): 1339-1347.
- Caughey B, Baron GS, Chesebro B, Jeffrey M. 2009. Getting a grip on prions: oligomers, amyloids and pathological membrane interactions. *Annual Review of Biochemistry*, **78**(1): 177-204.
- Chandler RL. 1961. Encephalopathy in mice produced by inoculation with scrapie brain material. *The Lancet*, **277**(7191): 1378-1379.
- Chianini F, Fernández-Borges N, Vidal E, Gibbard L, Pintado B, Castro JD, Priola SA, Hamilton S, Eaton SL, Finlayson J, Pang Y, Steele P, Reid HW, Dagleish MP, Castilla J. 2012. Rabbits are not resistant to prion infection. *Proceedings of the National Academy of Sciences of the United States of America*, **109**(13): 5080-5085.
- Collinge J, Clarke AR. 2007. A general model of prion strains and their pathogenicity. *Science*, **318**(5852): 930-936.
- Collinge J, Sidle KCL, Meads J, Ironside J, Hill AF. 1996. Molecular analysis of prion strain variation and the aetiology of 'new variant' CJD. *Nature*, **383**(6602): 685-690.
- Collins SJ, Lawson VA, Masters CL. 2004. Transmissible spongiform encephalopathies. *The Lancet*, **363**(9402): 51-62.
- Courageot MP, Daude N, Nonno R, Paquet S, Di Bari MA, Le Dur A, Kunming Institute of Zoology (CAS), China Zoological Society
- Chapuis J, Hill AF, Agrimi U, Laude H, Vilette D. 2008. A cell line infectible by prion strains from different species. *Journal of General Virology*, **89**(1): 341-347.
- Daude N, Westaway D. 2011. Biological properties of the PrP-like Shadoo protein. *Frontiers in Bioscience*, **16**: 1505-1516.
- Fernández-Borges N, Chianini F, Eraña H, Vidal E, Eaton SL, Pintado B, Finlayson J, Dagleish MP, Castilla J. 2012. Naturally prion resistant mammals: A utopia? *Prion*, **6**(5): 425-429.
- Fernandez-Funez P, Zhang Y, Casas-Tinto S, Xiao X, Zou WQ, Rincon-Limas DE. 2010. Sequence-dependent prion protein misfolding and neurotoxicity. *Journal of Biological Chemistry*, **285**(47): 36897-36908.
- Fernandez-Funez P, Zhang Y, Sanchez-Garcia J, Jensen K, Zou WQ, Rincon-Limas DE. 2011. Pulling rabbits to reveal the secrets of the prion protein. *Communicative & Integrative Biology*, **4**(3): 262-266.
- Gibbs CJ, Gajdusek DC. 1973. Experimental subacute spongiform virus encephalopathies in primates and other laboratory animals. *Science*, **182**(4107): 67-68.
- Haase B, Doherr MG, Seuberlich T, Drögemüller C, Dolf G, Nicken P, Schiebel K, Ziegler U, Groschup MH, Zurbriggen A, Leeb T. 2007. PRNP promoter polymorphisms are associated with BSE susceptibility in Swiss and German cattle. *BMC Genet*, **8**(1): 15.
- Harman JL, Silva CJ. 2009. Bovine spongiform encephalopathy. *Journal of the American Veterinary Medical Association*, **234**(1): 59-72.
- Hill AF, Desbruslais M, Joiner S, Sidle KC, Gowland I, Collinge J, Doey LJ, Lantos P. 1997. The same prion strain causes vCJD and BSE. *Nature*, **389**(6650): 448-450.
- Hill AF, Joiner S, Linehan J, Desbruslais M, Lantos PL, Collinge J. 2000. Species-barrier-independent prion replication in apparently resistant species. *Proceedings of the National Academy of Sciences of the United States of America*, **97**(18): 10248-10253.
- Hornemann S, Glockshuber R. 1998. A scrapie-like unfolding intermediate of the prion protein domain PrP (121-231) induced by acidic pH. *Proceedings of the National Academy of Sciences of the United States of America*, **95**(11): 6010-6014.
- Imran M, Mahmood S, Babar ME, Hussain R, Yousaf MZ, Abid NB, Lone KP. 2012. PRNP gene variation in Pakistani cattle and buffaloes. *Gene*, **505**(1): 180-185.
- Imran M, Mahmood S. 2011. An overview of animal prion diseases. *Virology Journal*, **8**(1): 493.
- Juling K, Schwarzenbacher H, Williams JL, Fries R. 2006. A major genetic component of BSE susceptibility. *BMC Biology*, **4**(1): 33.
- Kaneko K, Zulianello L, Scott M, Cooper CM, Wallace AC, James TL, Cohen FE, Prusiner SB. 1997. Evidence for protein X binding to a discontinuous epitope on the cellular prion protein during scrapie prion propagation. *Proceedings of the National Academy of Sciences of the United States of America*, **94**(19): 10069-10074.
- Khan MQ, Sweeting B, Mulligan VK, Arslan PE, Cashman NR, Pai EF, Chakrabartty A. 2010. Prion disease susceptibility is affected by β -

- structure folding propensity and local side-chain interactions in PrP. *Proceedings of the National Academy of Sciences of the United States of America*, **107**(46): 19808-19813.
- Kimberlin RH, Walker CA. 1977. Characteristics of a short incubation model of scrapie in the golden hamster. *Journal of General Virology*, **34**(2): 295-304.
- Kirkwood JK, Cunningham AA. 1994. Epidemiological observations on spongiform encephalopathies in captive wild animals in the British Isles. *Veterinary Record*, **135**(13): 296-303.
- Lasmézas CI, Deslys JP, Robain O, Jaegly A, Beringue V, Peyrin JM, Fournier JG, Hauw JJ, Rossier J, Dormont D. 1997. Transmission of the BSE agent to mice in the absence of detectable abnormal prion protein. *Science*, **275**(5298): 402-404.
- Lin DH, Wen W. 2011. Progresses on prion proteins. *Scientia China: Chimica*, **41**(4): 683-698.
- Lloyd S, Mead S, Collinge J. 2011. Genetics of prion disease. *Topics in Current Chemistry*, **305**: 1-22.
- Lysek DA, Schom C, Nivon LG, Esteve-Moya V, Christen B, Calzolari L, Schroetter CV, Fiorito F, Herrmann T, Guntert P, Wüthrich K. 2005. Prion protein NMR structures of cats, dogs, pigs, and sheep. *Proceedings of the National Academy of Sciences of the United States of America*, **102**(3): 640-645.
- Manson JC, Clarke AR, McBride PA, McConnell I, Hope J. 1994. PrP gene dosage determines the timing but not the final intensity or distribution of lesions in scrapie pathology. *Neurodegeneration*, **3**(4): 331-340.
- McKinley MP, Bolton DC, Prusiner SB. 1983. A protease-resistant protein is a structural component of the scrapie prion. *Cell*, **35**(1): 57-62.
- Msalya G, Shimogiri T, Ohno S, Okamoto S, Kawabe K, Minezawa M, Maeda Y. 2011. Evaluation of PRNP expression based on genotypes and alleles of two indel loci in the medulla oblongata of Japanese Black and Japanese Brown cattle. *PLoS One*, **6**(5): e18787.
- Nicholson EM, Brunelle BW, Richt JA, Kehrl Jr ME, Greenlee, JJ. 2008. Identification of a heritable polymorphism in bovine PRNP associated with genetic transmissible spongiform encephalopathy: evidence of heritable BSE. *PLoS One*, **3**(8): e2912.
- Nisbet RM, Harrison CF, Lawson VA, Masters CL, Cappai R, Hill AF. 2010. Residues surrounding the glycosylphosphatidylinositol anchor attachment site of PrP modulate prion infection: insight from the resistance of rabbits to prion disease. *Journal of Virology*, **84**(13): 6678-6686.
- Novakofski J, Brewer MS, Mateus-Pinilla N, Killefer J, McCusker RH. 2005. Prion biology relevant to bovine spongiform encephalopathy. *Journal of Animal Science*, **83**(6): 1455-1476.
- Oztabak K, Ozkan E, Soysal I, Paya I, Ün C. 2009. Detection of prion gene promoter and intron1 indel polymorphisms in Anatolian water buffalo (*Bubalus bubalis*). *Journal of Animal Breeding and Genetics*, **126**(6): 463-467.
- Pan KM, Baldwin M, Nguyen J, Gasset M, Serban A, Groth D, Mehlhorn I, Huang Z, Fletterick RJ, Cohen FE. 1993. Conversion of alpha-helices into beta-sheets features in the formation of the scrapie prion proteins. *Proceedings of the National Academy of Sciences of the United States of America*, **90**(23): 10962-10966.
- Pérez DR, Damberger FF, Wüthrich K. 2010. Horse prion protein NMR structure and comparisons with related variants of the mouse prion protein. *Journal of Molecular Biology*, **400**(2): 121-128.
- Polymenidou M, Trusheim H, Stallmach L, Moos R, Julius C, Miele G, Lenz-Bauer C, Aguzzi A. 2008. Canine MDCK cell lines are refractory to infection with human and mouse prions. *Vaccine*, **26**(21): 2601-2614.
- Premzl M, Sangiorgio L, Strumbo B, Marshall Graves JA, Simonic T, Gready JE. 2003. Shadoo, a new protein highly conserved from fish to mammals and with similarity to prion protein. *Gene*, **314**: 89-102.
- Prusiner SB. 1982. Novel proteinaceous infectious particles cause scrapie. *Science*, **216**(4542): 136-144.
- Prusiner SB. 1998. Nobel lecture: Prions. *Proceedings of the National Academy of Sciences of the United States of America*, **95**(23): 13363-13383.
- Sander P, Hamann H, Drögemüller C, Kashkevich K, Schiebel K, Leeb T. 2005. Bovine Prion protein gene (PRNP) promoter polymorphisms modulate PRNP expression and may be responsible for differences in bovine spongiform encephalopathy susceptibility. *Journal of Biology Chemistry*, **280**(45): 37408-37414.
- Sander P, Hamann H, Pfeiffer I, Wemheuer W, Brenig B, Groschup MH, Ziegler U, Distl O, Leeb T. 2004. Analysis of sequence variability of the bovine prion protein gene (PRNP) in German cattle breeds. *Neurogenetics*, **5**(1): 19-25.
- Seuberlich T, Botteron C, Wenker C, Café-Marçal V, Oevermann A, Haase B, Leeb T, Heim D, Zurbriggen A. 2006. Spongiform encephalopathy in a miniature zebu. *Emerging Infectious Diseases*, **12**(12): 1950-1953.
- Sigurdson CJ, Joshi-Barr S, Bett C, Winson O, Manco G, Schwarz P, Rulicke T, Nilsson KPR, Margalith I, Raeber A, Peretz D, Hornemann S, Wuthrich K, Aguzzi A. 2011. Spongiform encephalopathy in transgenic mice expressing a point mutation in the $\beta 2$ - $\alpha 2$ loop of the prion protein. *Journal of Neuroscience*, **31**(39): 13840-13847.
- Stewart P, Campbell L, Skogtvedt S, Griffin KA, Arnemo JM, Tryland M, Girling S, Miller MW, Tranulis MA, Goldmann W. 2012. Genetic predictions of prion disease susceptibility in carnivore species based on variability of the prion gene coding region. *PLoS One*, **7**(12): e50623.
- Thomzig A, Cardone F, Krüger D, Pocchiari M, Brown P, Beekes M. 2006. Pathological prion protein in muscles of hamsters and mice infected with rodent-adapted BSE or vCJD. *Journal of Neuroscience*, **26**(1): 251-254.
- Uchida L, Heriyanto A, Thongchai C, Hanh TT, Horiuchi M, Ishihara K, Tamura Y, Muramatsu Y. 2014. Genetic diversity in the prion protein gene (PRNP) of domestic cattle and water buffaloes in Vietnam, Indonesia and Thailand. *Journal of Veterinary Medical Science*, in press.
- Vidal E, Fernández-Borges N, Pintado B, Ordóñez M., Márquez M, Fondevila D, Torres JM, Pumarola M, Castilla J. 2013. Bovine spongiform encephalopathy induces misfolding of alleged prion-resistant species cellular prion protein without altering its pathobiological features. *Journal of Neuroscience*, **33**(18): 7778-7786.
- Vilette D, Andreoletti O, Archer F, Madelaine MF, Vilotte JL, Lehmann S, Laude H. 2001. Ex vivo propagation of infectious sheep scrapie

- agent in heterologous epithelial cells expressing ovine prion protein. *Proceedings of the National Academy of Sciences of the United States of America*, **98**(7): 4055-4059.
- Vorberg I, Groschup MH, Pfaff E, Priola SA. 2003. Multiple amino acid residues within the rabbit prion protein inhibit formation of its abnormal isoform. *Journal of Virology*, **77**(3): 2003-2009.
- Wang JY, Hao Z, Xu M, Wang X, Wu SB, Song BC, Liu WS, Li JP, Meng KY, Li ZY, Gao HW. 2010. Mapping the interaction site of prion protein and Sho. *Molecular Biology Reports*, **37**(5): 2295-2300.
- Wang SQ, Zhao H, Zhang YP. 2014. Advances in research on Shadoo, Shadow of prion protein. *Chinese Science Bulletin*, **59**(9): 821-827.
- Watts JC, Drisaldi B, Ng V, Yang J, Strome B, Horne P, Sy M, Young R, Mastrangelo P, Bergeron C, Fraser PE, Carlson GA, Mount HTJ, Schmitt-Ulms G, Westaway D. 2007. The CNS glycoprotein Shadoo has PrPC-like protective properties and displays reduced levels in prion infections. *The EMBO Journal*, **26**(17): 4038-4050.
- Watts JC, Stöhr J, Bhardwaj S, Wille H, Oehler A, DeArmond SJ, Giles K, Prusiner SB. 2011. Protease-resistant prions selectively decrease Shadoo protein. *PLoS Pathogens*, **7**(11): e1002382.
- Wells GA, Scott AC, Johnson CT, Gunning RF, Hancock RD, Jeffrey M, Dawson M, Bradley R. 1987. A novel progressive spongiform encephalopathy in cattle. *Veterinary Record*, **121**(18): 419-420.
- Wen Y, Li J, Yao WM, Xiong MQ, Hong J, Peng Y, Xiao GF, Lin DH. 2010a. Unique structural characteristics of the rabbit prion protein. *Journal of Biological Chemistry*, **285**(41): 31682-31693.
- Wen Y, Li J, Xiong M, Peng Y, Yao WM, Hong J, Lin DH. 2010b. Solution structure and dynamics of the I214V mutant of the rabbit prion protein. *PLoS One*, **5**(10): e13273.
- Westaway D, Genovesi S, Daude N, Brown R, Lau A, Lee I, Mays CE, Coomaraswamy J, Canine B, Pitstick R, Herbst A, Yang J, Ko KWS, Schmitt-Ulms G, Dearmond SJ, McKenzie D, Hood L, Carlson GA. 2011. Down-regulation of Shadoo in prion infections traces a pre-clinical event inversely related to PrPSc accumulation. *PLoS Pathogens*, **7**(11): e1002391.
- Westaway D, Mirenda C A, Foster D, Zebajadian Y, Scott M, Torchia M, Yang S, Serban H, Dearmond SJ, Ebeling C, Prusiner SB, Carlson GA. 1991. Paradoxical shortening of scrapie incubation times by expression of prion protein transgenes derived from long incubation period mice. *Neuron*, **7**(1): 59-68.
- Westaway D, Zuliani V, Cooper C M, Costa MD, Neuman S, Jenny AL, Detwiler L, Prusiner SB. 1994. Homozygosity for prion protein alleles encoding glutamine-171 renders sheep susceptible to natural scrapie. *Genes and Development*, **8**(8): 959-969.
- Wopfner F, Weidenhöfer G, Schneider R, Brunn AV, Gilch S, Schwarz TF, Werner T, Schätzl HM. 1999. Analysis of 27 mammalian and 9 avian PrPs reveals high conservation of flexible regions of the prion protein. *Journal of Molecular Biology*, **289**(5): 1163-1178.
- Yuan Z, Zhao D, Yang L. 2013. Decipher the mechanisms of rabbit's low susceptibility to prion infection. *Acta Biochimica et Biophysica Sinica*, **45**(11): 899-903.
- Zhang JP. 2009. Studies on the structural stability of rabbit prion probed by molecular dynamics simulations. *Journal of Biomolecular Structure and Dynamics*, **27**(2): 159-162.
- Zhang JP. 2010. Studies on the structural stability of rabbit prion probed by molecular dynamics simulations of its wild-type and mutants. *Journal of Theoretical Biology*, **264**(1): 119-122.
- Zhang JP. 2011a. The nature of the infectious agents: PrP models of resistant species to prion diseases (dog, rabbit and horses). In: Verdier JM. Prions and prion diseases: New developments. Chapter 2. New York: NOVA Science Publishers, 41-48.
- Zhang JP, Liu DDW. 2011. Molecular dynamics studies on the structural stability of wild-type dog prion protein. *Journal of Biomolecular Structure and Dynamics*, **28**(6): 861-869.
- Zhang JP. 2011b. The structural stability of wild-type horse prion protein. *Journal of Biomolecular Structure and Dynamics*, **29**(2): 369-377.
- Zhao H, Liu LL, Du SH, Wang SQ, Zhang YP, Forloni G. 2012. Comparative analysis of the Shadoo gene between cattle and buffalo reveals significant differences. *PLoS One*, **7**(10): e46601.
- Zhou Z, Yan X, Pan K, Chen J, Xie ZS, Xiao GF, Yang FQ, Liang Y. 2011. Fibril formation of the rabbit/human/bovine prion proteins. *Biophysical Journal*, **101**(6): 1483-1492.

科铭牌生化检测试剂盒：产品实用、服务实在和价格实惠

简介：Comin 牌检测试剂盒由苏州科铭生物技术有限公司自主研发、生产和销售，目前包括 26 个系列 200 种常用测定指标 330 种检测试剂盒。苏州科铭率先研发并且独家拥有辅酶 I、辅酶 II、维生素 C、脂肪酸、淀粉、蔗糖、P450、土壤和转氢酶等系列检测试剂盒。科铭生物深知用户花钱购买试剂盒，就是为了简便快捷地获得可靠的实验数据，因此致力于以实用的产品、实在的服务和实惠的价格来赢得广大用户青睐。目前 Comin 牌检测试剂盒用户广泛分布于中科院系统、中国农科院系统、综合性大学、医科大学、农业大学和林业大学等科研单位以及专业公司。用户可以直接登录苏州科铭官网 www.cominbio.com 或者联系当地经销商选购。

产品实用：科铭生物致力于产品实用性和系列成套，全面满足用户需求。在保证检测专一性、灵敏度和重复性的基础上，通过测定方法优选、测定体系优化和测定步骤简化，力求测定数据可靠和操作简便，以最大限度地提高用户科研效率，保证顺利结题和按时毕业。产品系列成套可以全面满足用户研究某个主题的需要，用户通过密切相关的几个指标的测定，得出明确结论，从而提高论文发表档次。

服务实在：科铭生物致力于提供实在服务，切实帮助用户取得可靠测定结果。科铭生物建立了资深研发人员组成的技术支持队伍，全面及时提供购买前咨询、使用中指导和结果分析建议等服务；先发货后付款，可以在收到试剂盒后一个月内付款。

价格实惠：科铭生物致力于价格实惠，真正保证用户物有所值。一方面在保证产品和服务质量的基础上，通过提高研发和生产效率，降低试剂采购、包装和运输成本；另一方面不搞促销让利等噱头，而是明码标价，根据用户单次和累计购买额提供明确折扣。从而保证合理利润以保证可持续发展的同时，真正降低用户的支出。例如科铭生物的线粒体复合体系列试剂盒，其定价只有市场上其它公司同样规格试剂盒的 37%。

注意事项：

1. 购买前认真咨询，以免误购、漏购和多购。建议购买前用户告知所研究材料、处理和研究目的以及拟测定指标，以便提供专业建议，以免误购和漏购。不建议用户一次大量购买同一种试剂盒，可以先少量购买，待确认试测定结果后再大量购买，以免造成重大损失。

2. 严格按照试剂盒所附说明书保存试剂盒和操作，以免测定失败。确有必要，请用户与科铭生物技术人员商量后再做出调整。如果因为用户擅自改变引起测定失败，科铭生物恕不负责。

3. 质量保证和投诉处理。科铭生物保证用户严格按照试剂盒所附说明书测定常规样品能够得到可靠数据。如果样品特殊或者特别贵重请与技术人员商量后再进行测定。建议用户先选取 1~2 个预期差异较大的样品做预实验。如果结果异常，请立即联系技术人员。为了保证双方利益，如果用户怀疑试剂盒存在质量问题，请在试剂盒用量不超过一半时提出具体证据，并且及时全面如实地与技术人员沟通，以便真正找出和解决问题，保证用户实验正常进行。双方确认试剂盒存在质量问题，用户必须退回试剂盒和发票，科铭生物免费提供新试剂盒或者免单。

联系电话：0512-62956165, 18112525205（张）。

QQ：1831895487, 1329548029。

Zoological Research Editorial Board

EDITOR-IN-CHIEF:

Yong-Gang YAO Kunming Institute of Zoology, CAS, China

ASSOCIATE EDITORS-IN-CHIEF:

Bing-Yu MAO Kunming Institute of Zoology, CAS, China
Ying-Xiang WANG Kunming Institute of Zoology, CAS, China
Yun ZHANG Kunming Institute of Zoology, CAS, China
Yong-Tang ZHENG Kunming Institute of Zoology, CAS, China

MEMBERS:

Jing CHE Kunming Institute of Zoology, CAS, China
Biao CHEN Capital Medical University, China
Ce-Shi CHEN Kunming Institute of Zoology, CAS, China
Gong CHEN Pennsylvania State University, USA
Jiong CHEN Ningbo University, China
Xiao-Yong CHEN Kunming Institute of Zoology, CAS, China
Michael H. Ferkin University of Memphis, USA
Nigel W. Fraser University of Pennsylvania, USA
Colin P. Groves Australian National University, Australia
Wen-Zhe HO Wuhan University, China
David Irwin University of Toronto, Canada
Nina G. Jablonski Pennsylvania State University, USA
Prithwiraj Jha Raiganj Surendranath Mahavidyalaya, India
Xiang JI Nanjing Normal University, China
Xue-Long JIANG Kunming Institute of Zoology, CAS, China
Le KANG Institute of Zoology, CAS, China
Ren LAI Kunming Institute of Zoology, CAS, China
Bin LIANG Kunming Institute of Zoology, CAS, China
Wei LIANG Hainan University, China
Si-Min LIN Taiwan Normal University, China
Huan-Zhang LIU Institute of Hydrobiology, CAS, China
Jie MA Harvard University, USA
Masaharu Motokawa Kyoto University Museum, Japan
Victor Benno Meyer-Rochow University of Oulu, Finland
Monica Mwale South African Institute for Aquatic Biodiversity, South Africa
Neena Singla Punjab Agricultural University, India
Bing SU Kunming Institute of Zoology, CAS, China
Wen WANG Kunming Institute of Zoology, CAS, China
Fu-Wen WEI Institute of Zoology, CAS, China
Jian-Fan WEN Kunming Institute of Zoology, CAS, China
Richard Winterbottom Royal Ontario Museum, Canada
Jun-Hong XIA Sun Yat-sen University, China
Lin XU Kunming Institute of Zoology, CAS, China
Jian YANG Columbia University, USA
Xiao-Jun YANG Kunming Institute of Zoology, CAS, China
Hong-Shi YU University of Melbourne, Australia
Li YU Yunnan University, China
Lin ZENG Academy of Military Medical Science, China
Xiao-Mao ZENG Chengdu Institute of Biology, CAS, China
Ya-Ping ZHANG Chinese Academy of Sciences, China

ZOOLOGICAL RESEARCH

EDITORIAL BOARD



中国科学院昆明植物研究所



动物学类核心期刊

Editors: Long NIE Su-Qing LIU Andrew Willden

Edited by Editorial Office of Zoological Research

(Kunming Institute of Zoology, Chinese Academy of Sciences, 32 Jiaochang Donglu, Kunming,
Yunnan, Post Code: 650223 Tel: +86 871 65199026 Fax: +86 871 65113532

E-mail: zoores@mail.kiz.ac.cn Website: <http://www.zoores.ac.cn>)

Editor-in-Chief: Yong-Gang YAO

Sponsored by Kunming Institute of Zoology, Chinese Academy of Sciences; China Zoological Society©

Published by Science Press (16 Donghuangchenggen Beijie, Beijing 100717, China)

Printed by Kunming Xiaosong Plate Making & Printing Co, Ltd

Domestic distribution by Yunnan Post and all local post offices in China

International distribution by China International Book Trading Corporation (Guoji Shudian) P.O.BOX 399,
Beijing 100044, China

ISSN 2095-8137/CN 53-1229/Q

Price: 10.00 USD/60.00 CNY Post No: BM358



9 772095 813148

09>